Hybrid Methods in Vehicle Dynamics State Estimation and Control

–

Exploiting Potentials and Ensuring Reliability of Artificial Intelligence

Von der Fakultät für Ingenieurwissenschaften,

Abteilung Maschinenbau und Verfahrenstechnik der

Universität Duisburg-Essen

zur Erlangung des akademischen Grades

eines

Doktors der Ingenieurwissenschaften

Dr.-Ing.

genehmigte Dissertation

von

Philipp Maximilian Sieberg

aus

Oberhausen (Rheinland)

Gutachter:

Prof. Dr.-Ing. Dr. h.c. Dieter Schramm

Prof. Dr.-Ing. Lars Mikelsons

Dr. rer. nat. habil. Robert Martin

Tag der mündlichen Prüfung: 27. Mai 2021

“Have the courage to follow your heart and intuition. They somehow already know what you truly want to become. Everything else is secondary.”

Steve Jobs

Abstract

Within the scope of this thesis, two hybrid methods are developed and presented, which allow to exploit the potentials and to ensure the reliability of artificial intelligence for vehicle dynamics state estimation and control systems. The two hybrid methods are applied for an implementation of a central predictive vehicle dynamics control system. The objectives are to increase the safety of vehicles and to improve the ride comfort. The implementation of vehicle dynamics control systems is a well-researched field, but still offers unused potential. To achieve the aforementioned objectives, hybrid methods are utilized to exploit the great potential of artificial intelligence.

The first hybrid method focuses on the task of state estimation. By default, physical models resulting from theoretical modeling are used for state estimation. Due to assumptions and simplifications such models always feature a limited accuracy. In contrast, there are models resulting from experimental modeling. These also include models based on artificial intelligence. Such models are not based on explicit assumptions or simplifications, which generally yields a higher potential of accuracy. The increased accuracy, however, is accompanied by a loss of reliability and safety. The hybrid method of state estimation addresses and solves this issue. Within the thesis, artificial neural networks are combined with simple physical models and thus secured by them. The hybrid method determines a confidence level, which represents the confidence in the artificial neural network. The combination is done by a Kalman filter, the confidence level thereby affects the covariances of transition and measurement. Due to this novel method, the artificial neural network is only trusted stronger in well trained areas. If unknown input data are present, the reliable physical model is completely trusted. This ultimately results in an increase of estimation accuracy, while providing a reliable and valid state estimation throughout. In principle, the hybrid method thus provides the foundation for a legally approvable implementation of artificial intelligence based models for state estimation in vehicles.

The second hybrid method relates to the implementation of the control itself. With the objective of increasing vehicle safety and ride comfort, a central predictive approach for the control of the vehicle dynamics is pursued in order to exploit unused synergies within the vehicle. The class of model-based predictive control algorithms addresses the required aspects of a central predictive control system. In principle, this class of algorithms exhibits an excellent control performance, but it often results in a strongly increased computational effort. This is also confirmed in the context of the thesis. The increased effort arises from the use of non-linear models for the prediction as well as the subsequent optimization. Since the optimization within this vehicle dynamics control is performed numerically, a non-real-time capable system is present.

One possibility to address these issues is the limitation of iteration steps or the use of linear models, which however result in a reduction of the excellent control quality. The hybrid method for control is an option to drastically reduce the computational effort while preserving the control quality. The original non-linear model-based predictive control is reproduced by a neuro-fuzzy system. Through the use of artificial intelligence, a fuzzy inference system becomes trainable and can thus reproduce the desired behavior. After training, a pure fuzzy inference system remains, which is much easier to comprehend than, for example, an artificial neural network. By using this hybrid method, the computational effort of the central predictive vehicle dynamics control is drastically reduced. At the same time, the original control quality is preserved. Furthermore, the fuzzy inference system is based on a direct and not iterative working principle. Thus, this hybrid method opens up the possibility to implement control systems which originally have a high computational effort, are non-real-time capable or feature both aspects.

Whereas the hybrid methods are presented in this thesis for one application in vehicle dynamics control systems, they both offer the prerequisite for the use in various fields of application.

Kurzfassung

Im Rahmen dieser Arbeit werden zwei hybride Methoden entwickelt und vorgestellt, die es ermöglichen, für Zustandsschätzungen und Regelungssysteme in der Fahrdynamik die Potentiale von künstlicher Intelligenz auszuschöpfen und die Zuverlässigkeit sicherzustellen. Die beiden hybriden Methoden werden dabei für die Entwicklung eines zentralen prädiktiven Fahrdynamikregelungssystems eingesetzt. Hierbei werden die Ziele verfolgt, Fahrzeuge immer sicherer zu machen und gleichzeitig den Fahrkomfort weiter zu erhöhen. Die Umsetzung von Fahrdynamikregelungssystemen stellt ein weit erforschtes Gebiet dar, bietet aber weiterhin noch ungenutztes Potential. Um die genannten Ziele zu erreichen, werden hybride Methoden eingesetzt, die das große Potenzial der künstlichen Intelligenz nutzen.

Die erste hybride Methode fokussiert dabei den Bereich der Zustandsschätzung. Standardmäßig werden für die Zustandsschätzung physikalische Modelle verwendet, welche aus einer theoretischen Modellbildung resultieren. Aufgrund von getroffenen Annahmen und Vereinfachungen besitzen solche Modelle auch nur eine begrenzte Genauigkeit. Dem gegenüber stehen Modelle resultierend aus experimenteller Modellbildung. Zu diesen Modellen zählen auch Modelle auf Basis von künstlicher Intelligenz. Dabei basieren solche Modelle nicht auf expliziten Annahmen oder Vereinfachungen, was grundsätzlich in einem höheren Genauigkeitspotential resultiert. Die erhöhte Genauigkeit geht jedoch mit einem Verlust an Zuverlässigkeit und Absicherbarkeit einher. Die hybride Methode der Zustandsschätzung greift diese Problematik auf und löst sie. Innerhalb der Arbeit werden dabei künstliche neuronale Netze mit simplen physikalischen Modellen kombiniert und durch diese abgesichert. Die hybride Methode ermittelt dabei ein Vertrauensmaß, welches das Vertrauen in das künstliche neuronale Netz bestimmt. Die Kombination erfolgt durch einen Kalman Filter, das Vertrauensmaß beeinflusst dabei die Kovarianzen der Transition sowie der Messung. Durch diese neuartige Methode wird dem künstlichen neuronalen Netz nur in gut trainierten Bereichen starkes Vertrauen entgegengebracht. Liegen unbekannte Eingangsdaten vor, so wird dem zuverlässigen physikalischen Modell vollständig vertraut. Daraus resultiert letztendlich eine Erhöhung der Schätzgenauigkeit, während zugleich durchgängig eine zuverlässige und valide Zustandsschätzung vorliegt. Grundsätzlich bildet sie daher die Grundlage für eine gesetzlich abnahmefähige Umsetzung von auf künstlicher Intelligenz basierenden Modellen zur Zustandsschätzung in Fahrzeugen.

Die zweite hybride Methode bezieht sich dabei auf die Umsetzung der Regelung selbst. Mit dem Ziel der Erhöhung von Fahrzeugsicherheit und Fahrkomfort, wird im Rahmen dieser Arbeit ein zentraler prädiktiver Ansatz zur Regelung der Fahrdynamik verfolgt. Dieser nutzt die

im Fahrzeug vorhandene Synergien aus. Die Klasse der modellbasierten prädiktiven Regelungsalgorithmen adressiert dabei die Anforderungen eines zentralen prädiktiven Regelungssystems. Grundsätzlich weist diese Klasse von Algorithmen eine exzellente Regelgüte auf, sie resultiert oftmals aber auch in einem stark erhöhten Rechenaufwand. Dieses wird im Rahmen der Arbeit ebenfalls bestätigt. Durch die Verwendung von nichtlinearen Modellen zur Prädiktion sowie der anschließenden Optimierung liegt hier ein sehr großer Rechenaufwand vor. Da die Optimierung innerhalb dieser Fahrdynamikregelung numerisch erfolgt, liegt zudem ein nichtechtzeitfähiges System vor. Eine Möglichkeit diese Problematik zu adressieren ist die Limitierung von Iterationen oder die Verwendung von linearen Modellen, was jedoch in einer Reduzierung der exzellenten Regelgüte resultieren würde. Die hybride Methode für die Regelung stellt hierbei eine Option dar, den Rechenaufwand drastisch zu reduzieren und dabei trotzdem die Regelgüte beizubehalten. Die ursprüngliche nichtlineare modellbasierte prädiktive Regelung wird dabei durch ein Neuro-Fuzzy System nachgebildet. Durch den Einsatz von künstlicher Intelligenz, wird das Fuzzy Inferenz System trainierbar und kann somit das vorgegebene Verhalten nachbilden. Im Anschluss an das Training bleibt dabei jedoch ein reines Fuzzy Inferenz System bestehen, welches deutlich besser nachzuvollziehen ist als beispielsweise ein künstliches neuronales Netz. Durch den Einsatz dieser hybriden Methode wird der Rechenaufwand der zentralen prädiktiven Fahrdynamikregelung drastisch reduziert. Zugleich wird die ursprüngliche Regelgüte grundlegend beibehalten. Darüber hinaus basiert das Fuzzy Inferenz System auf einer direkten und nicht iterativen Arbeitsweise. Somit eröffnet diese hybride Methode die Möglichkeit Regelungssysteme umzusetzen welche ursprünglich einen hohen Rechenaufwand besitzen, nicht echtzeitfähig sind oder beide Aspekte aufweisen.

Während die beiden hybriden Methoden im Rahmen dieser Arbeit für eine Anwendung in der Fahrdynamikregelung vorgestellt werden, bieten beide Methoden die Voraussetzung für den Einsatz in verschiedensten Anwendungsgebieten.

Table of Contents

List of Figures

List of Tables

List of Symbols

Indexing

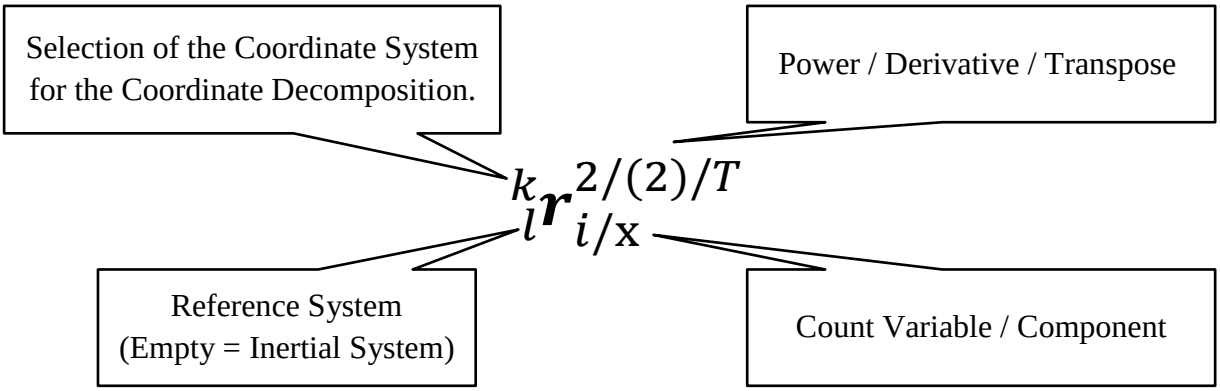

Latin Letters

Symbol	Unit	Description
$\boldsymbol{A}$	-	Transition Matrix
$\boldsymbol{B}$	-	Input Matrix
C_{H1}	-	Auxiliary Coordinate System
C_{H2}	-	Auxiliary Coordinate System
C_{I}	-	Inertial Coordinate System
$C_{R,C}$	-	Instantaneous Center of Rotation Opposite Steering
$C_{R,O}$	-	Instantaneous Center of Rotation Front Wheel Steering
$C_{R,P}$	-	Instantaneous Center of Rotation Parallel Steering
C_{V}	-	Body-Fixed Coordinate System
$\boldsymbol{D}$	-	Feedthrough Matrix
$E(\ \ )$	-	Loss Function
$EI(\ \ )$	-	Expected Improvement of the Hyperparameter Optimization
F_{A}	N	Force Due to Longitudinal Acceleration
F_{C}	N	Centrifugal Force

Symbol	Unit	Description
F_{D}	N	Damper Force
$\Delta F_{\mathrm{D,max}}$	N	Maximum Possible Damper Force Difference of the Semi-Active Damper
$\dot{F}_{\mathrm{D,max}}$	N/s	Maximum Changing Rate of the Damper Force Difference of the Semi-Active Damper
$F_{\mathrm{D,p}}$	N	Damping Force within the Determination of the Reference Value
$F_{\mathrm{D},\theta}$	N	Damping Force Depending on the Pitch Behavior
$F_{\mathrm{D},\varphi}$	N	Damping Force Depending on the Roll Behavior
F_{G}	N	Gravitational Force
$F_{\mathrm{S},\theta}$	N	Spring Force Depending on the Pitch Behavior
$F_{\mathrm{S},\varphi}$	N	Spring Force Depending on the Roll Behavior
F_{St}	N	Stabilizer Force
$F_{\mathrm{St,p}}$	N	Stabilizer Force with the Determination of the Reference Value
F_y	N	Lateral Force
$F_{y,\mathrm{C}}$	N	Lateral Force within the Control
F_z	N	Wheel Load
F_{z0}	N	Nominal Wheel Load
$F_{z,\mathrm{C}}$	N	Wheel Load within the Control
$\boldsymbol{H}$	-	Output Matrix
$\boldsymbol{I}$	-	Identity Matrix
I_{A}	A	Armature Current of the DC Motor
I_{C}	A	Coil Current of the Semi-Active Damper
I_{D}	A	Applied Current of the Semi-Active Damper
$I_{\mathrm{D,max}}$	A	Maximal Current of the Semi-Active Damper
$I_{\mathrm{D,min}}$	A	Minimal Current of the Semi-Active Damper
J_{DC}	kgm²	Moment of Inertia of the Rotor of the DC Motor
J_{xx}	kgm²	Moment of Inertia of the Vehicle Body Around the Longitudinal Axis
J_{yy}	kgm²	Moment of Inertia of the Vehicle Body Around the Lateral Axis

Symbol	Unit	Description
$\boldsymbol{K}$	-	Kalman Gain
K_{E}	Vs/rad	Counter-Electromotive Force Constant of the DC Motor
K_{T}	Nm/A	Torque Constant of the DC Motor
L	-	Parameter Quantifying the Number of Sigma Points
L_{A}	H	Armature Inductance of the DC Motor
L_{C}	H	Inductance of the Semi-Active Damper
MAE( )	-	Mean Absolute Error
$\mathcal{N}$( )	-	Normal Probability Distribution
O_{I}	-	Origin of the Inertial Coordinate System
O_{V}	-	Origin of the Vehicle Body-Fixed Coordinate System
$\boldsymbol{P}$	-	A Posteriori Covariance
$\boldsymbol{P}_{\hat{\boldsymbol{x}}(k+1)\hat{\boldsymbol{y}}(k+1)}$	-	Cross Correlation Covariance
$P_{\hat{\boldsymbol{y}}(k+1)\hat{\boldsymbol{y}}(k+1)}$	-	Covariance of the Predicted Measurement
$\boldsymbol{P}^{-}$	-	A Priori Covariance
$\boldsymbol{Q}$	-	Covariance of the Process Noise
$\boldsymbol{Q}_{\mathrm{HSE}}$	-	Covariance of Transition of the Hybrid Method of State Estimation
$\boldsymbol{Q}_{\mathrm{N}}$	-	Neutral Covariance of Transition
$\boldsymbol{R}$	-	Covariance of the Measurement Noise
R_{A}	Ω	Armature Resistance of the DC Motor
R_{C}	Ω	Resistance of the Semi-Active Damper
R_{F}	-	Number of Rule of the Neuro-Fuzzy Inference System
R_{HSE}	-	Covariance of Measurement of the Hybrid Method of State Estimation
R_{N}	-	Neutral Covariance of Measurement
RMSE( )	-	Root Mean Squared Error
SSG_{C}	rad·s²/m	Self-Steering Gradient within the Control
SSG_{Ref}	rad·s²/m	Reference Self-Steering Gradient
SSG_{Stat}	rad·s²/m	Constant Self-Steering Gradient
T	Nm	Counter Roll Torque
T_{A}	Nm	Pitch Torque due to the Longitudinal Acceleration

Symbol	Unit	Description
T_{C}	Nm	Counter Roll Torque within the Control
T_{Canfis}	Nm	Counter Roll Torque of the Co-Active Neuro-Fuzzy Inference System
T_{Ce}	Nm	Roll Torque due to the Centrifugal Force
T_{DC}	Nm	Applied Torque of the DC Motor
$T_{\mathrm{DC,req}}$	Nm	Required Torque of the DC Motor
$T_{G,\theta}$	Nm	Pitch Torque due to the Gravitational Force
$T_{\mathrm{G},\varphi}$	Nm	Roll Torque due to the Gravitational Force
T_{L}	Nm	Load Torque of the DC Motor
T_{max}	Nm	Maximal Counter Roll Torque
T_{min}	Nm	Minimal Counter Roll Torque
T_{Mpc}	Nm	Counter Roll Torque of the Non-Linear Model-Based Predictive Control
T_{St}	Nm	Actuated Variable of the Stabilizer Torque
$T_{\mathrm{St,C}}$	Nm	Manipulated Variable of the Stabilizer Torque
$T_{\mathrm{St,max}}$	Nm	Maximal Stabilizer Torque
$T_{\mathrm{St,min}}$	Nm	Minimal Stabilizer Torque
T_{T}	Nm	Total Counter Roll Torque
ΔT_{C}	Nm	Counter Roll Torque Deviation
U_{A}	V	Armature Voltage of the DC Motor
$U_{\mathrm{C,N}}$	V	Voltage of the Semi-Active Damper
W	-	Weighting of the Sigma Point
$\boldsymbol{W}_{\mathrm{hf}}$	-	Weighting Matrix of the Short-Term State in the Forget Gate
$\boldsymbol{W}_{\mathrm{hg}}$	-	Weighting Matrix of the Short-Term State in the Input Gate
$\boldsymbol{W}_{\mathrm{hi}}$	-	Weighting Matrix of the Short-Term State in the Input Gate
$\boldsymbol{W}_{\mathrm{ho}}$	-	Weighting Matrix of the Short-Term State in the Output Gate
$\boldsymbol{W}_{\mathrm{zf}}$	-	Weighting Matrix of the Input Vector in the Forget Gate
$\boldsymbol{W}_{\mathrm{zg}}$	-	Weighting Matrix of the Input Vector in the Input Gate

Symbol	Unit	Description
$\boldsymbol{W}_{\mathrm{zi}}$	-	Weighting Matrix of the Input Vector in the Input Gate
$\boldsymbol{W}_{\mathrm{zo}}$	-	Weighting Matrix of the Input Vector in the Output Gate
$\boldsymbol{a}$	-	Coefficients of the Polynomials within the Control
a_{HP}	-	Parameter of the Generalized Bell Function
a_{N}	-	Minimum Value of the Min-Max Normalization
a_{St}	m	Effective Length of the Stabilizer
a_x	$\mathrm{m/s^2}$	Longitudinal Acceleration
a_y	$\mathrm{m/s^2}$	Lateral Acceleration
$\boldsymbol{b}_{\mathrm{f}}$	-	Bias Vector in the Forget Gate
$\boldsymbol{b}_{\mathrm{g}}$	-	Bias Vector in the Input Gate
b_{HP}	-	Parameter of the Generalized Bell Function
$\boldsymbol{b}_{\mathrm{i}}$	-	Bias Vector in the Input Gate
b_{N}	-	Maximum Value of the Min-Max Normalization
$\boldsymbol{b}_{\mathrm{o}}$	-	Bias Vector in the Output Gate
b_{St}	m	Lever Arm of the Stabilizer
$\boldsymbol{c}$	-	Long-Term State
c_α	N/rad	Cornering Stiffness
$c_{\alpha,\mathrm{C}}$	N/rad	Cornering Stiffness within the Control
c_{HP}	-	Parameter of the Generalized Bell Function
c_{S}	N/m	Spring Constant
$c_{\mathrm{St,P}}$	N/m	Stabilizer Stiffness of the Passive Stabilizer
c_{T1}	-	Parameter of the Semi-Empirical Tire Model
c_{T2}	-	Parameter of the Semi-Empirical Tire Model
d	Ns/m	Damping Factor of the Semi-Active Damper
d_{C}	Ns/m	Damping Factor of the Semi-Active Damper within the Control
d_{Canfis}	Ns/m	Damping Factor of the Semi-Active Damper of the Co-Active Neuro-Fuzzy Inference System
d_{DC}	Nms/rad	Viscosity Coefficient of the DC Motor
d_{max}	Ns/m	Maximal Damping Factor of the Semi-Active Damper
d_{min}	Ns/m	Minimal Damping Factor of the Semi-Active Damper

Symbol	Unit	Description
d_{Mpc}	$\mathrm{Ns/m}$	Damping Factor of the Semi-Active Damper of the Non-Linear Model-Based Predictive Control
d_{p}	$\mathrm{Ns/m}$	Damping Factor of the Passive Damper
Δd_{C}	$\mathrm{Ns/m}$	Damping Factor Deviation of the Semi-Active Damper
$\boldsymbol{e}$	-	Error of the A Posteriori State Estimation
$\boldsymbol{e}^{-}$	-	Error of the A Priori State Estimation
$\boldsymbol{f}$	-	Intermediate State of the Forget Gate
f_{a}	-	Activation Function
f_{C}	-	Cost Function within the Control
f_{HP}	-	Loss Function of the Hyperparameter Optimization
f_{HP}^{*}	-	Loss Function of the Hyperparameter Optimization
f_{I}	-	Transition Function
f_{i}	-	Identity Function
f_{log}	-	Logistic Function
f_{O}	-	Output Function
f_{tanh}	-	Hyperbolic Tangent
$\boldsymbol{g}$	-	Intermediate State of the Input Gate
g	$\mathrm{m/s^2}$	Acceleration due to Gravity
$g_{\mathrm{HP}}(\ \ )$	-	Density of the Hyperparameter Optimization
$\boldsymbol{h}$	-	Short-Term State
h_{G}	m	Height of the Center of Gravity
h_{GP}	m	Height Distance between the Center of Gravity and the Pitch Center
h_{GR}	m	Height Distance between the Center of Gravity and the Roll Center
h_{P}	m	Pitch Center Height
h_{R}	m	Roll Center Height
$\boldsymbol{i}$	-	Intermediate State of the Input Gate
i_{SR}	-	Steering Gear Ratio
k	-	Discrete Time Step

Symbol	Unit	Description
k_{G}	-	Number of Cells of One Input Quantity of the Hybrid Method of State Estimation
l_{D}	m	Distance between Damper Force Application and Center of Gravity
l_{f}	m	Distance between the Front Axle and the Center of Gravity
$l_{\mathrm{HP}}(\ \ )$	-	Density of the Hyperparameter Optimization
l_{r}	m	Distance between the Rear Axle and the Center of Gravity
l_{S}	m	Distance between the Spring Force Application and the Center of Gravity
l_{St}	m	Distance between the Stabilizer Force Application and the Center of Gravity
m	kg	Mass of the Vehicle Body
n_{F}	-	Number of Input Quantities of the Co-Active Neuro-Fuzzy Inference System
n_{I}	-	Dimension of the Input Space of the Hybrid Method of State Estimation
n_{MS}	-	Number of Membership Functions per Input Quantity of the Co-Active Neuro-Fuzzy Inference System
n_{p}	-	Prediction Horizon
n_{W}	$1/\mathrm{s}$	Wheel Speed
$\bar{n}_{\mathrm{V}}$	$1/\mathrm{s}$	Average Wheel Speed
$\boldsymbol{o}$	-	Intermediate State of the Output Gate
$p(\ \ )$	-	Probability Distribution
p_{DC}	-	Number of Pole Pairs of the DC Motor
r_{DC}	-	Gear Ratio of the DC Motor
p_k	-	Number of Data Within a Cell of the Hybrid Method of State Estimation
$p_{\max}$	-	Characteristic Value of the Hybrid Method of State Estimation
$\boldsymbol{r}_{\mathrm{V}}$	m	Spatial Vector
s_{D}	m	Distance between the Damper Force Application and the Vehicle Center Plane

Symbol	Unit	Description
s_{S}	m	Distance between the Spring Force Application and the Vehicle Center Plane
s_{St}	m	Distance between the Stabilizer Force Application and the Vehicle Center Plane
$\boldsymbol{s}_{\mathrm{V}}$	-	Sensor Data Vector
$\boldsymbol{s}_{\mathrm{V,Ann}}$	-	Sensor Input Data of the Artificial Neural Networks
$\boldsymbol{s}_{\mathrm{V,P}}$	-	Sensor Input Data of the Physical Models
t_{S}	s	Step Size
$\boldsymbol{u}$	-	Input Vector
u	-	Manipulated Variable within the Control
$\boldsymbol{u}_{\mathrm{C}}$	-	Manipulated Variables Vector
$\boldsymbol{u}_{\mathrm{Canfis}}$	-	Manipulated Variables of the Co-Active Neuro-Fuzzy Inference System
$\boldsymbol{u}_{\mathrm{HSE}}$	-	Input Vector of the Unscented Kalman Filter
$\boldsymbol{u}_{\mathrm{Mpc}}$	-	Manipulated Variables of the Non-Linear Model-Based Predictive Control
u_{n}	-	Result of the Weighted Sum
$\boldsymbol{u}_{\mathrm{P}}$	-	Manipulated Variables Vector within the Control
$\boldsymbol{u}_{\mathrm{R}}$	-	Actuating Variables Vector
$\boldsymbol{v}$	-	Measurement Noise Vector
v	m/s	Vehicle Velocity
v_{D}	m/s	Compression Velocity of the Semi-Active Damper
$\boldsymbol{w}$	-	Process Noise Vector
$\boldsymbol{w}_{\mathrm{z}}$	-	Weighting Vector
w_{b}	-	Weighting of the Bias
$\boldsymbol{x}$	-	State Vector
$\hat{\boldsymbol{x}}$	-	A Posteriori State Vector
$\boldsymbol{x}_{\mathrm{C}}$	-	States to be Controlled within the Control
$\boldsymbol{x}_{\mathrm{Est}}$	-	Estimated States by the Hybrid Method of State Estimation
x_{I}	-	Longitudinal Axis of the Inertial Coordinate System
$\boldsymbol{x}_{\mathrm{Ref}}$	-	Reference States within the Control

Symbol	Unit	Description
x_{V}	-	Longitudinal Axis of the Body-Fixed Coordinate System
$\hat{\boldsymbol{x}}^{-}$	-	A Priori State Vector
${}^{\mathrm{I}}x_{\mathrm{V}}$	m	Longitudinal Component of the Spatial Vector
$\boldsymbol{y}$	-	Output Vector
y	-	Output
y_{Ann}	-	Estimation Quantity of the Artificial Neural Network
y_{I}	-	Lateral Axis of the Inertial Coordinate System
y_{V}	-	Lateral Axis of the Body-Fixed Coordinate System
$\hat{y}^{-}$	-	Predicted Measurement of the Unscented Kalman Filter
${}^{\mathrm{I}}y_{\mathrm{V}}$	m	Lateral Component of the Spatial Vector
$\boldsymbol{z}$	-	Input Vector of the Artificial Neural Network
z_{b}	-	Bias
z_{I}	-	Vertical Axis of the Inertial Coordinate System
z_{N}	-	Normalized Input Quantity of the Artificial Neural Network
z_{V}	-	Vertical Axis of the Body-Fixed Coordinate System
${}^{\mathrm{I}}z_{\mathrm{V}}$	m	Vertical Component of the Spatial Vector

Greek Letters

Symbol	Unit	Description
$\boldsymbol{\Upsilon}$	-	Sigma Points of the Predicted Measurement
$\mathbf{X}$	-	Sigma Points of the State
α	rad	Slip Angle
α_{C}	rad	Slip Angle within the Control
α_{K}	-	Parameter of the Sigma Points Spreading
α_{L}	-	Learning Rate
$\tilde{\alpha}_{\mathrm{Canfis}}$	rad	Pseudo Quantity of the Self-Steering Behavior of the Co-Active Neuro-Fuzzy Inference System

Symbol	Unit	Description
$\tilde{\alpha}_{\mathrm{Est,Canfis}}$	rad	Pseudo Quantity of the Collaborative Setup of the Hybrid Methods
$\tilde{\alpha}_{\mathrm{Mpc}}$	rad	Pseudo Quantity of the Self-Steering Behavior of the Non-Linear Model-Based Predictive Control
$\tilde{\alpha}_{\mathrm{Pas}}$	rad	Pseudo Quantity of the Self-Steering Behavior of a Vehicle With Passive Chassis
$\tilde{\alpha}_{\mathrm{P,Mpc}}$	rad	Pseudo Quantity of the Physical Setup
$\tilde{\alpha}_{\mathrm{Ref}}$	rad	Reference Pseudo Quantity of the Self-Steering Behavior
$\Delta\tilde{\alpha}$	rad	Pseudo Quantity Deviation
β	rad	Side-Slip Angle
β_{Ann}	rad	Artificial Neural Network Estimation of the Side-Slip Angle
β_{C}	rad	Side-Slip Angle within the Control
β_{Est}	rad	Hybrid Method Estimation of the Side-Slip Angle
β_{Meas}	rad	Ground Truth Side-Slip Angle
β_{P}	rad	Physical Estimation of the Side-Slip Angle
β_{U}	-	Specification of the Distribution
$\Delta\beta$	rad	Side-Slip Angle Deviation
$\dot{\beta}$	rad/s	Time Derivative of the Side-Slip Angle
$\dot{\beta}_{\mathrm{C}}$	rad/s	Time Derivative of the Side-Slip Angle within the Control
$\dot{\beta}_{\mathrm{P}}$	rad/s	Physical Estimation of the Time Derivative of Side-Slip Angle
γ_{HP}	-	Probability Distribution of the Hyperparameter Optimization
δ	rad	Steering Angle
δ_{SW}	rad	Steering Wheel Angle
θ	rad	Pitch Angle
θ_{Ann}	rad	Artificial Neural Network Estimation of the Pitch Angle
θ_{C}	rad	Pitch Angle within the Control

Symbol	Unit	Description
θ_{Canfis}	rad	Pitch Angle of the Co-Active Neuro-Fuzzy Inference System
θ_{Est}	rad	Hybrid Method Estimation of the Pitch Angle
$\theta_{\mathrm{Est,Canfis}}$	rad	Pitch Angle of the Collaborative Setup of the Hybrid Methods
θ_{Meas}	rad	Ground Truth Pitch Angle
θ_{Mpc}	rad	Pitch Angle of the Non-Linear Model-Based Predictive Control
θ_{P}	rad	Physical Estimation of the Pitch Angle
θ_{Pas}	rad	Pitch Angle of a Vehicle With Passive Chassis
$\varphi_{\mathrm{P,Mpc}}$	rad	Pitch Angle of the Physical Setup
θ_{Ref}	rad	Reference Pitch Angle
θ_{Stat}	rad	Constant Pitch Angle
$\Delta\theta$	rad	Pitch Angle Deviation
$\dot{\theta}$	rad/s	Pitch Rate
$\dot{\theta}_{\mathrm{C}}$	rad/s	Pitch Rate within the Control
$\dot{\theta}_{\mathrm{Est}}$	rad/s	Hybrid Method Estimation of the Pitch Rate
$\dot{\theta}_{\mathrm{P}}$	rad/s	Physical Estimation of the Pitch Rate
$\ddot{\theta}_{\mathrm{C}}$	rad/s²	Pitch Acceleration within the Control
$\ddot{\theta}_{\mathrm{P}}$	rad/s²	Physical Estimation of the Pitch Acceleration
κ	-	Parameter of the Sigma Points Spreading
λ	-	Scaling Parameter of the Sigma Points
$\boldsymbol{\lambda}_{\mathrm{HP}}$	-	Hyperparameter Configurations
$\boldsymbol{\lambda}_{\mathrm{HP}}^{*}$	-	Hyperparameter Configuration
$\boldsymbol{\lambda}_{\mathrm{C}}$	-	Weighting Factors within the Control
$\mu(\ \ )$	-	Membership Function
ξ_{R}	-	Scaling Factor of the Reference Roll Angle
τ_{Ann}	-	Lookback of the Artificial Neural Network
τ_{C}	s	Inductive Time Delay of the Semi-Active Damper
τ_{H}	s	Hydraulic Time Delay of the Semi-Active Damper

Symbol	Unit	Description
τ_{HSE}	-	Confidence Level of the Hybrid Method of State Estimation
φ	rad	Roll Angle
φ_{Ann}	rad	Artificial Neural Network Estimation of the Roll Angle
φ_{C}	rad	Roll Angle within the Control
$\varphi_{\mathrm{Canfis}}$	rad	Roll Angle of the Co-Active Neuro-Fuzzy Inference System
φ_{Est}	rad	Hybrid Method Estimation of the Roll Angle
$\varphi_{\mathrm{Est,Canfis}}$	rad	Roll Angle of the Collaborative Setup of the Hybrid Methods
φ_{Meas}	rad	Ground Truth Roll Angle
φ_{Mpc}	rad	Roll Angle of the Non-Linear Model-Based Predictive Control
φ_{P}	rad	Physical Estimation of the Roll Angle
φ_{Pas}	rad	Roll Angle of a Vehicle With Passive Chassis
$\varphi_{\mathrm{P,Mpc}}$	rad	Roll Angle of the Physical Setup
φ_{T}	rad	Roll Angle of a Vehicle With Passive Chassis to Determine the Reference Roll Angle
φ_{Ref}	rad	Reference Roll Angle
$\Delta\varphi$	rad	Roll Angle Deviation
$\dot{\varphi}$	rad/s	Roll Rate
$\dot{\varphi}_{\mathrm{C}}$	rad/s	Roll Rate within the Control
$\dot{\varphi}_{\mathrm{Est}}$	rad/s	Hybrid Method Estimation of the Roll Rate
$\dot{\varphi}_{\mathrm{P}}$	rad/s	Physical Estimation of the Roll Rate
$\dot{\varphi}_{\mathrm{P}}$	rad/s	Roll Rate of a Vehicle With Passive Chassis to Determine the Reference Roll Angle
$\ddot{\varphi}_{\mathrm{C}}$	rad/s²	Roll Acceleration within the Control
$\ddot{\varphi}_{\mathrm{P}}$	rad/s²	Physical Estimation of the Roll Acceleration
$\ddot{\varphi}_{\mathrm{T}}$	rad/s²	Roll Acceleration of a Vehicle With Passive Chassis to Determine the Reference Roll Angle
ψ	rad	Yaw Angle
$\dot{\psi}$	rad/s	Yaw Rate

Symbol	Unit	Description
$\dot{\psi}_{\mathrm{C}}$	rad/s	Yaw Rate within the Control
$\ddot{\psi}_{\mathrm{C}}$	rad/s²	Yaw Acceleration within the Control
ω_{DC}	rad/s	Angular Velocity of the DC Motor

1 Introduction

This thesis is intended to be a fundamental contribution towards developing the vehicle of the future. The underlying motivation is to contribute to safer vehicles while additionally enhancing the ride comfort. In principle, this is achieved by making even greater use of additional intelligence in the vehicle. In the context of this thesis the potentials of artificial intelligence are exploited for this purpose. Furthermore, a novel methodology to ensure the reliability of models based on artificial intelligence is introduced. These aspects are presented and validated for the application case of vehicle dynamics control systems.

1.1 Motivation and Context

Motorized vehicles have accompanied humankind far more than a century now. Since then, it has ensured the individual mobility of people and, in addition to its use in local transportation systems, has also made it possible to cover long distances.

Increasing the vehicle safety has always been one of the most important driving forces behind the continuous development of vehicles. This aspect is further reflected in the vision zero initiative considering a future scenario in which individual mobility does not lead to any fatalities, serious injuries or even accidents in an ideal case, (Johansson, 2009).

In order to achieve the objectives of this initiative it is indispensable to increase vehicle safety significantly. Various possibilities of intervention are available for this purpose, which already have been used in the past as well. These include legal regulations, passive safety systems and active safety systems.

An increase in vehicle safety has so far been successfully achieved by legal regulations. Especially the introduction of speed limits, the regulation of alcohol limits for drivers and the introduction of sanctions for seat belt violations have to be emphasized, (Mann et al., 2001, De Pauw et al., 2014). Alongside the legal regulations, the development and integration of passive safety systems has contributed to the increase in vehicle safety. This includes the introduction and improvement of structural deformation zones, the introduction of airbags and the utilization of seat belts, (Robertson, 1996, Griffin et al., 2018).

Whereas passive safety systems primarily minimize damage in accidents, active safety systems are used to increase vehicle safety by actively preventing accidents, (Jarašūniene and Jakubauskas, 2007). These active safety systems comprise vehicle dynamics control systems and advanced driver assistance systems. Whereas advanced driver assistance systems mainly assist in the driving task of guidance, vehicle dynamics control systems support the driving task of stabilization, (Eckstein and Zlocki, 2013). Especially the applications of vehicle dynamics control systems have contributed significantly to the reduction of accidents and thus to the enhancement of vehicle safety, (Schramm et al., 2020). The anti-lock braking system and the electronic stability control system are particularly noteworthy in this context. By using the electronic stability control system, the risk of accidents is reduced approximately between 30 % and 35 %, (Farmer, 2004, Rieger et al., 2005).

The improvement of the ride comfort is a further key driving force within the vehicle development. In this context, the chassis is essential for improving ride comfort. Whereas the design of a passive chassis during the development process totally defines the influence on the ride comfort, semi-active and active chassis elements offer the possibility to adapt the influence on the ride comfort during operation. The design of a passive chassis therefore always represents a compromise between ride comfort and performance, (Sharp and Crolla, 1987). In contrast, the use of semi-active and active chassis elements offers more flexibility. The systematic adjustment of the semi-active and active chassis elements during operation is thereby also classified in the category of vehicle dynamics control systems.

Vehicle dynamics control systems thus represent a possibility to influence and ultimately improve two decisive characteristics of a vehicle, the safety and the ride comfort. Especially with regard to a visionary implementation in combination with highly respectively fully automated vehicles, the area of vehicle dynamics control possesses unexploited potential. With the development towards highly respectively fully automated driving, drivers become passengers. This obviously alters the general perception of passengers and thus also the perception of comfort, (Elbanhawi et al., 2015). Moreover, the safety needs to be ensured in emergency evasive maneuvers as well.

The implementation of a central predictive vehicle dynamics control is addressing the unused potential and exploits it by synergy effects and a modified mode of operation. Instead of a purely reactive mode of operation, it acts with foresight. Consequently, both vehicle safety and ride comfort can be further improved.

1.2 Problem Statement

In order to contribute to even safer vehicles along with an enhanced ride comfort of vehicles in the future, the potentials of a central predictive vehicle dynamics control system are exploited within this thesis. To accomplish these objectives, artificial intelligence is utilized, providing

additional potential which can be used to surpass the emerging challenges. These challenges are composed mainly of the minimization of costs, the enhancement of accuracy, the assurance of reliability and the reduction of computational effort.

In particular, the costs are largely determined by the effort to acquire the vehicle dynamic states. The knowledge must be available to realize a central predictive vehicle dynamics control at full potential. This indispensable knowledge can be provided by additional sensors, which directly measure the corresponding vehicle dynamics states. However, additional sensors result in increased costs, which should be avoided if possible. An already common practice is the use of state estimators, which are able to estimate the relevant states on the basis of already installed sensors. This reduces additional costs. Moreover, also states which are very difficult to measure can be estimated.

In principle, state estimators resulting from theoretical modeling are used. However these are based on simplification and assumptions due to the kind of modeling. Thus the state estimation loses accuracy. The enhancement of accuracy concerning the state estimation is thus a second challenge. In order to overcome this challenge, state estimators based on artificial intelligence are used within this thesis. Based on training data, these methods represent the corresponding transfer behavior. Since no explicit modeling based on physical laws is applied, also no conscious simplifications are implemented. Thus these estimators exhibit great potential with respect to the accuracy of the state estimation.

The increased estimation accuracy is however expensively acquired on the basis of decreasing reliability. In particular in combination with a control system the state estimations must be reliable and valid. To ensure the reliability equals a further challenge. A not reliable respectively an invalid state estimation violates directly one objective of this thesis, which is formulated by the increase of vehicle safety. Therefore, a novel method is developed and validated, which allows a reliable and valid state estimation based on artificial intelligence. Obviously, it must also be possible to secure this hybrid method of state estimation for particular extreme conditions such as sensor malfunctions or signal failures.

A last challenge which has to be overcome for the implementation of the central predictive vehicle dynamics control is the reduction of the computational effort. By default, model-based predictive control approaches are used for predictive control systems. Within this type of control, mathematical models of the system to be controlled are used to predict its behavior. This prediction is then optimized and adapted in a coherent step with respect to the desired behavior. An increasing model complexity in the form of non-linearities leads to the consequence that the optimization problem is solved numerically. This step, however, involves an increased computational effort. Furthermore, the iterative solution of the optimization problem results without additional restrictions in a non-real-time capable system. With regard to the implementation in vehicles, this problem will also be solved by using artificial intelligence.

In conclusion, the objective is the implementation of a central predictive control system with respect to the vehicle dynamics. On the one hand, this control system is based on a hybrid method of state estimation. This method must fulfill the following criteria:

- Enhancement of estimation accuracy,
- Assurance of estimation reliability.

On the other hand, the control system is based on a hybrid method with respect to a central predictive vehicle dynamics control. For this purpose the following criteria have to be fulfilled:

- Reduction of computational effort,
- Preservation of control quality.

The corresponding criteria are evaluated in contrast to conventional methods excluding the use of artificial intelligence and relying purely on the evaluation of physical principles.

1.3 Outline

This thesis is divided into seven Chapters. The outline of the thesis is illustrated in Figure 1.1.

The first Chapter represents the introduction to the thesis, which in addition to the fundamental motivation focuses primarily on the research issue to be discussed. For this purpose, the classification in the scientific context is presented. Afterwards the problem statement of the thesis is formulated. Furthermore, an overview of the structure of the thesis is given.

The second Chapter presents the current state of the art concerning the research objectives. At first, the general principles of vehicle dynamics are introduced. Subsequently, well established and more recent approaches in estimating and controlling the vehicle dynamics are discussed. Moreover, the present research gaps are identified, which are addressed and overcome within this thesis.

Within the third Chapter the development framework used in this thesis is introduced. For this purpose the software tools utilized in the simulation environment are presented. Furthermore, the targets of the vehicle dynamics control and the associated state estimation are defined. The equipment of the vehicle in terms of sensors and actuators is elaborated. Moreover, the driving scenarios used to create the database for the implementation of the data-driven models are introduced.

In the fourth Chapter, the hybrid method of state estimation is presented and developed. Both the physical models and the models based on artificial intelligence in the form of artificial neural networks are developed. Afterwards the novel hybrid method of combining the different types of models is presented and evaluated in a first open-loop validation.

In the fifth Chapter the focus is on the central predictive control of the vehicle dynamics. For this purpose, both a non-linear model-based predictive control and a control based on a neuro-fuzzy system are derived. These elaborated control systems are likewise evaluated in a first brief open-loop validation.

The sixth Chapter presents the closed-loop validations of the developed hybrid methods of state estimation and vehicle dynamics control. Especially the mutual influence in a closed-loop mode of operation is considered.

The thesis is closed in the seventh Chapter by a conclusion. For this purpose, it is summarized first. Subsequently, the scientific contributions of the thesis are pointed out. The achieved results are then critically reviewed within a discussion part. Finally an outlook on further research activities is provided.

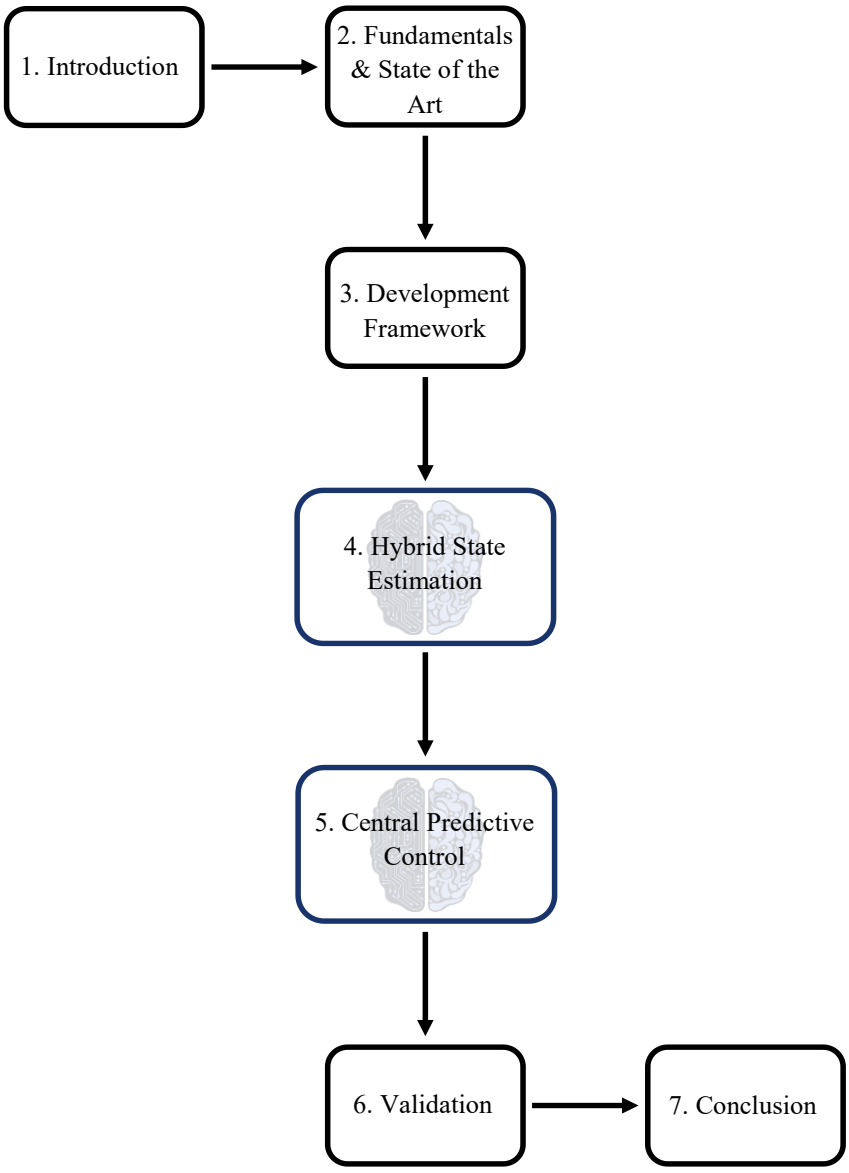

Figure 1.1 Outline of the Thesis

2 Fundamentals and State of the Art

In this Chapter the theoretical foundation of the thesis is presented. First of all, the general definitions concerning vehicles and vehicle dynamics are introduced. Subsequently, the focus is on the state of the art and the fundamentals regarding state estimation in the field of vehicle dynamics. The main distinction is made by the type of modeling. Finally, the domain of vehicle dynamics control is reviewed. In addition to general control concepts, the fundamentals as well as the state of the art of two specific types of control algorithms are outlined.

2.1 Vehicle Dynamics

The motion of a vehicle in the presence of internal and external forces as well as torques is defined as vehicle dynamics, (Schramm et al., 2018). The vehicle can be divided into three assemblies:

- Drivetrain,
- Tires and wheel suspensions,
- Vehicle body.

The tires are used for the targeted transfer of the forces induced by the drivetrain towards the road. The wheel suspensions are used to adjust the wheel position in order to ensure an optimal transmission behavior. Consequently, the wheel suspensions have an immense impact on the movement of the vehicle body and thus on the safety and ride comfort.

The movement of the vehicle can be subdivided into longitudinal dynamics, lateral dynamics and vertical dynamics in normal driving operation. The closer the vehicle approaches the vehicle dynamics limits, the greater is the coupling between the individual vehicle dynamics domains. The position of the vehicle in space and thus also its movement is described by the body-fixed coordinate system $C_\mathrm{V} = \{O_\mathrm{V};\ x_\mathrm{V}, y_\mathrm{V}, z_\mathrm{V}\}$ in relation to the inertial coordinate system $C_\mathrm{I} = \{O_\mathrm{I};\ x_\mathrm{I}, y_\mathrm{I}, z_\mathrm{I}\}$, (Schramm et al., 2020). The relation is illustrated in Figure 2.1.

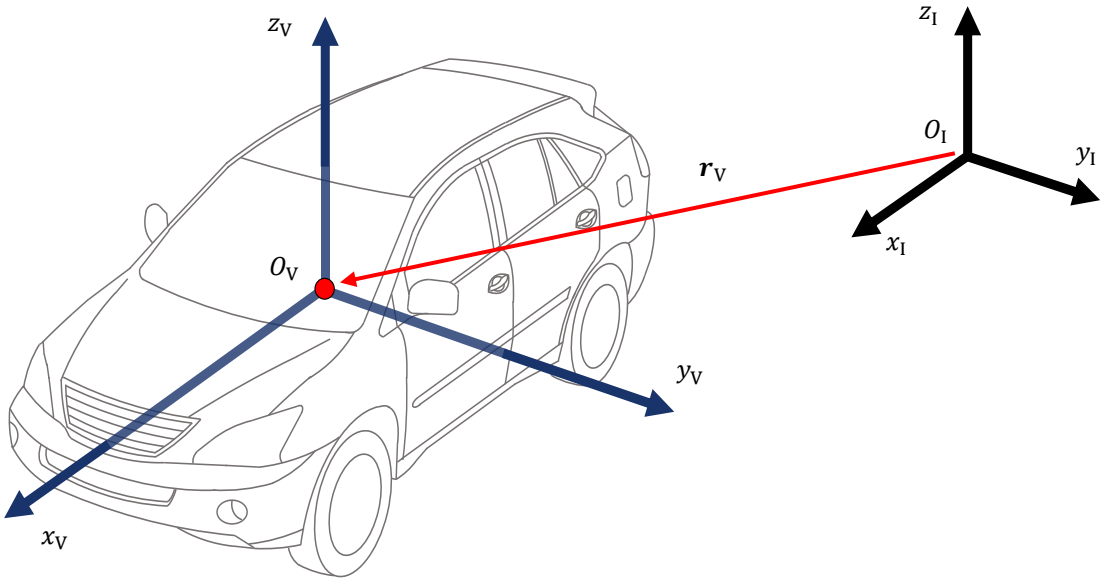

Figure 2.1 Coordinate Systems

The origin of the body fixed coordinate system O_V is located at the center of gravity of the vehicle body, (ISO, 2011b). It is constructed in such a way that the x_V-axis points to the front in the longitudinal direction of the vehicle, the y_V-axis to the left in the lateral direction and the z_V-axis upwards in the vertical direction.

In order to describe the spatial position and orientation of the vehicle in more detail, first the degrees of freedom of the vehicle body are introduced. The vehicle body is considered as a rigid body. The spatial position and orientation of the vehicle body can therefore be unambiguously described using its six degrees of freedom. The degrees of freedom can be divided into translational and rotational degrees of freedom, (ISO, 2011b). The translational degrees of freedom are defined by

- the longitudinal movement along the x_V-axis denoted as jerk,
- the lateral movement along the y_V-axis denoted as push and
- the vertical movement along the z_V-axis denoted as heave.

The rotational degrees of freedom are specified by

- the rotation around the x_V-axis with the angle φ denoted as roll,
- the rotation around the y_V-axis with the angle θ denoted as pitch and
- the rotation around the z_V-axis with the angle ψ denoted as yaw.

Figure 2.2 provides an overview of the translational and rotational degrees of freedom of the vehicle body. By using these degrees of freedom the spatial position and the orientation of the vehicle can be described unambiguously.

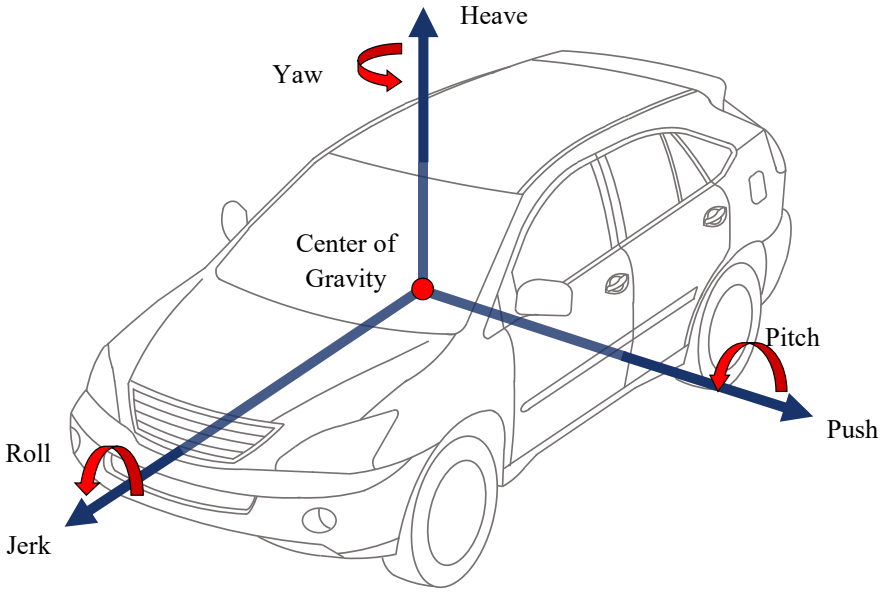

Figure 2.2 Degrees of Freedom

The spatial position of the vehicle can be described by the position vector $\boldsymbol{r}_{\mathrm{V}} = \left({}^{\mathrm{I}}x_{\mathrm{V}} \quad {}^{\mathrm{I}}y_{\mathrm{V}} \quad {}^{\mathrm{I}}z_{\mathrm{V}} \right)$ in coordinates of the inertial coordinate system C_{I}. The position vector $\boldsymbol{r}_{\mathrm{V}}$ points from the origin of the inertial coordinate system O_{I} to the origin of the body-fixed coordinate system O_{V} and thus to the center of gravity of the vehicle body as shown in Figure 2.1, (Heißing and Ersoy, 2011, Schramm et al., 2018).

The orientation of the vehicle in relation to the inertial coordinate system can be described for example by the CARDAN angles, (Schramm et al., 2020). Using three defined rotations, the orientation of the vehicle can be derived from the inertial orientation determined by C_{I}:

1. Rotation of the inertial coordinate system C_{I} around its z_{I}-axis with the yaw angle ψ resulting in a coordinate system C_{H1}.
2. Rotation of the coordinate system C_{H1} around its y_{H1}-axis with the pitch angle θ resulting in a coordinate system C_{H2}.
3. Rotation of the coordinate system C_{H2} around its x_{H2}-axis with the roll angle φ resulting in the vehicle body-fixed coordinate system C_{V}.

2.2 Vehicle Dynamics State Estimation

The following Section deals in detail with the estimation of vehicle dynamic states. For this purpose the fundamentals of established methods within the state estimation are introduced. Furthermore, the state of the art of these methods for the application within vehicle dynamics is presented.

In general a state estimation is required, whenever states are not measureable directly or the measurement itself is complex and thus expensive, (Sieberg et al., 2019a).

Two general approaches can be distinguished in the derivation of state estimators. The approach of theoretical modeling is based on explicit model knowledge. In contrast to this, the approach of experimental modeling operates without explicit model knowledge and only reproduces available information regarding the transfer behavior, (Schramm et al., 2018).

Theoretical modeling usually results in so-called white-box models. These models are based for example on physical laws and therefore result in completely comprehensible models. In contrast there are black-box models, which are not completely comprehensible, (Sjöberg et al., 1995). Black-box models usually result from experimental modeling, since only an input-output relationship is represented by mathematical relationships, without using explicit model knowledge inside. In order to combine the advantages of the respective modeling approaches and thus use synergies between them, hybrid methods of state estimation exist in addition, (Sieberg et al., 2019a, Sieberg et al., 2021a).

In the following, approaches of state estimation based on theoretical modeling are presented. Afterwards an introduction to approaches based on experimental modeling is given. Hybrid methods are then introduced which combine models resulting from both modeling approaches. Finally, the research gap addressed within this thesis with respect to state estimation is highlighted.

2.2.1 Theoretical Modeling Approaches

The theoretical modeling depends on explicit model knowledge to be able to reproduce a desired behavior. In the present case of the estimation of vehicle dynamic states, this explicit model knowledge results from physical laws, (Isermann and Münchhof, 2011). Therefore, white-box models arise, whose comprehensibility and traceability is completely ensured, (Sjöberg et al., 1995).

In principle, different methods of state estimation can be distinguished as a result of theoretical modeling. These are composed of the method of observers, the method of Kalman filters and the method of particle filters. By these methods internal states can be determined by establishing a mathematical model of the system. The fundamental idea of these methods is based on the principle that internal states of a system can be determined on the basis of known input and output quantities. First a brief overview of the method of observers is given, followed by a more detailed focus on the method of Kalman filters. The method for particle filters is not presented in detail due to the increased computational effort to be expected for this method, (György et al., 2014).

Observer

The method of observers is suitable to estimate the states of a deterministic system, (Luenberger, 1971). The states of such a system can be reconstructed entirely if the system is

completely observable. A complete observability of a system is given, whenever the initial state can be determined from the sequences of the input variables and the output variables over a finite interval, (Kalman, 1959b). In order to determine the observability of a system established methods are available, (Kalman, 1959a, Gilbert, 1963, Kalman, 1963).

For state estimation within linear systems the method of the Luenberger observer is well established, (Luenberger, 1964). Using an adequate proportional feedback of the deviation between the measured and estimated output variables, the deviation between the actual and the estimated states approaches asymptotically zero, (Luenberger, 1971). For the application to non-linear systems the Luenberger observer is not particularly appropriate, thus additional modifications are necessary. The extension of the feedback of a Luenberger observer by an integral path results in a proportional-integral observer, which is able to reconstruct the states of a dynamic system with non-linearities, (Söffker et al., 1995). A further possibility of implementing observers is the class of sliding-mode observers, whereby the state estimation results in output variables, which become identical to the measured output variables within a finite time. An overview regarding sliding-mode observers is given in (Spurgeon, 2008). An overview of additional possibilities to observe the states of non-linear systems is presented in (Misawa and Hedrick, 1989).

Kalman Filter

A further possibility of state estimation based on theoretical modeling is represented by the Kalman filter, which will be discussed in detail in the following. For this purpose the fundamental principles as well as the state of the art in the field of vehicle dynamics state estimation are presented.

Fundamentals

The method of the Kalman filter applies to the state estimation of stochastic systems. In the following the functionality of the Kalman filter is presented for a discrete linear stochastic system, according to (Kalman, 1960). The system is defined by the discrete state space representation

$$\boldsymbol{x}(k+1) = \boldsymbol{A}\boldsymbol{x}(k) + \boldsymbol{B}\boldsymbol{u}(k) + \boldsymbol{w}(k+1), \tag{2.1}$$

$$\boldsymbol{y}(k) = \boldsymbol{H}\boldsymbol{x}(k) + \boldsymbol{v}(k). \tag{2.2}$$

Here $\boldsymbol{x}$ represents the state vector, $\boldsymbol{u}$ the input vector and $\boldsymbol{y}$ the output vector, which contains the measurements. Furthermore $\boldsymbol{A}$ is the transition matrix, $\boldsymbol{B}$ is the input matrix and $\boldsymbol{H}$ is the output matrix, relating the states $\boldsymbol{x}$ with the measured quantities $\boldsymbol{y}$. k represents the current time step. The vectors $\boldsymbol{w}$ and $\boldsymbol{v}$ represent the process noise respectively the measurement noise. Both, the process noise $\boldsymbol{w}$ and the measurement noise $\boldsymbol{v}$, are assumed to be white noise.

Furthermore, they are independent of each other and exhibit a normal probability distribution, (Welch and Bishop, 1995):

$$p(\boldsymbol{w}) \sim \mathcal{N}(\boldsymbol{0}, \boldsymbol{Q}), \tag{2.3}$$

$$p(\boldsymbol{v}) \sim \mathcal{N}(\boldsymbol{0}, \boldsymbol{R}). \tag{2.4}$$

$\boldsymbol{Q}$ represents the covariance of the process noise and $\boldsymbol{R}$ the covariance of the measurement noise. Fundamentally, the Kalman filter establishes a recursive solution regarding the state estimation, which is based on two parts, the time update and the measurement update.

Within the time update the system behavior is predicted

$$\hat{\boldsymbol{x}}^{-}(k+1) = \boldsymbol{A}\hat{\boldsymbol{x}}(k) + \boldsymbol{B}\boldsymbol{u}(k), \tag{2.5}$$

$$\boldsymbol{P}^{-}(k+1) = \boldsymbol{A}\boldsymbol{P}(k)\boldsymbol{A}^{\mathrm{T}} + \boldsymbol{Q}(k). \tag{2.6}$$

This results in an a priori state $\hat{\boldsymbol{x}}^{-}(k+1)$ and an associated a priori covariance $\boldsymbol{P}^{-}(k+1)$ which characterizes the error of the a priori state estimation $\boldsymbol{e}^{-}(k+1)$:

$$\boldsymbol{e}^{-}(k+1) = \boldsymbol{x}(k+1) - \hat{\boldsymbol{x}}^{-}(k+1). \tag{2.7}$$

In the step of the measurement update the estimated a priori state $\hat{\boldsymbol{x}}^{-}(k)$ is corrected to an improved a posteriori state $\hat{\boldsymbol{x}}(k)$ by using the measured quantities $\boldsymbol{y}(k)$. For this purpose, first a Kalman gain $\boldsymbol{K}(k)$ is determined, which minimizes the a posteriori covariance $\boldsymbol{P}(k)$, (Brown and Hwang, 1997):

$$\boldsymbol{K}(k) = \boldsymbol{P}^{-}(k)\boldsymbol{H}^{\mathrm{T}}\left(\boldsymbol{H}\boldsymbol{P}^{-}(k)\boldsymbol{H}^{\mathrm{T}} + \boldsymbol{R}(k)\right)^{-1}. \tag{2.8}$$

This covariance $\boldsymbol{P}(k)$ characterizes the error of the a posteriori state estimation $\boldsymbol{e}(k)$

$$\boldsymbol{e}(k) = \boldsymbol{x}(k) - \hat{\boldsymbol{x}}(k). \tag{2.9}$$

Based on the Kalman gain $\boldsymbol{K}(k)$ the a posteriori state $\hat{\boldsymbol{x}}(k)$ is calculated, using the a priori estimations $\hat{\boldsymbol{x}}^{-}(k)$ and the measured quantities $\boldsymbol{y}(k)$

$$\hat{\boldsymbol{x}}(k) = \hat{\boldsymbol{x}}^{-}(k) + \boldsymbol{K}(k)\left(\boldsymbol{y}(k) - \boldsymbol{H}\hat{\boldsymbol{x}}^{-}(k)\right). \tag{2.10}$$

In the final step of the measurement update the a posteriori covariance $\boldsymbol{P}(k)$ is determined with

$$\boldsymbol{P}(k) = (\boldsymbol{I} - \boldsymbol{K}(k)\boldsymbol{H})\boldsymbol{P}^{-}(k). \tag{2.11}$$

The Kalman filter is thus based on a predictor-corrector algorithm. Figure 2.3 illustrates this mode of operation of the Kalman filter for a linear system.

The described implementation of the Kalman filter is suitable for linear systems. For the consideration of non-linear systems an extended Kalman filter can be applied. With the extended Kalman filter the non-linear system equations are linearized around the respective working point, (Jazwinski, 1970, Sorenson, 1985). The linearization follows the principle of the Taylor

series with the order one, (Welch and Bishop, 1995). The further procedure for the extended Kalman filter is similar to the Kalman filter. The predictor-corrector scheme is retained.

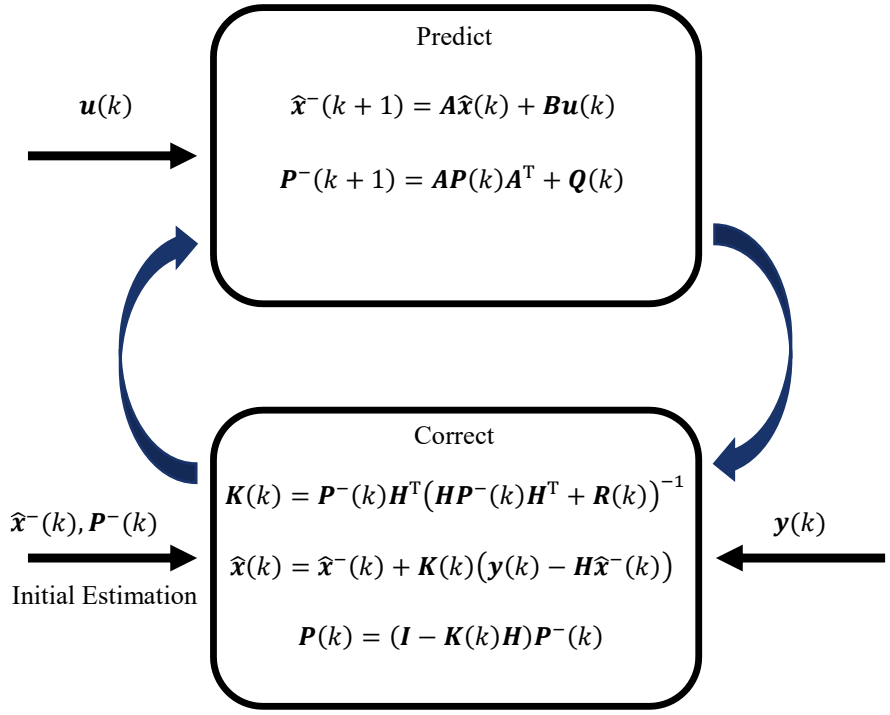

Figure 2.3 Structure of the Kalman Filter for Linear Systems

A further possibility to consider non-linearities within the state estimation is represented by the unscented Kalman filter, (Julier and Uhlmann, 1997). Instead of a linearization, the non-linearities are considered by an unscented transformation. In comparison to linearization, the unscented transformation is a direct and explicit method to transfer the information regarding mean and covariances, (Julier and Uhlmann, 2004). This enables an accurate estimation also for high order non-linearities, where the extended Kalman filter results in greater inaccuracies due to linearization errors, (Wan and Merwe, 2000). In principle, the unscented Kalman filter is likewise based on the predictor-corrector scheme of the Kalman filter.

State of the Art

In the following a review on the state of the art of state estimation in the field of vehicle dynamics using Kalman filters is given.

In (Chen et al., 2010), Kalman filters are used to estimate the roll angle and roll rate for a subsequent control. The impact of the underlying physical models on the estimation accuracy is investigated. A model with one degree of freedom is compared to a model with three degrees of freedom. The estimation of the roll angle only based on the lateral acceleration yields better results.

(Nam et al., 2013) use a Kalman filter to determine the roll angle of an electric vehicle with in-wheel motors. By integrating a pseudo-measurement quantity, the lateral vehicle velocity, the

Kalman filter achieves a sufficient estimation accuracy. The validation is done experimentally by test drives.

In (Guzman et al., 2018b), Kalman filters are used to estimate the roll angle of a vehicle using low-cost sensor equipment. Both a Kalman filter and an unscented Kalman filter are applied. The unscented Kalman filter provides more accurate results than the Kalman filter. In contrast, the Kalman filter exhibits a lower computational effort.

Based on a magnetometer and non-holonomic constraints, (Won et al., 2015) estimate not only the roll angle but also the pitch angle using an extended Kalman Filter. The estimated states are used to improve the inertial navigation performance. The validation is performed experimentally.

In (Ahmed and Tahir, 2017), a Kalman filter is expanded by a second measurement update and thus a second correction step. This allows the estimation of roll and pitch angles with high accuracy based on low-cost sensors. The proposed structure of the Kalman filter is validated by both simulations and experiments.

An adaptive unscented Kalman filter is presented in (Wang et al., 2017) to estimate the roll and pitch rate. The covariances of transition and measurement noise are dependent on the road conditions. Eight classes of road conditions are considered. By adapting the respective road condition class, the adaptive unscented Kalman filter achieves a higher estimation quality in the simulation than an unscented Kalman filter without any adaption.

In (Chen and Hsieh, 2008), the side-slip angle is estimated by using an extended Kalman filter. The extended Kalman filter is based on a kinematic model and noisy measurements of longitudinal acceleration, lateral acceleration and yaw rate. Within simulations, the quality of the estimation increases in comparison to a linear observer and to a pure use of the kinematic model. The validation is done at high and at low road friction conditions.

An unscented Kalman filter is used in (Doumiati et al., 2009b) to estimate the side-slip angle besides the lateral tire forces. In addition to a model for the description of the vehicle dynamics, a tire model is integrated. Thereby, the presented unscented Kalman filter achieves a high accuracy in experimental test drives.

(Gadola et al., 2014) use an extended Kalman filter to estimate the side-slip angle based on the input variables of the longitudinal velocity, the steering angle, the lateral acceleration and the yaw rate. Both within simulations and based on noisy measurements occurring in experimental test drives an estimation with adequate accuracy is achieved.

In (Doumiati et al., 2009a), an extended Kalman filter and an unscented Kalman filter for side-slip angle estimation are validated and benchmarked. Especially in regions of high order non-linearities the unscented Kalman filter is superior to the extended Kalman filter.

Similar results are presented by (Antonov et al., 2011) for vehicle dynamics state estimation. Again, a comparison between an extended Kalman filter and an unscented Kalman filter is conducted. In this case the unscented Kalman filter outperforms the extended Kalman filter, especially at larger sampling times. This is caused by the linearization error within the extended Kalman filter.

Comparable results are presented in (Wielitzka et al., 2014) for the estimation of the lateral dynamics.

2.2.2 Experimental Modeling Approaches

Experimental modeling, in contrast to theoretical modeling, is not based on explicit model knowledge in the form of physical laws. Rather, a desired transfer behavior is mapped on the basis of a defined, in most cases mathematically formulated, model structure. With existing data in relation to input and output quantities, the parameters of the model are adjusted so that the transfer behavior is reproduced, (Schramm et al., 2018).

A possible application of experimental modeling is the domain of machine learning. Machine learning represents a subsection of artificial intelligence, (Goodfellow et al., 2016). Within machine learning methods, mathematical models are created that can map and predict system behavior based on training data, (Mitchell, 1999).

In the field of machine learning there are numerous different approaches. These include support vector machines, probabilistic models such as Bayesian networks as well as decision trees and artificial neural networks, (Cortes and Vapnik, 1995, Jensen and Nielsen, 2007, Rokach and Maimon, 2008, Schmidhuber, 2015).

Regarding vehicle dynamics state estimation artificial neural networks are focused. These represent a proven method in this context, (Guo et al., 2018). In the following, the fundamentals of artificial neural networks are presented. Subsequently, an overview of the state of the art in vehicle dynamics state estimation by artificial neural networks is outlined.

Fundamentals

The concept of artificial neural networks is based on the model of the human brain, which is fundamentally based on interconnected neurons, (McCulloch and Pitts, 1943). A simple artificial neuron consists of input connections, which mimic the dendrites, a cell core and an output connection, similar to an axon. The input variables $\boldsymbol{z}$ are weighted and then accumulated in the cell core. This is realized by the weightings $\boldsymbol{w}_{\mathrm{z}}$.

$$\boldsymbol{z} = (z_1, \dots, z_n, z_{\mathrm{b}})^{\boldsymbol{T}} \tag{2.12}$$

$$\boldsymbol{w}_{\mathrm{z}} = (w_1, \dots, w_n, w_{\mathrm{b}})^{\mathrm{T}} \tag{2.13}$$

A special element within the input variables is the bias z_b, which corresponds to a constant value and thus represents a possibility to interact independently of the further input variables. The resulting weighted sum is then evaluated according to the biological model using a threshold value. In the artificial neuron, this is achieved by an activation function f_a, (Patterson, 1998). The schematic structure of a simple artificial neuron is shown in Figure 2.4.

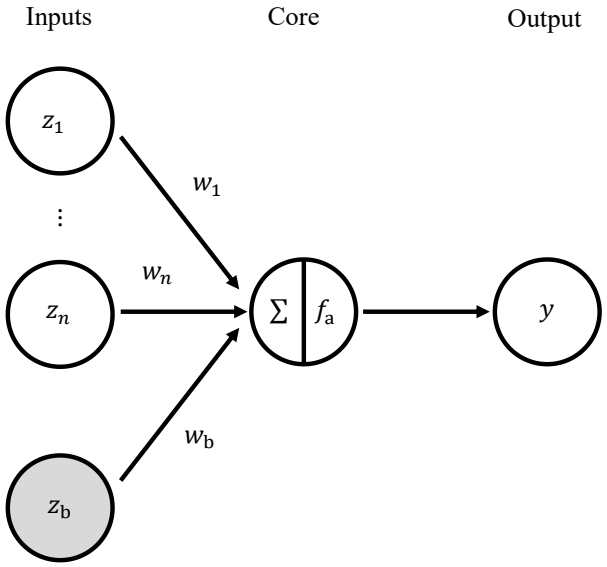

Figure 2.4 Structure of a Simple Neuron

The output quantity y of the simple artificial neuron represents the weighted sum of the input quantities evaluated by the activation function f_a

$$y = f_\mathrm{a}\left(w_\mathrm{b} z_\mathrm{b} + \sum_{i=1}^{n} w_n\, z_n\right). \tag{2.14}$$

The activation function can be implemented by linear or non-linear functions, whereby non-linear activation functions are required for the representation of non-linear processes. By default, these are usually differentiable and increasing monotonously, (Patterson, 1998). Activation functions used for regression problems are an identity function f_i, a logistic function f_log respectively an activation function f_tanh based on a hyperbolic tangent:

$$f_\mathrm{i}(u_\mathrm{n}) = u_\mathrm{n}, \tag{2.15}$$

$$f_\mathrm{log}(u_n) = \frac{1}{1 + e^{-u_n}}, \tag{2.16}$$

$$f_\mathrm{tanh}(u_n) = \frac{e^{u_n} - e^{-u_n}}{e^{u_n} + e^{-u_n}}. \tag{2.17}$$

In this context u_n represents the result of the weighted sum of the input variables $\boldsymbol{z}$.

Within artificial neural networks, neurons are arranged in layers. In the majority of cases an artificial neural network consists of an input layer, an output layer and at least one layer in

between. The number of these so-called hidden layers is not limited. Whereas the number of neurons in the input respectively output layer corresponds to the number of input respectively output quantities, the number of neurons within the hidden layers is freely selectable.

In principle, artificial neural networks can be distinguished by their topology. If a data flow within the layers of an artificial neural network only proceeds in the direction of the output variables, this artificial neural network is denoted as a feedforward artificial neural network. In this case, neurons of one layer are only connected to neurons of the following layer, (Bishop, 2006). If there is an interconnection between neurons within one layer or to neurons from previous layers, the artificial neural network is referred to as a recurrent artificial neural network, (Rumelhart et al., 1986). Recurrent artificial neural networks are able to map sequential relationships in the data due to this coupling. Thus, an output quantity can be determined from a temporal sequence, as it occurs for example in the estimation of states within vehicle dynamics.

In order to reproduce long-term dependencies, the long short-term memory architecture developed by (Hochreiter and Schmidhuber, 1997) is particularly suitable, which is classified into the topology of recurrent artificial neural networks. Following the extension of (Gers et al., 2000), a long short-term memory cell can be characterized by three gates. Due to this structure, the long short-term memory cell is able to store, add and forget information. The schematic structure of a long short-term memory cell is shown in Figure 2.5.

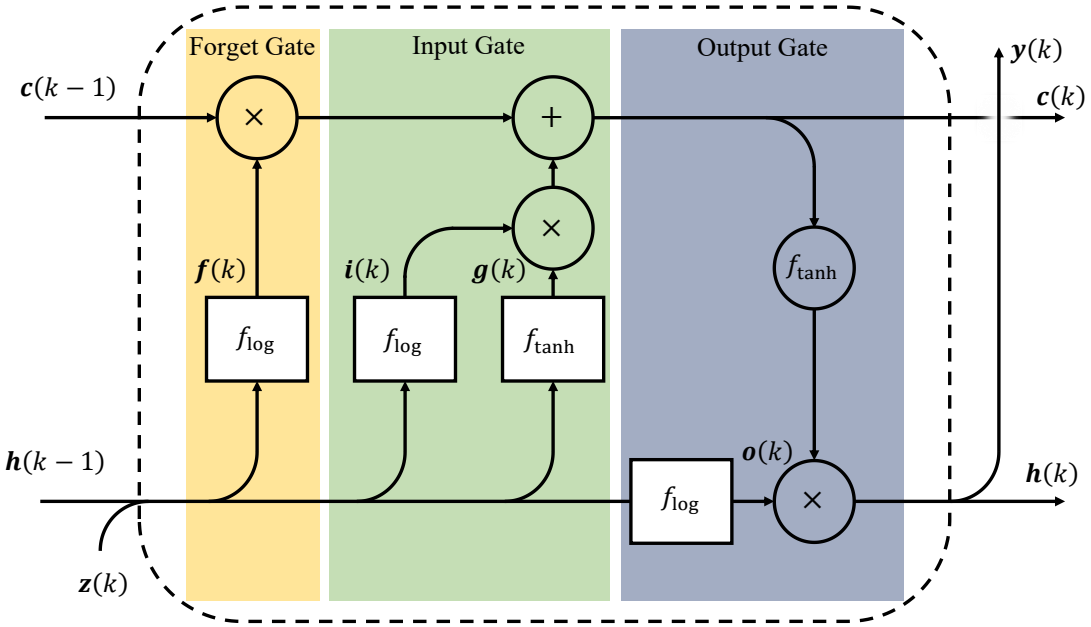

Figure 2.5 Structure of a Long Short-Term Memory Cell

Both a short-term state $\boldsymbol{h}(k-1)$ and a long-term state $\boldsymbol{c}(k-1)$ are introduced, which are used in addition to the further input quantities $\boldsymbol{z}(k)$ to predict the output $\boldsymbol{y}(k)$.

A forget gate is used to determine which parts of the long-term state $\boldsymbol{c}(k-1)$ are forgotten or retained. For this purpose the short-term states $\boldsymbol{h}(k-1)$ as well as the input variables $\boldsymbol{z}(k)$ are fed into a fully connected layer with a logistic activation function $f_{\log}$.

Thereafter, the long-term state $\boldsymbol{c}(k-1)$ is processed with the resulting intermediate state $\boldsymbol{f}(k)$ via the Hadamard product to perform the forgetting operation.

$$\boldsymbol{f}(k) = f_{\log}\left(\boldsymbol{W}_{\mathrm{zf}}^{\mathrm{T}}\boldsymbol{z}(k) + \boldsymbol{W}_{\mathrm{hf}}^{\mathrm{T}}\boldsymbol{h}(k-1) + \boldsymbol{b}_{\mathrm{f}}\right) \tag{2.18}$$

$\boldsymbol{W}_{\mathrm{hf}}$ and $\boldsymbol{W}_{\mathrm{zf}}$ represent the weighting factor matrices of the fully connected layer for the short-term state $\boldsymbol{h}(k-1)$ respectively the input variable $\boldsymbol{z}(k)$ within the forget gate. Additionally, $\boldsymbol{b}_{\mathrm{f}}$ denotes the bias of the fully connected layer.

Within the input gate it is determined, which parts of the short-term state $\boldsymbol{h}(k-1)$ and the input variable $\boldsymbol{z}(k)$ are incorporated into the long term state $\boldsymbol{c}(k)$.

$$\boldsymbol{i}(k) = f_{\log}\left(\boldsymbol{W}_{\mathrm{zi}}^{\mathrm{T}}\boldsymbol{z}(k) + \boldsymbol{W}_{\mathrm{hi}}^{\mathrm{T}}\boldsymbol{h}(k-1) + \boldsymbol{b}_{\mathrm{i}}\right) \tag{2.19}$$

$$\boldsymbol{g}(\boldsymbol{k}) = f_{\tanh}\left(\boldsymbol{W}_{\mathrm{zg}}^{\mathrm{T}}\boldsymbol{z}(\boldsymbol{k}) + \boldsymbol{W}_{\mathrm{hg}}^{\mathrm{T}}\boldsymbol{h}(\boldsymbol{k}-\boldsymbol{1}) + \boldsymbol{b}_{\mathrm{g}}\right) \tag{2.20}$$

To determine the long terms state $\boldsymbol{c}(k)$ both a fully connected layer with logistic activation function $f_{\log}$ and one based on the hyperbolic tangent $f_{\tanh}$ are processed. The resulting intermediate states $\boldsymbol{i}(k)$ and $\boldsymbol{g}(k)$ are likewise processed by the Hadamard product, which is illustrated by $\circ$. $\boldsymbol{W}_{\mathrm{hi}}$, $\boldsymbol{W}_{\mathrm{zi}}$, $\boldsymbol{W}_{\mathrm{hg}}$ and $\boldsymbol{W}_{\mathrm{zg}}$ accordingly represent the weighting matrices. Respectively $\boldsymbol{b}_{\mathrm{i}}$ and $\boldsymbol{b}_{\mathrm{g}}$ denote the bias within the input gate.

The long-term state $\boldsymbol{c}(k)$ is calculated using the forget and the input gate

$$\boldsymbol{c}(k) = \boldsymbol{f}(k) \circ \boldsymbol{c}(k-1) + \boldsymbol{i}(k) \circ \boldsymbol{g}(k). \tag{2.21}$$

In a final step, the output gate determines which part of the long-term state $\boldsymbol{c}(k)$ is transferred to the short-term state $\boldsymbol{h}(k)$. For this purpose, the short-term state $\boldsymbol{h}(k-1)$ as well as the input quantity $\boldsymbol{z}(k)$ are processed by a fully connected layer with logistic activation function $f_{\log}$:

$$\boldsymbol{o}(k) = f_{\log}\left(\boldsymbol{W}_{\mathrm{zo}}^{\mathrm{T}}\boldsymbol{z}(k) + \boldsymbol{W}_{\mathrm{ho}}^{\mathrm{T}}\boldsymbol{h}(k-1) + \boldsymbol{b}_{\mathrm{o}}\right). \tag{2.22}$$

$\boldsymbol{W}_{\mathrm{ho}}$,$\boldsymbol{W}_{\mathrm{zo}}$ and $\boldsymbol{b}_{\mathrm{o}}$ represent the weighting matrices respectively the bias within the output gate. The resulting intermediate state $\boldsymbol{o}(k)$ is likewise incorporated via the Hadamard product together with the long-term state $\boldsymbol{c}(k)$ processed by a hyperbolic tangent $f_{\tanh}$ to obtain the short-term state $\boldsymbol{h}(k)$

$$\boldsymbol{h}(k) = \boldsymbol{y}(k) = \boldsymbol{o}(k) \circ f_{\tanh}\left(\boldsymbol{c}(k)\right). \tag{2.23}$$

The short term state $\boldsymbol{h}(k)$ is identical to the output $\boldsymbol{y}(k)$ of the long short-term memory cell.

In addition to the network topology, artificial neural networks can also be distinguished with respect to their learning strategy. There are basically three different learning strategies.

In supervised learning both input and output data are available for the training. The weights of the artificial neural network are adapted and optimized in such a way that the output variables are determined in the best possible way based on the present input variables. The objective of the supervised learning is to enable the artificial neural network to determine correct output data for unknown input data after the training.

In unsupervised learning only input data are available for the training of the artificial neural network. The main objective of unsupervised learning is to cluster the input data of the artificial neural network.

The third strategy of learning is represented by reinforcement learning. Depending on the actions of the artificial neural network and the resulting reaction of the environment, the actions are evaluated and rewarded or penalized. The objective of reinforcement learning is to maximize the rewards, which is equivalent to achieving a desired behavior. (Goodfellow et al., 2016)

During the training phase, the weights of the artificial neural network are adjusted. A common algorithm for adjusting the weights is the gradient descent method. In this method, the weights are adapted via the gradient of the loss function $E(\boldsymbol{w}_\mathrm{z})$

$$\boldsymbol{w}_\mathrm{z}(k+1) = \boldsymbol{w}_\mathrm{z}(k) - \alpha_\mathrm{L} \nabla E\big(\boldsymbol{w}_\mathrm{z}(k)\big). \tag{2.24}$$

Thus, the loss function $E(\boldsymbol{w}_\mathrm{z})$ is minimized by adjusting the weights $\boldsymbol{w}_\mathrm{z}$ in the direction of its negative gradient. α_L determines the step size within the gradient descent procedure and is denoted as learning rate. Common loss functions are the mean squared error and the mean absolute error, (Bishop, 2006).

In order to adapt the weights for multilayer artificial neural networks and thus make them trainable, the principle of error propagation is applied together with the gradient descent method. Using the chain rule, the error is traced back to the hidden layers, which in turn allows to adjust the weights within these layers according to the gradient descent method, (Hecht, 1989).

To adjust and thus train recurrent neural networks, error backpropagation through time is applied. The recurrent artificial neural network is unfolded along the time axis and the principle of backpropagation is applied to this structure, (Werbos, 1990). The adjustment of the weights is done by the gradient method, (Goodfellow et al., 2016).

In case an artificial neural network is not able to achieve the desired quality of representation for the training data, it is referred to as underfitted. One possibility to counteract underfitting is to increase the capacity of the artificial neural network, which characterizes the number of layers and neurons. The capacity of an artificial neural network increases with the number of layers and the number of neurons within the layers, (Goodfellow et al., 2016). In general, the capacity

of a neural network should be chosen as small as possible with respect to the problem to be solved in order to obviate an overfitting.

Besides the underfitting the threat of overfitting arises. Overfitting implies the excessive adaptation of an artificial neural network to its training data while losing the ability to generalize on data not included in the training. To prevent overfitting, regularizations are integrated during the training. A regularization can be implemented via a penalty term into the gradient descent method as well as via a dropout, (Krogh and Hertz, 1991). Dropout involves the random deactivation of a defined number of neurons within an iteration of the training, (Srivastava et al., 2014).

Due to their structure artificial neural networks in general result in black-box models whose inner comprehensibility cannot be completely achieved, (Sjöberg et al., 1995).

State of the Art

In the following an overview of the state of the art in vehicle dynamics state estimation by artificial neural networks is outlined analogously to Section 2.2.1.

In (Sanchez et al., 2004), a recurrent artificial neural network is implemented for the state estimation. Besides the roll angle, the lateral acceleration and the tire normal forces are also taken into account as the estimation targets. In this case the artificial neural network corresponds to a recurrent higher-order artificial neural network. The recurrent artificial neural network is used as an input into a roll control to reduce the rollover risk. The implementation and validation of the state estimation is done by simulations.

(Guzman et al., 2018a) use a simple feedforward artificial neural network with one hidden layer to estimate the roll angle. The estimation is based on low cost sensor equipment. The validation is done experimentally by test drives. The artificial neural network is able to meet the real time conditions defined in the article, however, it generates a partially noisy estimation of the roll angle.

In (Blume et al., 2019), a recurrent artificial neural network is used to estimate the roll angle. This artificial neural network is based on a long short-term memory architecture. The roll angle estimation based on the artificial neural network is further integrated into a roll control system. By embedding the recurrent artificial neural network the control performance is improved compared to the use of a physical state estimator within the control loop.

(Gonzalez et al., 2020) use an artificial neural network to simultaneously determine the roll angle and the side-slip angle. The feedforward artificial neural network possesses five fully connected hidden layers containing 450 neurons in total. The training of the artificial neural network is purely based on simulated data. In contrast, the validation is based on both simulated as well as experimental data obtained during test drives. The quality of the state estimation for the simulation data is considerably superior to that of the experimental data.

In (Sasaki and Nishimaki, 2000), a fully connected feedforward artificial neural network with one hidden layer is used to estimate the side-slip angle. The artificial neural network is both trained and validated with experimental data. The estimation of the side-slip angle is done with the input quantities of the lateral acceleration and the yaw rate. The artificial neural network generates reasonable estimations only up to a velocity of 50 km/h. In this case the small amount of training data is one limiting factor.

(Melzi and Sabbioni, 2011) present an artificial neural network for estimating the side-slip angle, which is adapted by a feedback of the estimated state leading to a recurrent artificial neural network. The recurrent artificial neural network is trained with simulation data and validated with experimental data. During the validation larger deviations occur.

In (Wei et al., 2016), a generalized regression artificial neural network is used to estimate the side-slip angle. The artificial neural network is trained and validated by two different simulated driving maneuvers. The lateral acceleration and the yaw rate constitute the input quantities.

(Chindamo et al., 2018) use a fully connected feedforward artificial neural network to estimate the side-slip angle. Here, both training and validation are based on simulation data. The artificial neural network features one hidden layer with ten neurons. The input variables for the state estimation are the longitudinal and the lateral acceleration as well as the yaw rate, the steering angle and the velocity.

In (Sieberg et al., 2021b), a recurrent artificial neural network is used to estimate the side-slip angle. The implementation is done with respect to an application with a vehicle dynamics control system. The input variables of the artificial neural network are composed of the manipulated variables of the control system as well as the steering angle, the velocity and the yaw rate. Training and validation are based on simulation data.

2.2.3 Hybrid Modeling Approaches

In the following, hybrid modeling approaches regarding vehicle dynamics state estimation are introduced. For this purpose, the fundamentals of hybrid modeling approaches are presented briefly. Subsequently, the state of the art concerning vehicle dynamics state estimation is outlined.

Fundamentals

Hybrid modeling approaches are defined within this thesis as a combination of models resulting from theoretical modeling and models resulting from experimental modeling. Within the state estimation of vehicle dynamics, in general one common structure of the hybrid approach is always present. Within this structure, two models by different modeling approaches are combined in such a way that a pseudo quantity is defined by a first model. This pseudo quantity is then made available to the second model. The pseudo quantity can correspond to the quantity

to be estimated, as well as to other auxiliary variables such as the time derivative of the quantity to be estimated.

State of the Art

In the following, an overview of the state of the art in hybrid estimation approaches is given.

In (Vargas-Melendez et al., 2016), the roll angle is estimated by a hybrid method. First a pseudo roll angle is determined by a fully connected feedforward artificial neural network. The input data into the artificial neural network consist of the longitudinal and lateral acceleration as well as the roll and yaw rate. The artificial neural network is based on one hidden layer with 15 neurons. The pseudo roll angle determined by the artificial neural network is then transferred to a Kalman filter as an input quantity. The Kalman filter is based on a linear physical description of the roll dynamics. The validation of the hybrid method is performed both by simulation and experimentally. By using the Kalman filter, the noise in the pseudo roll angle resulting by the artificial neural network is reduced. Furthermore, using an artificial neural network in combination with the Kalman filter shows a considerable improvement in the estimation quality in contrast to the use of a pseudo roll angle based on the suspension deflection as an input quantity into the Kalman filter.

(Boada et al., 2018) implement a comparable structure for estimating the roll angle. First an estimation of a pseudo roll angle by an artificial neural network is performed. This artificial neural network is a fully connected feedforward artificial neural network with one hidden layer and 15 neurons after (Vargas-Melendez et al., 2016). The resulting pseudo roll angle is used as input into an H∞ observer. The further input variable into the H∞ observer is the roll rate measured by an inertial measurement unit. The H∞ observer is based on a linear physical roll model with uncertainties. The validation is done experimentally. The hybrid structure reduces the noise in the pseudo roll angle estimated by the artificial neural network. Compared to the pure consideration of the roll rate as an input quantity into the H∞ observer the quality of the estimation is increased.

In (Sieberg et al., 2019a), the roll angle is also estimated, though the procedure is slightly different from (Vargas-Melendez et al., 2016, Boada et al., 2018). In principle an artificial neural network is used again to determine a pseudo roll angle. The artificial neural network is based on gated recurrent units arranged in one hidden layer, which yields a recurrent artificial neural network. The temporal lookback equals three time steps. The input variables into the recurrent artificial neural network are the lateral acceleration, the longitudinal velocity and the yaw rate. Subsequently, the pseudo roll angle is considered as an input variable into an unscented Kalman filter in addition to a lateral acceleration term. A non-linear physical roll model is stored within the unscented Kalman filter. The special characteristic of this hybrid method is the combination of the two models within the unscented Kalman filter. Depending on the lateral acceleration present, either the recurrent artificial neural network or the physical model is trusted more

within the merge. This is realized by manipulating the covariances of the unscented Kalman filter. The result is an improvement in the estimation quality compared to the pure consideration of the artificial neural network respectively the physical model. The validation is based on simulation data.

In (Boada et al., 2016), an adaptive neuro-fuzzy inference system is used instead of an artificial neural network to determine a pseudo side-slip angle. The procedure is analogous to (Vargas-Melendez et al., 2016, Boada et al., 2018). This adaptive neuro-fuzzy inference system is based on the representation of a fuzzy inference system as an artificial neural network to make it trainable. Fundamentals concerning adaptive neuro-fuzzy inference systems and fuzzy inference systems in general are presented in Section 2.3.2. The pseudo side-slip angle is further processed by an unscented Kalman filter to reduce the noise and to minimize the variance of the estimation. The validation is done purely by simulation data.

In (Novi et al., 2018), the side-slip angle is estimated based on an inertial measurement unit by an artificial neural network in combination with an unscented Kalman filter using the same structure as (Vargas-Melendez et al., 2016). The artificial neural network determines a pseudo side-slip angle which serves as input variable into the unscented Kalman filter. The training of the artificial neural network is done by simulation data. Within the unscented Kalman filter a kinematic model with uncertainties is used. The validation is done on simulated and experimental data.

(Gräber et al., 2019) pursue the objective of the side-slip angle estimation. At first the estimation of an auxiliary quantity is done by a physical model, the single-track model. The auxiliary quantity represents the time derivative of the side-slip angle. It is then made available to a recurrent artificial neural network in order to estimate the side-slip angle. The artificial neural network consists of a feedforward layer followed by a layer based on gated recurrent units. The validation is performed experimentally for different road properties. The integration of the physical knowledge in terms of the time derivative of the side-slip angle improves the estimation quality for dry, wet and snowy surfaces, in contrast to the pure use of a recurrent artificial neural network.

2.2.4 Research Gap

The publications listed can be summarized in terms of their motivation to increase the quality of the estimation by a hybrid methodology. This objective is achieved by combining models resulting from theoretical modeling and models based on experimental modeling. The use of models based on experimental modeling, however, results in black-box models that are difficult to validate and to be safeguarded, which also affects the presented hybrid methods. Whenever the data-driven models of experimental modeling result in incorrect or failed estimations, these also apply to the hybrid methods. Regarding the applicability within a vehicle dynamics control

system, an incorrect estimation would have fatal consequences. Therefore, the need of safeguarding data-driven state estimators arises.

To intercept such cases and to pursue the objective of improving the estimation quality as well, a novel hybrid method of state estimation is introduced in this thesis. Within this hybrid method of state estimation a model based on artificial intelligence is merged and safeguarded by a reliable physical model. The task of safeguarding is realized by the determination of a confidence level. This confidence level represents the confidence in the black-box model based on artificial intelligence. The merge of both model types is conducted based on the confidence level. Next to a partly confidence, thus also a pure confidence either in the artificial intelligence based model or in the reliable physical model are possible. By this working principle the hybrid method establishes a safe and reliable foundation for the application and the associated exploitation of the potential of data-driven state estimators in a closed-loop system incorporating vehicle dynamics control.

2.3 Vehicle Dynamics Control

The control of vehicle dynamics is an important aspect to increase the safety of a vehicle and the ride comfort. In the following, fundamental control concepts with respect to the overall vehicle dynamics are presented. Subsequently, the focus is on selected control implementations. At first, an insight into model-based predictive control algorithms is given. Especially with regard to highly respectively fully automated driving, a predictive control becomes necessary in order to act in a predictive manner instead of merely reacting. One objective pursued is to further increase the comfort for the passengers. In addition the method of fuzzy control is introduced, which is based on the theory of fuzziness and attempts to reproduce human actions. The Section concludes with an outline of the research gap which is addressed by this thesis concerning the vehicle dynamics control.

2.3.1 Control Concepts

Control concepts in the context of vehicle dynamics control represent architectures in which different types of control systems are implemented within the same vehicle. The concepts distinguish with respect to the degree of the interconnection regarding the individual control systems.

A self-sufficient control concept is present whenever there are no connections between various control systems within one vehicle. In this context, each control system runs independently, (Heißing and Ersoy, 2011). The advantage of the self-sufficient control concept is the possibility of an individual and independent design of each control system. Due to the absence of interconnections between the individual control systems, however, negative mutual influences

can arise. In order to avoid this, the adaptation in the vehicle requires a high effort. Moreover, the potentials of synergies resulting from different control systems cannot be exploited.

A first level of interconnectivity within the control systems is described by a peaceful coexistence concept. The interconnection is realized in terms of sensor data and states of vehicle dynamics. Within the manipulated variables there is no interconnection. This architecture ensures that the individual control systems do not have any mutual impacts, (Heißing and Ersoy, 2011). A further advantage is the partial independence in the design of the control systems, which is analogous to the self-sufficient concept, (Fan et al., 2008). Disadvantages of the concept of peaceful coexistence are the remaining adaptation effort and the absence of the opportunity to exploit synergies.

In case the interconnection is expanded into the range of the manipulated variables, a peaceful coexistence transforms into a cooperative coexistence. Not only sensor data respectively system states are shared, but the individual control systems can support each other in addition and thus pursue common objectives. Negative mutual influences can be avoided and even synergies can be exploited to a certain extent. Since in the case of cooperative coexistence, the control systems remain separated from each other, an adaptation effort still persists, (Heißing and Ersoy, 2011).

A central control approach represents the highest level of interconnection, (Fan et al., 2008). Within this architecture, one integrated control system is designed and installed to achieve the defined objectives of vehicle dynamics control. Since one control system handles all manipulated variables, no negative mutual effects are present and existing synergies can be completely exploited, (Chen et al., 2016). The central control system can also minimize the adaptation effort within the vehicle. A disadvantage is the increased effort required in the central design of the integrated control system.

Table 2.1 summarizes the control concepts and provides an overview of the individual advantages and disadvantages.

Table 2.1 Control Concepts – Overview

Control Concept	Advantages	Disadvantages
Central Control	Minimized Adaptation Effort Avoidance of Negative Mutual Interactions Exploitation of Synergies	Complex Control Design
Cooperative Coexistence	Avoidance of Negative Mutual Interactions Restricted Exploitation of Synergies	Adaptation Effort Agreements in Control Design
Peaceful Coexistence	Avoidance of Negative Mutual Interactions Partial Independence in Control Designs	Adaptation Effort No Exploitation of Synergies
Self-Sufficient Control	Independence in Control Designs	Increased Adaptation Effort Negative Mutual Interactions No Exploitation of Synergies

2.3.2 Control Approaches

In the following, the two approaches to control a system relevant in this thesis are considered in detail. First, model-based predictive control systems are introduced. Afterwards the focus is on fuzzy control systems.

Model-Based Predictive Control

Within a model-based predictive control, a mathematical model of the system is used to predict the system behavior in order to adapt it optimally to a desired behavior over a future time horizon. First, the fundamentals of model-based predictive control are introduced. Subsequently, the current state of the art concerning this control technique in the field of vehicle dynamics control is presented.

Fundamentals

In general, the category of model-based predictive control is based on mathematical models that are used to predict the future behavior of the system to be controlled. The working principle of a model-based predictive control can be basically divided into the steps of prediction and optimization, (Rossiter, 2004).

Within the prediction, a mathematical model of the system to be controlled is used to predict the future behavior as a function of the manipulated variables, (Camacho and Bordons, 1998). The most recently manipulated variables, states and measured variables can be used for initialization of the prediction. The time period for which the system behavior is predicted is defined by the prediction horizon.

Additionally, a control horizon can be introduced. This horizon describes the time period for which the manipulated variables will be adjusted. After the control horizon the manipulated variables are kept constant for the further prediction. The control horizon is thus smaller or equal to the prediction horizon. The application of a smaller control horizon can be used to reduce the calculation effort. The mathematical model which is used to describe the system behavior can be linear or non-linear, (Grüne and Pannek, 2017).

In the second step of the model-based predictive control the predicted system behavior is adapted and optimized under consideration of a quality criterion. In many applications, this quality criterion includes besides the control deviations also expressions related to the manipulated variables. By this inclusion, the utilization of the manipulated variables can be adapted to a desired behavior. The cost function, which is minimized in this step, includes the predicted behavior of the variables over the entire prediction horizon. These predicted variables are aligned with reference variables, which represent the desired behavior. The reference variables are likewise provided as trajectories over the prediction horizon. The cost function can thus be

used to minimize both the control deviations and the utilization of manipulated variables over the prediction horizon.

An important aspect that can be considered in the model-based predictive control is the limitation especially of the manipulated variables but also of further variables of the system model, (Camacho and Bordons, 1998). Thus, exemplary physical limits of actuators can already be embedded in the control system and the optimization can be performed according to these requirements. The result of the optimization is an optimal course of the manipulated variables for the predicted time period. Depending on the definition of the cost function, the consideration of constraints and the properties of the mathematical model for the prediction, the optimization is performed analytically or numerically as an iterative optimization, (Rossiter, 2004).

The basic principle of the model-based predictive control is illustrated in Figure 2.6.

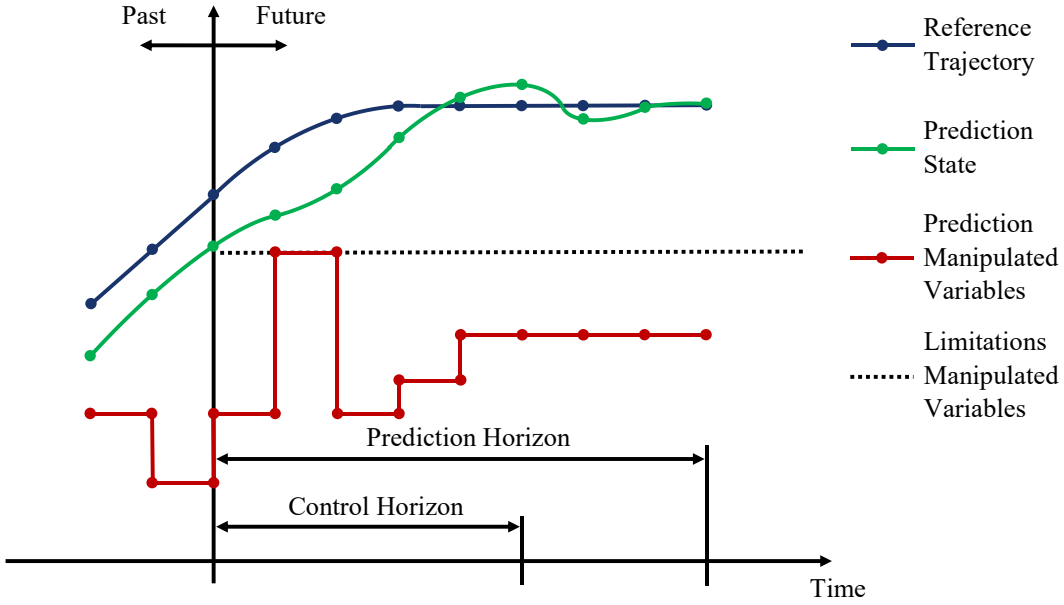

Figure 2.6 Model-Based Predictive Control – Working Principle

In general, a principle of the receding horizon is applied for the model-based predictive control comprising prediction and optimization. Only the values for the next time step of the optimal manipulated variable trajectories are passed on to the system to be controlled. Subsequently, the process consisting of prediction and optimization is performed again. Thus, also non-modeled disturbances can be considered optimally, (Michalska and Mayne, 1993).

State of the art

In the following, the state of the art in the field of vehicle dynamics control with respect to model-based predictive control algorithms is presented.

(Beal and Gerdes, 2010) compare two model-based predictive controllers for the control of the roll behavior. The two control algorithms differ with respect to their manipulated variables. On

the one hand, the steering angles at the front and rear axle form the manipulated variables. On the other hand, the drive torque at the rear axle serves as a manipulated variable in addition to the steering angle at the front axis. Both algorithms are based on linear models and also incorporate restrictions for manipulated variables and states. The implementation is done by simulations. Due to the linear models, the optimization in the model-based predictive controllers is conducted with a particular speed according to a predefined real time. Basically, the model-based predictive control based on the steering angles features a better performance.

In (Sieberg et al., 2018), a non-linear model-based predictive control is compared against a linear model-based predictive control. The control objective equals an active roll stabilization. The implementation and validation of the control algorithms is done by simulation. The non-linear model-based predictive control uses a non-linear roll model as a basis for control and incorporates a total counter roll torque as well as a total damping factor as manipulated variables. The linear model-based predictive control contains a linear roll model with the manipulated variable of the total counter roll torque. The dampers are adjusted via a skyhook control, according to (Liu et al., 2005). The solution of the optimization problem is done iteratively with the non-linear model-based predictive control and analytically with the linear model-based predictive control. This results in a lower computational effort for the linear model-based predictive control. At the same time, the non-linear model-based predictive control achieves a significantly improved control quality.

(Sieberg et al., 2019b) present a central vehicle dynamics control based on a non-linear model based predictive control algorithm. The integrated control pursues the objectives of an active roll stabilization and a pitch reduction. Within the cost function, the control quality as well as the manipulated variables are considered to take into account the energy demand of the actuators within the optimization. The manipulated variables consist of a total counter roll torque and individual damping factors at the wheel suspensions. During the optimization, restrictions of the manipulated variables are additionally considered. The non-linear model-based predictive control achieves excellent control quality within the simulation, however, it also results in an increased computational effort.

(Mehra et al., 1997) use a model-based predictive control to increase the ride comfort. The objective is to reduce vertical motions of the vehicle body. For this purpose, a linear model is stored in the model-based predictive control, which uses the forces of active suspensions as manipulated variables. Restrictions in compression and rebound travel are considered within the control. The validation is done by simulation. By using the model-based predictive control, the ride comfort is significantly improved compared to a vehicle equipped with passive suspensions.

In (Canale et al., 2006), semi-active suspensions are controlled by means of a model-based predictive control. The damping forces serve as manipulated variables. These are restricted within the optimization so that the actuator limits are preserved. A linear model is used within

the model-based predictive control. The implementation and validation is also carried out in simulations. The model-based predictive control is compared against a skyhook and a clipped control strategy, (Hrovat, 1997, Giua et al., 1999). The validation of the controllers is conducted in relation to different road excitations. In all cases the model-based predictive control provides the best control quality in terms of sprung mass accelerations.

In (Canale et al., 2011) a non-linear model-based predictive control is used for the yaw control. Thereby, the yaw behavior can be influenced by a steer-by-wire system at the front axle. The non-linear model specifically maps the transition behavior in relation to the yaw behavior. It has been parametrized with measurement data. In the simulative validation this non-linear model-based predictive control is compared with a model-based predictive control based on a non-linear physical model and an internal model control. Hereby, better closed-loop robustness is achieved using the parametrized non-linear model.

(Beal and Gerdes, 2013) use a model-based predictive control to stabilize the vehicle at the limits of vehicle dynamics. A linear single-track model in combination with a linearized tire model is used within the controller. The manipulated variable is incorporated by a steer-by-wire system at the front axle. Within the model-based predictive control, the yaw rate and the side-slip angle are restricted in such a way that the vehicle is stabilized within the limits of the vehicle dynamics. The validation is done experimentally with a test vehicle. Due to the chosen linear model structure the model-based predictive control can be applied inside the test vehicle.

In (Choi and Choi, 2014) a model-based predictive control is used for a direct yaw control. A linear single-track model combined with a linearized tire model is used within the control. The manipulated variable is represented by a total counter yaw torque. The optimization problem is solved analytically. The counter yaw torque is further converted by braking individual wheels. The implementation and the validation are done with simulation data. Roads with high friction coefficients as well as roads with low friction coefficients are investigated. By taking the tire characteristics into account, the quality of the control increases compared to a model-based predictive control with an exclusive consideration of a linear single-track model.

Fuzzy-Control

In the following, the subject of fuzzy control is introduced. At first, the fundamentals of fuzzy control are presented. This is followed by an overview of the state of the art of fuzzy control in the field of vehicle dynamics.

Fundamentals

Fuzzy control is based on fuzzy logic. The fuzzy logic is an extension of the classical set theory, (Klir and Yuan, 1994). Whereas in the classical set theory a variable x belongs to a set or is excluded from it, in fuzzy logic the possibility of a partial membership to a set is present. The implementation of this fuzziness is done by membership functions $\mu(x)$, which describe the

membership of a variable x to a fuzzy set μ. A degree of membership of $\mu(x) = 1$ corresponds to the complete membership of the variable x and a degree of membership of $\mu(x) = 0$ implies that the variable x is not included in the set. Thus the boundary cases correspond to the classical set theory. In fuzzy logic a partial membership of the variable x is feasible. A higher value corresponds to a greater degree of membership, (Zadeh, 1988).

Based on the fuzzy logic, fuzzy inference systems can be defined, which allow to determine relations between single fuzzy sets. These fuzzy inference systems are thereby suitable for the application within control systems, (Sugeno, 1985). A fuzzy inference system can be divided into three sections. Within the so-called fuzzification, crisp input signals are fuzzificated. Common types of membership functions include a triangular function, a trapezium function, a generalized bell function and a Gaussian function, (Jantzen, 2007). Inside the inference, the fuzzificated input variables are subsequently evaluated based on a rule base, which incorporates "if-then" rules. The inference can be divided into the segments of premise and consequence. Within the premise the "if" parts of the rules are evaluated. The consequence comprises the evaluation of the "then" parts of the rules. Fuzzy operations are used for the processing within the inference. This includes the union as well as the intersection. The union is typically performed by the maximum function or the algebraic sum. For the intersection the minimum function or the algebraic product are used analogously, (Jang and Sun, 1996). The result of the rule base evaluation needs to be transformed back into a crisp output variable, which can be denoted as defuzzification, (Passino and Yurkovich, 1997). The two most common types of fuzzy controllers are presented subsequently.

In the fuzzy control according to (Mamdani and Assilian, 1975), fuzzy sets are used within the consequence likewise to the use in the premise. Within the premise first the firing strengths of all rules are determined using an intersection fuzzy operation, which correspond to the degrees of fulfillment of the rules. The determination of the intersection considering the firing strengths as well as the fuzzy sets of the consequence and the following union of the results yield a fuzzy output variable. In order to obtain a crisp output value, a defuzzification needs to be performed afterwards. Common defuzzification methods are based on the center of gravity method, the center of area method and on maxima methods, (Leekwijck and Kerre, 1999). Due to this representation this type of fuzzy control is easily comprehensible. However, the necessary defuzzification also increases the computational effort, (Jang and Sun, 1996).

The fuzzy control according to (Takagi and Sugeno, 1985) differs from the controller according to (Mamdani and Assilian, 1975) in the evaluation of the consequences. Instead of fuzzy sets, functional rules are used to calculate the controller output as a function of the crisp input variables. This also results in crisp values arising from the rule evaluations. Usually zero-order or first-order functions are used, (Jang and Chuen-Tsai, 1995). For the determination of the output quantity of the fuzzy controller the individual rule evaluations in combination with the respective firing strengths resulting from the premise are evaluated. For this purpose the weighted

average or the weighted sum are used in common. The procedure directly results in a crisp output variable, thus eliminating the step of defuzzification, (Takagi and Sugeno, 1985).

Establishing a fuzzy controller containing a rule base, a premise and a consequence can be done in two different ways.

One way is to design a fuzzy controller manually. For this purpose, membership functions have to be defined, a rule base has to be created and, depending on the type of controller, additional output functions have to be defined manually. Depending on the complexity of the system to be controlled, a comprehensive expert knowledge is required. As a result, the manual creation can be very complex.

The second possibility of creating a fuzzy inference system uses methods of machine learning, so that no expert knowledge is needed. These methods are distinguished as neuro-fuzzy control systems. In the following, these are presented using the example of an adaptive neuro-fuzzy inference system.

In an adaptive neuro-fuzzy inference system a fuzzy inference system according to (Takagi and Sugeno, 1985) is represented as an artificial neural network. Thereby, the fuzzy-inference system becomes trainable, (Jang, 1993). An adaptive neuro-fuzzy inference system is represented as a feedforward artificial neural network with five hidden layers. Though, the fuzzy inference system is preserved so that it remains more comprehensible compared to a pure artificial neural network, (Wu et al., 2011). The structure of an adaptive neuro-fuzzy inference system with two input quantities is illustrated in Figure 2.7.

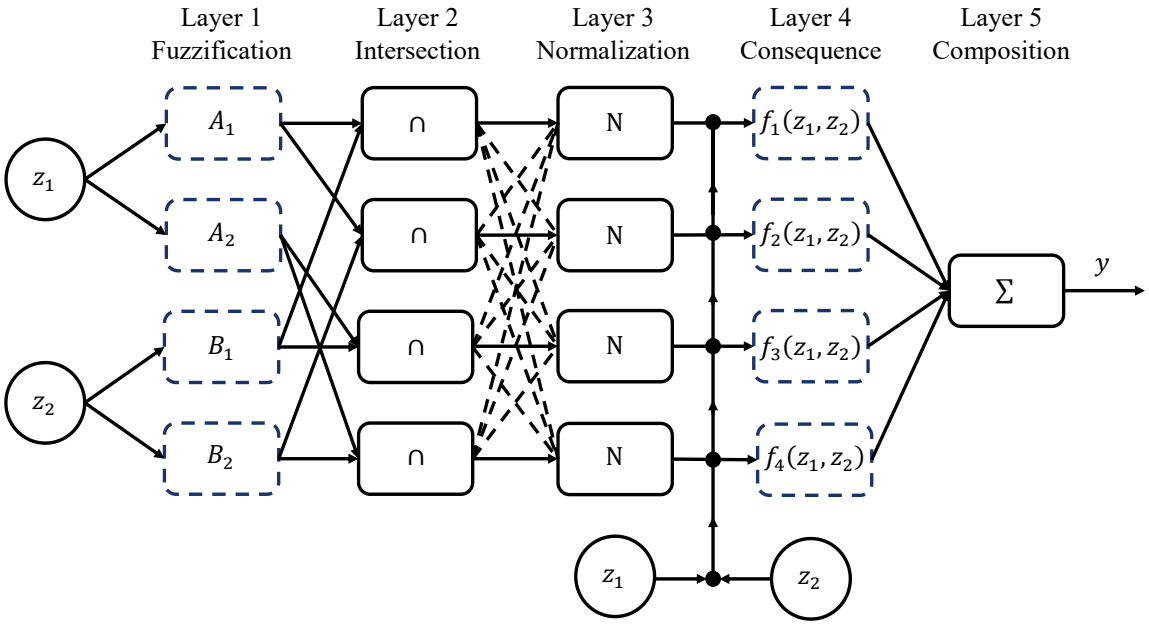

Figure 2.7 Adaptive Neuro-Fuzzy Inference System – Structure

Within the first layer the input variables are fuzzificated. For this purpose membership functions are defined for each input variable. Typically, type and number of the membership functions are consistent across all input variables, (Jang, 1993). The output quantities of the first layer therefore correspond to the membership values of the input variables towards the membership functions. In the second layer these membership values are used to determine the firing strengths of the rules. For this purpose the intersection fuzzy operation is applied. The third layer normalizes the firing strengths. In the fourth layer the input values are processed with respect to functional rules and multiplied by the normalized firing strengths. Within the fifth and last layer the rules are composed. Due to the chosen structure of the previous layers, this is done by a summation. The output of the fifth layer is equal to the output of the adaptive neuro-fuzzy inference system. Within the field of control this output is equal to the manipulated variable, (Karaboga and Kaya, 2019).

Within the training of adaptive neuro-fuzzy inference system only the parameters of the first and fourth layer are adjusted. The further layers remain invariable. For this purpose a hybrid algorithm can be applied for supervised learning, according to (Jang, 1993).

In a forward pass the parameters of the consequence, which are located in the fourth layer, are adjusted. The input data are propagated through the adaptive neuro-fuzzy inference system. In the forward pass the premise parameters in the first layer are kept constant as well. In order to adapt the fourth layer, the linear dependency between the output quantity and the consequence parameters is used. Thus, a linear system of equations is solved analytically to adjust it. For this purpose the least squares estimation method can be used, (Sorenson, 1970).

In a backward pass the parameters of the premise, which are located in the first layer, are then adjusted. The parameters determined in the forward pass are kept constant. Between the output variable and the premise parameters there is no linear relationship. Therefore, the method of error backpropagation is used for the adjustment of the premise parameters, (Rumelhart and McClelland, 1987, Hecht, 1989).

The creation of the rule base of adaptive neuro-fuzzy inference system depends on the partitioning of the input variables, which initializes the membership functions for the inputs.

One method of input partitioning is the grid partitioning. In this method the value ranges of each input variable are divided into equal areas. Corresponding to each of these areas a membership function is initialized. The number as well as the type of the membership functions are selectable. The rule base then comprises all combinations of membership functions of all inputs with each other.

A further possibility of input partitioning is clustering, (Chiu, 1994). Here the input data space is analyzed and clusters are created in areas of high data density. Then a rule is defined for each cluster. In comparison to the method of grid partitioning, this results in a significantly smaller

rule base in most cases. However, this also leads to a loss of accuracy of the adaptive neuro-fuzzy inference system.

An adaptive neuro-fuzzy inference system represents a multiple input single output system. For the use as multiple input multiple output system there are in principle two possibilities of implementation.

One possibility is the parallel arrangement of individual adaptive neuro-fuzzy inference systems, which is denoted as a multiple adaptive neuro-fuzzy inference system. For each output variable a separate adaptive neuro-fuzzy inference system is created, including its own premise, rule base and consequence, (Jang and Sun, 1996). One disadvantage is the increased training effort, since a complete training has to be performed for each output variable. Likewise, a multiple adaptive neuro-fuzzy inference system does not allow to realize interconnections between individual output variables, thus these are completely independent of each other.

The second option is represented by a co-active neuro-fuzzy inference system, according to (Mizutani and Jang, 1995). In this case the adaptive neuro-fuzzy inference system is adapted in such a way that for each output variable a separate consequence is defined including its own functional rules. These consequences are denoted as local experts. The further structure of the adaptive neuro-fuzzy inference system remains the same. Therefore, a co-active neuro-fuzzy inference system possesses only one premise and one rule base for all output variables. This structure is illustrated in Figure 2.8.

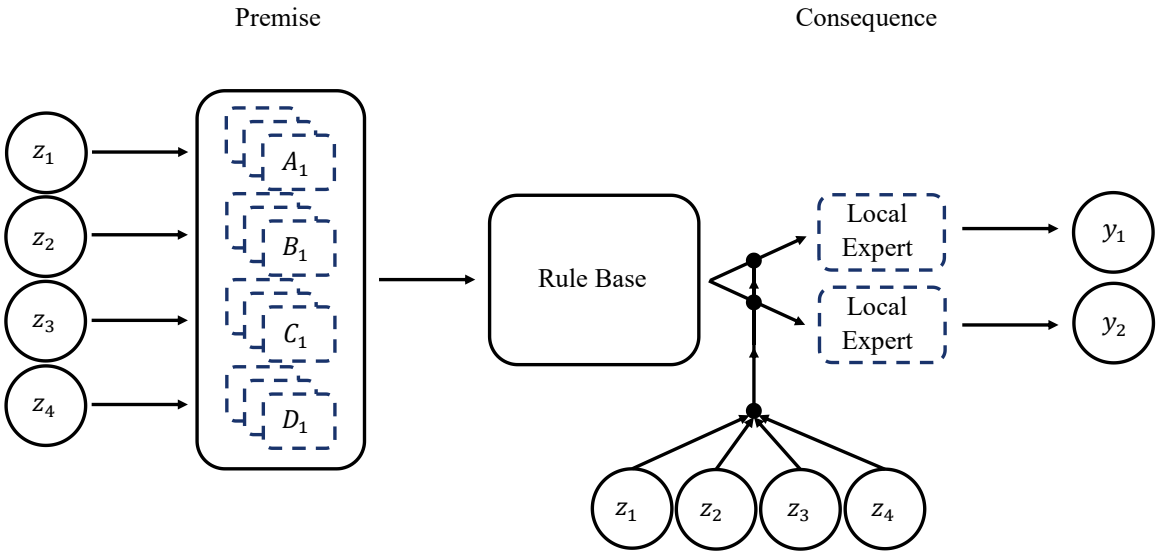

Figure 2.8 Co-Active Neuro-Fuzzy Inference System – Structure

For the training of the co-active neuro-fuzzy inference system, the hybrid learning algorithm can be adapted in such a way that the forward pass is performed separately for each local expert and during the backward pass the cumulated error over all local experts is back propagated,

(Mizutani and Jang, 1995). Due to this structure the training effort is reduced compared to a multiple adaptive neuro-fuzzy inference system. Furthermore, interconnections between output variables can be modeled, (Sieberg et al., 2020).

State of the Art

In the following, the state of the art in the field of vehicle dynamics based on fuzzy control systems is presented.

(Miao et al., 2008) use a fuzzy neural network controller to improve the vehicle stability. A fuzzy neural network controller also represents a trainable fuzzy inference system. The fuzzy control is first designed and trained by simulation. The validation is done both in simulation and experimentally. The input variables into the fuzzy neural network controller are the roll angle, the pitch angle and the vertical position of the center of gravity. The output variables are composed of the vertical forces at the wheel suspensions, which can be adjusted by magnetorheological dampers. The fuzzy neural network controller reduces roll, pitch and vertical body movements to a greater extent than a control based on the skyhook principle, according to (Ahmadian et al., 2004).

In (Singh and Darus, 2011), a fuzzy inference system according to (Mamdani and Assilian, 1975) is used to control the roll behavior of a vehicle. The implementation as well as the validation is done by simulation. The definition of the fuzzy inference system is based on expert knowledge. The input variables consist of the steering angle with seven membership functions and the longitudinal velocity with five membership functions. The output variable is the counter roll torque with seven membership functions. All membership functions are of the type of a Gaussian function. In total the fuzzy inference system comprises 35 rules. By using the fuzzy controller both roll angle and roll rate are reduced compared to a passive vehicle.

In (Tahami et al., 2004), a fuzzy controller is used for direct yaw control of a vehicle with in-wheel motors. In addition, the individual in-wheel motors are controlled in a lower level by separate fuzzy inference systems concerning the slip. The implementation and validation is done by simulation. The inputs into the fuzzy inference system for the direct yaw control include the yaw rate deviation from a reference variable and the time derivative thereof. The output variable represents a counter yaw torque. For the inputs as well as for the output seven membership functions each are defined. Each of the fuzzy inference systems in the lower level features the wheel slip as well as the angular acceleration of the wheel as input variables and an output variable which affects the torque of the in-wheel motors. By using the fuzzy inference systems the safety of the vehicle is ensured compared to a passive vehicle respectively a pure application of the direct yaw controller.

A multiple adaptive neuro-fuzzy inference system is used in (Hou et al., 2008) to control the vehicle in terms of yaw rate and side-slip angle. The input variables into the multiple adaptive neuro-fuzzy inference system are the deviation from reference variables in yaw rate and side-

slip angle respectively. Five membership functions are defined per input. The outputs represent throttle or brake. The implementation and validation is done by simulation. The multiple adaptive neuro-fuzzy inference system is then combined with a fractional proportional-integral-derivative controller which controls an active front steering system. The integrated vehicle dynamics control increases safety compared to stand-alone systems.

In (Fan et al., 2011) a fuzzy inference system according to (Mamdani and Assilian, 1975) is applied for a direct yaw control. The input variables are the deviation of the yaw rate from a reference yaw rate and the time derivative of this deviation. The output quantity is a counter yaw torque. The input variables are each covered by seven triangular membership functions. The output quantity is represented by five triangular and two trapezoidal membership functions. The rule base comprises 49 rules. The implementation and validation of the fuzzy inference system is done by simulation. Through the use of the fuzzy inference system for a direct yaw control a passive vehicle can be stabilized.

2.3.3 Research Gap

In order to optimize vehicle dynamics control for future applications, in particular highly respectively fully automated driving, two aspects have to be covered to achieve further improvements in vehicle safety and ride comfort. As drivers become passengers, comfort becomes an increasingly decisive feature of the vehicle. Furthermore, vehicle safety must also be ensured in the case of emergency evasive maneuvers at the limits of vehicle dynamics. The two aspects to be covered are characterized by a predictive mode of operation and by the utilization of the available synergy potential and the avoidance of negative influences within the control structure. A central model-based predictive control is an appropriate solution for that purpose. To achieve a full exploitation of the control performance, this type of control results in an enormous computational effort. Furthermore, the optimization within the model-based predictive control without additional restrictions leads to a non-real-time capable system. With regard to the application in vehicles, both aspects represent enormous challenges. One way to evade these challenges is to reduce the computational effort by using simplified models and by restricting the number of iterations or even by solving the optimization problem in an analytical way. However, all these adjustments reduce the control quality, (Sieberg et al., 2018).

In the context of this thesis, a novel approach is presented to reduce the computational effort while preserving the control quality. Within this approach a central non-linear model-based predictive control featuring an excellent control quality is represented by a neuro-fuzzy system. The neuro-fuzzy system drastically reduces the computational effort without deteriorating the control quality. Moreover, it is based on a direct mode of operation and is basically real-time capable. A neuro-fuzzy system represents a fuzzy inference system in the form of an artificial neural network. Thus, the fuzzy inference system is trainable and can reproduce the desired

behavior. After the training, a pure fuzzy inference system ultimately remains, resulting in a more comprehensible system compared to an artificial neural network.

3 Development Framework

This Chapter presents the framework used for the development and implementation of the vehicle dynamics state estimation and control. First, the simulation environment is outlined. The following Section introduces the control objectives. Then the selected vehicle is presented. Two main considerations in this context are actuators and sensors. Regarding the actuators, the possibilities to influence the vehicle dynamics are presented and subsequently selected based on a utility analysis. Furthermore, the simulation models of the selected actuators are derived. Considering the sensors, the measurement equipment of the vehicle is presented. Then the quantities for the vehicle dynamics state estimation are specified. In a final Section, the driving scenarios used to implement the data-driven models are presented.

3.1 Simulation Environment

To realize the vehicle dynamics state estimation and control, a simulation environment based on a co-simulation between two simulation tools is utilized. The simulation software IPG CarMaker implements vehicles and driver models as well as environmental effects, so that it can conduct virtual test scenarios. A multibody simulation is performed within IPG CarMaker to describe the vehicle dynamics in detail. The impact of the driver on the vehicle dynamics can be investigated by varying driver models. Furthermore, other traffic participants can be integrated into IPG CarMaker and the characteristics of the road as well as the entire surrounding area can be parameterized. Thus, the software can generate scenarios close to reality, which are necessary for the development of the hybrid methods regarding vehicle dynamics state estimation and control.

In addition to IPG CarMaker, the software tool MATLAB & Simulink is used to develop the hybrid methods and finally use them inside the co-simulation for state estimation and control of the vehicle dynamics. In addition to the tasks of state estimation and control, the deployed actuators are also simulated in MATLAB & Simulink. A schematic structure of the simulation environment is shown in Figure 3.1.

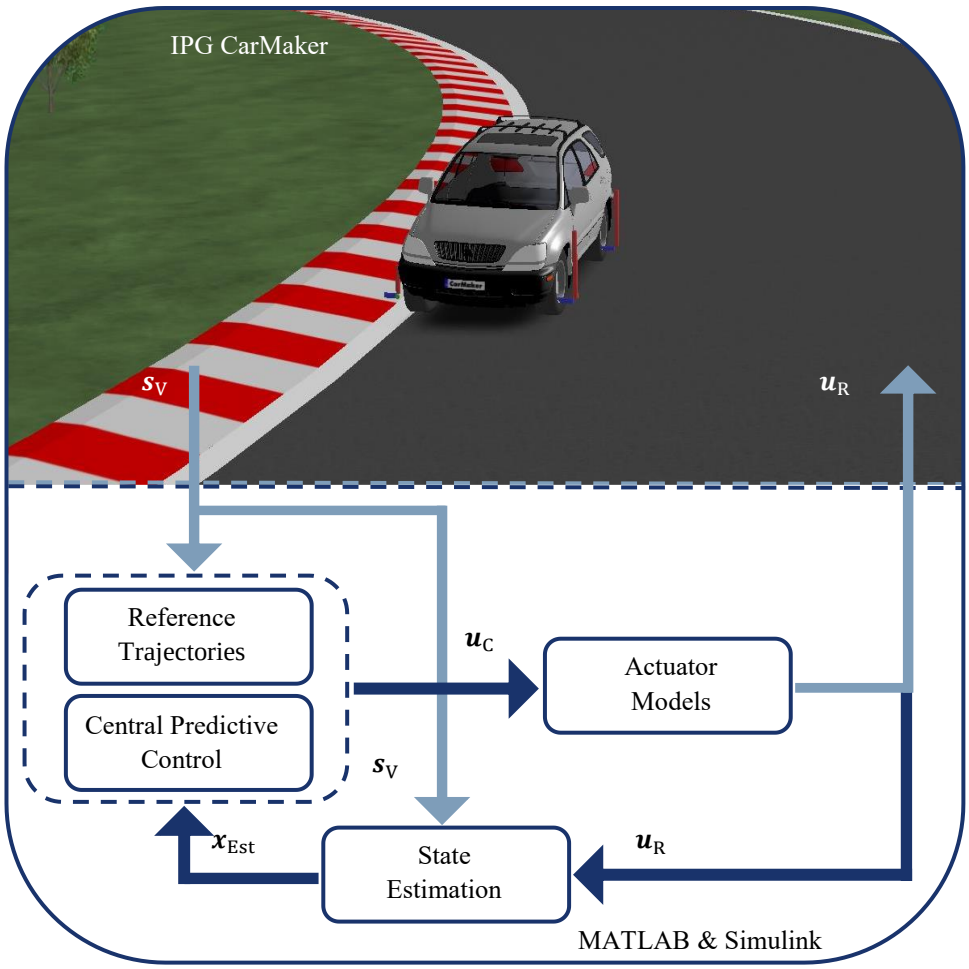

Figure 3.1 Simulation Environment

The co-simulation is performed with a fixed step size of $t_S = 0.001$ s. The step size applied within IPG CarMaker as well as within MATLAB & Simulink is also fixed to $t_S = 0.001$ s. First, IPG CarMaker performs a simulation step, in which the vehicle is simulated based on the vehicle dynamics and all additional influences from the driver and the environment. Subsequently, sensor data listed in $\boldsymbol{s}_V$, which describe the vehicle dynamics, are transferred from IPG CarMaker to MATLAB & Simulink. The sensors used to measure the vehicle dynamics are described in Section 3.3.2.

Based on the sensor data $\boldsymbol{s}_V$ the central predictive control is prepared. For this purpose, the available information regarding vehicle dynamics is used to determine reference trajectories for the controlled variables. The central predictive control is executed taking into account the sensor data $\boldsymbol{s}_V$ and the reference trajectories, which specify the target variables of the control. Furthermore, the central predictive control utilizes the states of the vehicle dynamics $\boldsymbol{x}_{Est}$ determined by the state estimation. The result of the predictive control is an optimal vector of the manipulation variables $\boldsymbol{u}_C$. Afterwards the actuator models process the manipulated variables in order to consider not only the actuator limitations but also the dynamics of the actuators. This yields the actuating variables $\boldsymbol{u}_R$ which are transferred to the state estimation. In addition to the actuating variables, the state estimation considers the available sensor data $\boldsymbol{s}_V$. Furthermore,

the actuating variables $\boldsymbol{u}_{\mathrm{R}}$ are transferred to IPG CarMaker, which takes into account these actuating variables $\boldsymbol{u}_{\mathrm{R}}$ to continue with the next step of the multibody simulation. Between the individual subareas, a delay time is taken into account. This provides a realistic representation of the transmission times within the vehicle.

3.2 Control Targets

The objective of the vehicle dynamics control within this thesis is to manipulate the rotational degrees of freedom of the vehicle body. Influencing these degrees of freedom enhances both vehicle safety and ride comfort. By implementing a central control system which is pursuing the control objectives in a holistic way, synergies are used and contrary interactions between the individual control variables are avoided, (Fan et al., 2008, Sieberg et al., 2019b). Within this thesis, three control objectives are addressed.

The control of the roll behavior of the vehicle body is one control objective. Thereby, the controlled variable equals the roll angle of the vehicle body. The risk of rollover during cornering is minimized by the systematic control of the roll angle. Furthermore, the comfort for the passengers is increased, (Mizuta et al., 2010).

A second control objective is the reduction of pitching movements of the vehicle body. Pitching movements occur mainly during acceleration or deceleration maneuvers. By reducing pitching movements, the comfort of the vehicle passengers is further improved, (Ikenaga et al., 2000).

The third control objective is to manipulate the self-steering behavior of the vehicle. Thereby, a desired self-steering behavior to be specified is adapted for the vehicle. As a result, the vehicle can be designed either in terms of vehicle stability or in terms of agility, (Jianyong et al., 2007). To improve vehicle stability, the vehicle is designed to achieve a greater understeering behavior. In contrast, the agility of the vehicle is increased by a more oversteering behavior, (Schramm et al., 2018).

3.3 Vehicle Setup

A test vehicle of the sport utility vehicle class is the starting point. The vehicle selected in this thesis is henceforth the sport utility vehicle Lexus RX 400h, which is one of the sample vehicles of IPG CarMaker. Table 3.1 lists basic vehicle parameters of the Lexus RX 400h.

The actuators, which can be integrated into the sport utility vehicle to accomplish the control objectives, are presented in the following. Subsequently, the composition of the sensor data $\boldsymbol{s}_{\mathrm{V}}$ is outlined, which are transferred from IPG CarMaker to MATLAB & Simulink.

Table 3.1 Vehicle Parameter Lexus RX 400h

Description	Parameter	Unit
Distance of the Center of Gravity to the Front Axle	1.343	m
Distance of the Center of Gravity to the Rear Axle	1.407	m
Driveline Model	All Wheel Drive	-
Height of the Center of Gravity	0.682	m
Height of the Center of Pitching	0.3257	m
Height of the Center of Rolling	0.2826	m
Moment of Inertia about the Lateral Axis	2,654	kgm²
Moment of Inertia about the Longitudinal Axis	760	kgm²
Moment of Inertia about the Vertical Axis	2,774	kgm²
Tires	235/55/R18	-
Track Width	1.538	m
Vehicle Body Mass	1,820	kg
Vehicle Mass	2,072	kg
Wheelbase	2.75	m

3.3.1 Actuators

First, different possibilities of manipulation opportunities are presented and subjected to a utility analysis. Based on defined criteria the actuators for further use are selected. Subsequently, the simulation models of these actuators are introduced, which are integrated into the co-simulation.

Manipulation Opportunities

In order to achieve the control objectives defined in 3.2, there are various ways of exerting influence. The chassis elements can be equipped with actuators to specifically influence the roll, pitch and self-steering behavior. Furthermore, concepts such as the distribution of drive torque to individual wheels and all-wheel steering can additionally affect the self-steering behavior. Subsequently, these actuators are presented with regard to their operating principle.

Active Stabilizers

Compared to a passive stabilizer, in an active stabilizer the two wheels of an axle are coupled by two stabilizer bars, which are connected by an actuator. Figure 3.2 illustrates an active stabilizer as a schematic sketch. By using an actuator, a torsion-independent cutting torque can be

generated. Thus an active torque can be impressed. Hydraulic swivel engines as well as electromechanical engines can be used for the actuation, (Heißing and Ersoy, 2011).

The use of a brushless electromechanical actuator reduces both the integration effort and the additional weight compared to a hydraulic actuator. Furthermore, the effort of maintenance and the fuel consumption are minimized. The electromechanical stabilizer features shorter operating times and can therefore follow the principle of power on demand, (Kraus, 2014, Sagewka et al., 2017). In contrast, hydraulic actuators offer a greater power density than electromechanical actuators, (Kim et al., 2011).

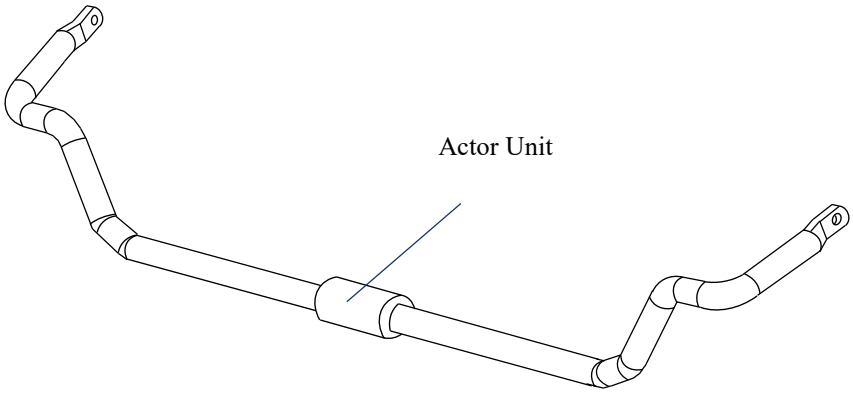

Figure 3.2 Active Stabilizer

Active stabilizers are used to manipulate the roll behavior. In addition, the self-steering behavior of the vehicle can be influenced. The vehicle can be designed to suit a situation by specifically assigning the stabilizer torques to the front and rear axles. The distribution of the active stabilizer torques in the direction of the front axle results in a more understeering behavior. Conversely, an assignment to the rear axle results in a more oversteering vehicle. Safety in critical driving situations and an agility desired by the driver can thus be optimally combined.

All-Wheel Steering

All-wheel steering indicates that in addition to the front wheels, the wheels of the rear axle can also be steered. In general, the wheels of the rear axle can be steered in the same direction or in the opposite direction to the steering at the front axle. Both possibilities are shown in Figure 3.3.

If the rear wheels are operating in a parallel direction steering, the instantaneous center of rotation $C_{R,P}$ is located further to the back compared to the instantaneous center of rotation $C_{R,O}$ of a purely front steered vehicle. This can be compared with a virtual extension of the wheelbase. A parallel direction steering indicates that the wheels of the rear axle are steered in the same direction as the wheels of the front axle. As a result, the side-slip angle is qualitatively reduced in this case compared to a vehicle that is steered exclusively at the front. Thereby, the vehicle

stability can be increased as the vehicle operates in a more understeering manner. In addition, due to the parallel steering direction for dynamic steering inputs, the lateral forces on the front and rear axle are built up faster and smoother. This improves the responsiveness from a steering input to a lateral acceleration, which improves the handling at high velocities.

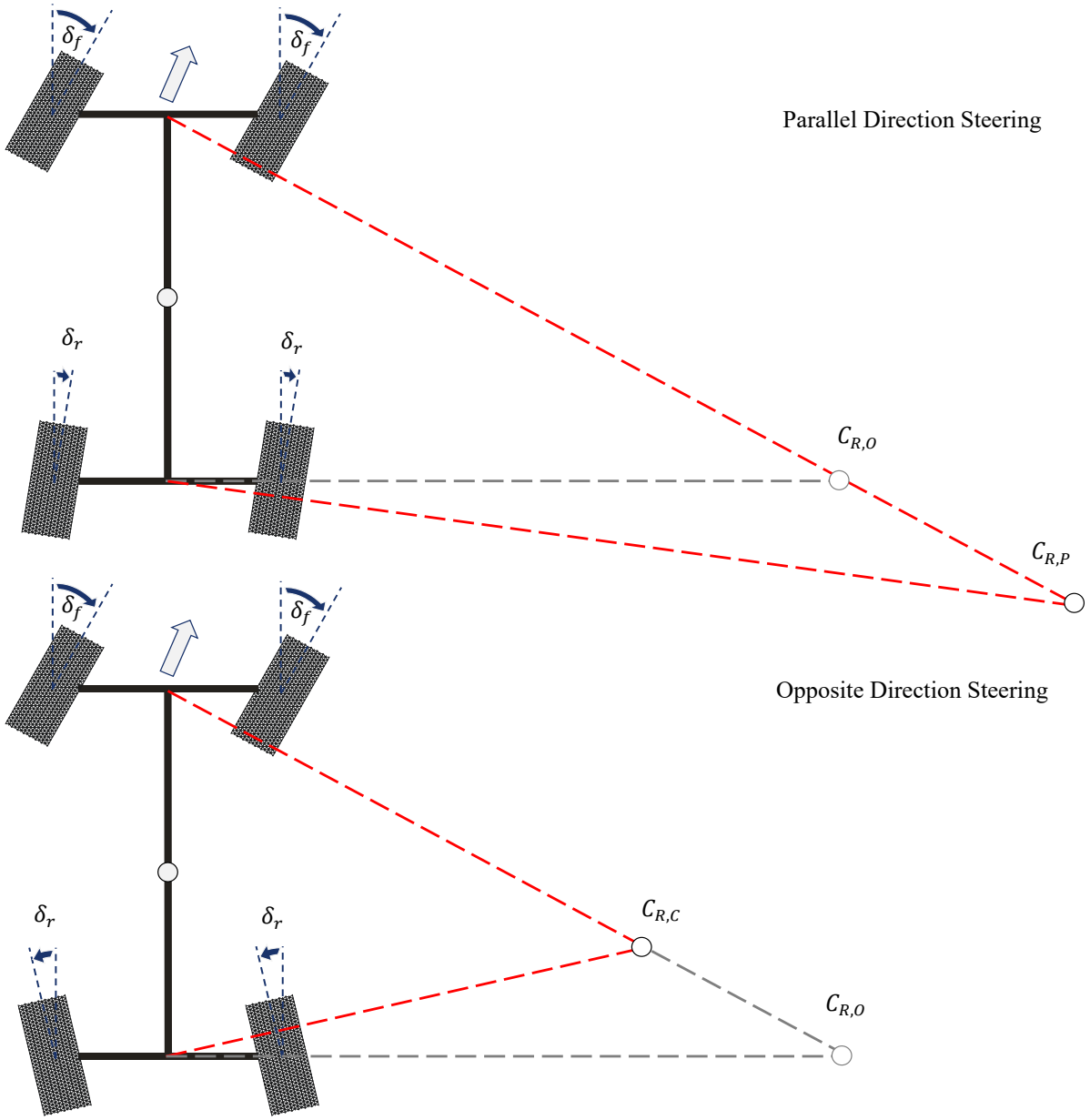

Figure 3.3 All-Wheel Steering, According to (Harrer and Pfeffer, 2017)

If the wheels of the rear axle are steered in the opposite direction of the front axle, the instantaneous center of rotation $C_{R,C}$ shifts further to the front compared to the instantaneous center of rotation $C_{R,O}$, as shown in Figure 3.3. This is equivalent to a virtual reduction of the wheelbase and results in a decrease of the cornering radius. Due to the steering in opposite directions, the direction of the lateral forces at the front and rear axle are initially opposed, which inhibits the initial lateral acceleration and results in yaw amplification. Thus the vehicle becomes more

agile. An opposite steering direction of the rear axle is therefore mainly used at low velocities. (Harrer and Pfeffer, 2017)

All-wheel steering can be used to influence the self-steering behavior of the vehicle. Furthermore, the steering effort can be reduced. Thus parking and maneuvering are simplified, which enhances the driving comfort.

Semi-Active Dampers

In order to vary the damping force of a conventional damper, two basic principles exist. One possibility is to regulate the damper force by an additional proportional valve in a twin-tube damper. Due to the valve, the flow between the two chambers can be adjusted and thus the damping force can be regulated continuously, (Heißing and Ersoy, 2011). Figure 3.4 shows two possibilities to realize such a damper.

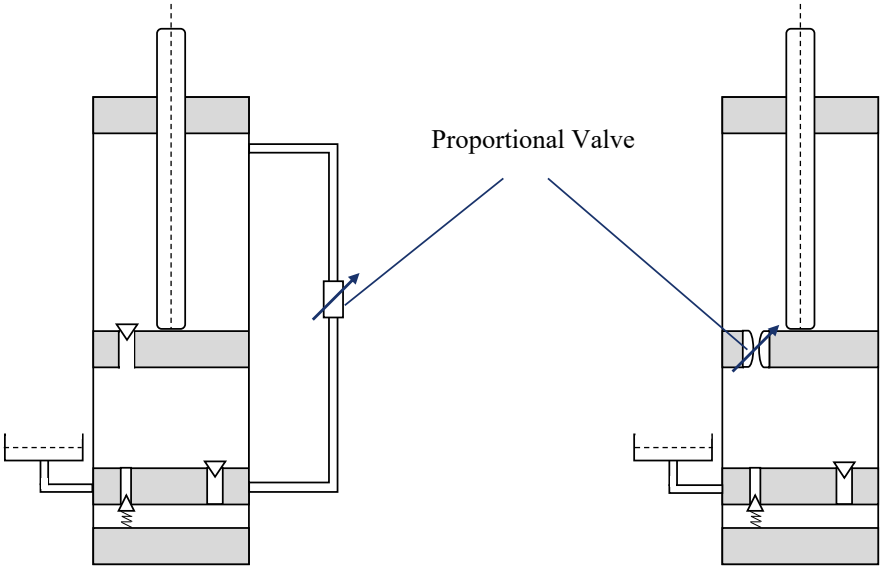

Figure 3.4 Semi-Active Damper – Left: Twin-Tube Dampers with External Proportional Valve; Right: Twin-Tube Dampers with Integrated Proportional Valve, According to (Heißing and Ersoy, 2011)

The left part of Figure 3.4 illustrates a solution with an external valve. The two chambers are connected by a bypass in which the proportional valve is located. In the right part of Figure 3.4 the proportional valve is integrated into the damper piston.

A second principle with which a variable damping force can be generated is based on the properties of magnetorheological fluids. For example, a magnetorheological fluid can be realized by adding very small iron particles to oil. When the fluid is inside of a magnetic field, the iron particles align themselves so that the shear stress in the fluid increases. This alignment of the particles is illustrated in Figure 3.5. The increase of the shear stress results in an increase of the damping force.

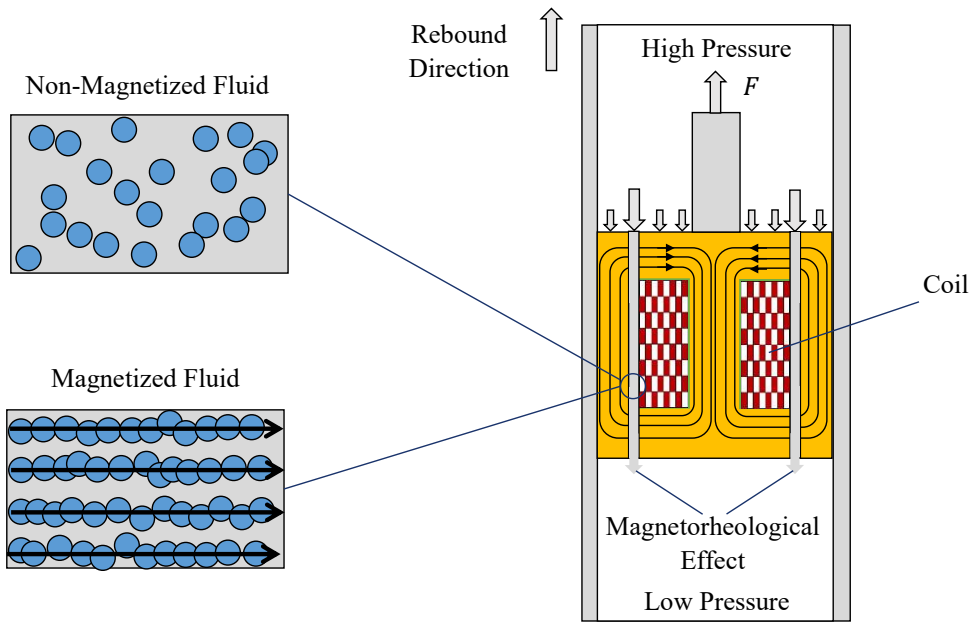

Figure 3.5 Semi-Active Damper – Magnetorheological Damper, According to (Heißing and Ersoy, 2011)

Semi-active dampers can reduce vertical movements of the vehicle body. As a result, vertical excitation induced by the road surface can be decreased. Moreover, semi-active dampers can reduce pitching and rolling movements. Semi-active dampers can also be used to adapt the forces in the tire contact surfaces. This can for example reduce the braking distance, especially on uneven roads, (Niemz, 2007).

Semi-Active Springs

Semi-active springs feature an adjustable spring force. One possibility to make the spring force adjustable is to change the length of the spring. This is done by adjusting the spring mount. The adjustment can be done either hydraulically or electromechanically. Figure 3.6 shows an electromechanical spring mount adjustment, according to (Münster et al., 2009). The upper end of the spring, which is usually connected to the vehicle body, is located on a movable piston. The piston is connected with a lead spindle drive, which enables the movement along the lead spindle. The position of the piston is controlled by an electric motor. Depending on the demand, the spring mount can be altered and hence the spring force can be adjusted. If a greater spring force is required, the piston moves downwards. If the required spring force is lower, the spring length is shortened by moving the piston upwards. In the hydraulic version, the adjustment of the spring mount is done by affecting the amount of the fluid inside a chamber system.

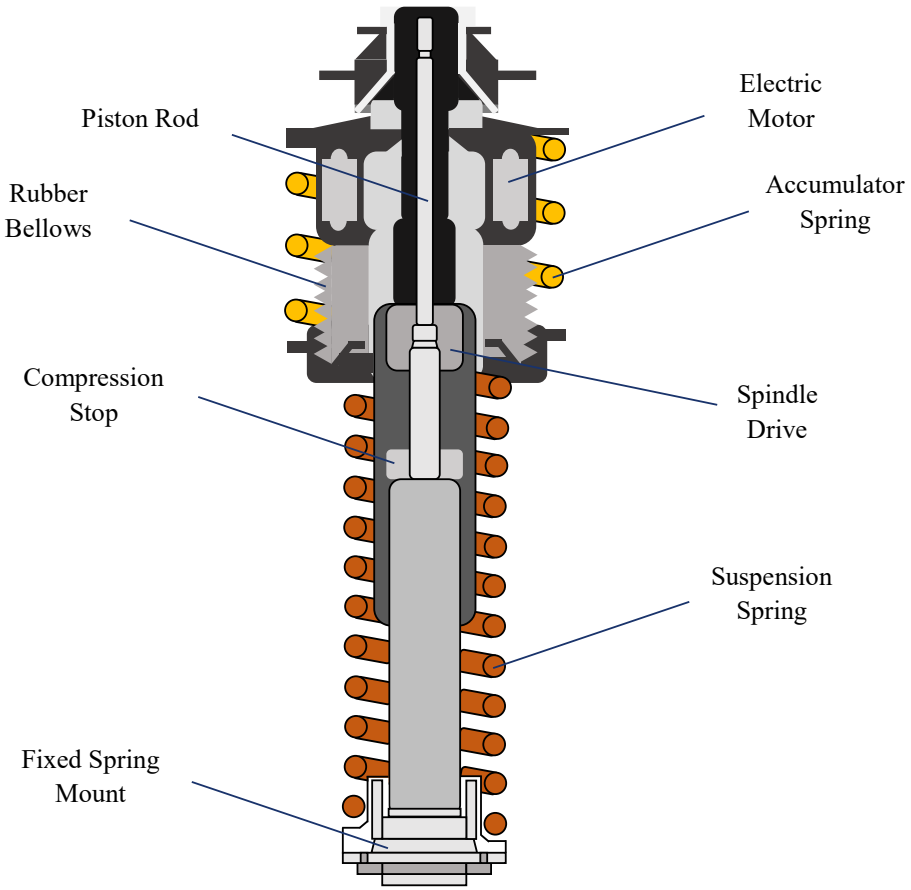

Figure 3.6 Semi-Active Spring – Spring Mount Adjustment, According to (Münster et al., 2009)

A second possibility for adjusting a spring force is to use air spring systems. Here, conventional steel springs are replaced by air-filled chambers. Depending on the required spring force, the amount of air and thus the pressure in the bellow is changed. The structure of a single-chamber air spring is shown in Figure 3.7. Air suspensions work according to the principle of volume suspension. The change of the spring force is based on the isentropic change of state of the enclosed air, (Pahl, 2016). Nowadays, multi-chamber air springs are used, for example three-chamber air springs. The rolling piston and an outer guide supporting the rolling process have a cylindrical contour. This ensures a constant effective area of the air spring bellows over the entire spring travel and prevents steps in the spring rate, (Boyraz et al., 2017b).

With the three-chamber air spring, the rolling process is carried out only for the main chamber. The two additional chambers are in a static form and serve to increase the total volume of the system. In the example of the three-chamber air spring, the air spring features the highest spring stiffness using only the main chamber. Generally, the spring rate decreases with increasing volume inside the air spring chambers. If the additional air chambers are merged with the main chamber, the spring rate of the air spring decreases, (Boyraz et al., 2017a).

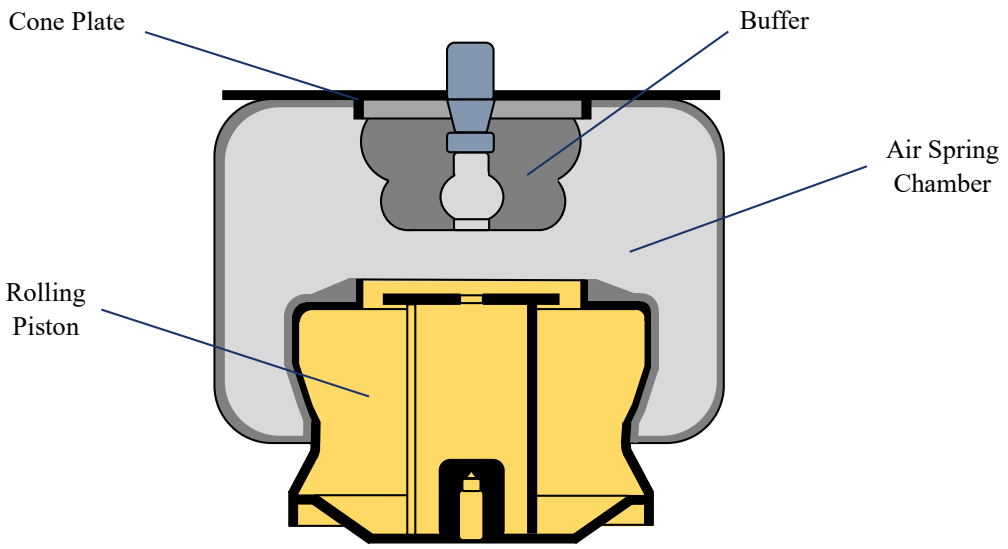

Figure 3.7 Semi-Active Spring – Air Spring, According to (Pahl, 2016)

Semi-active springs can be used to manipulate pitching, rolling and vertical movements of the vehicle body. In addition, the vehicle height level can be adjusted by semi-active springs, regardless of the payload.

Torque Vectoring

Torque vectoring allows the drive torque to be distributed to individual wheels. One possibility to implement the distribution is a brake intervention, which reduces the drive torque on individual wheels. Due to the brake intervention, this type of torque vectoring results in both increased fuel consumption and increased strain on the brake system.

A more efficient way to perform torque vectoring is to use an active differential. One way of implementing an active differential is to modify a bevel gear differential so that it can transmit motion to clutch housings. Thereby, clutch friction discs are attached to the differential output axles. The structure of this active differential is shown in Figure 3.8.

The transmission ratio between the input shaft of the bevel gear and the clutch housings is designed in such a way that the clutch housings rotate faster than the discs. Therefore, the clutch torque sign is known. Accordingly, the magnitude of the torque depends purely on the actuating force of the clutch.

In (Canale et al., 2007), this force is generated by an electro-hydraulic system. The dynamics of the active differential depends mainly on the valves which adjust the fluid pressure within the hydraulic system and thereby generate the clutch forces. The transmission of the drive torque in this system is merely limited by the internal transmission ratio.

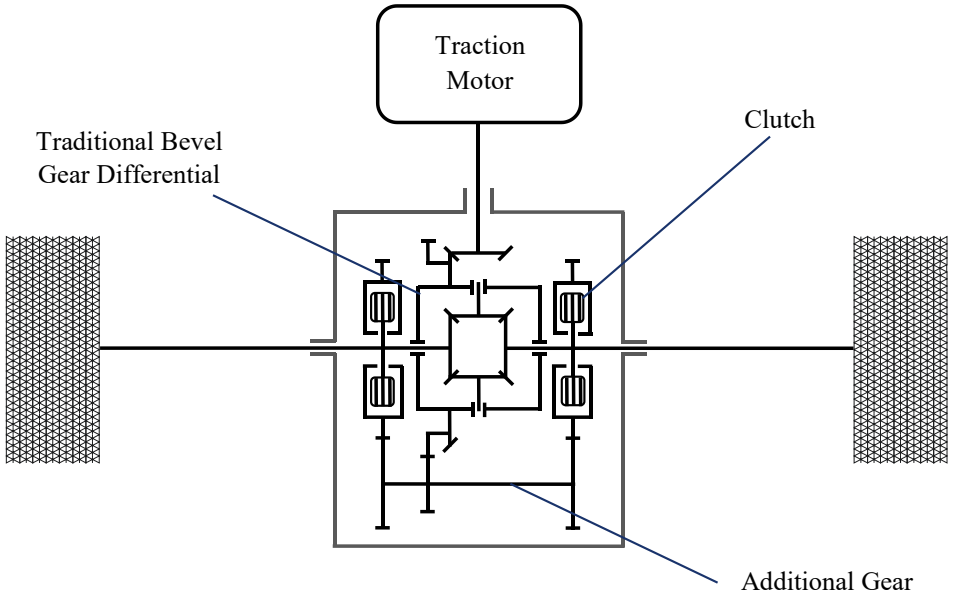

Figure 3.8 Torque Vectoring – Active Rear Differential, According to (Canale et al., 2007)

Another way of implementing an active differential is to integrate an electric motor into the differential. The scheme is shown in Figure 3.9. The internal transmission ratio and the adjustable clutches enable individual drive torque settings for each wheel. By using the electric motor in both, motoric operation as well as a generator, the drive torque can be adjusted. If the electric motor is not actuated, the electromechanical differential operates as an open differential, (Rahimi Fetrati et al., 2016a, Rahimi Fetrati et al., 2016b).

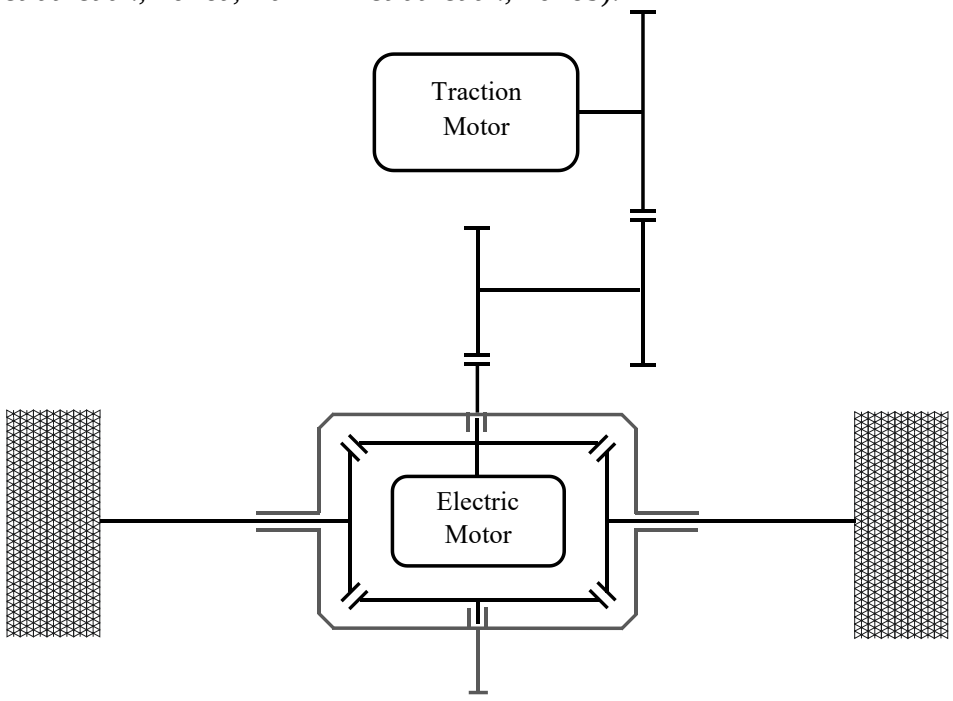

Figure 3.9 Torque Vectoring – Active Electromechanical Differential, According to (Rahimi Fetrati et al., 2016a)

Torque vectoring generates an additional yaw torque, which results from the individual adjustment of the drive torques for each wheel. Therefore, torque vectoring systems can be used to affect the self-steering behavior of a vehicle. The vehicle acts in a more oversteering manner and is consequently more agile if the drive torque is shifted in the direction of the curve's outer wheels during cornering. If the drive torque is shifted in the direction of the curve's inner wheels, a greater understeering behavior is obtained, which increases the stability of the vehicle.

Utility Analysis

In the following Section, the actuators with which the sport utility vehicle will be equipped are selected. The selection is based on a utility analysis under consideration of the overall suitability for the final application. Three concepts are considered as possible setups. Each concept is capable of achieving the control objectives defined in Section 3.2. Besides the control objectives, the concepts are evaluated with regard to their costs, the availability of additional functions and the integration complexity into the test vehicle. Table 3.2 gives an overview of the evaluation criteria, including the corresponding weightings. These have been determined with regard to the control objectives and economic efficiency by a pair-by-pair comparison, which is provided in Table A-1 of the Appendix.

Table 3.2 Assessment Criteria of the Utility Analyses

Assessment Criteria	**Weighting**
Additional Costs	19.44 %
Additional Functions	5.56 %
Integration Effort	11.11 %
Manipulation of the Pitch Behavior	19.44 %
Manipulation of the Roll Behavior	30.56 %
Manipulation of the Self-Steering Behavior	13.89 %

Subsequently, the vehicle configuration concepts are presented. The composition of the concepts as well as the surcharges to be considered are based on the equipment possibilities of a Porsche Cayenne due to availability, (PorscheAG, 2020). The surcharges to be paid are used as indicators to evaluate the additional costs. An overview of the concepts is given in Table 3.3.

Table 3.3 Vehicle Configuration Concepts

	Concept 1	**Concept 2**	**Concept 3**
Utilized Actors	Four-Wheel Steering Semi-Active Dampers Semi-Active Springs Torque Vectoring	Active Stabilizers Semi-Active Dampers	Active Stabilizers Four-Wheel Steering Semi-Active Dampers Semi-Active Springs
Surcharges	5,955.95 €	4,819.50 €	7,740.95 €

The first configuration concept includes an air spring system, four-wheel steering, semi-active dampers and electromechanical differentials respectively torque vectoring. The surcharges indicating the additional costs are 5,955.95 €. The air spring and the semi-active dampers can be used to manipulate the roll and pitch behavior of the vehicle body. The self-steering behavior is adjusted by the four-wheel steering and the torque vectoring. Additional functions, which are covered by the setup, are a variable height adjustment of the vehicle, an optimization of the braking distance and the adjustment of vertical movements.

The second configuration concept features active stabilizers and semi-active dampers. Therefore, it is the most minimalistic one of the three concepts. The surcharges sum up to 4,819.50 €. The semi-active dampers are used to influence the roll and pitch behavior of the vehicle body. The active stabilizers serve on the one hand to control the roll behavior. On the other hand, the distribution of the stabilizer torques between the front and rear axle is used to affect the self-steering behavior of the vehicle. Additional functions covered by this concept are an optimization of the braking distance and the compensation of vertical movements of the vehicle body.

Within the third configuration concept, the sport utility vehicle is equipped with an air spring system, active stabilizers, four-wheel steering and semi-active dampers. This leads to surcharges indicating the additional costs of 7,740.95 €. The roll behavior of the vehicle body is manipulated by the air spring, the active stabilizers and the semi-active dampers. The pitch behavior of the vehicle body is affected by the air springs and the semi-active dampers. In addition to the four-wheel steering, the active stabilizers are used to influence the self-steering behavior by distributing the torque between the front and rear axle. As with the first configuration setup, additional functions are the variable height adjustment of the vehicle, the optimization of the braking distance and the adjustment of the vertical movements of the vehicle.

The three different vehicle configuration concepts are evaluated using the criteria listed in Table 3.2. The assessment scale consists of four scores. Zero points are awarded for very poor performance in one criterion. For a poor fulfilment of a criterion, one point is granted. In case a criterion is fulfilled properly, then two points are scored. An excellent fulfilment corresponds to a score of three points. The score is then multiplied by the weighting of the corresponding assessment criterion. Table 3.4 depicts an overview of the assessment of the three concepts by the author. The weighted scores of the individual concepts are summed to obtain the results of the utility analysis.

As a result of the utility analysis, configuration concept 2 is selected, which includes active stabilizers and semi-active dampers. In comparison to the other two concepts, it fulfills the specified requirements in the best way with a score of 2.25001.

Table 3.4 Vehicle Setup – Utility Analyses

Assessment Criteria	Concept 1	Concept 2	Concept 3
Additional Costs	0.19444	0.38889	0
Additional Functions	0.11111	0.05556	0.16667
Integration Effort	0.11111	0.22222	0
Manipulation of the Pitch Behavior	0.58333	0.38889	0.58333
Manipulation of the Roll Behavior	0.61111	0.91667	0.91667
Manipulation of the Self-Steering Behavior	0.41667	0.27778	0.41667
Results	**2.02777**	**2.25001**	**2.08334**

Actuator Models

Subsequently, the models of the actuators are presented, which are integrated into the sport utility vehicle due to the results of the utility analysis. Owing to a realistic representation, it is essential to use actuator models. By using actuator models, the actuator dynamics can be mapped and furthermore the physical limitations of the actuators can be considered. Moreover, the requirements of discrete and real-time capable operation must be preserved for actuator modeling.

Active Stabilizer

The active stabilizers used in this thesis are based on an electromechanical design. The active part, which connects the two sides of the stabilizer, is implemented by a DC motor together with a gearbox. The parameterization of the DC motor is listed in Table 3.5, according to (Buma et al., 2010).

Table 3.5 Active Stabilizer – DC Motor & Gearbox Parameter

Description	Parameter	Unit
Armature Inductance L_A	0.5	H
Armature Resistance R_A	0.204	Ω
Nominal Armature Voltage U_A	12	V
Counter-Electromotive Force Constant K_E	0.5	Vs/rad
Gear Ratio r_{DC}	1/200	-
Internal Torque Control PI Controller	Proportional Part 0.0391 Integral Part 563.0720	-
Moment of Inertia of the Rotor J_{DC}	0.000196	kgm²
Number of Pole Pairs p_{DC}	1	-
Torque Constant K_T	0.15	Nm/A
Viscosity Coefficient d_{DC}	0.3	Nms/rad

The DC motor primarily determines the behavior of the electromechanical stabilizer. In the following, the behavior of the DC motor is mapped using a discrete state space model

$$\boldsymbol{x}(k+1) = \boldsymbol{A}\boldsymbol{x}(k) + \boldsymbol{B}\boldsymbol{u}(k), \tag{3.1}$$

$$\boldsymbol{y}(k) = \boldsymbol{C}\boldsymbol{x}(k) + \boldsymbol{D}\boldsymbol{u}(k), \tag{3.2}$$

which results in

$$\begin{bmatrix} \omega_{\mathrm{DC}}(k+1) \\ I_{\mathrm{A}}(k+1) \end{bmatrix} = \begin{bmatrix} -\frac{d_{\mathrm{DC}}}{J_{\mathrm{DC}}} & \frac{K_{\mathrm{T}}}{J_{\mathrm{DC}}} \\ -\frac{K_{\mathrm{E}}}{L_{\mathrm{A}}} & \frac{R_{\mathrm{A}}}{L_{\mathrm{A}}} \end{bmatrix} \cdot \begin{bmatrix} \omega_{\mathrm{DC}}(k) \\ I_{\mathrm{A}}(k) \end{bmatrix} + \begin{bmatrix} -\frac{1}{J_{\mathrm{DC}}} & 0 \\ 0 & \frac{1}{L_{\mathrm{A}}} \end{bmatrix} \cdot \begin{bmatrix} T_{\mathrm{L}}(k) \\ U_{\mathrm{A}}(k) \end{bmatrix}, \tag{3.3}$$

$$\begin{bmatrix} T_{\mathrm{DC}}(k) \\ I_{\mathrm{A}}(k) \end{bmatrix} = \begin{bmatrix} -d_{\mathrm{DC}} & K_{\mathrm{T}} \\ 0 & 1 \end{bmatrix} \cdot \begin{bmatrix} \omega_{\mathrm{DC}}(k) \\ I_{\mathrm{A}}(k) \end{bmatrix} + \begin{bmatrix} -1 & 0 \\ 0 & 0 \end{bmatrix} \cdot \begin{bmatrix} T_{\mathrm{L}}(k) \\ U_{\mathrm{A}}(k) \end{bmatrix}. \tag{3.4}$$

The angular velocity ω_{DC} of the DC motor and the armature current I_{A} form the state vector. The two input variables are the load torque T_{L} and the armature voltage U_{A}. The output variables are the armature current I_{A} and the applied torque T_{DC} of the DC motor. Furthermore, the viscosity coefficient d_{DC}, the torque constant K_{T} and the moment of inertia of the rotor J_{DC} act on the mechanical characteristics of the DC motor model. The electrical characteristics are affected by the armature resistance R_{A}, the armature inductance L_{A} and the counter-electromotive force constant K_{E}. In addition, a torque control is integrated into the DC motor model to enable adjustment of the stabilizer torque determined by the central predictive control. The dynamic behavior of the DC motor corresponds to a first order delay element. In order to compensate the delay the torque control is achieved by a proportional-integral controller. Figure 3.10 illustrates the schematic structure of the active stabilizer model.

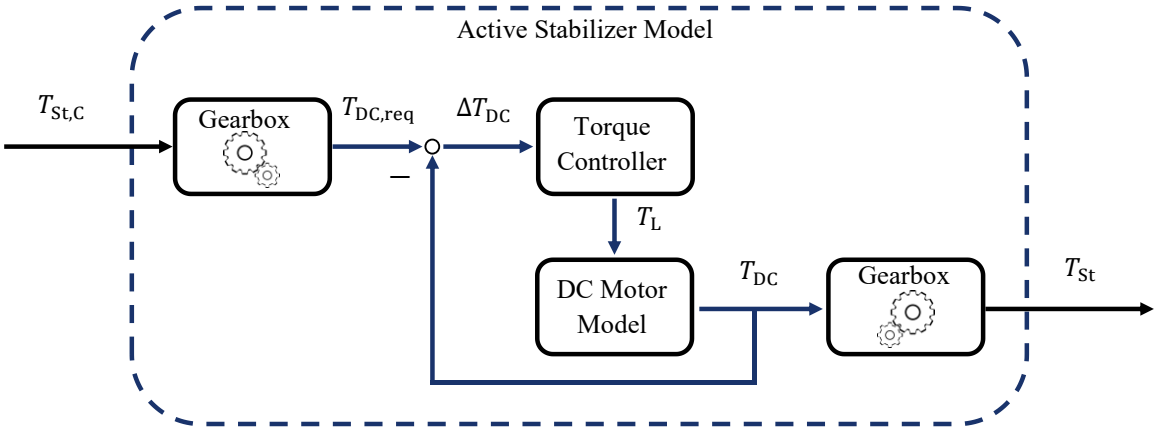

Figure 3.10 Active Stabilizer Model – Schematic Structure

The stabilizer torque $T_{\mathrm{St,C}}$ specified by the central predictive control system is converted into the required torque $T_{\mathrm{DC,req}}$ for the DC motor via a gear ratio. Moreover, the torque T_{DC} of the

DC motor is likewise converted back into the actuated variable of the stabilizer torque T_{St} via the ratio of the gearbox.

Semi-Active Damper

In order to model the behavior of the semi-active dampers, a magnetorheological design of a damper is considered within this thesis. Data obtained during experimental test series are available for modeling the semi-active damper. The semi-active damper can be operated in a defined current range. Depending on the compression velocity v_{D} of the damper and the applied current I_{D}, a resulting damping force is generated. The characteristic map of the magnetorheological damper is illustrated in Figure 3.11. The current can be set within the range of $I_{\mathrm{D,min}}$ and $I_{\mathrm{D,max}}$.

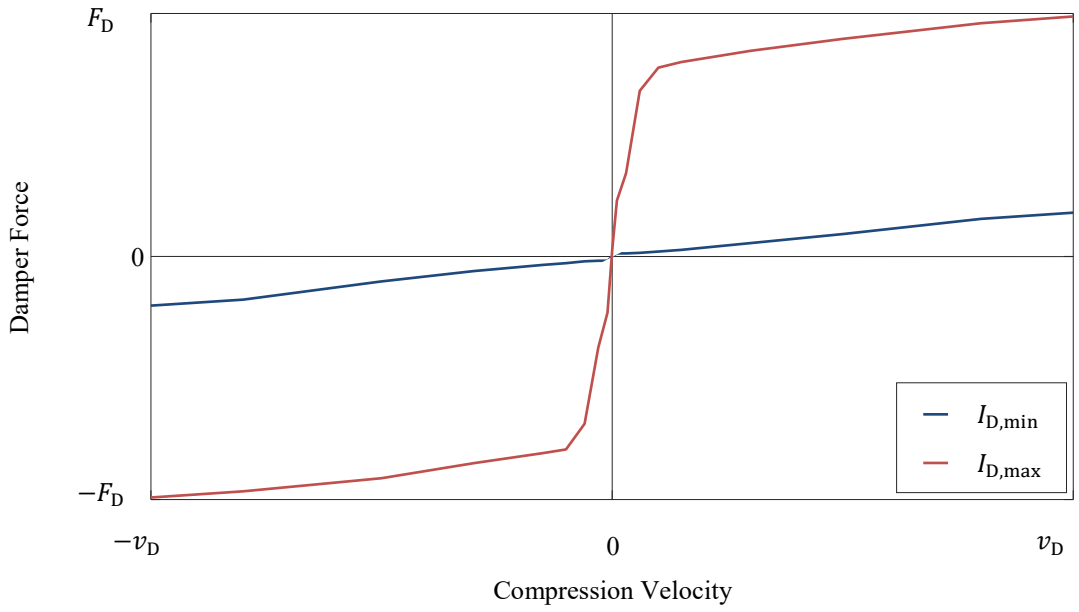

Figure 3.11 Semi-Active Damper Model – Characteristic Map

The basis of the damper model is the characteristic map, which is embedded into the simulation environment as a lookup table. Depending on the applied current and the compression velocity of the damper a corresponding damper force is determined, which is within the physical boundaries of the magnetorheological damper.

Another important aspect in the modeling of the actuator is the representation of the actuator dynamics. In order to reproduce the dynamics using the characteristic map, delay times are taken into account. On the one hand, an inductive delay time τ_{C} is integrated into the model. This considers the dynamic behavior of the coil, which is used to build up the magnetic field of the semi-active damper. The inductive delay time τ_{C} is specified by

$$\tau_{\mathrm{C}} = \frac{L_{\mathrm{C}}}{R_{\mathrm{C}}}. \tag{3.5}$$

The coil for building up the magnetic field features the inductance L_C and the resistance R_C. By taking the inductive delay time τ_C into account, the current I_C acts like a first order delay element, (Lei and Shiguo, 2006). Considering the operation at specified DC voltage $U_\mathrm{C,N}$, the dynamic behavior of the current I_C can be determined by

$$I_C = \begin{cases} \frac{U_\mathrm{C,N}}{R_\mathrm{C}}\left(1 - e^{-\frac{t_\mathrm{C}}{\tau_\mathrm{C}}}\right) & \frac{dI_\mathrm{C}}{dt_\mathrm{C}} > 0 \\ \frac{U_\mathrm{C,N}}{R_\mathrm{C}} & \frac{dI_\mathrm{C}}{dt_\mathrm{C}} = 0 \\ \frac{U_\mathrm{C,N}}{R_\mathrm{C}} e^{-\frac{t_\mathrm{C}}{\tau_\mathrm{C}}} & \frac{dI_\mathrm{C}}{dt_\mathrm{C}} < 0 \end{cases}. \tag{3.6}$$

After a period of $t_\mathrm{C} = 5\tau_\mathrm{C}$ the coil current I_C corresponds to 99.32621 % of the target value, in terms of an increasing coil current I_C. The second time delay, which is considered in the model of the magnetorheological damper, describes the dynamic behavior of the fluid within the damper. The hydraulic delay time τ_H has been determined during the experimental test series, which has served to record the characteristic map. τ_H is the time required to build up the maximum possible damper force difference $\Delta F_\mathrm{D,max}$, excluding the inductive time constant τ_C. A linear behavior is assumed for building up the damper force in terms of hydraulic characteristics. Under consideration of the inductive delay time τ_C and the hydraulic delay time τ_H the maximum changing rate of the damper force

$$\dot{F}_\mathrm{D,max} = \Delta F_\mathrm{D,max} \frac{1}{5\tau_\mathrm{C} + \tau_\mathrm{H}} \tag{3.7}$$

is calculated. $\dot{F}_\mathrm{D,max}$ incorporates the physical boundaries of the magnetorheological damper. Thus the characteristic map of the semi-active damper is extended by a description of the dynamic behavior.

3.3.2 Sensors

The sensor equipment of the sport utility vehicle corresponds to a minimalistic specification. In this configuration, a minimum number of sensors are installed in order to keep the costs for the hardware setup as low as possible. For this purpose, sensors are used that are already available as a standard for the electronic stability control. Due to a regulation of the European Union in 2009, it is mandatory for vehicles to be equipped with an electronic stability control system in order to be licensed, (EuropeanUnion, 2009). The sensor signals required for an electronic stability control system are composed of the lateral acceleration, the steering wheel angle, the velocity, the wheel speeds and the yaw rate of the vehicle, (Liebemann et al., 2005). Furthermore, the information regarding the drive train is made available to the electronic stability control system, whereby the brake pressure, the engine torque, the transmission ratio and each pedal

position within the pedal set are known. For passenger safety, airbags are standard in the vehicle. The airbags are essentially controlled on the basis of the longitudinal acceleration of the vehicle, (Aljazzar et al., 2009, Reif, 2014, Schramm et al., 2020).

In the present case of the basic sensor equipment, an inertial measurement unit is incorporated in the center of gravity of the vehicle. The inertial measurement unit consists of two acceleration sensors and one gyroscope. The lateral acceleration and the longitudinal acceleration as well as the yaw rate of the vehicle are monitored by this inertial measurement unit. Furthermore, the steering wheel angle and the corresponding steering velocity are measured by a steering angle sensor. In addition, wheel speed sensors are used to determine not only the wheel speed but also the velocity of the vehicle, (Bosch, 2020).

Table 3.6 provides an overview of the sensors installed. This sensor equipment serves as a basis for the sensor data $\boldsymbol{s}_{\mathrm{V}}$ which are transferred from the sport utility vehicle within IPG CarMaker to MATLAB & Simulink.

Table 3.6 Sensor Setup

Sensor	Measured Quantity	Unit
Inertial Measurement Unit at the Center of Gravity	Lateral Acceleration a_y	m/s²
	Longitudinal Acceleration a_x	m/s²
	Yaw Rate $\dot{\psi}$	rad/s
Steering Angle Sensor	Steering Wheel Angle δ_{SW}	rad
Wheel Speed Sensors	Vehicle Velocity v	m/s
	Wheel Speeds $n_{\mathrm{W},ij}$	1/s

In the context of this thesis, it is assumed that the sensor signals have already been pre-processed by filtering. Therefore, ideal sensor signals are used in the further course.

3.4 Estimation Targets

In order to achieve the control objectives defined in Section 3.2, it is necessary to possess information regarding other variables of vehicle dynamics besides the quantities defined by the sensor signals in Section 3.3.2. The unknown vehicle dynamics states are determined by state estimators within this thesis. These state estimators predict the unknown states on the basis of the available sensor data and the actuating variables.

For a successful control of the roll behavior of the vehicle body, the vehicle dynamic states of the roll angle φ and the roll rate $\dot{\varphi}$ are estimated. In conjunction with the reduction of the pitch behavior, the pitch angle θ and the pitch rate $\dot{\theta}$ of the vehicle body are estimated. Moreover, in order to affect the self-steering behavior, the side-slip angle β of the vehicle is estimated. Table 3.7 provides an overview of the quantities along with the corresponding units, which are determined by the state estimation.

Table 3.7 Estimation Quantities

Estimation Quantity	Unit
Pitch Angle θ	rad
Pitch Rate $\dot{\theta}$	rad/s
Roll Angle φ	rad
Roll Rate $\dot{\varphi}$	rad/s
Side-Slip Angle β	rad

3.5 Driving Scenarios

In order to create the data-driven models within the state estimation as well as the control, training data are required. The composition of the training data takes into account three driving conditions. These are composed of driving straight ahead, cornering and the transition area between these two. The training data are generated within the development framework. This enables the closed-loop characteristic and the interaction between state estimation and control to be mapped. For the state estimation the physical models are used within the framework, which are introduced in Chapter 4.1. The controller is based on the non-linear model-based predictive control, which is introduced in Chapter 5.2. By the pure use of models based on physical model knowledge within the development framework for the generation of the training data, these data are completely comprehensible. To generate the data-driven state estimators as well as the control, one database is used. This database relies on standardized driving maneuvers which are briefly presented in the following.

The vehicle behavior of driving straight ahead is subdivided into the driving maneuvers acceleration test and braking test. During the acceleration test, the test vehicle is accelerated from standstill to a defined velocity. Depending on the target velocity, gears are changed during the acceleration phase. The driving maneuver acceleration test is varied for two parameters. In addition to the target velocity, which varies from 30 km/h to 130 km/h, the lateral road gradient is altered in a corridor from -6 % to 6 %. The increments are 20 km/h for the velocity and 1 % for the lateral road gradient. Besides the acceleration test, the driving maneuver braking test is used to describe the vehicle behavior of driving straight ahead. Within this driving maneuver, the test vehicle is decelerated from a defined velocity to standstill by an emergency braking. The braking test is also varied for two parameters. Again, in addition to the lateral road gradient ranging from -6 % to 6 % in 1 % increments, the velocity from which the emergency braking takes place is varied. The velocity is modified in 20 km/h steps in an interval of 30 km/h up to 130 km/h.

The cornering behavior is covered by two driving maneuvers. The first driving maneuver is based on the steady-state circular driving, according to (ISO, 2012). The objective of the driving

maneuver is to determine the steady-state behavior of the vehicle during cornering. Four different parameters are varied during the steady-state circular travel. These are kept constant during each run of the driving maneuver. The parameters are the cornering radius, the lateral road gradient, the steering direction and the velocity of the vehicle. As for the cornering radius, 40 m and 100 m are preset. The lateral road gradient alters between -6 % and 6 % again in 1 % increments. The steering direction is either clockwise or counterclockwise. The velocity is varied again in an interval from 30 km/h to 130 km/h in increments of 20 km/h. The second driving maneuver describing the cornering behavior is based on the maneuver braking in a turn, according to (ISO, 2019). This driving maneuver aims at determining the vehicle reaction to a braking action during steady-state circular driving. The driving maneuver braking in a turn is modified for different parameters, which are composed by the longitudinal deceleration during the braking action, the lateral road gradient and the steering direction. The longitudinal deceleration is varied between 2.5 m/s² and 10.0 m/s² with an incremental step of 0.5 m/s². The lateral road gradient is adjusted within the range of -6 % and 6 % in increments of 1 %. In addition, both clockwise and counterclockwise steering directions are applied. The cornering radius as well as the velocity within this driving maneuver are constantly set to 100 m and 100 km/h, respectively.

Beside the two areas of driving straight ahead and cornering, the transition behavior between these areas is used to create the training data. As with the other two areas, two driving maneuvers are utilized here as well. One driving maneuver applied is the double lane change defined in (ISO, 2018). The objective of the driving maneuver is to explore the dynamic behavior of the vehicle during several lane changes. The vehicle changes the lane and returns to the original lane subsequently. The geometric dimensions of the lanes for the double lane change are fixed. The driving maneuver is variable in three parameters. Besides the lateral road gradient and the velocity, both steering directions of the first lane change, clockwise and counterclockwise, are used. The lateral road gradient alters in 1 % increments between -6 % and 6 % and the velocity is varied between 30 km/h and 130 km/h in steps of 20 km/h. During the double lane change the driver attempts to preserve a constant velocity. The second driving maneuver to describe the transition behavior between driving straight ahead and cornering is based on the step steering input test, (ISO, 2011a). The objective of the driving maneuver is to determine the transient response behavior of the vehicle in the time domain. During the driving maneuver, a step change in the steering wheel angle is applied while driving straight ahead at constant velocity. Taking into account the feasibility, this steering wheel angle step is performed as a steering wheel angle ramp. The driving maneuver is varied in four parameters. These are composed of the lateral road gradient, the velocity, the amplitude of the steering wheel angle and the steering direction. The lateral road gradient and the velocity are varied consistently with the other driving maneuvers in the ranges -6 % to 6 % in 1 % steps and 30 km/h to 130 km/h in 20 km/h steps. The amplitude of the steering wheel angle is varying between 60° and 180° in increments

of 60°. The gradient of the steering wheel angle ramp is consistently 30°/s. Furthermore, both clockwise and counterclockwise steering directions are covered.

A database with 1,508 simulated test drives results from the variation of the six different driving maneuvers. Table 3.8 summarizes the driving maneuvers, the adjustable parameters and their value ranges.

Table 3.8 Driving Scenarios

Driving Maneuver	Parameter	Values	Unit
Acceleration Test	Lateral Road Gradient	-6 to 6	%
	Velocity	30 to 130	km/h
Braking in a Turn	Lateral Road Gradient	-6 to 6	%
	Longitudinal Deceleration	2.5 to 10	m/s²
	Steering Direction	Clockwise / Counterclockwise	-
Braking Test	Lateral Road Gradient	-6 to 6	%
	Velocity	30 to 130	km/h
Double Lane Change	Lateral Road Gradient	-6 to 6	%
	Steering Direction	Clockwise / Counterclockwise	-
	Velocity	30 to 130	km/h
Step Steering Input Test	Lateral Road Gradient	-6 to 6	%
	Steering Amplitude	60 to 180	°
	Steering Direction	Clockwise / Counterclockwise	-
	Velocity	30 to 130	km/h
Steady-State Circular Drive	Cornering Radius	40 / 100	m
	Lateral Road Gradient	-6 to 6	%
	Steering Direction	Clockwise / Counterclockwise	-
	Velocity	30 to 130	km/h

The value ranges for the parameters were determined under consideration of public standards. The absolute, maximum lateral road gradient in Germany is 6 %, whereby this serves as the limit for the driving maneuvers, (FGSV, 2011, 2012). The limits of the velocity take into account the driving behavior in urban areas with 30 km/h and 130 km/h as the recommended velocity on the highway. Moreover, a maximum deceleration of 10 m/s² can be assumed according to (Kudarauskas, 2007). For purposes of completeness, both steering directions were taken into account. The further limits of the value ranges result from the individual standards of the driving maneuvers.

4 Hybrid State Estimation

The hybrid method of state estimation combines and safeguards models obtained by machine learning methods with simple physical models. Models based on machine learning methods feature a reduced modeling effort as well as a high potential of representation quality. However, models resulting from experimental modeling lead to the consequence that the inner workings are not or only partially comprehensible. By introducing physical model knowledge through simple models based on theoretical modeling, these incomprehensible models can be safeguarded. The simple physical models are introduced first. Subsequently the state estimators based on machine learning methods are presented in the form of artificial neural networks. In a further step both model architectures are combined and safeguarded by the hybrid method. A first validation of the hybrid state estimators is performed with test data in an open-loop operation mode.

4.1 State Estimation Based on Physical Models

The method of theoretical modeling is applied for the generation of the state estimators based on physical model knowledge. In this kind of modeling, a system behavior is described with the use of mathematical equations, which are derived from physical laws, (Schramm et al., 2018). In the following, three state estimators based on physical knowledge are implemented for the quantities to be estimated as defined in Section 3.4, the roll angle φ and roll rate $\dot{\varphi}$, the pitch angle θ and pitch rate $\dot{\theta}$ as well as the side-slip angle β. In addition to a number of measured quantities, the manipulated variables also serve as inputs to these state estimators. For this purpose, the actuating variables $\boldsymbol{u}_{\mathrm{R}}$ represented by the actuator models are used. This ensures that, in addition to the actuator thresholds, the dynamics of the actuators are also incorporated. Consequently, these input variables into the state estimators are more accurate and realistic.

4.1.1 Roll Behavior

The physical characteristic of the vehicle's roll behavior is based on a non-linear roll model. To derive the model, the vehicle body is cut free in the y-z plane, according to (Schramm et al., 2018). Furthermore, the following assumptions are made for the construction of the non-linear roll model:

- A quasi-stationary balance of forces acts in the lateral direction.
- The geometry of the chassis does not alter under the impact of the applied forces.
- The centrifugal force F_C due to the lateral acceleration a_y acts as an external force.
- The front and rear axle are combined to one axle at the plane of the center of gravity.
- The mass of the vehicle body m is concentrated at the center of gravity.
- The vehicle body is symmetrical to its longitudinal axis.

Figure 4.1 illustrates the free cut of the vehicle body under consideration of these assumptions.

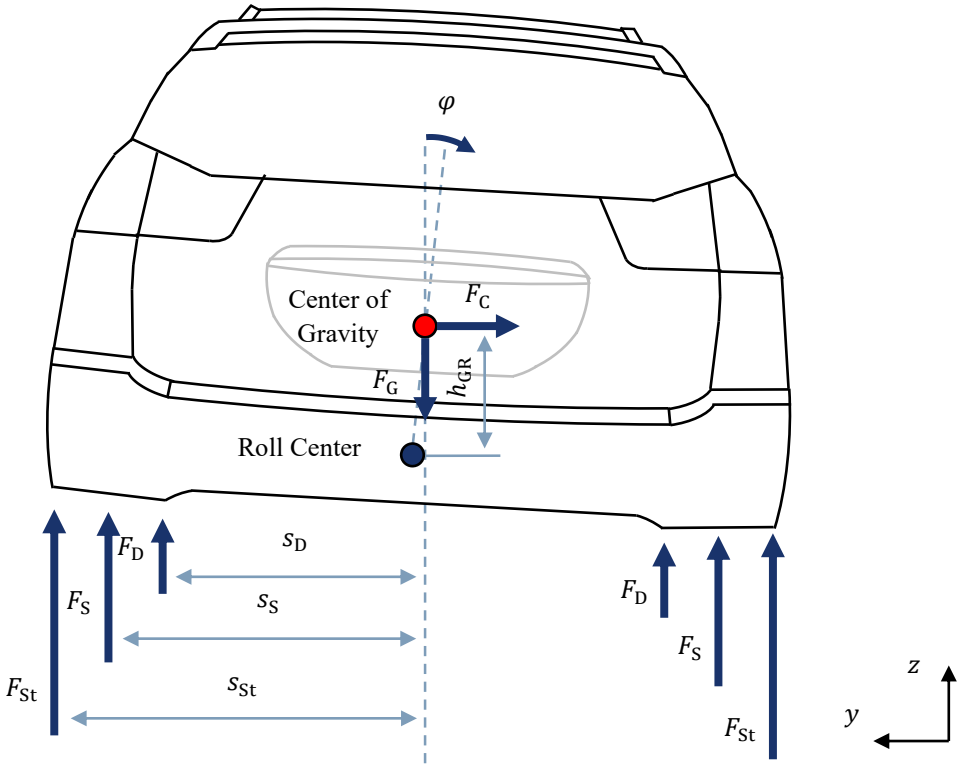

Figure 4.1 Roll Model – Free Cut

To describe the roll behavior of the vehicle body, the principle of angular momentum is set up for the roll center. On the one hand, the gravitational force F_G and the centrifugal force F_C affect the vehicle body. These two forces are regarded as external input quantities which cannot be affected. The gravitational and the centrifugal force act at the center of gravity of the vehicle body. They are specified by

$$F_G = mg, \tag{4.1}$$

$$F_C = ma_y, \tag{4.2}$$

where m is the mass of the vehicle body, g the acceleration due to gravity and a_y the lateral acceleration. Both forces affect the rolling motion by the lever arm

$$h_{\mathrm{GR}} = h_{\mathrm{G}} - h_{\mathrm{R}}, \tag{4.3}$$

which defines the distance between the height of the center of gravity h_{G} and the height of the roll center h_{R}. This results in the corresponding torques based on the two forces in dependency of the roll angle φ:

$$T_{\mathrm{G},\varphi}(\varphi) = h_{\mathrm{GR}} m g \sin\varphi, \tag{4.4}$$

$$T_{\mathrm{Ce}}(\varphi) = h_{\mathrm{GR}} m a_y \cos\varphi\,. \tag{4.5}$$

Besides the two external force influences, the forces of the chassis elements also act on the vehicle body. In the present case, these are composed of the spring force F_{S}, the damper force F_{D} and the force resulting from the stabilizer F_{St}. The latter two are actively influenced by the control system, while the spring operates as a passive suspension element. The forces of the chassis in relation to the roll motion are accordingly based on

$$F_{\mathrm{D},\varphi,ij}(\varphi) = d_{ij} s_{\mathrm{D},i} \dot{\varphi} \cos\varphi, \tag{4.6}$$

$$F_{\mathrm{S},\varphi,i}(\varphi) = c_{\mathrm{S},i} s_{\mathrm{S},i} \sin\varphi\,, \tag{4.7}$$

$$F_{\mathrm{St},i} = \frac{T_i}{2 s_{\mathrm{St},i}}. \tag{4.8}$$

Here, $s_{\mathrm{D},i}$, $s_{\mathrm{S},i}$ and $s_{\mathrm{St},i}$ represent the distance from the respective points of force application of the damper, the spring and the stabilizer to the center plane of the vehicle. The spring constant $c_{\mathrm{S},i}$ determines the characteristic behavior of the spring. In addition, the damping factor d_{ij} and the counter roll torque T_i denote the variables represented by the actuator models, via which the roll behavior is systematically controlled. The roll rate is defined by $\dot{\varphi}$. The index i further indicates which vehicle axle is considered:

$$i \in \{\mathrm{f}, \mathrm{r}\}. \tag{4.9}$$

The index value f indicates the front axle whereas the index value r indicates the rear axle. In addition to the index i, the index j indicates which side of the vehicle is involved. The index value l denotes the left side of the vehicle and the index value r the right side of the vehicle:

$$j \in \{\mathrm{l}, \mathrm{r}\}. \tag{4.10}$$

The counter roll torque T_i can be determined by the stabilizer geometry using the stabilizer torque $T_{\mathrm{St},i}$

$$T_i = \frac{a_{\mathrm{St},i}}{b_{\mathrm{St},i}} T_{\mathrm{St},i}. \tag{4.11}$$

In this context, $a_{\mathrm{St},i}$ denotes the effective length and $b_{\mathrm{St},i}$ the lever arm of the stabilizer. Taking into account the lever arms of the chassis forces to the roll center, the principle of angular momentum for the rolling motion of the vehicle body can be set up, which is used to describe the roll behavior based on physical knowledge:

$$\begin{aligned}\ddot{\varphi}_{\mathrm{P}}(k) = \frac{1}{J_{xx}}\Big[&h_{\mathrm{GR}} m a_y(k)\cos\varphi_{\mathrm{P}}(k) + h_{\mathrm{GR}} m g \sin\varphi_{\mathrm{P}}(k) - T_{\mathrm{f}}(k) - T_{\mathrm{r}}(k)\\ &- 2\left(s_{\mathrm{S,f}}^2 c_{\mathrm{S,f}} + s_{\mathrm{S,r}}^2 c_{\mathrm{S,r}}\right)\sin\varphi_{\mathrm{P}}(k)\\ &- \left(\left(d_{\mathrm{fl}}(k) + d_{\mathrm{fr}}(k)\right)s_{\mathrm{D,f}}^2\right)\dot{\varphi}_{\mathrm{P}}(k)\cos\varphi_{\mathrm{P}}(k)\\ &- \left(\left(d_{\mathrm{rl}}(k) + d_{\mathrm{rr}}(k)\right)s_{\mathrm{D,r}}^2\right)\dot{\varphi}_{\mathrm{P}}(k)\cos\varphi_{\mathrm{P}}(k)\Big].\end{aligned} \tag{4.12}$$

Therefore, the variables describing the roll behavior, the roll acceleration $\ddot{\varphi}_{\mathrm{P}}$, the roll rate $\dot{\varphi}_{\mathrm{P}}$ and the roll angle φ_{P} are labeled with the index P. The roll acceleration $\ddot{\varphi}_{\mathrm{P}}$ at time $t = k$ is determined by transforming the principle of angular momentum. The calculation is based on quantities at $t = k$. J_{xx} denotes the moment of inertia of the vehicle body around the longitudinal axis. Based on the roll acceleration $\ddot{\varphi}_{\mathrm{P}}(k)$, the roll rate $\dot{\varphi}_{\mathrm{P}}(k+1)$ and the roll angle $\varphi_{\mathrm{P}}(k+1)$ can be estimated by integration respectively double integration. The explicit Euler method is used for the discrete integration, (Butcher, 2016):

$$\dot{\varphi}_{\mathrm{P}}(k+1) = \dot{\varphi}_{\mathrm{P}}(k) + \ddot{\varphi}_{\mathrm{P}}(k) t_{\mathrm{S}}, \tag{4.13}$$

$$\varphi_{\mathrm{P}}(k+1) = \varphi_{\mathrm{P}}(k) + \dot{\varphi}_{\mathrm{P}}(k) t_{\mathrm{S}}. \tag{4.14}$$

The fixed step size for the physical estimation of the roll behavior is $t_{\mathrm{S}} = 0.001$ s. The input quantities into the physical model regarding the estimation of the roll behavior are listed in Table 4.1.

Table 4.1 Input Quantities Physical Model – Roll Behavior Estimation

Input Quantity	**Unit**
Counter Roll Torques T_i	Nm
Damping Factors d_{ij}	Ns/m
Lateral Acceleration a_y	m/s²

4.1.2 Pitch Behavior

For the physical description of the pitch behavior a non-linear pitch model is set up. Analogous to the setup of the non-linear roll model, the vehicle body is cut free to derive the non-linear pitch model. In this case, the free cut is done in the x-z plane.

The following assumptions are made:

- A quasi-stationary balance of forces acts in the longitudinal direction.
- The geometry of the chassis does not alter under the impact of the applied forces.
- The force F_A due to the longitudinal acceleration a_x acts as an external force.
- The mass of the vehicle body m is concentrated at the center of gravity.
- The left and right side are front and rear axle are merged in the vehicle center plane.

The resulting free cut of the vehicle body is shown in Figure 4.2.

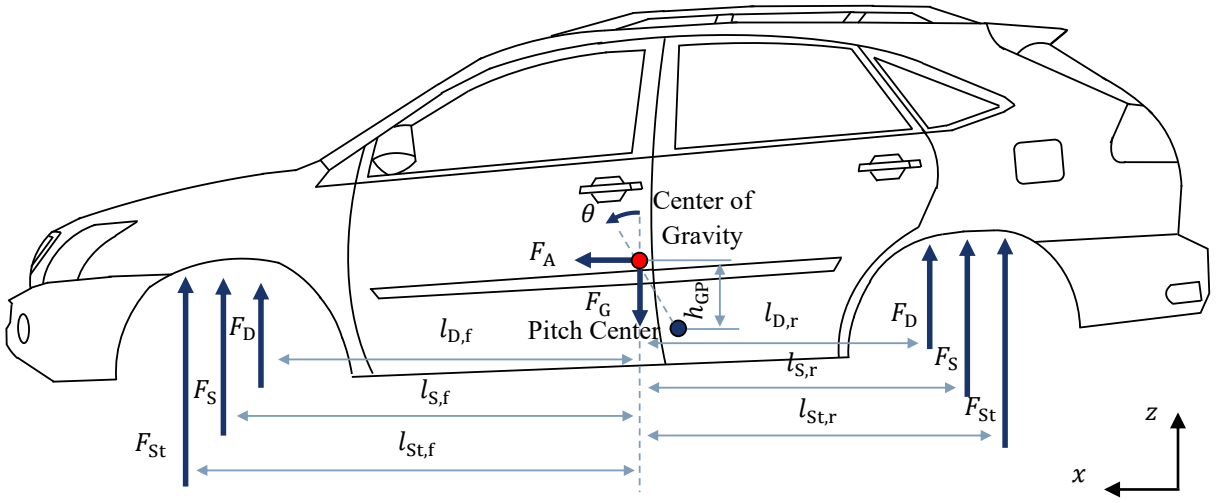

Figure 4.2 Pitch Model – Free Cut

In addition to the gravitational force F_G, the force F_A resulting from the longitudinal acceleration of the vehicle affects the vehicle body as an external influence factor:

$$F_A = ma_x. \tag{4.15}$$

The longitudinal acceleration of the vehicle is given by a_x. The two external forces act via the lever arm h_{GP} on the pitching motion of the vehicle body. h_{GP} denotes the distance between the height of the center of gravity h_G and the height of the pitch center h_P

$$h_{GP} = h_G - h_P. \tag{4.16}$$

Taking into account the lever arm h_{GP}, the gravitational and acceleration forces result in dependency of the pitch angle θ in two corresponding torques $T_{G,\theta}$ and T_A, which influence the pitch behavior of the vehicle body:

$$T_{G,\theta}(\theta) = h_{GP} mg \sin\theta, \tag{4.17}$$

$$T_A(\theta) = h_{GP} ma_x \cos\theta\,. \tag{4.18}$$

In addition to the external force influences, the forces resulting from the chassis elements further affect the pitching motion of the vehicle body.

The damper forces $F_{\mathrm{D},\theta,ij}$ and spring forces $F_{\mathrm{S},\theta,i}$ are formulated as a function of the present pitch behavior:

$$F_{\mathrm{D},\theta,ij}(\theta) = d_{ij} l_{\mathrm{D},i} \dot{\theta} \cos\theta, \tag{4.19}$$

$$F_{\mathrm{S},\theta,i}(\theta) = c_{\mathrm{S},i} l_{\mathrm{S},i} \sin\theta\,. \tag{4.20}$$

The horizontal distances from the application points of the chassis element forces to the center of gravity plane are defined by $l_{\mathrm{D},i}$, $l_{\mathrm{S},i}$ and $l_{\mathrm{St},i}$. As a result the pitch acceleration $\ddot{\theta}_{\mathrm{P}}$ is

$$\begin{aligned}\ddot{\theta}_{\mathrm{P}}(k) = \frac{1}{J_{yy}} \Bigg[& h_{\mathrm{GP}} m a_x(k) \cos\theta_{\mathrm{P}}(k) + h_{\mathrm{GP}} m g \sin\theta_{\mathrm{P}}(k) \\ & - 2\left(l_{\mathrm{S,f}}^2 c_{\mathrm{S,f}} + l_{\mathrm{S,r}}^2 c_{\mathrm{S,r}}\right) \sin\theta_{\mathrm{P}}(k) - T_{\mathrm{f}}(k) \frac{l_{\mathrm{St,f}}}{s_{\mathrm{St,f}}} - T_{\mathrm{r}}(k) \frac{l_{\mathrm{St,r}}}{s_{\mathrm{St,r}}} \\ & - \left(\left(d_{\mathrm{fl}}(k) + d_{\mathrm{fr}}(k)\right) l_{\mathrm{D,f}}^2\right) \dot{\theta}_{\mathrm{P}}(k) \cos\theta_{\mathrm{P}}(k) \\ & - \left(\left(d_{\mathrm{rl}}(k) + d_{\mathrm{rr}}(k)\right) l_{\mathrm{D,r}}^2\right) \dot{\theta}_{\mathrm{P}}(k) \cos\theta_{\mathrm{P}}(k) \Bigg].\end{aligned} \tag{4.21}$$

By applying the principle of angular momentum to the vehicle body regarding the pitch center, the pitch acceleration $\ddot{\theta}_{\mathrm{P}}$ at the time $t = k$ can be calculated. The moment of inertia around the lateral axis is defined as J_{yy}. Based on this pitch acceleration $\ddot{\theta}_{\mathrm{P}}(k)$, the pitch rate $\dot{\theta}_{\mathrm{P}}(k+1)$ and the pitch angle $\theta_{\mathrm{P}}(k+1)$ can be determined by single respectively double integration:

$$\dot{\theta}_{\mathrm{P}}(k+1) = \dot{\theta}_{\mathrm{P}}(k) + \ddot{\theta}_{\mathrm{P}}(k) t_{\mathrm{S}}, \tag{4.22}$$

$$\theta_{\mathrm{P}}(k+1) = \theta_{\mathrm{P}}(k) + \dot{\theta}_{\mathrm{P}}(k) t_{\mathrm{S}}. \tag{4.23}$$

Analogous to the physical roll estimation, the explicit Euler method is used as the integration method. The input quantities used for the physical estimation of the pitch behavior are shown in Table 4.2.

Table 4.2 Input Quantities Physical Model –Pitch Behavior Estimation

Input Quantity	**Unit**
Counter Roll Torques T_i	Nm
Damping Factors d_{ij}	Ns/m
Longitudinal Acceleration a_x	m/s²

4.1.3 Side-Slip Angle

In addition to the roll and pitch behavior, it is further required to estimate the side-slip angle of the vehicle. The single-track model provides a physical description of vehicle behavior with respect to the side-slip angle, (Schramm et al., 2020, Sieberg et al., 2021b).

The following assumptions are made to generate the single-track model:

- The velocity of the vehicle's center of gravity is considered constant along the longitudinal axis of its trajectory.
- Longitudinal tire forces are neglected.
- The trail and the aligning torque due to slip angles are neglected.
- The mass of the vehicle body m is concentrated at the center of gravity.
- The front and rear tires are merged in the vehicle center plane.

The single-track model in the x-y plane resulting from these assumptions is shown in Figure 4.3.

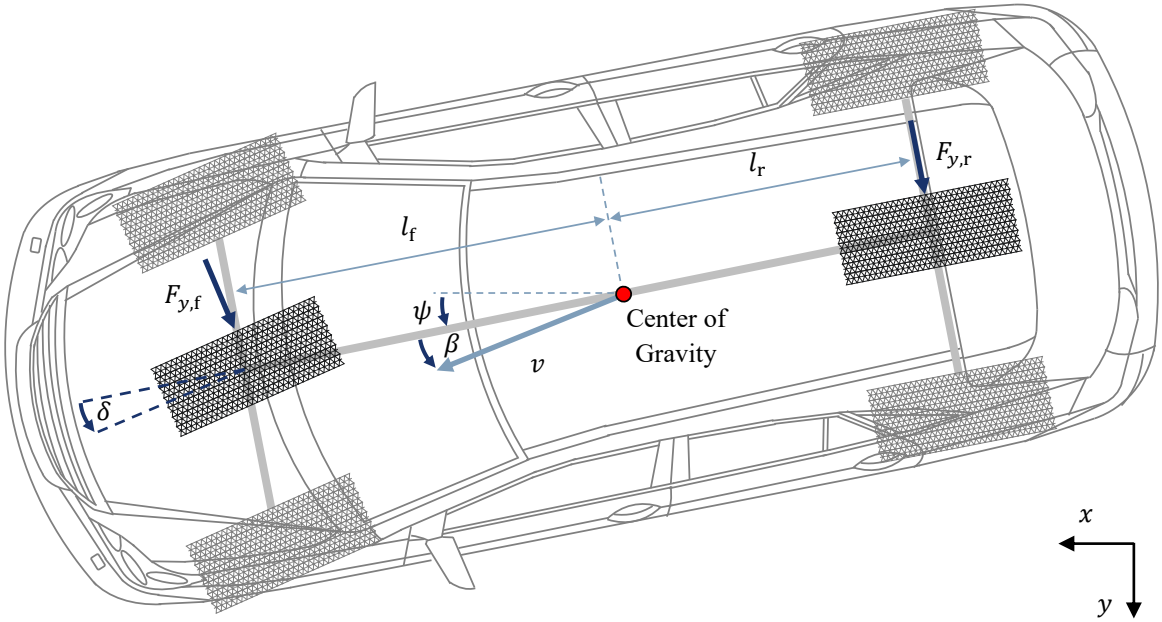

Figure 4.3 Single-Track Model

In order to achieve the physical estimation of the side-slip angle β, Newton's principle for the lateral direction of the vehicle is first established using Figure 4.3:

$$mv(\dot{\psi} + \dot{\beta})\cos\beta = \cos\delta\, F_{y,\mathrm{f}} + F_{y,\mathrm{r}}. \tag{4.24}$$

Here, $\dot{\psi}$ denotes the yaw rate and $\dot{\beta}$ the time derivative of the side-slip angle. The steering angle at the front axle is represented by δ. The steering angle δ can be calculated from the steering wheel angle δ_{SW} using the steering ratio i_{SR}. The lateral forces at the front and rear axle are $F_{y,\mathrm{f}}$ and $F_{y,\mathrm{r}}$, respectively. These are the result of the addition of the lateral forces acting on the wheels of an axle:

$$F_{y,\mathrm{f}} = F_{y,\mathrm{fl}} + F_{y,\mathrm{fr}}, \tag{4.25}$$

$$F_{y,\mathrm{r}} = F_{y,\mathrm{rl}} + F_{y,\mathrm{rr}}. \tag{4.26}$$

The lateral tire forces $F_{y,ij}$ can be determined in a simplified way by the relationship between the cornering stiffness $c_{\alpha,ij}$ and the slip angle α_{ij}. In the present model the cornering stiffness $c_{\alpha,ij}$ is not constant but depends on the respective wheel load $F_{z,ij}$.

$$F_{y,ij} = c_{\alpha,ij}\left(F_{z,ij}\right)\alpha_{ij} \tag{4.27}$$

The relationship between cornering stiffness and wheel load is shown qualitatively in Figure 4.4. A degressive characteristic is given.

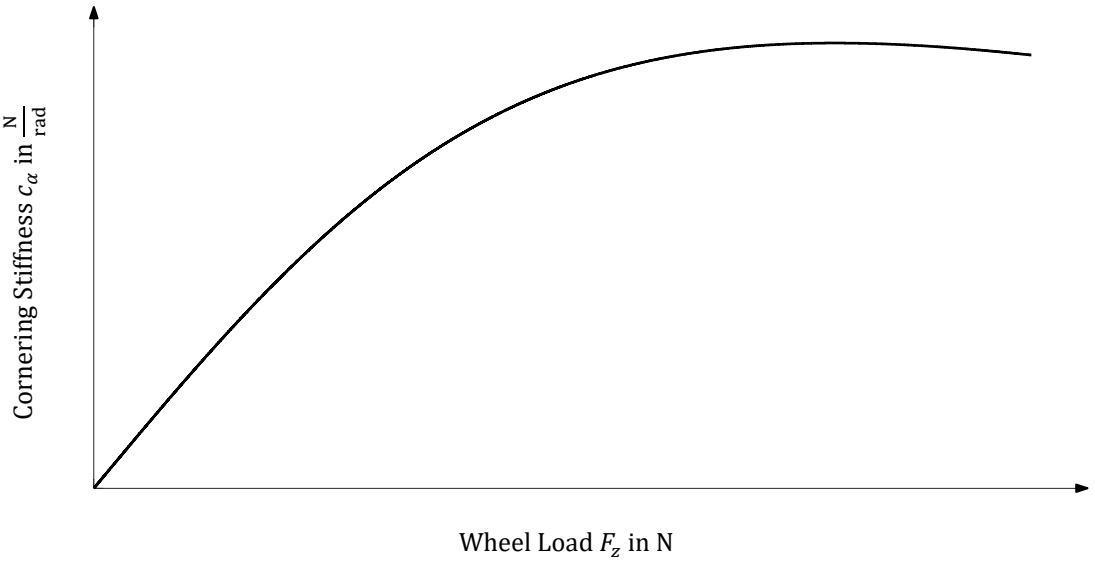

Figure 4.4 Relationship between the Cornering Stiffness and the Wheel Load

A semi-empirical approach according to (Pacejka, 2006) is used to map this degressive dependency between cornering stiffness and wheel load. This kind of description expresses the relationship by means of mathematical equations, which are parameterized with data obtained by empirical measurements

$$c_{\alpha,ij} = c_{\mathrm{T1}} c_{\mathrm{T2}} F_{z0,ij} \sin\left(2 \arctan\left(\frac{F_{z,ij}}{c_{\mathrm{T2}} F_{z0,ij}}\right)\right). \tag{4.28}$$

$F_{z0,ij}$ represents the nominal wheel load, which is determined under static conditions. The parameters c_{T1} and c_{T2} result from a parameter optimization, which is done to correspond to the existing tire characteristics. The tire characteristics result from the stored tire data in IPG CarMaker.

To determine the cornering stiffness the corresponding wheel load is required. The wheel load is composed of a static part, which only depends on the weight distribution, and a variable part. The chassis elements affect the variable part of the wheel load, (Sieberg et al., 2021b).

Due to the common reference to lateral dynamics, the forces of the chassis elements are specified depending on the roll behavior, (4.6) - (4.8):

$$F_{z,\mathrm{fl}} = \frac{l_\mathrm{r}}{l_\mathrm{f}+l_\mathrm{r}}\left(0.5mg - d_\mathrm{fl}s_{\mathrm{D,f}}\,\dot{\varphi}_\mathrm{P}\cos\varphi_\mathrm{P} - s_{\mathrm{S,f}}c_{\mathrm{S,f}}\sin\varphi_\mathrm{P} - \frac{1}{2s_{\mathrm{St,f}}}T_\mathrm{f}\right), \tag{4.29}$$

$$F_{z,\mathrm{fr}} = \frac{l_\mathrm{r}}{l_\mathrm{f}+l_\mathrm{r}}\left(0.5mg + d_\mathrm{fr}s_{\mathrm{D,f}}\,\dot{\varphi}_\mathrm{P}\cos\varphi_\mathrm{P} + s_{\mathrm{S,f}}c_{\mathrm{S,f}}\sin\varphi_\mathrm{P} + \frac{1}{2s_{\mathrm{St,f}}}T_\mathrm{f}\right), \tag{4.30}$$

$$F_{z,\mathrm{rl}} = \frac{l_\mathrm{f}}{l_\mathrm{f}+l_\mathrm{r}}\left(0.5mg - d_\mathrm{rl}s_{\mathrm{D,r}}\,\dot{\varphi}_\mathrm{P}\cos\varphi_\mathrm{P} - s_{\mathrm{S,r}}c_{S,\mathrm{r}}\sin\varphi_\mathrm{P} - \frac{1}{2s_{\mathrm{St,r}}}T_\mathrm{r}\right), \tag{4.31}$$

$$F_{z,\mathrm{rr}} = \frac{l_\mathrm{f}}{l_\mathrm{f}+l_\mathrm{r}}\left(0.5mg + d_\mathrm{rr}s_{\mathrm{D,r}}\,\dot{\varphi}_\mathrm{P}\cos\varphi_\mathrm{P} + s_{\mathrm{S,r}}c_{\mathrm{S,r}}\sin\varphi_\mathrm{P} + \frac{1}{2s_{\mathrm{St,r}}}T_\mathrm{r}\right). \tag{4.32}$$

Here, l_f and l_r denote the distances between the center of gravity and the front respectively the rear axle. Based on (4.29) - (4.32), the cornering stiffness $c_{\alpha,ij}$ of the individual wheels can be determined. Assuming that the slip angles at one axle are equal, the cornering stiffness of the merged tire at the axle can be determined by the addition of the corresponding cornering stiffnesses

$$c_{\alpha,\mathrm{f}} = c_{\alpha,\mathrm{fl}} + c_{\alpha,\mathrm{fr}}, \tag{4.33}$$

$$c_{\alpha,\mathrm{r}} = c_{\alpha,\mathrm{rl}} + c_{\alpha,\mathrm{rr}}. \tag{4.34}$$

The slip angles at the front and rear axles α_f and α_r can be determined in a simplified way by assuming small side-slip and steering angles, (Schramm et al., 2020):

$$\alpha_\mathrm{f} = \delta - \beta - l_\mathrm{f}\frac{\dot{\psi}}{v}, \tag{4.35}$$

$$\alpha_\mathrm{r} = -\beta + l_\mathrm{r}\frac{\dot{\psi}}{v}. \tag{4.36}$$

Using the relationship of (4.33) and (4.34) as well as substituting (4.35) and (4.36) in (4.27), the time derivative of the side-slip angle $\dot{\beta}_\mathrm{P}$ at time $t = k+1$ can be determined with the aid of Newton's principle for the lateral direction (4.24). The index P consistently indicates the underlying estimation based on physical model knowledge.

$$\begin{aligned}\dot{\beta}_\mathrm{P}(k) = &\left(-v(k) - \frac{1}{v(k)}\frac{c_{\alpha,\mathrm{f}}(k)\,l_\mathrm{f} + c_{\alpha,\mathrm{r}}(k)\,l_\mathrm{r}}{m}\right)\frac{\dot{\psi}(k)}{v(k)}\\ &-\left(\frac{1}{v(k)}\frac{c_{\alpha,\mathrm{f}}(k)+c_{\alpha,\mathrm{r}}(k)}{m}\right)\beta_\mathrm{P}(k) + \left(\frac{1}{v(k)}\frac{c_{\alpha,\mathrm{f}}(k)}{m}\right)\delta(k)\end{aligned} \tag{4.37}$$

The yaw rate $\dot{\psi}$ and the velocity v are external input variables and are available due to the existing sensor equipment.

By integrating $\dot{\beta}_{\mathrm{P}}(k)$ with the explicit Euler method, the side-slip angle $\beta_{\mathrm{P}}(k+1)$ is determined with

$$\beta_{\mathrm{P}}(k+1) = \beta_{\mathrm{P}}(k) + \dot{\beta}_{\mathrm{P}}(k) t_{\mathrm{S}}. \tag{4.38}$$

Table 4.3 summarizes the input quantities of the physical estimation model regarding the side-slip angle.

Table 4.3 Input Quantities Physical Model –Side-Slip Angle Estimation

Input Quantity	**Unit**
Counter Roll Torques T_i	Nm
Damping Factors d_{ij}	Ns/m
Estimated Roll Angle φ_{P}	rad
Estimated Roll Rate $\dot{\varphi}_{\mathrm{P}}$	rad/s
Steering Angle δ	rad
Velocity v	m/s
Yaw Rate $\dot{\psi}$	rad/s

4.2 State Estimation Based on Artificial Neural Networks

Alongside the approach of theoretical modeling, experimental modeling can be conducted to create state estimators. In contrast to theoretical modeling, experimental modeling only represents the transfer behavior of a system without explicit consideration of physical laws respectively model knowledge. In the course of this thesis, artificial neural networks are used as a method of experimental modeling to build the state estimation.

In order to enable the artificial neural network to map the vehicle dynamic behavior and accomplish the task of state estimation, the transfer behavior needs to be trained. The training is done in Python using the open source deep learning library Keras, (Gulli and Pal, 2017). The data stream oriented framework TensorFlow is used as a backend, (Abadi et al., 2016). The driving maneuvers described in Section 3.5 are used as the database.

The state estimation of the vehicle dynamics variables is a time series dependent modeling task. Based on this, recurrent artificial neural networks are used to accomplish the required functions. In order to realize these recurrent artificial neural networks, a sequencing of the database is required. Depending on a defined lookback τ_{Ann}, a sequence is created for each time step, which describes the past course of variables. Thereby, the lookback τ_{Ann} defines the number of previous time steps within a sequence. Besides the sequencing, a normalization of the input

variables of the artificial neural network is performed. The normalization avoids a varying impact of different orders of magnitude by the input quantities, (Ioffe and Szegedy, 2015). The normalization method used is min-max-normalization:

$$z_{i,j,\mathrm{N}} = \frac{\left(z_{i,j} - \min(\boldsymbol{z_i})\right)(b_\mathrm{N} - a_\mathrm{N})}{\max(\boldsymbol{z_i}) - \min(\boldsymbol{z_i})}. \tag{4.39}$$

In this process a single value $z_{i,j}$ of the input quantity vector $\boldsymbol{z}$ is scaled to the value range $[a_\mathrm{N}, b_\mathrm{N}]$:

$$z_{i,j,\mathrm{N}} \in \{[a_\mathrm{N}, b_\mathrm{N}]\}. \tag{4.40}$$

After the training, the artificial neural network is exported and a corresponding MATLAB & Simulink model is created.

In the following, the state estimators based on artificial neural networks are presented. As a consistent approach to the physical state estimators, one artificial neural network is created for each behavior regarding the vehicle dynamics segments. A hyperparameter optimization is performed initially. Subsequently, the individual artificial neural networks are introduced, which have been parameterized with optimal hyperparameters.

4.2.1 Hyperparameter Optimization

The optimal hyperparameters for the artificial neural networks are determined by a hyperparameter optimization. Hyperparameters in general represent the parameters of an artificial neural network which are not adjusted during training. Nevertheless, hyperparameters affect the quality of the artificial neural network and the speed of the training process.

In the course of this thesis, a sequential model-based global optimization is used for the hyperparameter optimization. This approach is part of informed, model-based hyperparameter optimization methods. This informed method is significantly superior to uninformed methods like grid search or random search, (Bergstra et al., 2011). Within the sequential model-based global optimization method, the objective function of the hyperparameter optimization is modeled by a probabilistic model. The probabilistic model is built and updated based on previously evaluated hyperparameter configurations as well as all prior available information. An acquisition function is used to select the next hyperparameter configuration. This function is employed to determine the predictive distribution of the probabilistic model for hyperparameter configurations. The acquisition function is therefore maximized over the search space so that the optimal hyperparameter configuration can be determined, (Hutter et al., 2015).

The hyperparameters that are optimized by the sequential model-based global optimization are listed in Table 4.4. These include besides the learning rate, the number of recurrent layers, the number of neurons in each recurrent layer and also the lookback of these layers. The hyperparameters of the number of neurons and the lookback are consistent for all recurrent layers. An

additional hyperparameter concerns the regularization. Furthermore, the search space for the hyperparameters is listed in Table 4.4.

Table 4.4 Hyperparameter Optimization Artificial Neural Networks – Search Space

Parameter	**Range**	
Learning Rate	0.0001	0.1
Lookback	3	10
Number of Recurrent Layers	1	4
Number of Neurons within one Recurrent Layer	Number of Input Quantities	150
Regularization	Dropout, L2, None	

In addition to the hyperparameters that are adjusted during optimization, the artificial neural network is further characterized by parameters that are fixed. These include the batch size, the evaluation metric during training, the number of epochs as well as the composition of the output layer. The recurrent layers are realized by long short-term memory layers, (Hochreiter and Schmidhuber, 1997). The initialization is done by the Glorot uniform method, (Glorot and Bengio, 2010). The optimization during the training is conducted by the Adam algorithm, (Kingma and Ba, 2015). These parameters are summarized in Table 4.5.

Table 4.5 Hyperparameter Optimization Artificial Neural Networks – Fixed Parameters

Parameter	**Value**
Batch Size	1024
Initialization	Glorot Uniform
Metric	Mean Absolute Error
Number of Epochs	50
Optimizer Training	Adam
Output Layer	Fully Connected Dense Layer with Linear Activation Function
Type of Recurrent Layers	Long Short-Term Memory

The sequential model-based global optimization is realized by the python library Hyperopt, (Bergstra et al., 2015). The expected improvement is utilized as the acquisition function, (Schonlau et al., 1998). Thereby, the tree-structured parzen estimator is applied. In contrast to the Gaussian process, the a priori distribution $p(f_{\mathrm{HP}}|\boldsymbol{\lambda}_{\mathrm{HP}})$ is not set up directly by the tree-structured parzen estimator but via the likelihood function using $p(\boldsymbol{\lambda}_{\mathrm{HP}}|f_{\mathrm{HP}})$ and $p(f_{\mathrm{HP}})$

$$p(f_{\mathrm{HP}}|\boldsymbol{\lambda}_{\mathrm{HP}}) = \frac{p(\boldsymbol{\lambda}_{\mathrm{HP}}|f_{\mathrm{HP}})}{p(\boldsymbol{\lambda}_{\mathrm{HP}})} p(f_{\mathrm{HP}}). \tag{4.41}$$

$\boldsymbol{\lambda}_{\mathrm{HP}}$ represents the observed hyperparameter configurations and f_{HP} their corresponding loss. $p(\boldsymbol{\lambda}_{\mathrm{HP}}|f_{\mathrm{HP}})$ is characterized within the tree-structured parzen estimator by the densities $l_{\mathrm{HP}}(\boldsymbol{\lambda}_{\mathrm{HP}})$ and $g_{\mathrm{HP}}(\boldsymbol{\lambda}_{\mathrm{HP}})$, which cover the configuration space:

$$p(\boldsymbol{\lambda}_{\mathrm{HP}}|f_{\mathrm{HP}}) = \begin{cases} l_{\mathrm{HP}}(\boldsymbol{\lambda}_{\mathrm{HP}}) & \text{if } f_{\mathrm{HP}} < f_{\mathrm{HP}}^{*} \\ g_{\mathrm{HP}}(\boldsymbol{\lambda}_{\mathrm{HP}}) & \text{if } f_{\mathrm{HP}} \geq f_{\mathrm{HP}}^{*} \end{cases}. \tag{4.42}$$

The density $l_{\mathrm{HP}}(\boldsymbol{\lambda}_{\mathrm{HP}})$ is created by considering hyperparameter configurations $\boldsymbol{\lambda}_{\mathrm{HP}}$ which result in a loss less than the threshold f_{HP}^{*}. The density $g_{\mathrm{HP}}(\boldsymbol{\lambda}_{\mathrm{HP}})$ represents the remaining configurations. Within the sequential model-based global optimization the expected improvement $EI(\boldsymbol{\lambda}_{\mathrm{HP}})$ of the hyperparameter configurations $\boldsymbol{\lambda}_{\mathrm{HP}}$ is maximized:

$$EI(\boldsymbol{\lambda}_{\mathrm{HP}}) = \int_{-\infty}^{f_{\mathrm{HP}}^{*}} (f_{\mathrm{HP}}^{*} - f_{\mathrm{HP}}) \frac{p(\boldsymbol{\lambda}_{\mathrm{HP}}|f_{\mathrm{HP}})p(f_{\mathrm{HP}})}{p(\boldsymbol{\lambda}_{\mathrm{HP}})} df_{\mathrm{HP}}. \tag{4.43}$$

To maximize the expected improvement $EI(\boldsymbol{\lambda}_{\mathrm{HP}})$, hyperparameter configurations $\boldsymbol{\lambda}_{\mathrm{HP}}$ having a high probability of belonging to $l_{\mathrm{HP}}(\boldsymbol{\lambda}_{\mathrm{HP}})$ and a low probability of belonging to $g_{\mathrm{HP}}(\boldsymbol{\lambda}_{\mathrm{HP}})$ are recommended. The optimization is performed iteratively, whereby the configuration $\boldsymbol{\lambda}_{\mathrm{HP}}^{*}$ with the highest expected improvement $EI(\boldsymbol{\lambda}_{\mathrm{HP}}^{*})$ found in each iteration step is also taken into account for the next iteration step. (Bergstra et al., 2011)

The driving maneuvers presented in Section 3.5 serve as the database for the hyperparameter optimization. In order to reduce the time required for optimization, a representative partial data set is used. For this purpose, 25 test drives are randomly selected per maneuver. Thus the database for the hyperparameter optimization comprises 150 driving maneuvers, which corresponds to about 10 % of the total database. In addition, 60 randomly selected driving maneuvers are used as validation data. The quantitative distribution across the individual maneuvers is identical. The sequential model-based global optimization is executed for 50 iterations.

In the following, the artificial neural networks are presented, which execute the state estimation in the three vehicle dynamics areas of rolling, pitching and self-steering behavior.

4.2.2 Roll Angle Estimation

For the estimation of the roll angle, on the one hand the manipulated variables of the vehicle dynamics control are used. Thereby, manipulated variables are summarized under consideration of their impact on the roll behavior.

This results in the total counter-torque T_T as well as the cumulated damping factor on the left d_l respectively right side d_ri of the vehicle as input variables:

$$T_\mathrm{T} = T_\mathrm{f} + T_\mathrm{r}, \tag{4.44}$$

$$d_\mathrm{l} = d_\mathrm{fl} + d_\mathrm{rl}, \tag{4.45}$$

$$d_\mathrm{ri} = d_\mathrm{fr} + d_\mathrm{rr}. \tag{4.46}$$

On the other hand, additional sensor signals are used as input variables. These input variables are explicitly different from the input variables based on sensor data of the respective physical model. This differentiation is made with respect to the mode of operation of hybrid state estimation presented in Section 4.3. The selection is based on expert knowledge. This yields further input variables of the steering wheel angle δ_SW, the velocity v as well as the yaw rate $\dot{\psi}$ of the vehicle. Table 4.6 provides an overview regarding the input variables.

Table 4.6 Input Quantities Artificial Neural Network – Roll Angle Estimation

Input Quantity	**Unit**
Total Counter Roll Torque T_T	Nm
Cumulated Damping Factors d_j	Ns/m
Steering Wheel Angle δ_SW	rad
Velocity v	m/s
Yaw Rate $\dot{\psi}$	rad/s

Inside the search space defined in Table 4.4 the hyperparameter optimization is executed for the composition of these input variables. This optimization is performed for 50 iterations. To evaluate the quality of the hyperparameter optimization, the best found metric is applied, according to (Dewancker et al., 2016). This evaluation metric determines the minimum validation error of the current iteration and all previous iterations. The minimum validation error can then be applied over the iterations and thus across the training process. Within the training of the artificial neural network, the validation error equals the mean absolute error

$$MAE(\varphi, \varphi_\mathrm{Ann}) = \frac{1}{n}\sum_{k=1}^{n} |\varphi(k) - \varphi_\mathrm{Ann}(k)|\,. \tag{4.47}$$

Here φ_Ann represents the roll angle estimated by the artificial neural network and φ indicates the ground truth roll angle. Figure 4.5 illustrates the best foundation metric of the mean absolute error for the training of the artificial neural network with the objective of roll angle estimation. In this context it should be considered that the estimation quantity has been standardized for the hyperparameter optimization.

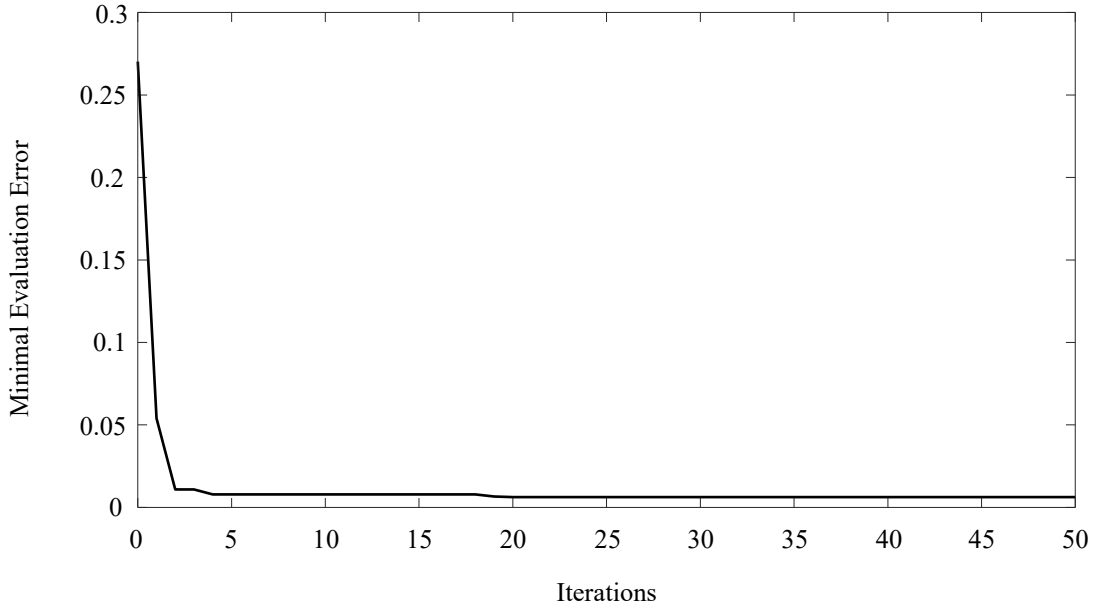

Figure 4.5 Results Sequential Model-Based Optimization – Roll Angle Estimation

The minimum validation error achieved in this hyperparameter optimization occurs in iteration 20. The hyperparameter configuration present at this epoch is listed in Table 4.7. The optimal configuration is based on four recurrent layers with 129 neurons in each layer. The lookback within these layers equals eight time steps. No regularization is performed. The learning rate in the beginning of the training process is 0.00245.

Table 4.7 Hyperparameters– Roll Angle Estimation

Parameter	**Value**
Learning Rate	0.00245
Lookback	8
Number of Recurrent Layers	4
Number of Neurons within one Recurrent Layer	129
Regularization	None

Based on this hyperparameter configuration the final training is performed. The artificial neural network is trained with 70 % of the entire database, which corresponds to 1,056 driving maneuvers, and is validated during the training with 15 % of the database, which corresponds to 226 driving maneuvers. The remaining 226 driving maneuvers are reserved for testing. The number of epochs is 200. During training, the learning rate is reduced if the validation error stagnates over several epochs, according to (Wilson and Martinez, 2001). The learning rate is reduced by 80 % in such a plateau situation. To avoid an overfitting of the artificial neural network, the option to end the training prematurely, thus before the 200 epochs, is selected, (Finnoff et al., 1993). This early stopping of the training is done if the validation error does not

decrease or even increases over several epochs. Figure 4.6 presents the course of the mean absolute error, both for the training and the validation data, over the epochs of the training.

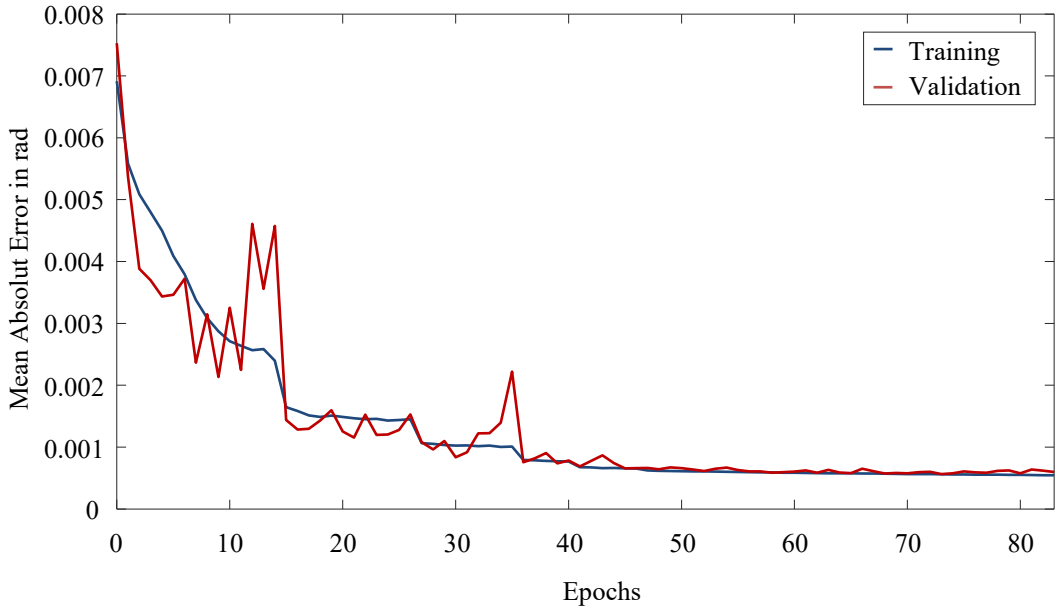

Figure 4.6 Mean Absolut Errors Artificial Neural Network – Roll Angle Estimation

The blue curve depicts the training error and the red curve represents the validation error. The training took place over 83 epochs and was therefore terminated by the option of early stopping to avoid overfitting. Both, training and validation errors, are not further reduced significantly after epoch 60. The mean absolute error for the training data set in the last epoch is 0.00055 rad which corresponds to 0.03151°. For the validation data set, the artificial neural network results in a mean absolute error of 0.00060 rad respectively 0.03438°.

4.2.3 Pitch Angle Estimation

The artificial neural network for the estimation of the pitch angle utilizes on the one hand input variables that represent the manipulated variables. Taking into account the potentials of influence, corresponding manipulated variables are aggregated analogous to the estimation of the roll angle. As a result, the input variables on the basis of the manipulated variables are composed of the counter roll torque acting at the front axle T_f respective rear axle T_r and the damping factors at the front axle d_f respectively rear axle d_r:

$$d_\mathrm{f} = d_\mathrm{fl} + d_\mathrm{fr}, \tag{4.48}$$

$$d_\mathrm{r} = d_\mathrm{rl} + d_\mathrm{rr}. \tag{4.49}$$

Sensor data are used as input variables on the other hand. These input data are composed of the velocity of the vehicle v and the time derivative of this velocity $\frac{dv}{dt}$. Analogous to the roll angle

estimation in Section 4.2, these are different from the input sensor data into the physical model. Table 4.8 lists the input variables of the artificial neural network for estimating the pitch angle.

Table 4.8 Input Quantities Artificial Neural Network – Pitch Angle Estimation

Input Quantity	**Unit**
Counter Roll Torques T_i	Nm
Cumulated Damping Factors d_i	Ns/m
Time Derivative of the Velocity $\frac{dv}{dt}$	m/s²
Velocity v	m/s

For this composition of the input variables, the hyperparameter optimization is performed for 50 iterations. This optimization is executed in the defined hyperparameter search space. As the evaluation criterion for the hyperparameter optimization, the best found metric based on the mean absolute error is used analogous to the remarks on the roll angle estimator.

$$MAE(\theta, \theta_{\text{Ann}}) = \frac{1}{n}\sum_{k=1}^{n} |\theta(k) - \theta_{\text{Ann}}(k)| \,. \tag{4.50}$$

As shown in Figure 4.7, the minimum validation error is plotted over the iterations of the optimization. The output variable, the pitch angle, has been standardized for the hyperparameter optimization likewise.

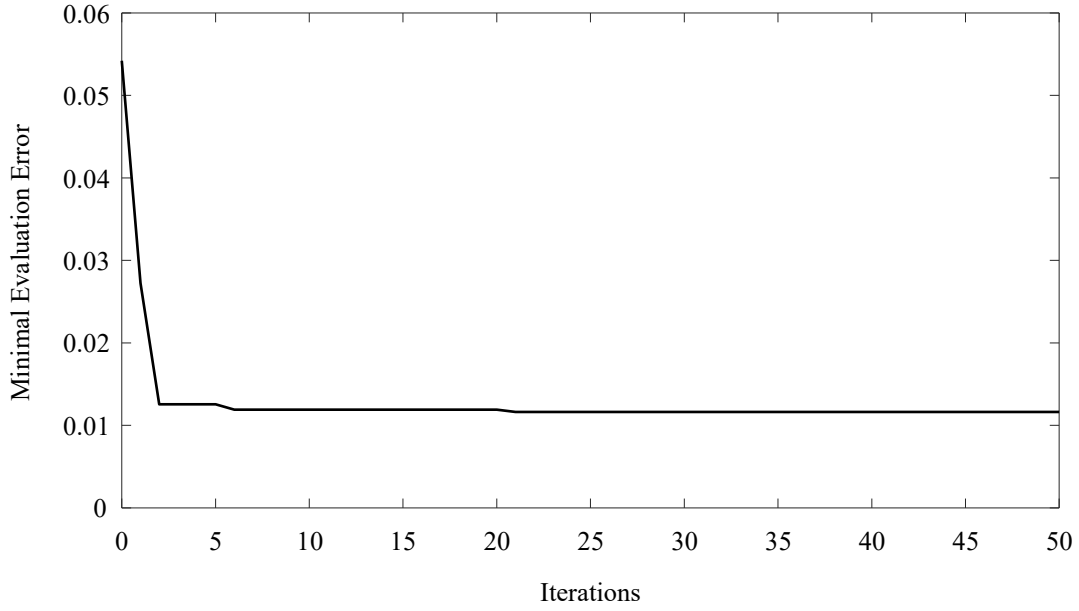

Figure 4.7 Results Sequential Model-Based Optimization – Pitch Angle Estimation

The minimum validation error is achieved in epoch 21 and equals 0.01163. The artificial neural network that generates the minimum validation error is based on two recurrent layers with 115

neurons each and a lookback of eight time steps. Furthermore, the learning rate is 0.00574 and no regularization is applied. An overview of the hyperparameters is given in Table 4.9.

Table 4.9 Hyperparameters– Pitch Angle Estimation

Parameter	Value
Learning Rate	0.00574
Lookback	8
Number of Recurrent Layers	2
Number of Neurons within one Recurrent Layer	115
Regularization	None

This hyperparameter configuration is then used to train the artificial neural network, which is used for pitch angle estimation. Analogous to the training of the roll angle estimator 1,056 respectively 226 driving maneuvers were used for the training respectively validation within the training. Furthermore, the options of reducing the learning rate in case of a stagnating validation error and stopping the training in case of further stagnation or even an increase were used to avoid overfitting. The evaluation metric, the mean absolute error, is plotted over the epochs of the training in Figure 4.8 for both the training data and the validation data.

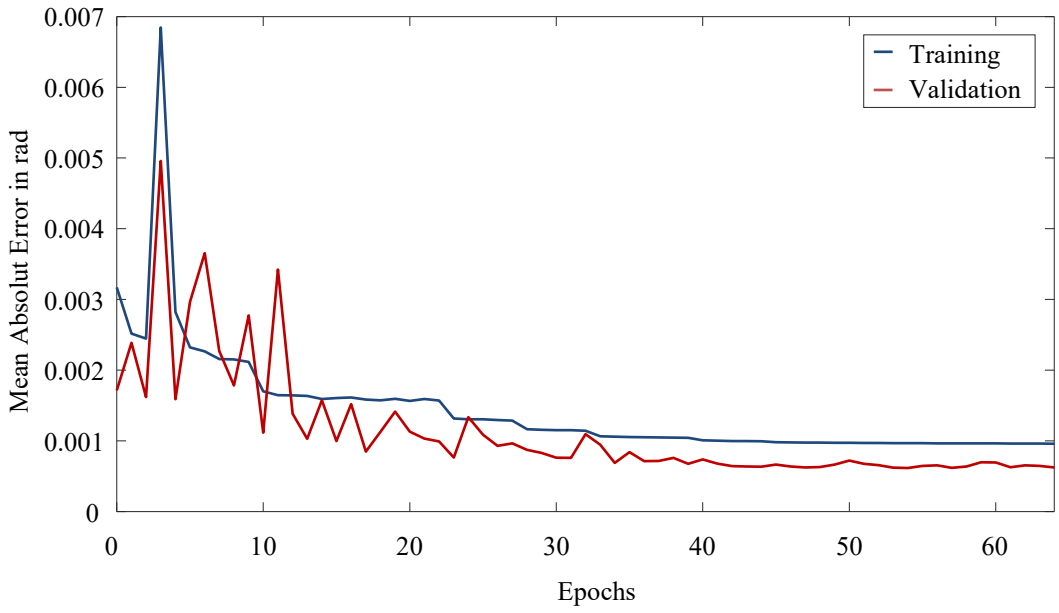

Figure 4.8 Mean Absolut Errors Artificial Neural Network – Pitch Angle Estimation

The training is carried out for 64 epochs before it is terminated to avoid an overfitting. Thereby, a mean absolute error of 0.00096 rad is obtained for the training data set, which corresponds to 0.05500°. In addition, a mean absolute error of 0.00062 rad, which is equivalent to 0.03552°, is achieved for the validation data. One possible reason that the validation error is smaller than

the training error is due to the random selection of validation maneuvers. The validation data set includes mainly driving maneuvers with small longitudinal accelerations respectively decelerations, for which the estimation of the pitch angle is facilitated.

4.2.4 Side-Slip Angle Estimation

For the estimation of the side-slip angle, the manipulated variables likewise serve as input variables for the artificial neural network. These consist of the counter roll torques at the front T_f respectively rear axle T_r as well as the damping factors at the front left d_fl, front right d_fr, rear left d_rl and rear right d_rr. As with the other artificial neural networks, the further sensory input quantities differ from the sensor input data of the physical model for the estimation of the side-slip angle. For the present artificial neural network, the average wheel speed $\bar{n}_\mathrm{V}$ is used in addition to the lateral acceleration a_y:

$$\bar{n}_\mathrm{V} = \frac{1}{4}\left(n_\mathrm{W,fl} + n_\mathrm{W,fr} + n_\mathrm{W,rl} + n_\mathrm{W,rr}\right). \tag{4.51}$$

An overview of the input variables for the side-slip angle estimation is provided in Table 4.10.

Table 4.10 Input Quantities Artificial Neural Network – Side-Slip Angle Estimation

Input Quantity	Unit
Counter Roll Torques T_i	Nm
Damping Factors d_{ij}	Ns/m
Lateral Acceleration a_y	m/s²
Average Wheel Speed $\bar{n}_\mathrm{V}$	1/s

With this setup the hyperparameter optimization is performed. The number of optimization iterations is consistently set to 50. Figure 4.9 shows the minimum validation error over the epochs using the best found metric. Analogous to the previous sequential model-based global optimizations, the output quantity is standardized for the hyperparameter optimization.

$$MAE(\beta, \beta_\mathrm{Ann}) = \frac{1}{n}\sum_{k=1}^{n}\left|\beta(k) - \beta_\mathrm{Ann}(k)\right|. \tag{4.52}$$

The minimum validation error during hyperparameter optimization is achieved with a mean absolute error of 0.00947 in iteration 49. The artificial neural network constructed in this iteration is based on one recurrent layer with 103 neurons and a lookback of eight time steps.

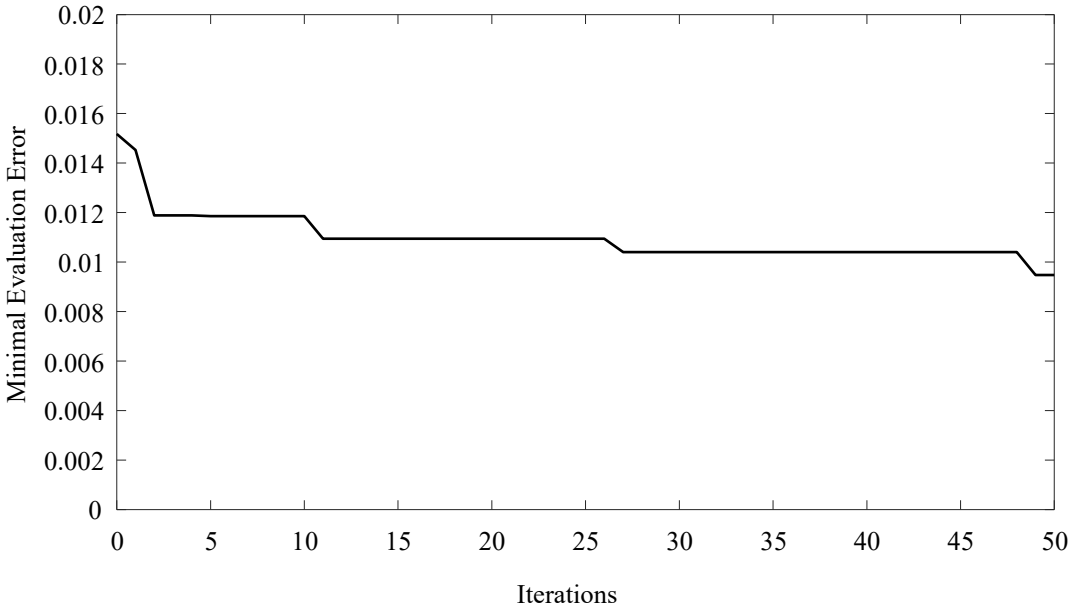

Figure 4.9 Results Sequential Model-Based Optimization – Side-Slip Angle Estimation

The learning rate of the training within this iteration equals 0.01204. Furthermore no regularization is used. Table 4.11 summarizes the results of the hyperparameter optimization.

Table 4.11 Hyperparameters– Side-Slip Angle Estimation

Parameter	**Value**
Learning Rate	0.01204
Lookback	8
Number of Recurrent Layers	1
Number of Neurons within one Recurrent Layer	103
Regularization	None

The training of the artificial neural network is performed with the hyperparameters resulting from this optimization. The database consists of 1,056 maneuvers for training and 226 maneuvers for validation. Furthermore, the already presented options of learning rate reduction on a plateau and of the early stopping are used. Thus overfitting can be avoided. The maximum number of training epochs is defined as 200. Figure 4.10 visualizes the mean absolute errors for the training data set and the validation data set.

The training of the artificial neural network is performed up to epoch 133 until it is terminated by the early stopping option. A minimum training error of 0.00173 rad or 0.09912° as well as a minimum validation error of 0.00195 rad or 0.11173° are achieved.

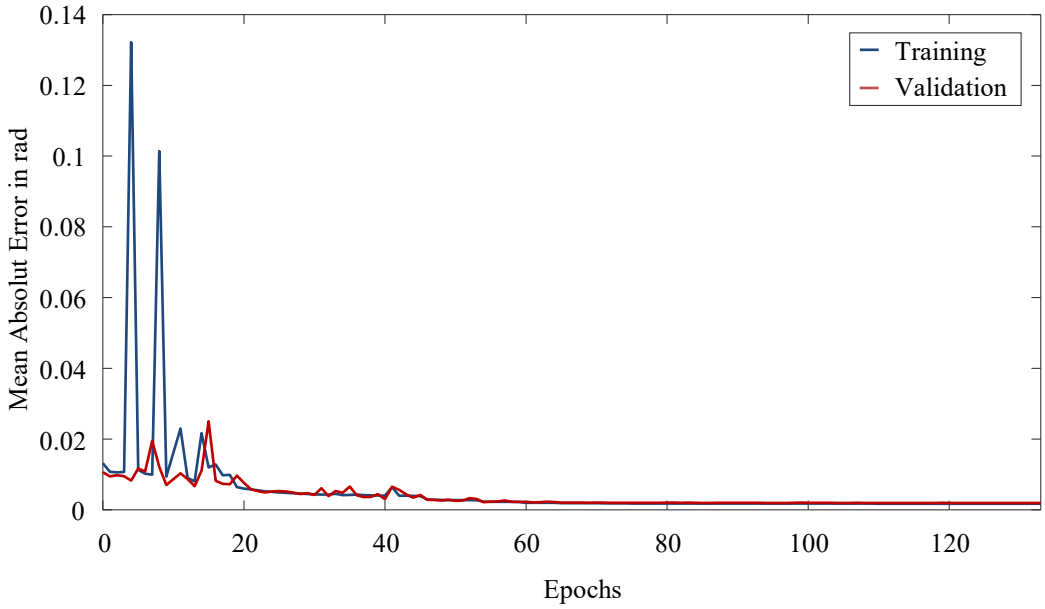

Figure 4.10 Mean Absolut Errors Artificial Neural Network – Side-Slip Angle Estimation

4.3 State Estimation Based on Hybrid Method

Within the hybrid method of state estimation, the physical models presented in Section 4.1 are merged with the artificial neural networks introduced in Section 4.2. (Sieberg et al., 2021a) present a first successful proof of concept of this hybrid method. In a first step the underlying structure of the hybrid method is presented. The determination of the confidence level is introduced, which indicates the degree of confidence in the different types of model. The conversion of the confidence level and thus the targeted fusion of the two estimator models is done by a Kalman filter. Finally, the hybrid method is validated against the physical models and the artificial neural networks in an open-loop operating mode.

4.3.1 Structure

The functional principle of the hybrid method can be divided into three parts. In a first step, the estimation of the vehicle dynamic state y_{Ann} is conducted by the artificial neural network. In a parallel step the input data of the artificial neural network are used to determine the confidence level τ_{HSE}. In a third step, the state estimated by the artificial neural network y_{Ann} is merged and safeguarded with the states from the physical model, taking into account the confidence level τ_{HSE}. The combination is done by an unscented Kalman filter, which takes into account the non-linearities of the physical model. This results finally in an estimated vehicle dynamics state vector $\boldsymbol{x}_{\mathrm{Est}}$ derived from the hybrid state estimations. This state vector $\boldsymbol{x}_{\mathrm{Est}}$ is then forwarded to the predictive control. The structure of the hybrid method is shown in Figure 4.11.

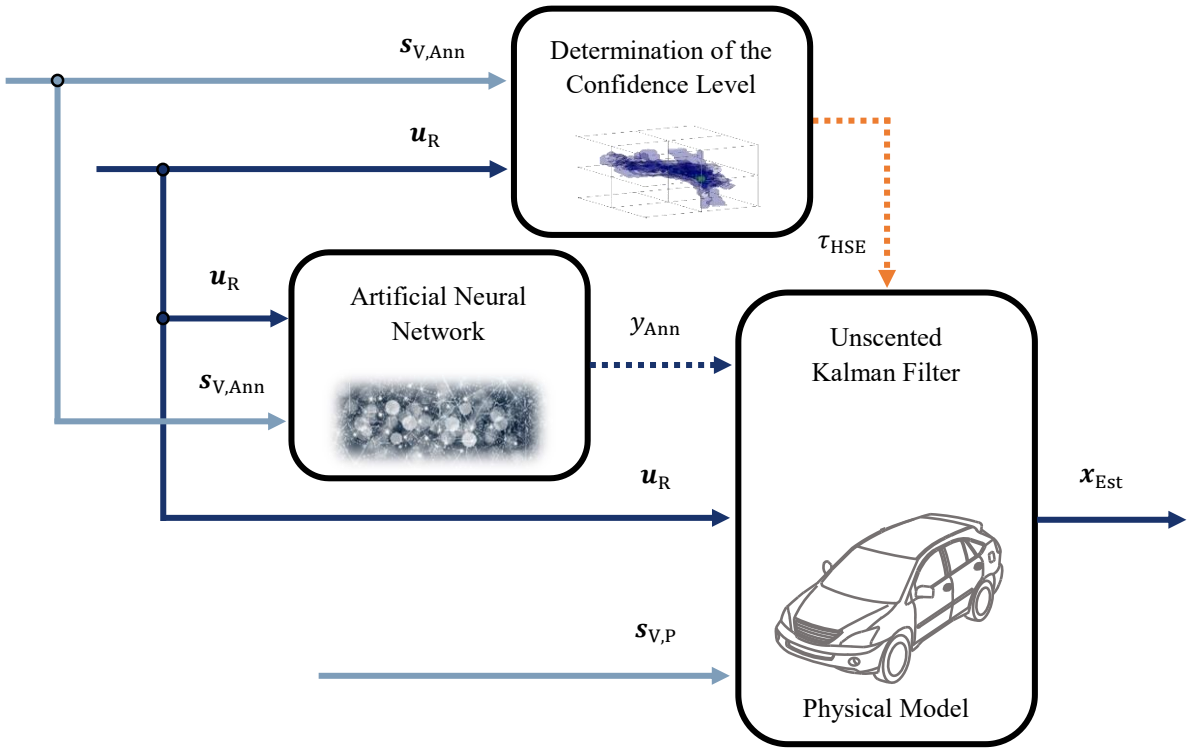

Figure 4.11 Hybrid State Estimation – Structure

The manipulated variables of the actuators $\boldsymbol{u}_R$ are used for both, the state estimators based on the artificial neural networks and the ones based on the physical models. In addition sensor signals are used. An important detail is that the sensor-based input data of the artificial neural networks $\boldsymbol{s}_{V,Ann}$ and of the physical models $\boldsymbol{s}_{V,P}$ are different. Due to this design, redundancies are created within the method, which enable a safe operation of the hybrid state estimation containing the artifcial neural network. In total three hybrid state estimators are thus constructed, one for each estimation target.

4.3.2 Adjustment of the Confidence Level

The most important characteristic of the hybrid method for state estimation is the confidence level τ_{HSE}. On the basis of this indicator it is decided which model is more or even completely trusted. Thus, especially the artificial neural network can be secured. In the following, the method for determining the confidence level τ_{HSE} is presented.

The main objective of the hybrid method is to secure an artificial neural network. Due to the black-box character of such a data-driven model, the internal interactions of these type of models cannot be fully comprehended. Therefore, these type of models are very difficult to secure in a holistic way. To determine the confidence level τ_{HSE}, the input data into the artificial neural network are processed.

Basically, the method relates the input data into the artificial neural network to the data used during the training. The more often the input data have been evaluated during training, the

greater the confidence level. More data correlate with an expected improvement in the quality of the artificial neural network, (Foody and Arora, 1997, Halevy et al., 2009, Sun et al., 2017). The composition of the input data for the individual time steps is deliberately taken into account, as they are interdependent and correlated. Only altogether the single input quantities are able to describe the dynamics at a certain time step.

In order to determine the confidence level, the data used during the training is processed prior to using the hybrid method. An input space is created from this training data. This input space is therefore invariable during the application of the hybrid method. The input space is n_I-dimensional, since the input data into the artificial neural network consists of n_I individual input quantities. The input space is further divided into k_G segments for each input variable, whereby the entire range of each input quantity is covered. This finally results in a grid structure with $k_\mathrm{G}^{n_\mathrm{I}}$ individual cells.

Subsequently, the data of the training are classified into this grid structure according to their values. Consequently, the more points are in a cell, the more often this area regarding vehicle dynamics has been considered in the training. p_k describes the number of data within one cell. Here, the latest input data into the artificial neural network are classified into the grid structure. The confidence level τ_HSE is derived from the ratio between the number of data in a specific cell p_k and the characteristic value p_max

$$\tau_\mathrm{HSE} = \frac{p_k}{p_\mathrm{max}} \,. \tag{4.53}$$

The characteristic value p_max is used for scaling and determines the threshold value at which the artificial neural network is completely trusted. Within this thesis p_max is set to the maximum number of data within one cell of the input space grid structure. By this choice of the characteristic value, the confidence level is automatically scaled between zero and one:

$$0 \leq \tau_\mathrm{HSE} \leq 1 \,. \tag{4.54}$$

Whereas a confidence level of $\tau_\mathrm{HSE} = 0$ causes the hybrid state estimator to be entirely based on the physical model, a confidence level of $\tau_\mathrm{HSE} = 1$ leads to complete confidence in the artificial neural network. Thus input data into the artificial neural network, which could result in unpredictable and thus invalid outputs, are detected and handled by the hybrid method. These input data include, for example, value ranges that have not been acquired during the training, as well as incorrect sensor signals, which may occur in case of sensor malfunctions respectively failures.

As a result of this methodology, unknown vehicle dynamics states that have not been used during training of the artificial neural network or incorrect sensor signals are detected and handled by the hybrid method. Due to the redundancy in the sensor input variables of the artificial neural network and of the physical model, even complete sensor failures can be compensated. In case of a sensor failure with respect to the physical estimations, the confidence level is set to

$\tau_{\mathrm{HSE}} = 1$. In general, however, the hybrid method mainly focuses on safeguarding the artificial neural network.

In the following, the three individual input spaces are briefly introduced regarding the estimation segments of rolling, pitching and the side-slip angle.

Roll Behavior

The input space, which is set up for the roll behavior, is based on six input variables. This results in a six-dimensional grid structure. In addition, the data based on the training input variables are divided into $k_{\mathrm{G}} = 19$ sections. The size of the partition represents a compromise between the level of detail of the individual cells and the size of the grid structure for the entire input space. In total, the size of the grid structure for the input space of the roll behavior equals $k_{\mathrm{G}}^{n_{\mathrm{I}}} = 19^6$.

Figure 4.12 provides an insight into the composition of the grid structure of the input space for the roll behavior. For this purpose, the partitioning of three input variables of the artificial neural network is shown as an example. This is done using histograms for the individual input variables. In addition, a three-dimensional distribution for this composition of the input variables is outlined, which shows the interrelated distribution of the data. Due to the dimensionality of the entire input space, this excerpt of the input space is used as an example.

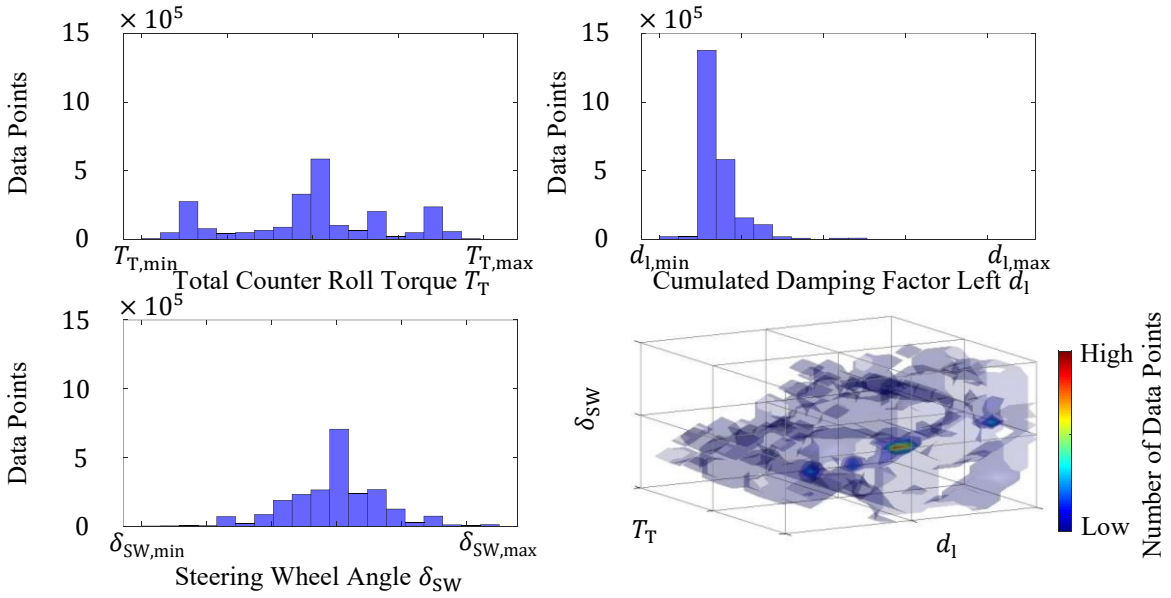

Figure 4.12 Confidence Level Determination Roll Behavior – Top Left: Input Distribution Total Counter Roll Torque; Top Right: Input Distribution Cumulated Damping Factor Left; Bottom Left: Input Distribution Steering Wheel Angle; Bottom Right: Interrelated 3D-Input Space

In this excerpt, the input variables of the total counter roll torque T_{T}, the cumulated damping factor on the left side of the vehicle d_{l} and the steering wheel angle δ_{SW} are visualized. In total 2,316,828 data points are located in the input space for each input quantity.

For the input variables of the total counter roll torque T_T as well as the steering wheel angle δ_SW, a point symmetry to zero is evident by the histograms illustrated in the top left respectively in the bottom left part of Figure 4.12. Small deviations in the symmetry, especially for larger absolute values of the two input variables, result from the selection of driving maneuvers for training, which occurred randomly and covers 70 % of the entire database. The greatest amounts of data for these two input variables cover the range around zero. The maximum number of data points within a segment for the total counter roll torque T_T equals $5.8545 \cdot 10^5$. With the selected segmentation there is a maximum number of $7.0519 \cdot 10^5$ data points for the steering wheel angle δ_SW. The third input variable of the shown excerpt represents the data distribution of the cumulated damping factor on the left side of the vehicle. This is shown in the top right part of Figure 4.12. The histogram shows that the majority of the data is located close to the minimum cumulated damping factor $d_\mathrm{l,min}$. The maximum number of data points within one segment across the entire input space is $1.3775 \cdot 10^6$ for the cumulated damping factor of the left side of the vehicle d_l. Thus for this input variable there are about two times more data points in the segment with the maximum data points than for the other two input variables illustrated.

In the bottom right part of Figure 4.12 the interrelated overview of these three exemplary input variables is visualized. Depending on the number of data points present, the ranges in which data points are present are displayed. Whereas a blue coloring represents a small number of data points, the color red is equivalent to the maximum number of data points. By this kind of representation the data coverage of the input space is evident.

Pitch Behavior

In total the input space of the hybrid state estimation for the pitch behavior has the dimension $k_\mathrm{G}^{n_\mathrm{I}} = 19^6$, since for the estimation of the artificial neural network altogether six input variables are used. In order to provide an overview of the input space of the hybrid state estimation with respect to the pitch behavior, an extract of the input variables is analyzed analogous to the roll behavior.

The input variables of the counter roll torque at the front axle T_f, the cumulated damping factor at the rear axle d_r and the velocity of the vehicle v are considered. For this purpose, the data distributions in relation to these input variables are processed via histograms representing the segmentation into $k_\mathrm{G} = 19$ sections. Figure 4.13 provides an overview of these data distributions.

The counter roll torque at the front axle T_f, which is shown in the upper left part, exhibits an approximately symmetrical data distribution to zero. The maximum amount of data available within one segment corresponds to $8.0295 \cdot 10^5$ and represents a counter roll torque close to zero. The data distribution of the velocity of the vehicle v over the entire velocity range is basically uniform, at the same time showing an accumulation of data at certain velocity intervals.

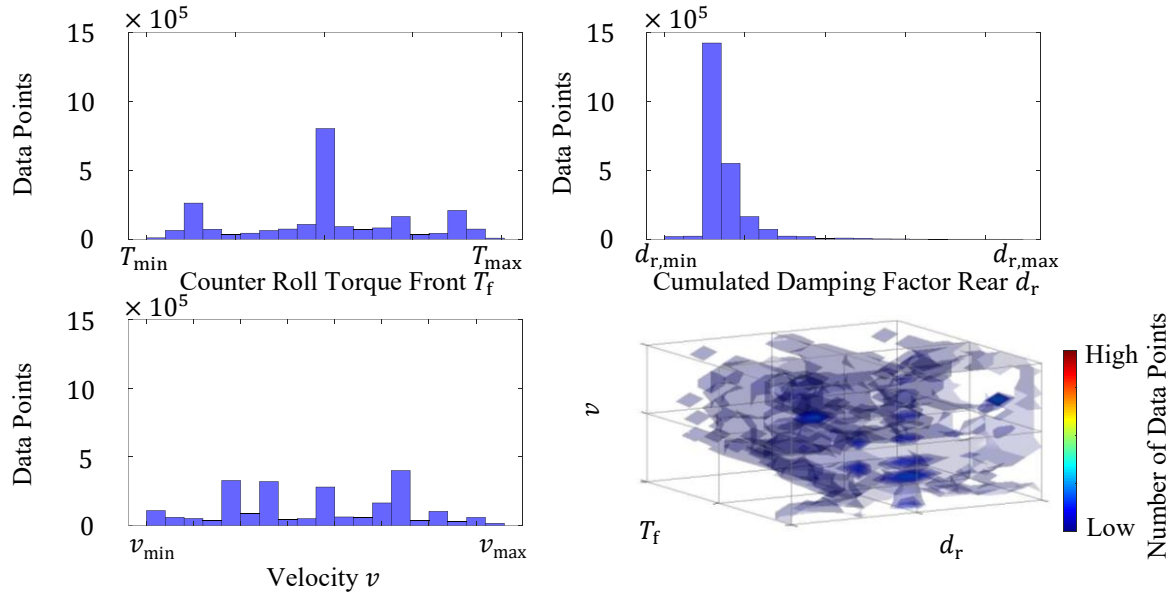

Figure 4.13 Confidence Level Determination Pitch Behavior – Top Left: Input Distribution Counter Roll Torque Front; Top Right: Input Distribution Cumulated Damping Factor Rear; Bottom Left: Input Distribution Velocity; Bottom Right: Interrelated 3D-Input Space

This distribution is illustrated in the bottom left part of Figure 4.13. These accumulations represent the defined velocities at which the driving maneuvers have been performed, according to Section 3.5. The third input variable from this extract, the cumulated damping value acting on the rear axle d_r, features a positive skewed data distribution as shown in the upper right part. The maximum number of data points in one segment equals $1.4239 \cdot 10^6$ close to the minimum cumulated damping factor acting at the rear axle $d_{\mathrm{r,min}}$. In the bottom right part of Figure 4.13 the interrelated input space is visualized for these three input variables. Thereby, the accumulations of the data points in single velocity ranges can be identified in the case of a small cumulated damping factor and counter roll torques close to zero.

Side-Slip Behavior

The artificial neural network for estimating the side-slip angle features eight input variables. The segmentation of the input data is done in analogy to the two already presented input spaces for $k_\mathrm{G} = 19$ sections. This results in an input space grid structure of $k_\mathrm{G}^{n_\mathrm{I}} = 19^8$ cells.

In the following an extract of the entire data distribution is presented in detail for three input variables. The input variables of the counter roll torque at the rear axle T_r, the damping factor at the front left suspension d_fl and the lateral acceleration a_y of the vehicle are considered for this visualization. The corresponding data distributions are displayed in Figure 4.14.

Both the data distribution of the counter roll torque acting at the rear axel T_r and the data distribution of the lateral acceleration a_y, which are displayed in the top left part respectively bottom left part, are approximately symmetrical to zero.

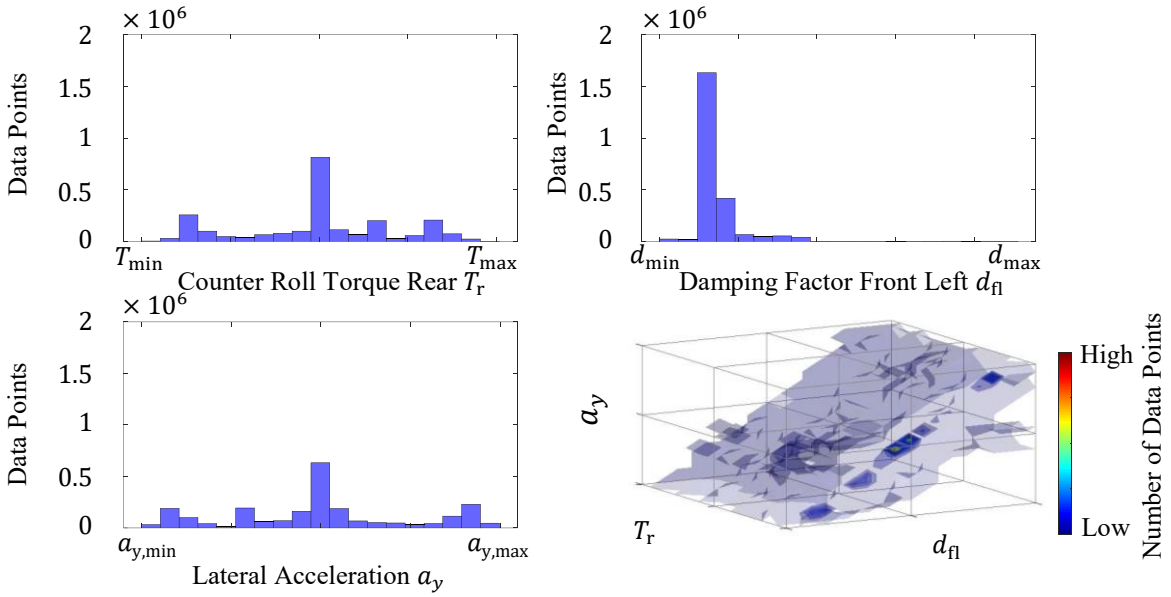

Figure 4.14 Confidence Level Determination Side-Slip Behavior – Top Left: Input Distribution Counter Roll Torque Rear; Top Right: Input Distribution Damping Factor Front Left; Bottom Left: Input Distribution Lateral Acceleration; Bottom Right: Interrelated 3D-Input

The sectors with the most data points are accordingly the sectors around zero. In these sectors, $0.8159 \cdot 10^6$ data points are allocated for the counter roll torque T_r and $0.6322 \cdot 10^6$ data points for the lateral acceleration a_y. The damping factor d_{fl} illustrated in the top right part of Figure 4.14 has a positive skewed data distribution as already evident in the cumulated damping factors. The segments with the most data points feature a total of $1.6325 \cdot 10^6$ data points. The interrelated data distribution with respect to these three selected input variables is shown in the bottom right part.

4.3.3 Combination of the Artificial Neural Networks and the Physical Estimators

The third part of the hybrid state estimation is the combination of the respective artificial neural network with the corresponding physical model. Depending on the confidence level τ_{HSE}, the particular model is trusted more or even entirely. A Kalman filter is used to merge the models. Due to the non-linearities in the physical models, an unscented Kalman filter is used for the implementation. In the following, the mode of operation of the unscented Kalman filter is briefly introduced, which has been modified with respect to the hybrid method. The basic mode of operation is according to (Julier and Uhlmann, 1997, Wan and Van Der Merwe, 2000).

Within the unscented Kalman filter the non-linearities of the physical models are considered by using an unscented transformation, (Julier, 2002). In this unscented transformation the state variables of the physical model $\boldsymbol{x}$ are represented by a probability distribution. This is achieved by means of $2L + 1$ sigma points $\mathbf{X}$ around the mean value $\hat{\boldsymbol{x}}$. Thereby, $\boldsymbol{P}$ quantifies the covariance of the state variables $\boldsymbol{x}$.

$$\left(\mathbf{X}(k)\right)_0 = \hat{\boldsymbol{x}}(k) \tag{4.55}$$

$$\left(\boldsymbol{X}(k)\right)_l = \hat{\boldsymbol{x}}(k) + \left(\sqrt[2]{(L+\lambda)\boldsymbol{P}(k)}\right), \qquad l = 1 \dots L \tag{4.56}$$

$$\left(\boldsymbol{X}(k)\right)_{l+L} = \hat{\boldsymbol{x}}(k) - \left(\sqrt[2]{(L+\lambda)\boldsymbol{P}(k)}\right), \qquad l = 1 \dots L \tag{4.57}$$

The index l indicates the respective column of $\mathbf{X}$. λ represents a scaling parameter for the calculation of the sigma points $\mathbf{X}$. It is calculated under consideration of the parameters α_K and κ, which determine the spreading of the sigma points around the mean value $\hat{\boldsymbol{x}}$:

$$\lambda = \alpha_\mathrm{K}^2(L+\kappa) - L. \tag{4.58}$$

Table 4.12 presents the assignment of the physical models in form of the state variables $\boldsymbol{x}$.

Table 4.12 Unscented Kalman Filters – Allocation of the Physical models

Estimation Targets	**State $\boldsymbol{x}$**	**Units**
Roll Behavior	Roll Angle φ_P	rad
	Roll Rate $\dot{\varphi}_\mathrm{P}$	rad/s
Pitch Behavior	Pitch Angle θ_P	rad
	Pitch Rate $\dot{\theta}_\mathrm{P}$	rad/s
Side-Slip Behavior	Side-Slip Angle β_P	rad

The states for the description of the roll behavior are the roll angle φ_P and the roll rate $\dot{\varphi}_\mathrm{P}$ of the physical model. In order to characterize the pitch behavior the states of the pitch angle θ_P and the pitch rate $\dot{\theta}_\mathrm{P}$ are used. The state for the side-slip behavior equals the side-slip angle β_P resulting from the physical model.

Based on the sigma points of the state variable $\left(\boldsymbol{X}(k)\right)_l$ at the time k, the transition function f_I is used to determine the sigma points of the state variable $\left(\mathbf{X}(k+1)\right)_l$ at the time $k+1$.

$$\left(\mathbf{X}(k+1)\right)_l = f_\mathrm{I}\left(\left(\boldsymbol{X}(k)\right)_l, \boldsymbol{u}_\mathrm{HSE}(k)\right), \qquad l = 0 \dots 2L \tag{4.59}$$

This calculation is done by additionally using the input variables $\boldsymbol{u}_\mathrm{HSE}$ into the physical model. These consist of the manipulated variables $\boldsymbol{u}_\mathrm{R}$ as well as the redundant sensor input variables $\boldsymbol{s}_\mathrm{V,P}$:

$$\boldsymbol{u}_\mathrm{HSE}(k) = \left(\boldsymbol{u}_\mathrm{R}(k), \boldsymbol{s}_\mathrm{V,P}(k)\right)^\mathrm{T}. \tag{4.60}$$

The transition functions f_I correspond to the calculation rules for the physical models presented in Section 4.1.

Using the sigma points $\left(\mathbf{X}(k+1)\right)_l$, the a priori state estimation $\hat{\boldsymbol{x}}^-(k+1)$ is calculated with

$$\hat{\boldsymbol{x}}^-(k+1) = \sum_{l=0}^{2L} W_l^{(m)} \left(\mathbf{X}(k+1)\right)_l. \tag{4.61}$$

$W_l^{(m)}$ represents the weightings corresponding to the sigma points $\left(\mathbf{X}(k+1)\right)_l$.

$$W_0^{(m)} = \frac{\lambda}{(L+\lambda)} \tag{4.62}$$

$$W_l^{(m)} = \frac{\lambda}{2(L+\lambda)}, \qquad l = 1 \dots 2L \tag{4.63}$$

The a priori covariance $\boldsymbol{P}^-(k+1)$ related to the a priori state estimation $\hat{\boldsymbol{x}}^-(k+1)$ is calculated by

$$\boldsymbol{P}^-(k+1) = \sum_{l=0}^{2L} W_l^{(c)} \left[\left(\mathbf{X}(k+1)\right)_l - \hat{\boldsymbol{x}}^-(k+1)\right]\left[\left(\mathbf{X}(k+1)\right)_l - \hat{\boldsymbol{x}}^-(k+1)\right]^T + \boldsymbol{Q}_{\mathrm{HSE}}(k+1). \tag{4.64}$$

using the weightings $W_l^{(c)}$

$$W_0^{(c)} = \frac{\lambda}{(L+\lambda)} + 1 - \alpha_{\mathrm{K}}^2 + \beta_{\mathrm{U}} \text{ and} \tag{4.65}$$

$$W_l^{(c)} = \frac{\lambda}{2(L+\lambda)}, \qquad l = 1 \dots 2L. \tag{4.66}$$

Thereby β_{U} is used to specify the distribution of $\boldsymbol{x}$.

Additionally, the covariance $\boldsymbol{Q}_{\mathrm{HSE}}(k+1)$ is considered, which usually describes the process noise. In the context of this thesis, though, this covariance $\boldsymbol{Q}_{\mathrm{HSE}}(k+1)$ is used to apply the confidence level $\tau_{\mathrm{HSE}}(k+1)$. (4.55) to (4.66) constitute the prediction step of the unscented Kalman filter.

In the subsequent correction step, the a posteriori state $\hat{\boldsymbol{x}}(k+1)$ is determined by

$$\hat{\boldsymbol{x}}(k+1) = \hat{\boldsymbol{x}}^-(k+1) + \boldsymbol{K}(k+1)\left(y_{\mathrm{Ann}}(k+1) - \hat{y}^-(k+1)\right). \tag{4.67}$$

$\boldsymbol{K}(k+1)$ represents the Kalman gain and $\hat{y}^-(k+1)$ indicates a predicted measurement and thus the mean value of the sigma points $\left(\boldsymbol{\Upsilon}(k+1)\right)_l$. These sigma points are determined by transforming the sigma points $\left(\boldsymbol{X}(k+1)\right)_l$ by the output function f_{O}.

$$\left(\boldsymbol{\Upsilon}(k+1)\right)_l = f_{\mathrm{O}}\left(\left(\boldsymbol{X}(k+1)\right)_l\right), \qquad l = 0 \dots 2L \tag{4.68}$$

$$\hat{y}^-(k+1) = \sum_{l=0}^{2L} W_l^{(m)} \left(\boldsymbol{\Upsilon}(k+1)\right)_l \tag{4.69}$$

The quantity $y_{\mathrm{Ann}}(k+1)$, which normally represents the measured quantity, contains the state variable predicted by the artificial neural network. For the roll behavior this quantity equals the roll angle φ_{Ann}, for the pitch behavior the pitch angle θ_{Ann} and for the side-slip behavior the side-slip angle β_{Ann}. Table 4.13 provides an overview of the values for the three areas.

Table 4.13 Unscented Kalman Filters – Virtual Measurements

Estimation Targets	**Virtual Measurements y_{Ann}**	**Units**
Roll Behavior	Roll Angle φ_{Ann}	rad
Pitch Behavior	Pitch Angle θ_{Ann}	rad
Side-Slip Behavior	Side-Slip Angle β_{Ann}	rad

For the calculation of the Kalman gain $\boldsymbol{K}(k+1)$ the covariance of the predicted measurement $P_{\hat{\boldsymbol{y}}(k+1)\hat{\boldsymbol{y}}(k+1)}$ as well as the cross correlation covariance $\boldsymbol{P}_{\hat{\boldsymbol{x}}(k+1)\hat{\boldsymbol{y}}(k+1)}$ are processed:

$$\boldsymbol{K}(k+1) = \boldsymbol{P}_{\hat{\boldsymbol{x}}(k+1)\hat{y}(k+1)} P^{-1}_{\hat{\boldsymbol{y}}(k+1)\hat{\boldsymbol{y}}(k+1)}. \tag{4.70}$$

For the calculation of the covariance $P_{\hat{\boldsymbol{y}}(k+1)\hat{\boldsymbol{y}}(k+1)}$ of the predicted measurement $\hat{y}^{-}(k+1)$, the covariance $R_{\mathrm{HSE}}(k+1)$ is additionally employed, which usually characterizes the measurement noise.

In the context of this thesis, the covariance is used analogous to the covariance $\boldsymbol{Q}_{\mathrm{HSE}}(k+1)$ for the realization of the confidence level $\tau_{\mathrm{HSE}}(k+1)$:

$$\begin{aligned} P_{\hat{\boldsymbol{y}}(k+1)\hat{y}(k+1)} = \sum_{l=0}^{2L} W_l^{(c)} \Big[\big(\boldsymbol{\Upsilon}(k+1)\big)_l \\ - \hat{y}^{-}(k+1) \Big] \Big[\big(\boldsymbol{\Upsilon}(k+1)\big)_l - \hat{y}^{-}(k+1) \Big]^{\mathrm{T}} + R_{\mathrm{HSE}}(k+1), \end{aligned} \tag{4.71}$$

$$\begin{aligned} \boldsymbol{P}_{\hat{\boldsymbol{x}}(k+1)\hat{y}(k+1)} = \sum_{l=0}^{2L} W_l^{(c)} \Big[\big(\mathbf{X}(k+1)\big)_l \\ - \hat{\boldsymbol{x}}^{-}(k+1) \Big] \Big[\big(\boldsymbol{\Upsilon}(k+1)\big)_l - \hat{y}^{-}(k+1) \Big]^{\mathrm{T}}. \end{aligned} \tag{4.72}$$

In the last part of the correction step the covariance $\boldsymbol{P}(k+1)$ of the a posteriori state $\hat{\boldsymbol{x}}(k+1)$ is determined by

$$\boldsymbol{P}(k+1) = \boldsymbol{P}^{-}(k+1) - \boldsymbol{K}(k+1) P_{\hat{\boldsymbol{y}}(k+1)\hat{\boldsymbol{y}}(k+1)} \boldsymbol{K}^{\boldsymbol{T}}(k+1). \tag{4.73}$$

The process of prediction (4.55) – (4.66) as well as correction (4.67) – (4.73) is performed in each time step.

The output quantities of the hybrid state estimation $\boldsymbol{x}_{\mathrm{Est}}$ are composed by the respective a posteriori states $\hat{\boldsymbol{x}}$ predicted by the unscented Kalman filters. Table 4.14 lists these output quantities.

Table 4.14 Unscented Kalman Filters – Outputs

Estimation Targets	Predicted States $\hat{\boldsymbol{x}}$	Units
Roll Behavior	Roll Angle φ_{Est}	rad
	Roll Rate $\dot{\varphi}_{\mathrm{Est}}$	rad/s
Pitch Behavior	Pitch Angle θ_{Est}	rad
	Pitch Rate $\dot{\theta}_{\mathrm{Est}}$	rad/s
Self-Steering Behavior	Side-Slip Angle β_{Est}	rad

In the following, the method for applying the confidence level is presented. For this application, the covariances $\boldsymbol{Q}_{\mathrm{HSE}}$ and R_{HSE} are defined as a function of the confidence level:

$$\boldsymbol{Q}_{\mathrm{HSE}}(k+1) = \tau_{\mathrm{HSE}}(k+1)\boldsymbol{Q}_{\mathrm{N}}, \tag{4.74}$$

$$R_{\mathrm{HSE}}(k+1) = \big(1 - \tau_{\mathrm{HSE}}(k+1)\big)R_{\mathrm{N}}. \tag{4.75}$$

$\boldsymbol{Q}_{\mathrm{N}}$ and R_{N} represent the fixed neutral covariance of the transition respectively the measurement. These neutral covariances are invariant and defined before the hybrid method is applied. By integrating the confidence level τ_{HSE} into the covariances $\boldsymbol{Q}_{\mathrm{HSE}}$ and R_{HSE}, the combination of the artificial neural network with the physical model is performed as intended. For this purpose the boundary conditions of the confidence level τ_{HSE} are considered and the resulting effects on the outputs of the hybrid state estimator $\boldsymbol{x}_{\mathrm{Est}}$ are investigated for the defined setup.

First the boundary condition is considered, where the confidence level approaches zero. If the confidence level approaches zero, the consequence is that the covariance of the transition $\boldsymbol{Q}_{\mathrm{HSE}}$ also approaches zero. In this case the covariance of the measurement R_{HSE} corresponds to the neutral covariance R_{N}:

$$\lim_{\tau(k+1)\to 0} \hat{\boldsymbol{x}}(k+1) = \lim_{\boldsymbol{Q}_{\mathrm{HSE}}(k+1)\to 0} \hat{\boldsymbol{x}}(k+1) = \hat{\boldsymbol{x}}^{-}(k+1). \tag{4.76}$$

The result is that the a posteriori state $\hat{\boldsymbol{x}}(k+1)$ is completely based on the predicted a priori state $\hat{\boldsymbol{x}}^{-}(k+1)$. This prediction is hereby completely based on the physical model. Thus, with a confidence level of $\tau_{\mathrm{HSE}} = 0$, the hybrid state estimation entirely trusts the physical model.

The opposite boundary condition to be considered occurs when the confidence level is approaching one. In this case the covariance of the transition $\boldsymbol{Q}_{\mathrm{HSE}}$ corresponds to the neutral covariance $\boldsymbol{Q}_{\mathrm{N}}$ and the covariance of the measurement R_{HSE} is approaching zero:

$$\lim_{\tau(k+1)\to 1} \hat{\boldsymbol{x}}(k+1) = \lim_{R_{\mathrm{HSE}}(k+1)\to 0} \hat{\boldsymbol{x}}(k+1) = f_{\mathrm{O}}^{-1}\big(y_{\mathrm{Ann}}(k+1)\big). \tag{4.77}$$

As a result, the a posteriori state $\hat{\boldsymbol{x}}(k+1)$ of the unscented Kalman filter is completely based on the quantity $y_{\mathrm{Ann}}(k+1)$. This quantity corresponds to the state variable predicted by the artificial neural network. With a confidence level of $\tau_{\mathrm{HSE}} = 1$, the artificial neural network is entirely trusted by the hybrid state estimation.

4.3.4 Open-Loop Validation

For the first evaluation of the functionality of the hybrid method for state estimation, the input data into the artificial neural network are manipulated. This results in unpredictable estimated output variables $\boldsymbol{y}_{\mathrm{Ann}}$ of the artificial neural networks. To verify the behavior of the state estimators, different driving maneuvers are used from the test data set of the driving scenarios, according to Section 3.5.

The manipulation of the input data into the neural network is done by means of the sensory input quantities $\boldsymbol{s}_{\mathrm{V,Ann}}$. Only one sensor signal is deliberately manipulated at a time in order to keep the detection difficulty for the hybrid method at a maximum. The manipulation is done by a drift respectively an offset in the sensor signal as well as the complete failure of one sensor. This results in three different test scenarios in the open loop validation which will be presented and investigated in the following.

Sensor Drift

A possibility of manipulating the input data into the artificial neural network is represented by a drift in one input signal. A drift in a sensor signal implies a challenging task in the detection of the malfunction itself, (Goebel and Yan, 2008).

In the present case the hybrid method for the application of the pitch behavior estimation is considered. The driving maneuver, in which the sensor error is applied, involves a braking in a turn. At the beginning of the driving maneuver, a left turn of 100 m radius is passed with a velocity of 100 km/h. There is no lateral road gradient present in this test maneuver. The braking is done with a deceleration of 4.5 m/s. Table 4.15 lists the parameters of this test driving maneuver.

Table 4.15 Hybrid State Estimation Open-Loop Validation – Driving Maneuver Sensor Drift

Driving Maneuver	Parameter	Values	Unit
Braking in a Turn	Cornering Radius	100	m
	Lateral Road Gradient	0	%
	Longitudinal Deceleration	4.5	m/s²
	Steering Direction	Counterclockwise	-
	Velocity	100	km/h

The drift in the input data is included in the signal of the time derivative of the vehicle velocity $\frac{dv}{dt}$. Starting from the tenth second of the driving maneuver, the derivative of the velocity is continuously distorted by -1m/s² per second. The resulting progression of the input variable is shown in the top part of Figure 4.15. The drift superimposes the original deceleration within the driving maneuver, which starts at the time of second 13.

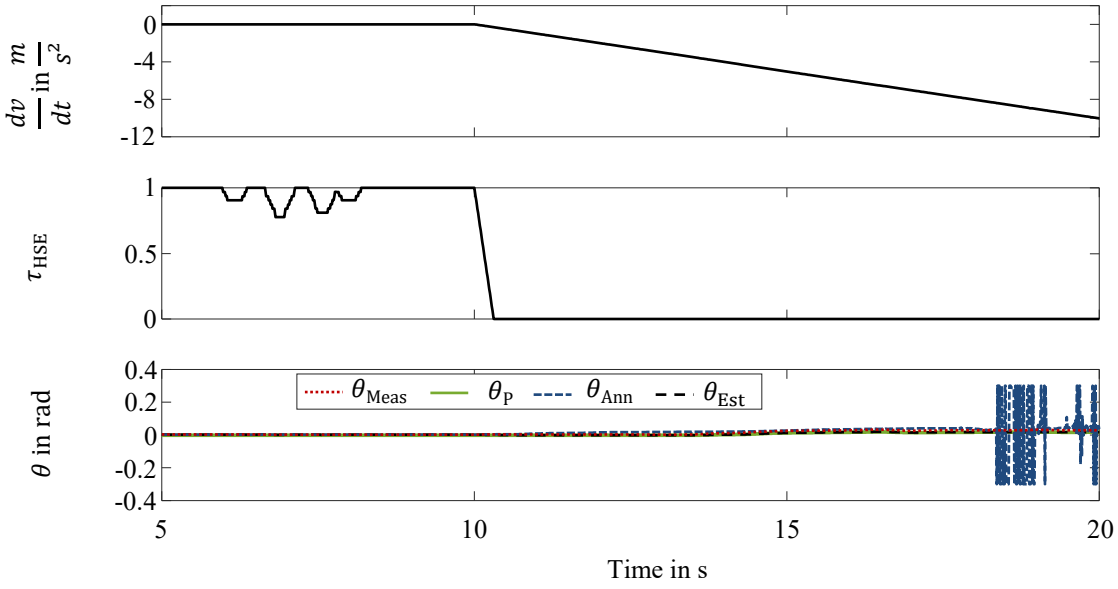

Figure 4.15 Hybrid State Estimation Open-Loop Validation – Reliability Sensor Drift: Top: Time Derivate of the Vehicle Velocity; Middle: Confidence Level; Bottom: Pitch Angle Curves

To investigate how the state estimators perform in this situation, the estimated states are plotted over time in the bottom part of Figure 4.15. A red dotted line represents the ground truth pitch angle θ_{Meas}. The pitch angle θ_{P} based on the physical model is represented by a solid green line. The fine dashed blue line indicates the pitch angle θ_{Ann} resulting from the artificial neural network. Besides, the pitch angle θ_{Est} of the hybrid method is visualized by a dashed black line.

The drift in the input variable of the artificial neural network also leads to a drift in the output variable estimated by the artificial neural network θ_{Ann}. This drift in the estimated pitch angle θ_{Ann} turns into strong oscillations from second 18.35 on. The results of the artificial neural network are no longer valid for this malfunction.

By using the hybrid method the malfunction is detected and can be handled. To illustrate the desired function, the confidence level τ_{HSE} is visualized in the middle part of Figure 4.15. Whereas the confidence level is high at the beginning of the driving maneuvers until the drift occurs, it decreases rapidly once the input variable is manipulated. The manipulation is thus detected by the hybrid method, which leads to a drop in the confidence level.

In order to obtain a detailed insight into the behavior of the state estimators, the deviations of the estimated pitch angle from the ground truth pitch angle are determined.

$$\Delta\theta_i = \theta_{\mathrm{Meas}} - \theta_i, \qquad i \in \{\mathrm{Ann}, \mathrm{Est}, \mathrm{P}\} \tag{4.78}$$

The deviations are displayed in Figure 4.16.

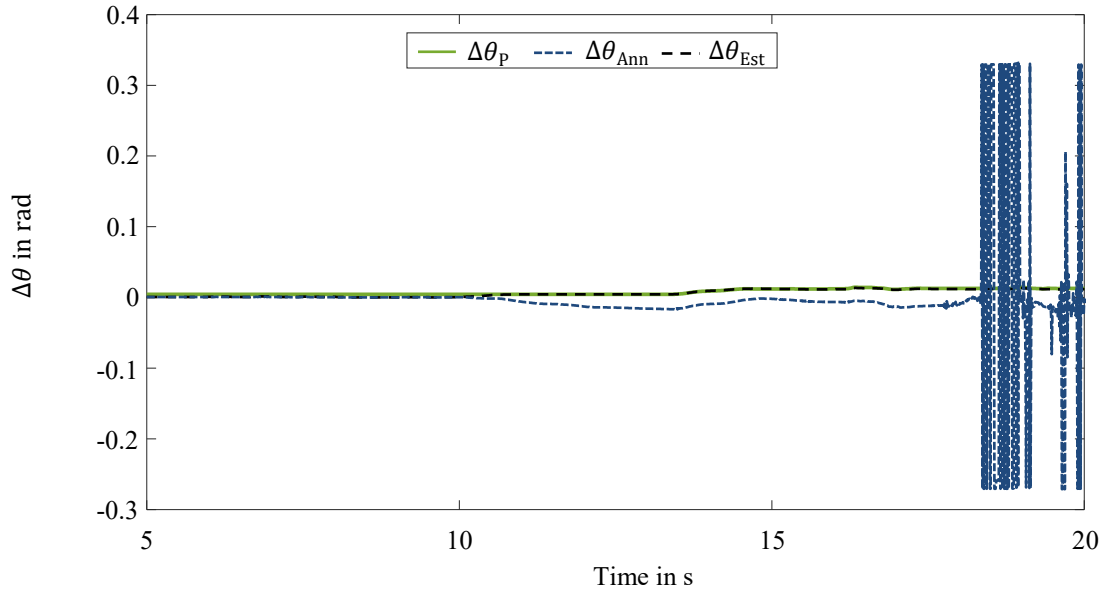

Figure 4.16 Hybrid State Estimation Open-Loop Validation – Reliability Sensor Drift: Pitch Angle Deviations

The coloring of the lines is consistent with the coloring used in the bottom part of Figure 4.15. By observing the deviations it is possible to highlight the drift in the output signal of the artificial neural network. Before the input signal is manipulated, meaning before second ten, the hybrid method θ_{Est} relies strongly on the estimation of the artificial neural network θ_{Ann}. As soon as the drift is detected by the confidence level, the estimation θ_{Est} shifts towards estimation of the physical model θ_{P}. From second 10.32 on, when the confidence level reaches $\tau_{\mathrm{HSE}} = 0$, the hybrid method trusts the physical model completely. Thus the state θ_{Ann}, which is incorrect due to the drift, is not considered in the output of the hybrid method θ_{Est}. Furthermore, the critical oscillations in the estimation of the artificial neural network do not affect the estimation of the hybrid method. A valid estimation is available over the whole period of time by applying the hybrid method.

Sensor Offset

A further possibility to manipulate the input data in the artificial neural network is to introduce an offset into the sensor signal. An offset represents a constantly added deviation, (Isermann, 2011).

The impact exerted by the sensor error of an offset is exemplarily evaluated using the hybrid method of state estimation for the application case of the roll behavior. A steady-state circular drive is considered as the driving maneuver. The test vehicle passes a right turn with a radius of 100 m. The velocity of the vehicle equals 90 km/h. There is no lateral road gradient present. Table 4.16 provides a summary of this driving maneuver.

Table 4.16 Hybrid State Estimation Open-Loop Validation – Driving Maneuver Sensor Offset

Driving Maneuver	Parameter	Values	Unit
Steady-State Circular Drive	Cornering Radius	100	m
	Lateral Road Gradient	0	%
	Steering Direction	Clockwise	-
	Velocity	90	km/h

The steering wheel angle δ_{SW} serves as the input variable into the artificial neural network which is manipulated. In a period of 20 to 25 seconds a positive offset of 65° is implemented. The driving maneuver is observed up to second 30, so that the transition into the offset as well as the transition out of the offset can be examined. The resulting steering wheel angle curve is shown in the top part of Figure 4.17.

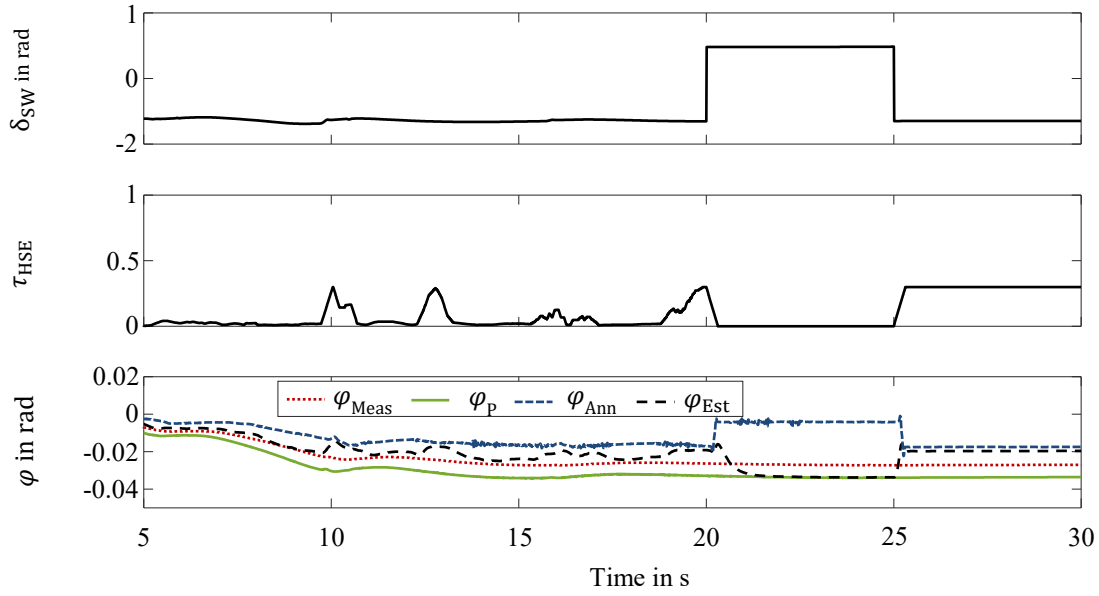

Figure 4.17 Hybrid State Estimation Open-Loop Validation – Reliability Sensor Offset: Top: Steering Wheel Angle; Middle: Confidence Level; Bottom: Roll Angle Curves

In the middle part of Figure 4.17 the confidence level τ_{HSE} is plotted over time. Basically, the confidence in the artificial neural network is not as strong in the unadulterated range as, for example, in the case of state estimation with respect to the pitch behavior during the driving maneuver shown in Figure 4.15. The offset is identified successfully by the hybrid method and thus the confidence level is set to $\tau_{\mathrm{HSE}} = 0$ for the period of the offset. Both prior to and subsequent to the offset, the hybrid method regains more confidence in the artificial neural network.

The effect of the offset on the state estimation concerning the roll angle is shown in the bottom part of Figure 4.17. The offset in the steering wheel angle δ_{SW} also distorts the roll angle estimated by artificial neural network φ_{Ann}. Thus the artificial neural network suggests a roll angle

close to zero during the offset, whereas the ground truth roll angle remains at $\varphi_{\mathrm{Meas}} = -0.02$ rad, which is equivalent to $-1.15°$. This incorrect estimation is detected by the confidence level and then handled by the hybrid method using the unscented Kalman filter. The state estimated by the hybrid method φ_{Est} is completely based on the physical model φ_{P} during the offset.

For a detailed analysis regarding the transition regions of the offset, the deviations of the estimated roll angles from the ground truth roll angle φ_{Meas} are determined.

$$\Delta\varphi_i = \varphi_{\mathrm{Meas}} - \varphi_i, \qquad i \in \{\mathrm{Ann}, \mathrm{Est}, \mathrm{P}\} \tag{4.79}$$

These deviations are visualized in Figure 4.18.

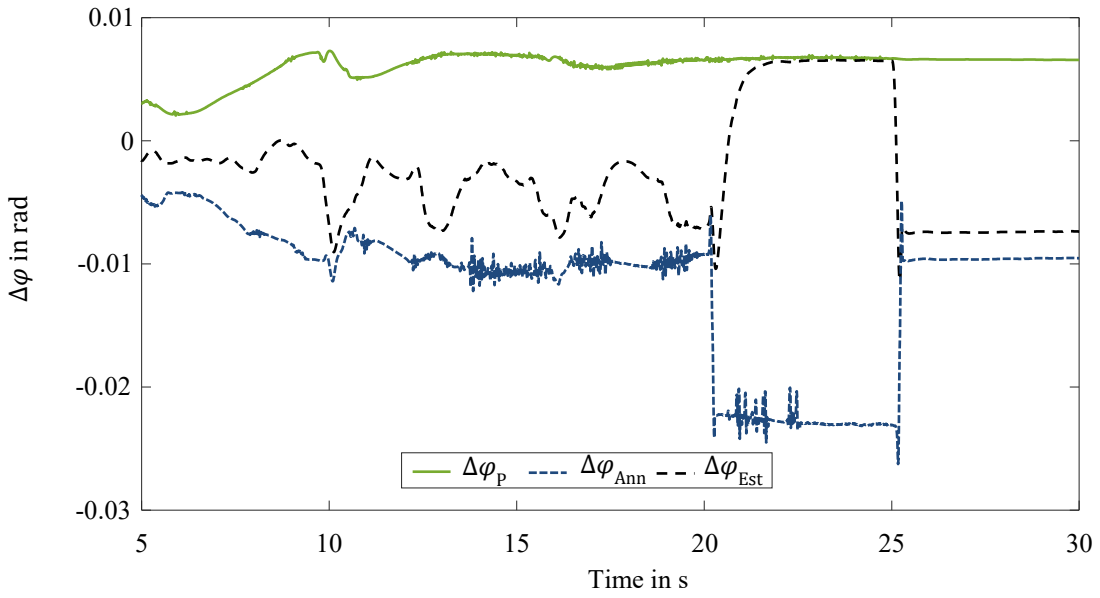

Figure 4.18 Hybrid State Estimation Open-Loop Validation – Reliability Sensor Offset: Roll Angle Deviations

First, the area prior to the offset is examined. The higher the confidence level, the stronger the artificial neural network is trusted. The deviations are approaching accordingly. A further advantage of using the hybrid method can be recognized in the period from 13.73 to 19.90 seconds. The artificial neural network has a partially noisy output signal for this period. The output signal of the physical model is also noisy, although the noise level is significantly lower. By using the unscented Kalman filter and the corresponding definition of the neutral covariances $\boldsymbol{Q}_{\mathrm{N}}$ and R_{N}, these noises are compensated. The estimation resulting from the hybrid method φ_{Est} does not show a noisy signal.

Whereas the physical model is completely trusted during the offset, there is a one-periodic oscillation at the beginning as well as at the end of the offset. For these instants steps in the steering wheel angle are present. Following these one-periodic oscillations, smooth signals are present both during and after the offset. By using the hybrid method the sensor malfunction of an

offset can be detected and handled as well. The hybrid method provides a valid estimate throughout.

The impact of the respective one-periodic oscillations in relation to the control is investigated within the closed-loop operation mode in Chapter 6.

Sensor Failure

A sensor failure represents an extremely dangerous situation concerning the state estimation. In the following, the behavior of the hybrid method in the case of such a failure of the sensor signal for an input quantity into the artificial neural network is examined. The further input variables remain unaltered.

The application example used in this case is the state estimation of the side-slip angle. For the analysis of the behavior of the individual state estimator the driving maneuver of the step steering input test is chosen. Here, the velocity of the vehicle is set to 90 km/h. The steering angle to be applied equals 60° which induces the vehicle to turn right. Moreover, no lateral road gradient is present. Table 4.17 provides an overview for this validation maneuver.

Table 4.17 Hybrid State Estimation Open-Loop Validation – Driving Maneuver Sensor Failure

Driving Maneuver	Parameter	Values	Unit
Step Steering Input Test	Lateral Road Gradient	0	%
	Steering Amplitude	60	°
	Steering Direction	Clockwise	-
	Velocity	90	km/h

The sensor failure in the present case involves the inertial measurement unit located at the center of gravity. The accelerometer for the lateral direction fails. The signal of the lateral acceleration a_y is therefore lost. The failure occurs at the time of 12 s of the driving maneuver. The course of the lateral acceleration a_y is shown in the top part of Figure 4.19. Due to the sensor failure, the lateral acceleration can accordingly only be visualized up to the time of 12 s.

In the middle part of Figure 4.19 the confidence level of the hybrid method τ_{HSE} arising for this driving maneuver is shown. Whereas the confidence level is quite high at the beginning of the maneuver during the initial driving straight ahead, it is rather low during the adjustment of the steering angle. The section of constant lateral acceleration features a similar confidence level as the hybrid method with respect to the roll behavior during the steady-state circular drive. The sensor failure is successfully detected by the hybrid method. The confidence level adopts permanently $\tau_{\mathrm{HSE}} = 0$ after the failure.

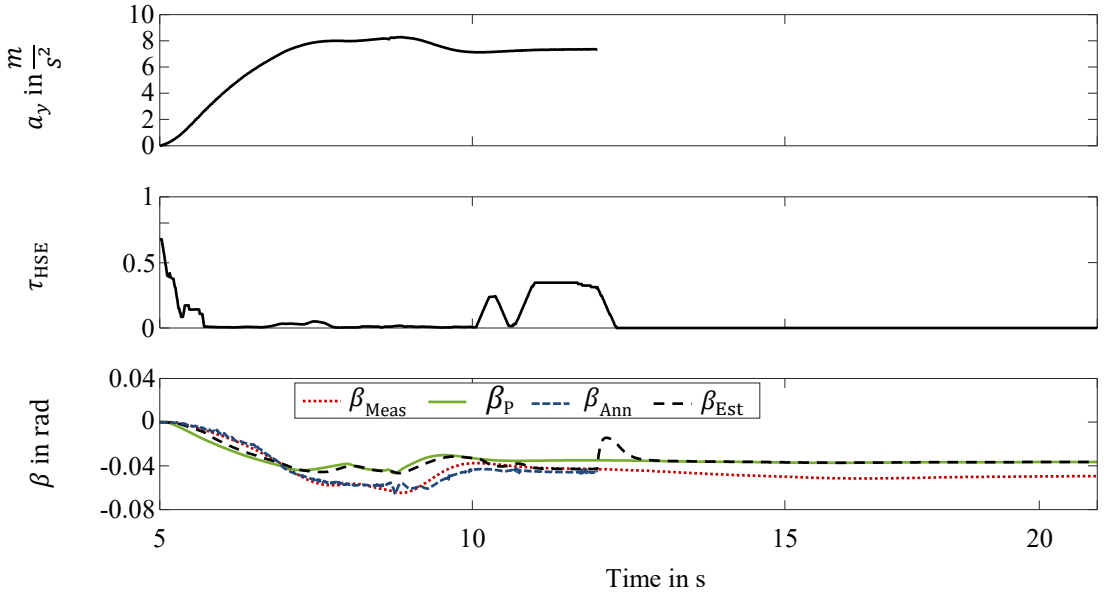

Figure 4.19 Hybrid State Estimation Open-Loop Validation – Reliability Sensor Failure: Top: Lateral Acceleration; Middle: Confidence Level; Bottom: Side-Slip Angle Curves

The consequences for the state estimations are visualized in the bottom part of Figure 4.19. Here the courses of the side-slip angle for the individual state estimators are plotted. Due to the fact that an input signal into the artificial neural network is lost from second 12 on, the artificial neural network likewise estimates only the side-slip angle β_{Ann} up to this instant. Beyond this time, no estimation of the artificial neural network β_{Ann} is present. Subsequent to the sensor failure, the only available estimation based on the physical model β_{P} is relied upon completely. In the transition area an overshoot is present.

In order to evaluate the behavior of the state estimators in more detail, the deviations $\Delta\beta_i$ from the ground truth side-slip angle β_{Meas} are determined.

$$\Delta\beta_i = \beta_{\mathrm{Meas}} - \beta_i, \qquad i \in \{\mathrm{Ann}, \mathrm{Est}, \mathrm{P}\} \tag{4.80}$$

These deviations for the driving maneuver are illustrated in Figure 4.20. The artificial neural network achieves a smaller deviation from the ground truth side-slip angle in contrast to the physical model. Through the conservative choice of the scaling factor p_{max}, the physical model is trusted more in the area of the steering wheel angle step. A more detailed examination of the influence of the choice of the scaling factor p_{max} is given in Chapter 7.3.

Furthermore, analogous to the observation on the sensor offset, the noise present in the signal of the estimated state β_{Ann} by the artificial neural network is filtered out by the unscented Kalman filter within the hybrid method. The estimated state of the hybrid method β_{Est} shows no noise.

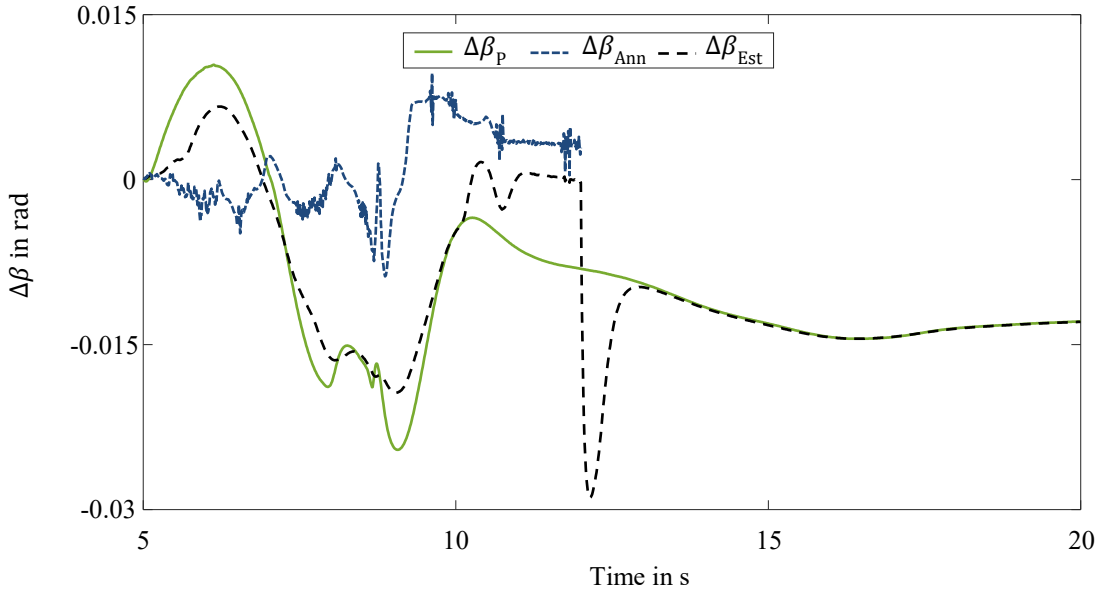

Figure 4.20 Hybrid State Estimation Open-Loop Validation – Reliability Sensor Failure: Side-Slip Angle Deviations

Following the sensor failure, there is a single overshoot exceeding the value estimated by the physical model before the estimated value by the hybrid method is permanently adapted to the physical model. The time between the sensor failure and the adoption of the state based on the physical model, which is equivalent to the time of the simple overshoot, lasts approximately one second. By using the hybrid method, the critical event of a sensor failure is recognized and compensated as well. A valid state estimation β_{Est} is available throughout.

The impact of the transition section in case of a sensor failure is additionally examined in Chapter 6. The focus is mainly on the interaction with the control of the vehicle dynamics in the closed-loop operation mode.

4.3.5 Conclusion

In conclusion, the hybrid method of state estimation detects incorrect input signals into the artificial neural networks and handles them accordingly. Due to the application of the confidence level, a valid state estimation based on the simple physical models is achieved despite the sensor malfunctions respectively the sensor failure. For further investigation, especially in connection with the vehicle dynamics control, a closed-loop validation of the hybrid method of state estimation is performed in Chapter 6. In this context, the impact of the short oscillations within the estimation on the subsequent control system is investigated, which occur in case of a significant drop of the confidence level due to incorrect input variables.

5 Central Predictive Control

This Chapter focuses on the hybrid method of vehicle dynamics control. In this context the hybrid method refers to the derivation of the central predictive control approach. First, a non-linear model-based predictive control is built within this derivation. This control is based on physical model knowledge. The non-linear model-based predictive control is then mapped by a neuro-fuzzy inference system, with the premise of drastically reducing the computational effort without affecting the control quality significantly. The neuro-fuzzy inference system represents a fuzzy inference system which is capable of learning and is thus trainable by its implementation as an artificial neural network. First, the reference trajectories that represent the control targets are introduced. Subsequently, the non-linear model-based control approach is derived. The implementation of the control based on the neuro-fuzzy inference system is presented in a third Section. Within this Section, the introduced hybrid method in terms of both vehicle dynamics control algorithms is additionally validated in an open-loop operation mode based on test data.

5.1 Reference Trajectories

According to Chapter 3.2, the control targets concern the manipulation of the roll behavior, the pitch behavior and the self-steering behavior. In the following, the detailed targets within these three areas are formulated. Corresponding target values are specified for each time step. In order to construct the reference trajectories required for the non-linear model-based predictive control, the specified target values are assumed to be constant over the prediction horizon within the control algorithm. As already with the state estimation, the three areas of roll, pitch and self-steering behavior are considered separately.

5.1.1 Roll Behavior

The objective of manipulating the roll behavior is to control the vehicle according to a reference roll angle φ_{Ref}. The roll behavior results mainly from the lateral dynamics of the vehicle. An

increasing lateral acceleration results in an increasing roll angle of the vehicle. The roll behavior thus provides the driver with indirect feedback on the driving status of the vehicle for the lateral dynamics, which has to be preserved. On this basis, the roll behavior of the vehicle is controlled by specifying a dynamic roll angle φ_{Ref}. The reference roll angle φ_{Ref} at a time step k is determined by scaling the roll angle φ_{T}, which would arise in a vehicle with passive chassis elements:

$$\varphi_{\mathrm{Ref}}(k) = \xi_{\mathrm{R}} \varphi_{\mathrm{T}}(k). \tag{5.1}$$

Here, ξ_{R} represents the corresponding scaling factor. To determine the passive roll behavior, the principle of angular momentum for the vehicle body is set up around the roll center, analogous to the physical model for the state estimation in Section 4.1. In this case, the forces of passive dampers and passive stabilizers must be taken into account:

$$F_{\mathrm{D,p},i}(\varphi) = d_{\mathrm{p},i} s_{\mathrm{D},i} \dot{\varphi} \cos\varphi\,, \tag{5.2}$$

$$F_{\mathrm{St,p},i}(\varphi) = \frac{c_{\mathrm{St},i} s_{\mathrm{St},i}}{b_{\mathrm{St},i}} \arcsin\left(\frac{a_{\mathrm{St},i}}{2 b_{\mathrm{St},i}} \sin\varphi\right). \tag{5.3}$$

The damping factors of the passive dampers and the stiffness of the passive stabilizers are denoted by $d_{\mathrm{p},i}$ and $c_{\mathrm{St},i}$, respectively. The damping factors at one axle are considered to be identical. The roll acceleration $\ddot{\varphi}_{\mathrm{T}}$ of the passive vehicle can be determined by applying the principle of angular momentum:

$$\begin{aligned}
\ddot{\varphi}_{\mathrm{T}}(k) = \frac{1}{J_{xx}} \Bigg[& h_{\mathrm{GR}} m a_y(k) \cos\varphi_{\mathrm{T}}(k) + h_{\mathrm{GR}} m g \sin\varphi_{\mathrm{T}}(k) \\
& - 2\left(s_{\mathrm{S,f}}^2 c_{\mathrm{S,f}} + s_{\mathrm{S,r}}^2 c_{\mathrm{S,r}}\right) \sin\varphi_{\mathrm{T}}(k) \\
& - 2\left(d_{\mathrm{p,f}} s_{\mathrm{D,f}}^2 + d_{\mathrm{p,r}} s_{\mathrm{D,r}}^2\right) \dot{\varphi}_{\mathrm{T}}(k) \cos\varphi_{\mathrm{T}}(k) \\
& - 2 \frac{c_{\mathrm{St,f}} s_{\mathrm{St,f}}}{b_{\mathrm{St,f}}} \arcsin\left(\frac{a_{\mathrm{St,f}}}{2 b_{\mathrm{St,f}}} \sin\varphi_{\mathrm{T}}(k)\right) \\
& - 2 \frac{c_{\mathrm{St,r}} s_{\mathrm{St,r}}}{b_{\mathrm{St,r}}} \arcsin\left(\frac{a_{\mathrm{St,r}}}{2 b_{\mathrm{St,r}}} \sin\varphi_{\mathrm{T}}(k)\right) \Bigg].
\end{aligned} \tag{5.4}$$

To determine the passive roll angle φ_{T}, the roll acceleration $\ddot{\varphi}_{\mathrm{T}}$ is integrated twice using the explicit Euler method:

$$\dot{\varphi}_{\mathrm{T}}(k+1) = \dot{\varphi}_{\mathrm{T}}(k) + \ddot{\varphi}_{\mathrm{T}}(k) t_{\mathrm{S}}, \tag{5.5}$$

$$\varphi_{\mathrm{T}}(k+1) = \varphi_{\mathrm{T}}(k) + \dot{\varphi}_{\mathrm{T}}(k) t_{\mathrm{S}}. \tag{5.6}$$

By using the dynamic roll angle specification φ_{Ref}, the feedback on the lateral dynamics to the driver is preserved, however, the roll behavior can still be reduced in a targeted manner.

5.1.2 Pitch Behavior

A further target of the control is to affect the pitch behavior of the vehicle. Due to the present actuator setup including semi-active dampers and active stabilizers, the pitching movements can be influenced indirectly. In the present case, the pitching movements can be reduced. The main factor determining the pitch behavior is the longitudinal acceleration of the vehicle. Pitching movements therefore occur primarily during acceleration or deceleration and during load changes. The basic objective is to avoid pitching movements in order to increase the comfort of the vehicle occupants. For this reason, no dynamic reference value specification is made in connection with the pitch behavior. Instead, the reduction of the pitch behavior is achieved by specifying the reference value θ_{Ref} by a constant pitch angle θ_{Stat}:

$$\theta_{\mathrm{Ref}} = \theta_{\mathrm{Stat}}. \tag{5.7}$$

This constant pitch angle θ_{Stat} represents the stationary pitch angle during standstill.

5.1.3 Self-Steering Behavior

In addition to the roll and pitch behavior, the self-steering behavior represents a third control target, for which a reference value has to be specified. The self-steering behavior is thereby manipulated via the self-steering gradient. The self-steering gradient quantifies the reaction of the vehicle to a steering input. Whereas a negative self-steering gradient reduces the steering angle demand for a defined circular path, it increases if the self-steering gradient is positive. This results in agility respectively stability during cornering. Understeering vehicle behavior is generally preferred, especially in critical driving situations, (Schramm et al., 2020).

In order to set a consistent self-steering behavior for the driver, the specification is based on a static self-steering gradient SSG_{Stat}. The reference value is thus a self-steering gradient SSG_{Ref} from which understeering vehicle behavior is obtained:

$$SSG_{\mathrm{Ref}} = SSG_{\mathrm{Stat}}. \tag{5.8}$$

5.2 Non-Linear Model-Based Predictive Control

The non-linear model-based predictive control algorithm is based on physical model knowledge and results from theoretical modeling, analogous to the physical models of state estimation. In principle, the mode of operation can be briefly summarized by the steps of prediction and the ensuing optimization. First the behavior to be controlled is predicted depending on the manipulated variables. Then these predictions are optimized with the objective of matching the reference trajectories. The optimization applies to the entire predicted time, (Sieberg et al., 2018, Sieberg et al., 2019b). This results in optimal trajectories for the individual manipulated variables. Using the principle of the moving horizon, only the first values of these trajectories are

passed on to the actuator models by the manipulated variables $\boldsymbol{u}_\mathrm{C}$. The process consisting of prediction and optimization is thus performed for each time step anew.

5.2.1 Prediction

During the prediction, the future system behavior concerning the control targets is forecasted. The time for which the prediction is made is quantified by the prediction horizon n_p. Subsequently, the prediction models used for the three control targets are introduced.

Roll Behavior

Analogous to the physical state estimation in Section 4.1, a theoretical modeling is carried out for the generation of the prediction model. In the present case, the vehicle body is likewise cut free in the y-z plane. Then the principle of angular momentum is set up with respect to the roll center. The same assumptions are applied as for the physical estimation model regarding the roll behavior, according to Section 4.1.

The roll acceleration $\ddot{\varphi}_\mathrm{C}$ can be determined by transforming the principle of angular momentum analogous to (4.12) into

$$\begin{aligned}\ddot{\varphi}_\mathrm{C}(k) = \frac{1}{J_{xx}}\Big[&h_\mathrm{GR} m a_y \cos\varphi_\mathrm{C}(k) + h_\mathrm{GR} m g \sin\varphi_\mathrm{C}(k) - u_1(k) - u_2(k)\\ &- 2\left(s_{\mathrm{S,f}}^2 c_{\mathrm{S,f}} + s_{\mathrm{S,r}}^2 c_{\mathrm{S,r}}\right)\sin\varphi_\mathrm{C}(k)\\ &- \left(\left(u_3(k) + u_4(k)\right)s_{\mathrm{D,f}}^2\right)\dot{\varphi}_\mathrm{C}(k)\cos\varphi_\mathrm{C}(k)\\ &- \left(\left(u_5(k) + u_6(k)\right)s_{\mathrm{D,r}}^2\right)\dot{\varphi}_\mathrm{C}(k)\cos\varphi_\mathrm{C}(k)\Big].\end{aligned} \tag{5.9}$$

The counter roll torque at the front and the rear axle are represented by u_1 and u_2, respectively. The damping factors at the front axle are indicated by u_3 for left vehicle side and u_4 for the right side. Accordingly, u_5 and u_6 denote the damping factors acting at the left respectively at the right side of the rear axle. For prediction, the roll acceleration $\ddot{\varphi}_\mathrm{C}$, the roll rate $\dot{\varphi}_\mathrm{C}$ and the roll angle φ_C are forecasted over the prediction horizon as a function of the manipulated variables. External influence quantities such as the lateral acceleration a_y are kept constant within the prediction. For the initialization of each prediction, the variables φ_Est and $\dot{\varphi}_\mathrm{Est}$ determined by the state estimation are used.

Based on the roll acceleration $\ddot{\varphi}_\mathrm{C}$ at the time $t = k$, the roll rate $\dot{\varphi}_\mathrm{C}$ and the roll angle φ_C for the time $t = k + 1$ are determined. The scheme of the semi-implicit Euler method is applied for this purpose, (Cromer, 1981):

$$\dot{\varphi}_\mathrm{C}(k+1) = \dot{\varphi}_\mathrm{C}(k) + \ddot{\varphi}_\mathrm{C}(k) t_\mathrm{S}, \tag{5.10}$$

$$\varphi_\mathrm{C}(k+1) = \varphi_\mathrm{C}(k) + \dot{\varphi}_\mathrm{C}(k+1) t_\mathrm{S}. \tag{5.11}$$

Pitch Behavior

In accordance with the prediction of the roll behavior, the prediction of the pitch behavior is again based on the theoretical modeling that has already been used in Section 4.1 to create the physical state estimation. For this purpose, the same assumptions are made for the preparation of the free cut of the vehicle body in the x-z plane. This leads analogous to (4.21) to the pitch acceleration $\ddot{\theta}_{\mathrm{C}}$ due to the formulation and subsequent transformation of the principle of angular momentum of the vehicle body around the pitch center:

$$\begin{aligned}\ddot{\theta}_{\mathrm{C}}(k) = \frac{1}{J_{yy}}\Big[& h_{\mathrm{GP}} m a_x \cos\theta_C(k) + h_{\mathrm{GP}} m g \sin\theta_{\mathrm{C}}(k) \\ & - 2\left(l_{\mathrm{S,f}}^2 c_{\mathrm{S,f}} + l_{\mathrm{S,r}}^2 c_{\mathrm{S,r}}\right)\sin\theta_{\mathrm{C}}(k) - u_1(k)\frac{l_{\mathrm{St,f}}}{s_{\mathrm{St,f}}} - u_2(k)\frac{l_{\mathrm{St,r}}}{s_{\mathrm{St,r}}} \\ & - \left(\left(u_3(k) + u_4(k)\right) l_{\mathrm{D,f}}^2\right)\dot{\theta}_{\mathrm{C}}(k)\cos\theta_{\mathrm{C}}(k) \\ & - \left(\left(u_5(k) + u_6(k)\right) l_{\mathrm{D,r}}^2\right)\dot{\theta}_{\mathrm{C}}(k)\cos\theta_{\mathrm{C}}(k)\Big].\end{aligned} \tag{5.12}$$

The pitch rate and the pitch angle are initialized with the pitch rate $\dot{\theta}_{\mathrm{Est}}$ and pitch angle θ_{Est} determined by the state estimation. External influence variables like the longitudinal acceleration a_x are kept constant over the prediction horizon. The prediction of the pitch behavior is further depending on the control variables. The pitch rate $\dot{\theta}_{\mathrm{C}}$ and the pitch angle θ_{C} are then predicted by applying the scheme of the semi-implicit Euler method

$$\dot{\theta}_{\mathrm{C}}(k+1) = \dot{\theta}_{\mathrm{C}}(k) + \ddot{\theta}_{\mathrm{C}}(k) t_{\mathrm{S}}, \tag{5.13}$$

$$\theta_{\mathrm{C}}(k+1) = \theta_{\mathrm{C}}(k) + \dot{\theta}_{\mathrm{C}}(k+1) t_{\mathrm{S}}. \tag{5.14}$$

Self-Steering Behavior

The theoretical modeling approach is likewise used for the prediction of self-steering behavior. The assumptions made in Section 4.1 for the generation of the single-track model are also used to predict the self-steering behavior within the non-linear model-based predictive control. In order to determine and then predict the self-steering behavior of the vehicle, it is necessary to determine the slip angles $\alpha_{\mathrm{C},i}$ with

$$\alpha_{\mathrm{C,f}}(k) = \delta - \arctan\left(\frac{l_{\mathrm{f}}\dot{\psi}_{\mathrm{C}}(k) + v\sin\beta_{\mathrm{C}}(k)}{v\cos\beta_{\mathrm{C}}(k)}\right), \tag{5.15}$$

$$\alpha_{\mathrm{C,r}}(k) = -\arctan\left(\frac{-l_{\mathrm{r}}\dot{\psi}_{\mathrm{C}}(k) + v\sin\beta_{\mathrm{C}}(k)}{v\cos\beta_{\mathrm{C}}(k)}\right). \tag{5.16}$$

With respect to a precise prediction over the entire prediction horizon, the determination of the slip angles $\alpha_{\mathrm{C},i}$ involves non-linearities in contrast to the modeling in the physical state estimation within Chapter 4.1.3.

Based on the information about the slip angles the self-steering gradient can be determined, which represents the control target associated with the self-steering behavior. The additionally required lateral acceleration a_y is available as a measured quantity and is assumed to be constant throughout the prediction.

$$SSG_{\mathrm{C}}(k) = \frac{\left(\alpha_{\mathrm{C,f}}(k) - \alpha_{\mathrm{C,r}}(k)\right)}{a_y} \tag{5.17}$$

Subsequently, the further correlations necessary for the prediction of the self-steering behavior are derived. In addition to the external influence variables of the vehicle's velocity v and steering angle δ, the yaw rate $\dot{\psi}_{\mathrm{C}}$ and the side-slip angle β_{C} are also required for this calculation. Whereas the majority of the external influencing variables, which are measured by the installed sensors, are kept constant over the prediction, some variables depend on the manipulated variables. Thereby, a special role is taken by the yaw rate $\dot{\psi}_{\mathrm{C}}$. The yaw rate is also considered to be variable over the prediction. For each prediction, the yaw rate and the side-slip angle are initialized with the value measured $\dot{\psi}$ respectively determined by the state estimator β_{Est}. For the prediction of the yaw rate $\dot{\psi}_{\mathrm{C}}$, the principle of angular momentum around the vertical axis of the vehicle is set up. The transformation of the principle of angular momentum provides the yaw acceleration $\ddot{\psi}_{\mathrm{C}}$

$$\ddot{\psi}_{\mathrm{C}}(k) = \frac{1}{J_{zz}}\left(l_{\mathrm{f}} \cos\delta \left(F_{y,\mathrm{C,fl}}(k) + F_{y,\mathrm{C,fr}}(k)\right) - l_{\mathrm{r}} \left(F_{y,\mathrm{C,rl}}(k) + F_{y,\mathrm{C,rr}}(k)\right)\right). \tag{5.18}$$

For the prediction of the side-slip angle β_{C}, Newton's principle is first applied with respect to the lateral vehicle axis and transformed according to the time derivative of the side-slip angle $\dot{\beta}_{\mathrm{C}}$:

$$\dot{\beta}_{\mathrm{C}}(k) = \frac{\left(\cos\delta \left(F_{y,\mathrm{C,fl}}(k) + F_{y,\mathrm{C,fr}}(k)\right) + \left(F_{y,\mathrm{C,rl}}(k) + F_{y,\mathrm{C,rr}}(k)\right)\right)}{mv\cos\beta_{\mathrm{C}}(k)} - \dot{\psi}_{\mathrm{C}}(k). \tag{5.19}$$

For the prediction of the yaw acceleration and the time derivative of the side-slip angle, nonlinearities are considered to achieve precise predictions over the entire prediction horizon in contrast to (4.37). By integrating the yaw acceleration $\ddot{\psi}_{\mathrm{C}}$ and the time derivative of the side-slip angle $\dot{\beta}_{\mathrm{C}}$, the yaw rate $\dot{\psi}_{\mathrm{C}}$ and the side-slip angle β_{C} are predicted. The explicit Euler method is used for the integration, (Butcher, 2016):

$$\dot{\psi}_{\mathrm{C}}(k+1) = \dot{\psi}_{\mathrm{C}}(k) + \ddot{\psi}_{\mathrm{C}}(k)t_{\mathrm{S}}, \tag{5.20}$$

$$\beta_{\mathrm{C}}(k+1) = \beta_{\mathrm{C}}(k) + \dot{\beta}_{\mathrm{C}}(k)t_{\mathrm{S}}. \tag{5.21}$$

The yaw rate $\dot{\psi}_{\mathrm{C}}$ and the side-slip angle β_{C} are determined and thus predicted as a function of the lateral forces $F_{y,\mathrm{C},ij}$ acting at the tires.

These are calculated using the relationship between the corresponding cornering stiffness $c_{\alpha,\mathrm{C},ij}$ and the slip angle $\alpha_{\mathrm{C},i}$ analogous to (4.27):

$$F_{y,\mathrm{C},ij}(k) = c_{\alpha,\mathrm{C},ij}(k)\alpha_{\mathrm{C},i}(k). \tag{5.22}$$

The cornering stiffnesses $c_{\alpha,\mathrm{C},ij}$ are again dependent on the wheel loads $F_{z,\mathrm{C},ij}$. Analogous to the determination in (4.28) within the state estimation in Section 4.1, the degressive dependency between the cornering stiffnesses $c_{\alpha,\mathrm{C},ij}$ and the wheel loads $F_{z,\mathrm{C},ij}$ is represented by a semi-empirical model, (Pacejka, 2006):

$$c_{\alpha,\mathrm{C},ij}(k) = c_{\mathrm{T}1}c_{\mathrm{T}2}F_{z0,ij}\sin\left(2\arctan\left(\frac{F_{z,\mathrm{C},ij}(k)}{c_{\mathrm{T}2}F_{z0,ij}}\right)\right). \tag{5.23}$$

The wheel loads are composed of a static part resulting from the gravitational force and a dynamic part resulting from the chassis elements. Analogous to (4.29) - (4.32), the actuators in particular influence the wheel loads via the control variables:

$$\begin{aligned} F_{z,\mathrm{C,fl}}(k) = \frac{l_\mathrm{r}}{l_\mathrm{f}+l_\mathrm{r}}\Bigg(&0.5mg - u_3(k)s_{\mathrm{D,f}}\,\dot{\varphi}_\mathrm{C}(k)\cos\varphi_\mathrm{C}(k) - s_{\mathrm{S,f}}c_{\mathrm{S,f}}\sin\varphi_\mathrm{C}(k) \\ &- \frac{1}{2s_{\mathrm{St,f}}}u_1(k)\Bigg), \end{aligned} \tag{5.24}$$

$$\begin{aligned} F_{z,\mathrm{C,fr}}(k) = \frac{l_\mathrm{r}}{l_\mathrm{f}+l_\mathrm{r}}\Bigg(&0.5mg + u_4(k)s_{\mathrm{D,f}}\,\dot{\varphi}_\mathrm{C}(k)\cos\varphi_\mathrm{C}(k) + s_{\mathrm{S,f}}c_{\mathrm{S,f}}\sin\varphi_\mathrm{C}(k) \\ &+ \frac{1}{2s_{\mathrm{St,f}}}u_1(k)\Bigg), \end{aligned} \tag{5.25}$$

$$\begin{aligned} F_{z,\mathrm{C,rl}}(k) = \frac{l_\mathrm{f}}{l_\mathrm{f}+l_\mathrm{r}}\Bigg(&0.5mg - u_5(k)s_{\mathrm{D,r}}\,\dot{\varphi}_\mathrm{C}(k)\cos\varphi_\mathrm{C}(k) - s_{\mathrm{S,r}}c_{\mathrm{S,r}}\sin\varphi_\mathrm{C}(k) \\ &- \frac{1}{2s_{\mathrm{St,r}}}u_2(k)\Bigg), \end{aligned} \tag{5.26}$$

$$\begin{aligned} F_{z,\mathrm{C,rr}}(k) = \frac{l_\mathrm{f}}{l_\mathrm{f}+l_\mathrm{r}}\Bigg(&0.5mg + u_6(k)s_{\mathrm{D,r}}\,\dot{\varphi}_\mathrm{C}(k)\cos\varphi_\mathrm{C}(k) + s_{\mathrm{S,r}}c_{\mathrm{S,r}}\sin\varphi_\mathrm{C}(k) \\ &+ \frac{1}{2s_{\mathrm{St,r}}}u_2(k)\Bigg). \end{aligned} \tag{5.27}$$

The forces resulting from the chassis elements are specified according to the motivation in Section 4.1 as a function of the roll behavior.

5.2.2 Optimization

Once the vehicle dynamics have been predicted as a function of the manipulated variables, the optimization is carried out taking the reference trajectories into account. The objective is to adapt the predicted vehicle dynamics to the reference trajectories. The entire predicted timespan is used for the optimization in order to design and adapt the manipulated variables over the complete prediction horizon under the premise of the reference trajectories.

The temporal aspect is already taken into account for the formulation of the manipulated variables. These are defined by polynomials which include the respective time step, (Sieberg et al., 2019b). The manipulated variables of the counter roll torques of the front axle u_1 and the rear axle u_2 are defined by cubic polynomials:

$$u_1(k) = a_{11} + a_{12}k + a_{13}k^2 + a_{14}k^3, \tag{5.28}$$

$$u_2(k) = a_{21} + a_{22}k + a_{23}k^2 + a_{24}k^3. \tag{5.29}$$

The manipulated variables which represent the damping factors of the semi-active dampers, are formulated using quadratic polynomials:

$$u_3(k) = a_{31} + a_{32}k + a_{33}k^2, \tag{5.30}$$

$$u_4(k) = a_{41} + a_{42}k + a_{43}k^2, \tag{5.31}$$

$$u_5(k) = a_{51} + a_{52}k + a_{53}k^2, \tag{5.32}$$

$$u_6(k) = a_{61} + a_{62}k + a_{63}k^2. \tag{5.33}$$

By formulating the manipulated variables using polynomials with a temporal background, the objective of continuous characteristics over the prediction horizon is pursued. The choice of the polynomial grades is made under consideration of the desired manipulated variable characteristics. Furthermore the polynomial degree of an actuator type is consistent.

In addition, limitations of the manipulated variables are considered within the optimization. The limitations result from the physical restrictions of the respective actuators. The stabilizers characteristics can be used to determine limitations for the counter roll torques according to the conversion presented in Section 4.1. As a result, the minimum and maximum stabilizer torque $T_{\mathrm{St,min}}$ and $T_{\mathrm{St,max}}$ yield a minimum and a maximum counter roll torque T_{min} and T_{max}:

$$T_{\mathrm{min}} = \frac{a_{\mathrm{St}}}{b_{\mathrm{St}}} T_{\mathrm{St,min}}, \tag{5.34}$$

$$T_{\mathrm{max}} = \frac{a_{\mathrm{St}}}{b_{\mathrm{St}}} T_{\mathrm{St,max}}. \tag{5.35}$$

The result of the manipulated variable optimization is thus limited to this solution space for the counter roll torques u_1 and u_2.

$$T_{\min} \leq u_i \leq T_{\max}, \qquad i \in \{1,2\} \tag{5.36}$$

Likewise, restrictions are also specified for the other manipulated variables. Both a minimum damping factor $d_{\min}$ and a maximum damping factor $d_{\max}$ are determined using the empirical measurement data of the damper characteristics.

$$d_{\min} \leq u_i \leq d_{\max}, \qquad i \in \{3,4,5,6\} \tag{5.37}$$

This also restricts the solution space for the manipulated variables which considers the semi-active dampers. The following notation is used to further describe the optimization problem:

$$\boldsymbol{u}_{\mathrm{P}}(k) = \left(u_1(k), \dots, u_6(k)\right)^{\mathrm{T}}, \tag{5.38}$$

$$\boldsymbol{a} = (a_{11}, \dots, a_{63})^{\mathrm{T}}. \tag{5.39}$$

The manipulated variables are summarized in the vector $\boldsymbol{u}_{\mathrm{P}}$. The parameter vector $\boldsymbol{a}$ comprises the individual polynomial parameters of the manipulated variables. These polynomial parameters are adjusted during the optimization. Furthermore, the control states of the vehicle dynamics predicted within the non-linear model-based predictive control which depend on the manipulated variables $\boldsymbol{u}_{\mathrm{P}}$ are summarized in $\boldsymbol{x}_{\mathrm{C}}$

$$\boldsymbol{x}_{\mathrm{C}}(k) = \left(\varphi_{\mathrm{C}}(k), \theta_{\mathrm{C}}(k), SSG_{\mathrm{C}}(k)\right)^{\mathrm{T}}. \tag{5.40}$$

The reference trajectories defined in Section 5.1 are included in $\boldsymbol{x}_{\mathrm{Ref}}$. These reference trajectories represent the target values of the control of the vehicle dynamics with

$$\boldsymbol{x}_{\mathrm{Ref}}(k) = \left(\varphi_{\mathrm{Ref}}(k), \theta_{\mathrm{Ref}}(k), SSG_{\mathrm{Ref}}(k)\right)^{\mathrm{T}}. \tag{5.41}$$

During the optimization, primarily the control deviations are focused. These result from the difference between the states $\boldsymbol{x}_{\mathrm{C}}$ predicted in the control and the reference variables $\boldsymbol{x}_{\mathrm{Ref}}$. In addition, the manipulated variables $\boldsymbol{u}_{\mathrm{P}}$ are incorporated into the optimization. Thus, the energy requirement of the actuators can be reduced by the optimization. This avoids excessive manipulated variables. The importance of the individual objectives within the optimization is determined by weighting factors $\boldsymbol{\lambda}_{\mathrm{C}}$

$$\boldsymbol{\lambda}_{\mathrm{C}} = (\lambda_{\mathrm{R}}, \lambda_{\mathrm{P}}, \lambda_{\mathrm{S}}, \lambda_{\mathrm{u1}}, \lambda_{\mathrm{u2}}, \lambda_{\mathrm{u3}}, \lambda_{\mathrm{u4}}, \lambda_{\mathrm{u5}}, \lambda_{\mathrm{u6}})^{\mathrm{T}}. \tag{5.42}$$

The parameterization of the weighting factors $\boldsymbol{\lambda}_{\mathrm{C}}$ is conducted under consideration of the utility analysis specified in Section 3.3.1.

In order to solve the optimization problem and to determine the optimal manipulated variable trajectories, the cost function f_C is minimized. The optimization is executed throughout the entire prediction horizon n_p. The manipulated variable trajectories are adapted via the polynomial parameters $\boldsymbol{a}$.

$$\begin{aligned}\min_{\boldsymbol{a}} f_\mathrm{C}\big(\boldsymbol{u}_\mathrm{P}(k),\boldsymbol{x}_\mathrm{C}(k),\boldsymbol{x}_\mathrm{Ref}(k)\big)\\ = \frac{1}{n_\mathrm{p}}\Bigg[\lambda_\mathrm{R}\sum_{k=0}^{n_\mathrm{p}}\big(\varphi_\mathrm{Ref}(k)-\varphi_\mathrm{C}(k)\big)^2+\lambda_\mathrm{P}\sum_{k=0}^{n_\mathrm{p}}\big(\theta_\mathrm{Ref}(k)-\theta_\mathrm{C}(k)\big)^2\\ +\lambda_\mathrm{S}\sum_{k=0}^{n_\mathrm{p}}\big(SSG_\mathrm{Ref}(k)-SSG_\mathrm{C}(k)\big)^2+\lambda_\mathrm{u1}\sum_{k=0}^{n_\mathrm{p}}\big(u_1(k)\big)^2\\ +\lambda_\mathrm{u2}\sum_{k=0}^{n_\mathrm{p}}\big(u_2(k)\big)^2+\lambda_\mathrm{u3}\sum_{k=0}^{n_\mathrm{p}}\big(u_3(k)\big)^2+\lambda_\mathrm{u4}\sum_{k=0}^{n_\mathrm{p}}\big(u_4(k)\big)^2\\ +\lambda_\mathrm{u5}\sum_{k=0}^{n_\mathrm{p}}\big(u_5(k)\big)^2+\lambda_\mathrm{u6}\sum_{k=0}^{n_\mathrm{p}}\big(u_6(k)\big)^2\Bigg]\end{aligned} \tag{5.43}$$

The optimization problem is solved in MATLAB & Simulink at each time step. The interior-point algorithm is utilized for this purpose applying the optimization toolbox of MATLAB, (Waltz et al., 2006). This algorithm first tries to solve the optimization problem by Newton-Raphson method, (Ypma, 1995). If the solution is deemed ineffective, a trust-region method is used for the optimization. Within this method conjugate gradient iterations are executed. By combining the two methods global convergence properties are obtained, (Waltz et al., 2006).

The result of the optimization are the optimal polynomial parameters $\boldsymbol{a}$. These constitute the manipulated variable trajectories over the prediction horizon n_p. In order to be capable of reacting to disturbances in an optimal way, the principle of a receding horizon is applied. Thereby, only the manipulated variables for the next future time step are transmitted to the actuator models. This results in the counter roll torques

$$T_\mathrm{f,C} = u_1(k=t_\mathrm{S}) = a_{11}+a_{12}t_\mathrm{S}+a_{13}t_\mathrm{S}^2+a_{14}t_\mathrm{S}^3, \tag{5.44}$$

$$T_\mathrm{r,C} = u_2(k=t_\mathrm{S}) = a_{21}+a_{22}t_\mathrm{S}+a_{23}t_\mathrm{S}^2+a_{24}t_\mathrm{S}^3 \tag{5.45}$$

and the damping factors

$$d_\mathrm{fl,C} = u_3(k=t_\mathrm{S}) = a_{31}+a_{32}t_\mathrm{S}+a_{33}t_\mathrm{S}^2, \tag{5.46}$$

$$d_\mathrm{fr,C} = u_4(k=t_\mathrm{S}) = a_{41}+a_{42}t_\mathrm{S}+a_{43}t_\mathrm{S}^2, \tag{5.47}$$

$$d_\mathrm{rl,C} = u_5(k=t_\mathrm{S}) = a_{51}+a_{52}t_\mathrm{S}+a_{53}t_\mathrm{S}^2, \tag{5.48}$$

$$d_\mathrm{rr,C} = u_6(k=t_\mathrm{S}) = a_{61}+a_{62}t_\mathrm{S}+a_{63}t_\mathrm{S}^2. \tag{5.49}$$

The transfer to the actuator models is done via

$$\boldsymbol{u}_{\mathrm{C}} = \left(T_{\mathrm{f,C}}, T_{\mathrm{r,C}}, d_{\mathrm{fl,C}}, d_{\mathrm{rl,C}}, d_{\mathrm{rl,C}}, d_{\mathrm{rr,C}}\right)^{\mathrm{T}}. \tag{5.50}$$

In the next time step, the procedure of prediction and optimization is executed again. This enables a predictive mode of operation of the control with simultaneous responsiveness to non-modeled disturbances, so that optimal control results can be achieved. Furthermore, the calculated optimal solution of the previous time step is used as a starting point for the solution of the optimization problem for the actual time step. Based on this warm-start method, the optimization can be solved by fewer iterations compared to the solution without knowledge of the previous solution, (Yildirim and Wright, 2002).

5.3 Control by Co-Active Neuro-Fuzzy Inference System

In the following a neuro-fuzzy inference system is used to reproduce the non-linear model-based predictive control. Due to the optimization problem within the model-based control, which is solved iteratively, an increased computational effort is incurred and without additional restrictions a non-real-time capable system results. By using neuro-fuzzy inference systems, this iterative mode of operation is replaced by a direct mode of operation and a real-time capable system is obtained with reduced computational effort. (Sieberg et al., 2019c, Sieberg et al., 2020) present a successful proof of concept of this hybrid method for both multiple input single output and multiple input multiple output systems.

Within this thesis the training of the neuro-fuzzy inference system is done in Python. The open source deep learning library Keras and the data stream oriented framework TensorFlow are used analogous to the training of the artificial neural networks from Section 4.2, (Abadi et al., 2016, Gulli and Pal, 2017). The resulting fuzzy inference system is exported to MATLAB & Simulink afterwards and thus integrated into the simulation environment.

On the one hand, sensor signals are used as input variables into the neuro-fuzzy inference system, which are measured by the inertial measurement unit located at the center of gravity of the vehicle. These include the measured variables of longitudinal acceleration a_x, lateral acceleration a_y and yaw rate $\dot{\psi}$.

On the other hand, the states which additionally describe the system behavior with respect to the control targets are also required for the implementation of the control algorithm. These internal state variables are not measured directly, but are determined via the state estimation. Therefore, the estimated values of the roll rate $\dot{\theta}_{\mathrm{Est}}$, the pitch rate $\dot{\varphi}_{\mathrm{Est}}$ and the side-slip angle β_{Est} are considered as input variables.

Furthermore, the deviations $\Delta\theta$ and $\Delta\varphi$ of the estimated pitch angle θ_{Est} respective the estimated roll angle φ_{Est} from the reference variables θ_{Ref} and φ_{Ref} are used as input variables:

$$\Delta\theta = \theta_{\mathrm{Ref}} - \theta_{\mathrm{Est}}, \tag{5.51}$$

$$\Delta\varphi = \varphi_{\mathrm{Ref}} - \varphi_{\mathrm{Est}}. \tag{5.52}$$

Table 5.1 provides a summary on the input variables into the neuro-fuzzy inference system.

Table 5.1 Neuro-Fuzzy Inference System – Input Quantities

Input Quantity	**Unit**
Lateral Acceleration a_y	m/s²
Longitudinal Acceleration a_x	m/s²
Pitch Angle Deviation $\Delta\theta$	rad
Pitch Rate $\dot{\theta}_{\mathrm{Est}}$	rad/s
Roll Angle Deviation $\Delta\varphi$	rad
Roll Rate $\dot{\varphi}_{\mathrm{Est}}$	rad/s
Side-Slip Angle β_{Est}	rad
Yaw Rate $\dot{\psi}$	rad/s

The output variables of the neuro-fuzzy inference system correspond to the manipulated variables of the non-linear model-based predictive control. These are composed of the counter roll torques acting at the front axle $T_{\mathrm{C,f}}$ and acting at the rear axle $T_{\mathrm{C,r}}$ as well as of the damping factors front left $d_{\mathrm{C,fl}}$, front right $d_{\mathrm{C,fr}}$, rear left $d_{\mathrm{C,rl}}$ and rear right $d_{\mathrm{C,rr}}$. An overview of the output variables of the neuro-fuzzy inference system is shown in Table 5.2.

Table 5.2 Neuro-Fuzzy Inference System – Output Quantities

Output Quantity	**Unit**
Counter Roll Torques $T_{\mathrm{C},i}$	Nm
Damping Factors $d_{\mathrm{C},ij}$	Ns/m

Due to the specified structure of the neuro-fuzzy inference system with eight input variables and six output variables, the control system is implemented by a co-active neuro-fuzzy inference system, according to (Sieberg et al., 2020).

In order to achieve a consistent order of magnitude for the training of the co-active neuro-fuzzy inference system, the input and output variables are normalized according to (4.39). The hybrid method according to (Jang and Sun, 1996) is used for the training respectively the optimization of the co-active neuro-fuzzy inference system within the training. This hybrid optimization method comprises a forward pass and a backward pass which are performed one after another.

Within this hybrid optimization method, the mean squared errors between the manipulated variables u_{Mpc} resulting from the non-linear model-based predictive control and the manipulated variables u_{Canfis} resulting from the co-active neuro-fuzzy inference system are minimized.

$$MSE\left(u_{\mathrm{Mpc}}, u_{\mathrm{Canfis}}\right) = \frac{1}{n}\sum_{k=1}^{n}\left(u_{\mathrm{Mpc}}(k) - u_{\mathrm{Canfis}}(k)\right)^2. \tag{5.53}$$

During the forward pass the premise and thus the membership functions of the input variables are kept constant. The objective of this step is to adjust the consequence section and thus the output functions within the local experts for each output variable in order to optimize them with respect to the desired behavior. Since the output variables are linearly dependent on the parameters within the consequences of the respective local experts, the adaptation of these parameters can be done by the analytical solution. For this purpose the method of least squares is used, (Sorenson, 1970).

Subsequently, the backward pass of the hybrid method is performed. The objective is to adapt the membership functions via their parameters, which are present in the premise. Thereby, the predetermined consequence parameters are kept constant. The relationship between the premise parameters and the desired output variables is non-linear. Thus, the method of error backpropagation is used for the adaptation, (Rumelhart and McClelland, 1987).

The training is based on the driving maneuvers described in Section 3.5. For this task, the same database is used as for the training of the artificial neural networks in Section 4.2. The data is derived from the closed-loop simulation based on the non-linear model-based predictive control and the physical state estimators. Initially, a hyperparameter optimization for the co-active neuro-fuzzy inference system is executed, followed by the final training of it based on the resulting optimal configuration.

5.3.1 Hyperparameter Optimization

The hybrid learning method adapts the parameters of the membership functions in the premise and the parameters of the output functions in the consequence during the training of the co-active neuro-fuzzy inference system. The number of membership functions per input variable, for example, is not changed during training. In order to obtain an appropriate starting condition for the training, a hyperparameter optimization is performed beforehand, which optimizes and determines exactly these parameters.

Among the hyperparameters considered are the number of membership functions. The search space is defined by either two membership functions per input or by three. In addition to the number of membership functions per input variable, the type of these membership functions is

also considered. Only continuous functions are taken into account. These include the generalized bell function and the Gaussian function. The number of membership functions as well as their type is consistent for all input variables.

Beside these hyperparameters, which describe the premise, another hyperparameter is evaluated for the consequence. This hyperparameter defines the type of the output functions in the consequence. Functions of zero order, so called singletons, as well as functions of first order, linear functions, are evaluated. Analogous to the number and the type of the membership function regarding the input variables, the type of the output functions is consistent for all output variables and thus in all local experts. Table 5.3 summarizes the search space of the hyperparameter optimization. The search space is chosen to be restricted in the context of this thesis in order to reduce the computational effort of the hyperparameter optimization.

Table 5.3 Hyperparameter Optimization Co-Active Neuro-Fuzzy Inference System– Search Space

Parameter	**Search Space**	
Number of Membership Functions	2	3
Type of Membership Function	Gaussian	Generalized Bell
Type of Consequence Function	Singleton	Linear Function

Besides the hyperparameters optimized and adapted during the hyperparameter optimization, the co-active neuro-fuzzy inference system is characterized by further invariant hyperparameters. These include the batch sizes that are used during the hybrid learning method. The batch sizes quantify how many data points of the training data set are grouped in one batch during the training. For the forward pass and therefore for the least squares estimate a batch size of 16,384 data points is chosen. The batch size used for the backward pass is four times smaller and accordingly contains 4,096 data points.

A further hyperparameter is the type of the used T-norm which is used to evaluate the intersection of fuzzy sets. In the present application this intersection is determined by the algebraic product. Furthermore, the initialization of the membership functions is determined by the method of grid partitioning. Thereby, the value range of the input variable is divided into equal parts depending on the number of membership functions. Each of these ranges is then initially covered by an own membership function.

The mean squared error is used as the evaluation metric in training. Furthermore the configurations of the co-active neuro-fuzzy inference system are trained for ten epochs within the hyperparameter optimization. An overview of the fixed parameters of the hyperparameter optimization is presented in Table 5.4.

Table 5.4 Hyperparameter Optimization Co-Active Neuro-Fuzzy Inference System – Fixed Parameters

Parameter	Value
Batch Size Gradient Descent	4,096
Batch Size Least Squares Estimation	16,384
Method of Intersection	Algebraic Product
Metric	Mean Squared Error
Number of Epochs	10
Initialization	Grid Partitioning

In order to optimize the hyperparameters, a grid search is performed. The hyperparameter settings defined in the search space are combined in all possible variations, (Larochelle et al., 2007, LeCun et al., 2012). The resulting configurations are then trained for ten epochs and the training errors are evaluated. This type of hyperparameter optimization is suitable for the present search space, since each hyperparameter has two defined, discrete setting options within the optimization. This ultimately results in eight different hyperparameter configurations. The configurations resulting from the grid search together with the minimum training errors are listed in Table 5.5.

Table 5.5 Hyperparameter Optimization Co-Active Neuro-Fuzzy Inference System– Results

Configuration	Parameter	Value	Error
1	Number of Membership Functions Type of Membership Functions Type of Consequence	2 Gaussian Singleton	0.35273
2	Number of Membership Functions Type of Membership Functions Type of Consequence	3 Gaussian Singleton	0.35267
3	Number of Membership Functions Type of Membership Functions Type of Consequence	2 Gaussian Linear Function	0.09628
4	Number of Membership Functions Type of Membership Functions Type of Consequence	3 Gaussian Linear Function	2.31023
5	Number of Membership Functions Type of Membership Functions Type of Consequence	2 Generalized Bell Singleton	0.09218
6	Number of Membership Functions Type of Membership Functions Type of Consequence	3 Generalized Bell Singleton	0.08843
7	Number of Membership Functions Type of Membership Functions Type of Consequence	2 Generalized Bell Linear Function	0.08872
8	Number of Membership Functions Type of Membership Functions Type of Consequence	3 Generalized Bell Linear Function	2.31027

Configuration six from Table 5.5 features the minimal training error of hyperparameter optimization. Within this configuration, three membership functions are used for each input variable. These membership functions are of the type generalized bell function.

Furthermore, singletons are used in the consequence as the output functions. This configuration results in an error of 0.08843 after ten training epochs, which is the error averaged over all six output variables.

After the hyperparameter optimization, this configuration is now trained further. The training is conducted over 20 epochs. During the training the premise parameters are adjusted, among other things. In the present case the membership functions are implemented as generalized bell functions. A generalized bell function is defined by three parameters $a_{\mathrm{HP}}, b_{\mathrm{HP}}, c_{\mathrm{HP}}$:

$$\mu(x) = \frac{1}{1 + \left|\frac{x - c_{\mathrm{HP}}}{a_{\mathrm{HP}}}\right|^{2b_{\mathrm{HP}}}}. \tag{5.54}$$

Exemplarily, the membership functions for the two input variables of the roll angle deviation $\Delta\varphi$ and side-slip angle β_{Est} are depicted in Figure 5.1.

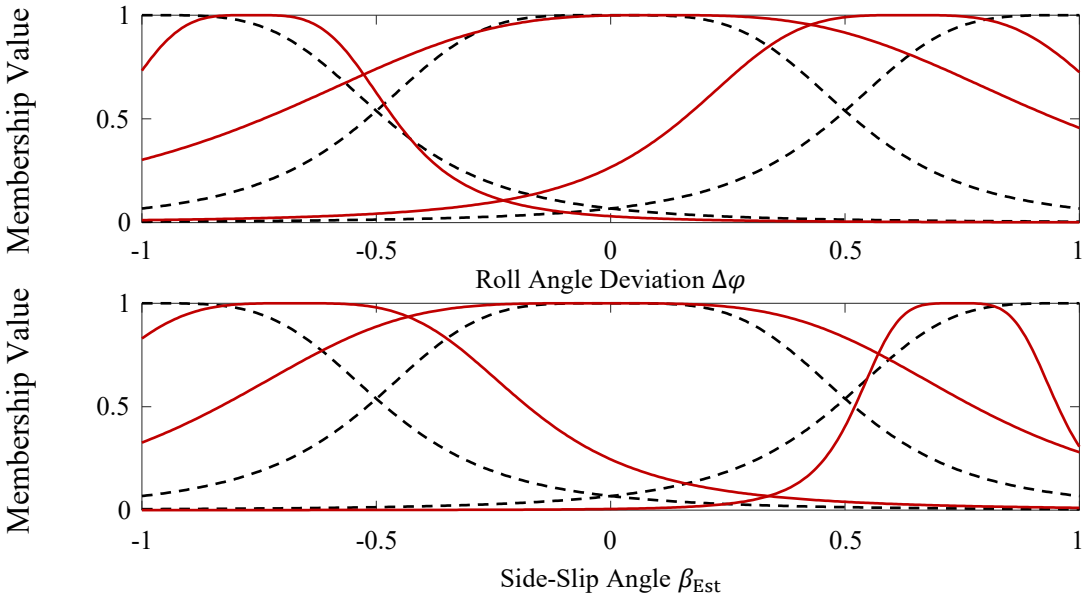

Figure 5.1 Co-Active Neuro-Fuzzy Inference System Membership Functions – Top: Scaled Roll Angle Deviation; Bottom: Scaled Side-Slip Angle

The initial definition of the membership functions covers the value range of the input variables according to the principle of grid partitioning. The initial membership functions are illustrated by black dashed lines. In addition to the initial membership functions, the optimized membership functions resulting from the training are also illustrated. These are represented by solid red lines.

The final selected co-active neuro fuzzy inference system features 6,561 rules based on the determined hyperparameters. The number of rules R_F is determined by the number of membership functions per input quantity n_MS to the power of the number of input quantities n_F

$$R_\mathrm{F} = (n_\mathrm{MS})^{n_\mathrm{F}}. \tag{5.55}$$

These rules are converted back into exact output values in each local expert by 6,561 singletons. In total, the layer of consequence comprising six local experts is thus defined by 39,366 parameters.

5.3.2 Open-Loop Validation

In analogy to the hybrid method of state estimation, the co-active neuro-fuzzy inference system is also evaluated in a first step through an open-loop validation. This open-loop validation involves the control system not yet being integrated into the simulation environment. The focus of the open-loop validation is therefore on the representation quality regarding the manipulated variables of the central model-based predictive vehicle dynamics control. Furthermore, the computational effort is evaluated. A closed-loop validation is presented in Chapter 6.

For this open-loop validation, a driving maneuver is used which has not been observed during the training of the controller. In the following the driving maneuver of the double lane change is selected. The double lane change is performed at a vehicle velocity of 70 km/h. The first lane change within the driving maneuver is clockwise. Furthermore, there is no lateral road gradient. Table 5.6 summarizes the parameters of the open-loop validation driving maneuver.

Table 5.6 Co-Active Neuro-Fuzzy Inference System Open-Loop Validation – Driving Maneuver

Driving Maneuver	Parameter	Values	Unit
Double Lane Change	Lateral Road Gradient	0	%
	Steering Direction	Clockwise	-
	Velocity	70	km/h

The driving maneuver of the double lane change is a representative driving maneuver of the test data set. The highly dynamic excitations within the driving maneuver are particularly challenging for the vehicle dynamics control.

The open-loop validation is conducted for two aspects. In a first step, the representation quality is investigated, which means how well the co-active neuro-fuzzy inference system can represent the manipulated variables of the non-linear model-based predictive vehicle dynamics control. In addition, the computational efforts for both vehicle dynamics controls are determined and evaluated.

Representation Quality

For the open-loop validation, the representation quality is first determined for the two manipulated variables of the counter roll torques. For this purpose, the counter roll torques at the front axle $T_{\mathrm{Canfis,f}}$ respectively the rear axle $T_{\mathrm{Canfis,r}}$ resulting from the co-active neuro-fuzzy inference system are plotted over time for the validation driving maneuver. This is shown in Figure 5.2. The manipulated variables resulting from the co-active neuro-fuzzy inference system are represented by black dashed lines.

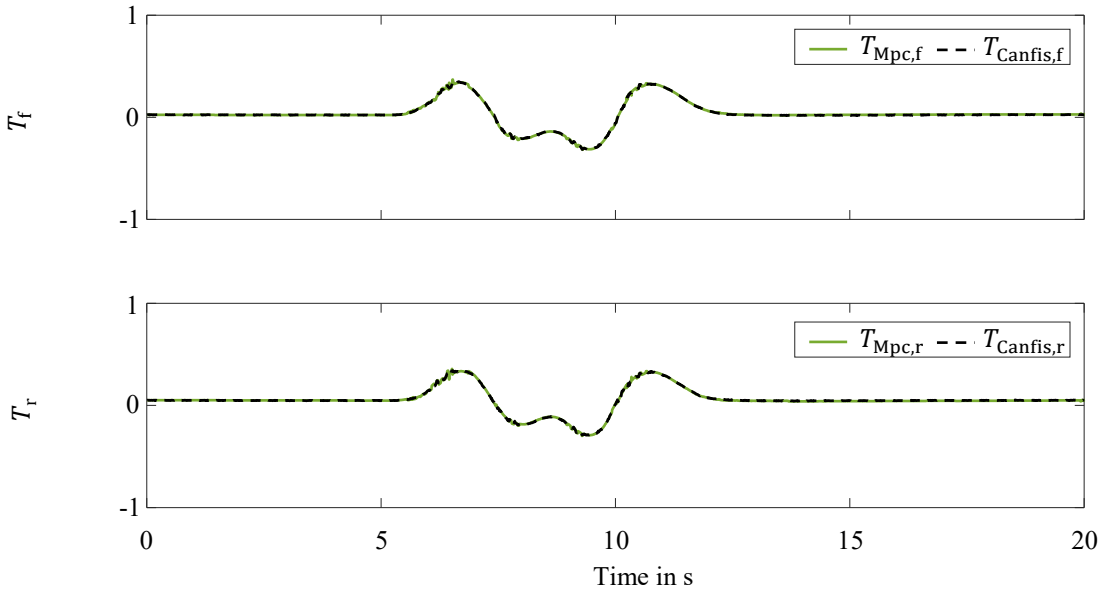

Figure 5.2 Co-Active Neuro-Fuzzy Inference System Open-Loop Validation – Representation Quality: Top: Counter Roll Torque Front; Bottom: Counter Roll Torque Rear

In addition, the manipulated variables resulting from the non-linear model-based predictive control are plotted in Figure 5.2. These are illustrated by solid green lines. The manipulated variables of the counter roll torque at the front axle $T_{\mathrm{Mpc,f}}$ respectively the rear axle $T_{\mathrm{Mpc,r}}$ are considered as reference variables for the co-active neuro-fuzzy inference system.

Both the representation of the counter roll torque at the front axle $T_{\mathrm{C,f}}$ as well as the counter roll torque at the rear axle $T_{\mathrm{C,r}}$ is done with a high quality. The examination of the courses of the counter roll torques $T_{\mathrm{C},i}$ in Figure 5.2 reveals no recognizable deviations. For this purpose the deviations of the manipulated variables resulting from the individual control algorithms are determined for a more detailed analysis by

$$\Delta T_{\mathrm{C},i} = T_{\mathrm{Mpc},i} - T_{\mathrm{Canfis},i}. \tag{5.56}$$

Thereby, a maximum absolute deviation of 0.05443 results for the representation of the counter roll torque at the front axle $T_{\mathrm{C,f}}$. For the representation of the counter roll torque at the rear axle $T_{\mathrm{C,r}}$, a maximum absolute deviation of 0.045854 is obtained. The deviations in relation to the counter roll torques $\Delta T_{\mathrm{C},i}$ are shown in Figure 5.3. The deviation for the counter roll torque at

the front axle $\Delta T_{\mathrm{C,f}}$ is represented by a solid red line and the deviation for the counter roll torque at the rear axle $\Delta T_{\mathrm{C,r}}$ by a dashed blue line.

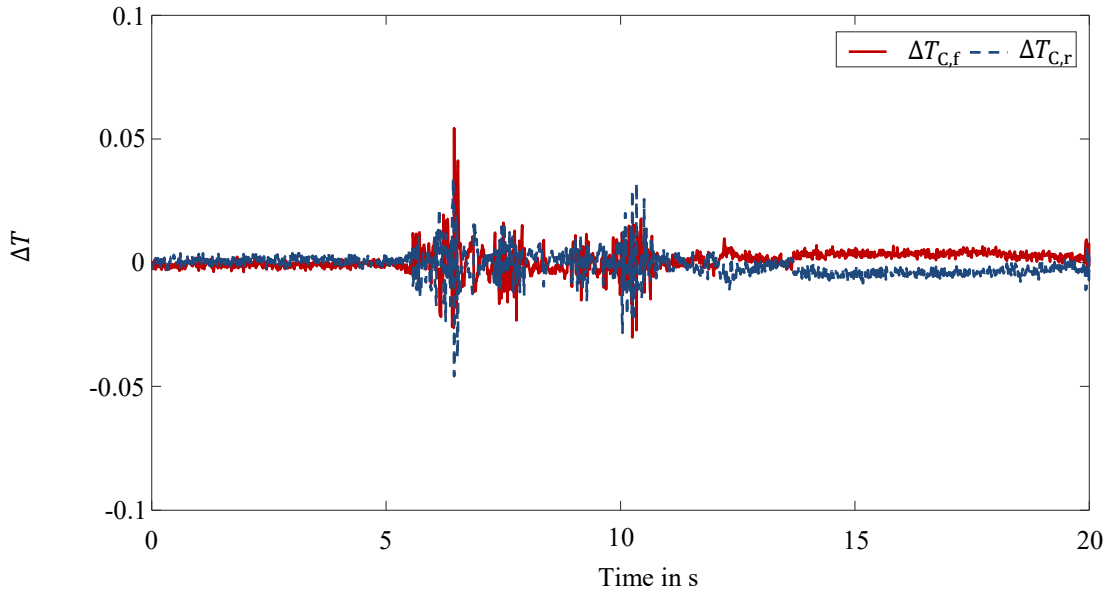

Figure 5.3 Co-Active Neuro-Fuzzy Inference System Open-Loop Validation – Representation Quality: Counter Roll Torque Deviations

In order to evaluate the representation quality regarding the entire validation maneuver, the metric of the root mean squared error is used:

$$RMSE\left(u_{\mathrm{Mpc}}, u_{\mathrm{Canfis}}\right) = \sqrt{\frac{\sum_{k=1}^{n}\left(u_{\mathrm{Mpc}}(k) - u_{\mathrm{Canfis}}(k)\right)^2}{n}}. \tag{5.57}$$

The counter roll torque at the front axle $T_{\mathrm{C,f}}$ results in a root mean squared error of 0.00455 and the counter roll torque at the rear axle $T_{\mathrm{C,r}}$ in a root mean squared error of 0.00498.

With respect to the entire validation maneuver, the representation of the counter roll torque at the front axle $T_{\mathrm{C,f}}$ thus features a slightly higher representation quality than the counter roll torque at the rear axle $T_{\mathrm{C,r}}$. In contrast, the representation of the counter roll torque at the rear axle $T_{\mathrm{C,r}}$ shows a smaller maximum absolute deviation than the counter roll torque at the front axle $T_{\mathrm{C,f}}$. In conclusion, both manipulated variables are represented very well and the small deviations for the two counter-torques lie in the same order of magnitude.

In the following, the open-loop validation with respect to the representation quality deals with the remaining manipulated variables, the damping factors $d_{\mathrm{C},ij}$. Exemplarily, the damping factors at the front left $d_{\mathrm{C,fl}}$ as well as at the rear right $d_{\mathrm{C,rr}}$ are evaluated. The representation of the further damping factors features a similar characteristic. The damping factors $d_{\mathrm{C,fl}}$ and $d_{\mathrm{C,rr}}$ are plotted over time for the validation maneuver, analogous to the manipulated variables of the counter roll torques. The damping factors of the non-linear model-based predictive control

$d_{\mathrm{Mpc},ij}$, which represent the reference variables, are illustrated by solid green lines. The damping factors resulting from the co-active neuro fuzzy inference system $d_{\mathrm{Canfis},ij}$ are likewise represented by black dashed lines. The course of the damping factors $d_{\mathrm{C},ij}$ is shown in Figure 5.4.

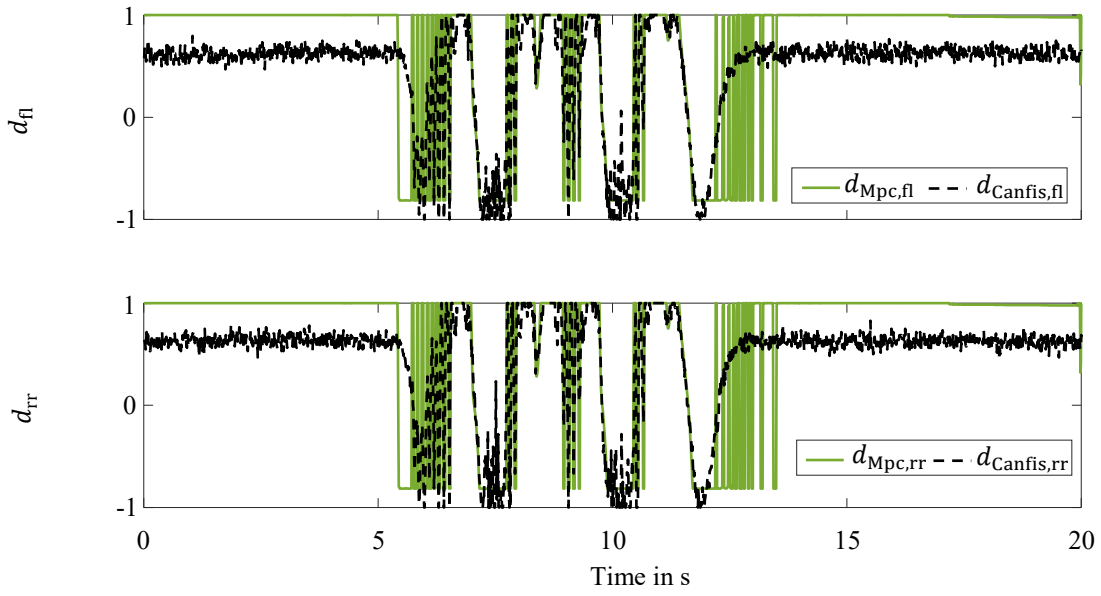

Figure 5.4 Co-Active Neuro-Fuzzy Inference System Open-Loop Validation – Representation Quality: Top: Damping Factor Front Left; Bottom: Damping Factor Rear Right

Basically, the damping factors resulting from co-active neuro-fuzzy inference system can follow the high dynamics of the damping factors resulting from the model-based predictive control only to a limited extent. In comparison to the representation of the counter roll torques, the quality of the representation is reduced in this case.

In order to evaluate the representation quality in more detail, the deviations with respect to the damping factors $\Delta d_{\mathrm{C},ij}$ are determined by

$$\Delta d_{\mathrm{C},ij} = d_{\mathrm{Mpc},ij} - d_{\mathrm{Canfis},ij}. \tag{5.58}$$

These deviations are shown in Figure 5.5. The deviation with respect to the front left damping factor $\Delta d_{\mathrm{C,fl}}$ is represented by a solid red line whereas the deviation with respect to the rear right damping factor $\Delta d_{\mathrm{C,rr}}$ is illustrated by a dashed blue line.

To evaluate the representation quality, the maximum absolute deviations for the damping factors are determined. The front left damping factor resulting from the co-active neuro-fuzzy inference system leads to a maximum absolute deviation of 1.50316. The rear right damping factor determined by the co-active neuro-fuzzy inference system yields a maximum absolute deviation of 1.60937.

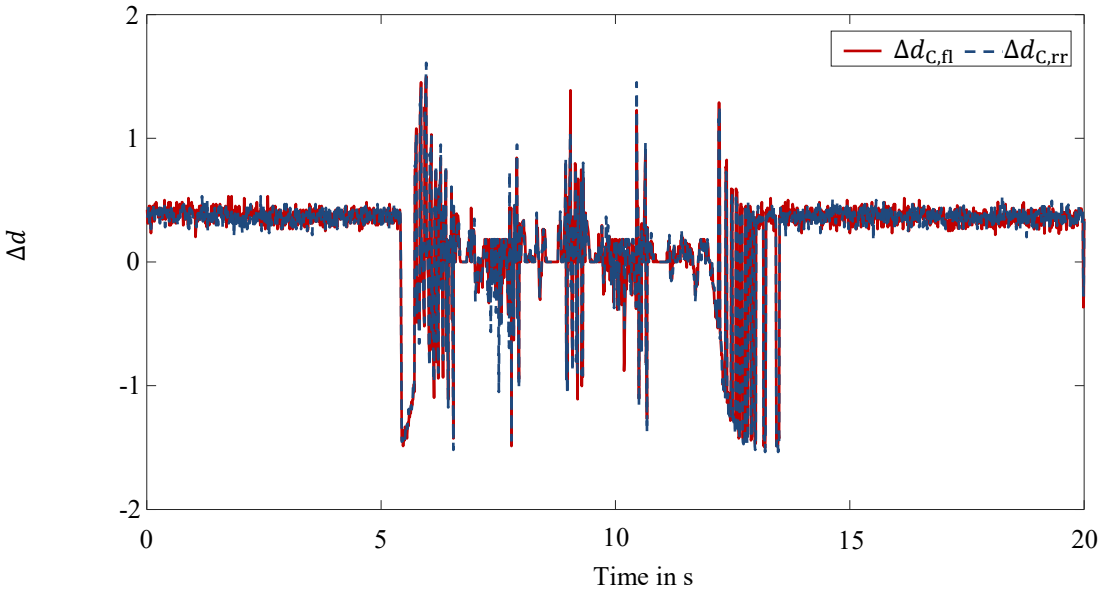

Figure 5.5 Co-Active Neuro-Fuzzy Inference System Open-Loop Validation – Representation Quality: Damping Factor Deviations

To determine the representation quality for the entire driving maneuver, the root mean squared errors for the manipulated variables of the damping factors is determined analogous to the evaluation of the counter roll torques. The representation of the damping factor front left $d_{C,fl}$ results in a root mean squared error of 0.44991. In the case of the representation of the rear right damping factor $d_{C,rr}$, the root mean squared error equals 0.44454.

Table 5.7 provides a comprehensive overview of all manipulated variables in relation to the root mean squared errors and thus the representation quality for the validation maneuver.

Table 5.7 Co-Active Neuro-Fuzzy Inference System Open-Loop Validation – Representation Quality: Root Mean Squared Errors

Manipulated Variable	**RMSE**
Counter Roll Torque Front $T_{C,f}$	0.00455
Counter Roll Torque Rear $T_{C,r}$	0.00498
Damping Factor Front Left $d_{C,fl}$	0.44991
Damping Factor Front Right $d_{C,fr}$	0.45004
Damping Factor Rear Left $d_{C,rl}$	0.43775
Damping Factor Rear Right $d_{C,rr}$	0.44454

In addition, one metric for the representation quality of all six manipulated variables is determined. This is conducted by the mean root mean squared error which equals 0.29863.

Computational Effort

In order to evaluate the computational effort, both control algorithms are considered in a stand-alone mode. For this purpose, the non-linear model-based predictive vehicle dynamics control as well as the co-active neuro-fuzzy inference system are integrated into separate models in MATLAB & Simulink. The evaluation of the calculation effort is likewise performed for the validation maneuver of the double lane change according to Table 5.6.

The control algorithms are run on a computer with 128 GB random access memory. Furthermore an Intel core i7 – 6850K with a clock frequency of 3.60 GHz and 12 individual cores form the central processing unit. Additionally the computer is equipped with four graphics processing units of the type NVIDIA GeForce GTX 1080 Ti. Table 5.8 summarizes the specifications of the computer.

Table 5.8 Co-Active Neuro-Fuzzy Inference System Open-Loop Validation – Hardware Setup

Component	Value
Central Processing Unit	Intel Core i7 – 6850K 12 Cores 3.60 GHz
Graphics Processing Unit	4 NVIDIA GeForce GTX 1080 Ti
Random Access Memory	128 GB

To evaluate the computational effort, the runtime for the simulation, the utilization of the central processing unit and the required random access memory for the corresponding processes are determined. In total the driving maneuver is simulated for ten cycles to obtain averaged values and to compensate fluctuations.

In a first step, the computational effort of the non-linear model-based predictive control is determined and evaluated. The runtime required for the validation driving maneuver based on the model-based predictive control is 149.11552 s on average. The duration of the validation driving maneuver equals 20.01 s. Thus, the model-based predictive vehicle dynamics control leads to a simulation that takes about 7.45 times longer to run compared to its duration. During the execution of the vehicle dynamics control an average utilization of the central processing unit of 8.85567 % is present. The maximum central processing unit utilization, which occurred during the execution, is in contrast 15.64100 %. In addition, the MATLAB & Simulink instance of the model-based predictive control occupies 2.43969 % of the random access memory.

In the following the co-active neuro-fuzzy inference system is examined regarding the computational effort. The execution of the control based on the co-active neuro-fuzzy inference system during the validation maneuver results in an average runtime of 17.62074 s. In this case the execution of the vehicle dynamics control is approximately 1.14 times faster than the duration of the driving maneuver. The average utilization of the central processing unit for the control

by the co-active neuro-fuzzy inference system equals 8.43133 %. The maximum central processing unit utilization that occurred during the execution of this control is 9.03775 %. Additionally the MATLAB & Simulink instance for the co-active neuro-fuzzy inference system utilizes on average 2.44023 % of the random access memory.

Table 5.9 provides an overview of the average values of the two vehicle dynamics control systems in terms of runtime, central processing unit utilization and random access memory allocation.

Table 5.9 Vehicle Dynamics Control Open-Loop Validation – Computational Effort

Control Algorithm	Criterion	Averaged Value	Unit
Co-Active Neuro-Fuzzy Inference System	Central Processing Unit Utilization	8.43133	%
	Random Access Memory Usage	2.44023	%
	Runtime	17.62074	s
Model-Based Predictive Control	Central Processing Unit Utilization	8.85567	%
	Random Access Memory Usage	2.43969	%
	Runtime	149.11552	s

5.3.3 Conclusion

In conclusion of the open-loop validation, the representation quality of the counter roll torques $T_{\mathrm{C},i}$ is very good with a mean root mean squared error of 0.00477. In contrast, the reproduction quality with respect to the damping factors $d_{\mathrm{C},ij}$ is reduced in comparison to the reproduction quality with respect to the counter roll torques $T_{\mathrm{C},i}$ resulting in a mean root squared error of 0.44556. A possible reason for this is the limited number of rules, which makes it difficult to adapt to the high dynamics of the non-linear model-based predictive control. The highly dynamic adjustments of the damping factors by the non-linear model-based predictive control result from the overall consideration of all control objectives and the objective to minimize the energy consumption of the actuators. The impact of these deviations on the control quality of the vehicle dynamics control is further validated for a closed-loop operation mode in Chapter 6.

With focus on the computational effort, the use of the co-active neuro-fuzzy inference system results in a significant reduction compared to the non-linear model-based predictive control. The runtime is reduced by a factor of approximately 8.46. This reduction of the runtime is not achieved at the cost of the central processing unit utilization. Compared to the model-based predictive control the co-active neuro-fuzzy inference system also reduces the average utilization of the central processing unit by a factor of 1.05. The maximum central processing unit utilization is even reduced by a factor of 1.73. Only the allocation of the random access memory is slightly increased by a factor of 1.00022 for the co-active neuro-fuzzy inference system. The reason for this is the usage of the consequence parameters within the co-active neuro-fuzzy

inference system. However, the increase of the random access memory utilization remains negligibly small. The effects on the computational effort with respect to the integration in the entire co-simulation will be considered further in Chapter 6 for the closed-loop operation mode.

6 Validation of the Hybrid State Estimation and Control

Within this Chapter the hybrid methods of vehicle dynamics state estimation and control are validated. For this purpose, first the validation maneuver, especially the fundamental track, is presented. Subsequently, the hybrid method of state estimation is validated individually. This is done in connection with the non-linear model-based predictive control in a first setup. The focus is on the estimation quality of the hybrid method. In a further Section the vehicle dynamics control based on the co-active neuro-fuzzy inference system is evaluated individually with respect to the control quality. This evaluation is conducted in connection with the state estimation based on the physical models. The final Section is the validation of both hybrid methods in collaboration. For this purpose the co-active neuro-fuzzy inference system is connected with the hybrid state estimation. The focus of this validation is mainly on the behavior of the holistic system with respect to malfunctions in input signals and the resulting disturbances.

6.1 Validation Scenario

For the closed-loop validation of the hybrid methods a part of the racetrack of the Hockenheimring is used. This choice of the validation scenario satisfies criteria necessary for the validation. The Hockenheimring racetrack was not included in the training data of the artificial neural networks respectively the co-active neuro-fuzzy system. Therefore, this validation scenario represents unseen data for the hybrid methods. The course of the validation track is shown in Figure 6.1.

Moreover, this validation maneuver poses additional challenges for the state estimation respectively the control within the vehicle dynamics. Due to the characteristics of a racetrack, the limits of vehicle dynamics are likewise excited within this validation scenario. For example a maximum velocity of the vehicle during the validation maneuver equals approximately 122.91 km/h. Moreover, a maximum longitudinal deceleration of about -6.59 m/s² is present.

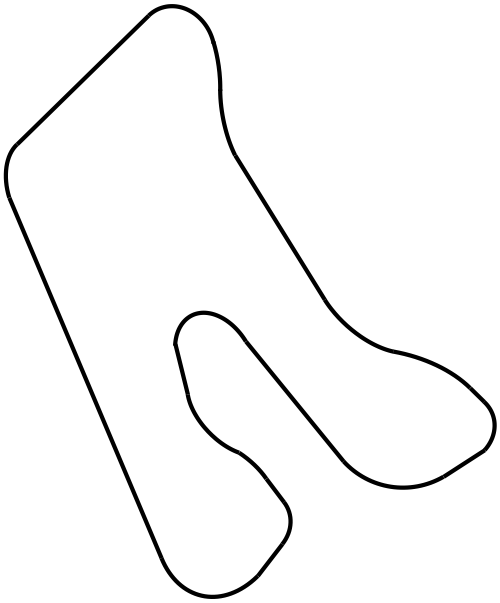

Figure 6.1 Validation Scenario – Hockenheimring

In addition to the increased excitation of the vehicle dynamics, the validation maneuver presents an increased challenge to the task of state estimation and control with respect to the road properties. Especially the lateral road gradient represents a decisive factor. The validation maneuver features a maximum absolute lateral road gradient of 8 %. Figure 6.2 illustrates the course of the lateral road gradient for one lap on the Hockenheimring racetrack.

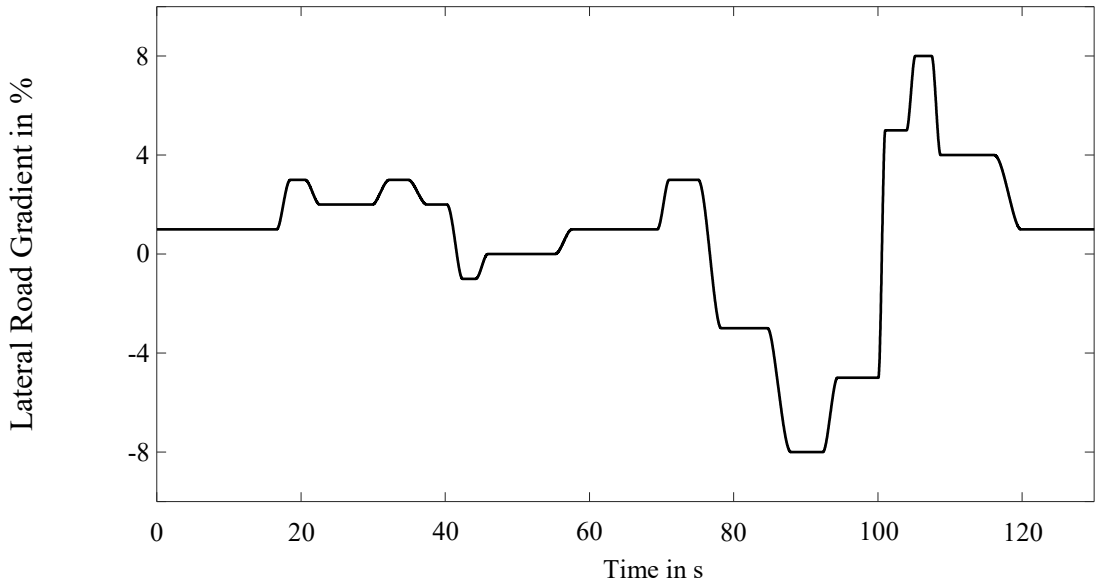

Figure 6.2 Validation Scenario – Lateral Road Gradient

Besides, the validation maneuver also exhibits longitudinal road gradients in the course of the track. There is a maximum absolute longitudinal road gradient of approximately 1.29 %. Both the extreme lateral road gradients as well as the presence of longitudinal road gradients within the track of the validation scenario exceed the characteristics prevailing in the training data as

shown in Table 3.8. A summary regarding the track characteristics of the validation scenario is provided in Table 6.1. One lap on this part of the Hockenheimring equals 2,600 m.

Table 6.1 Validation Scenario – Hockenheimring

Parameter	Value	Unit
Maximal Lateral Road Gradient	8.00000	%
Minimal Lateral Road Gradient	-8.00000	%
Maximal Longitudinal Road Gradient	1.12561	%
Minimal Longitudinal Road Gradient	-1.28740	%
Total Lap Length	2,600	m

For the following validations, the simulated IPG driver is also included besides the state estimation and the control in a closed-loop operation.

6.2 Validation of the Hybrid State Estimation

In the following, the hybrid method of state estimation is evaluated individually for the validation maneuver of the Hockenheimring racetrack. The focus is on the estimation quality. For this purpose the estimation quality is determined for the three targets of roll, pitch and side-slip behavior. In this Section, the non-linear model-based predictive control is used as the control algorithm. Table 6.2 summarizes the present setup.

Table 6.2 Hybrid State Estimation Validation – Setup

Task	Method
Control	Non-Linear Model-Based Predictive Control
State Estimation	Hybrid State Estimation

The Section concludes with a review of the results obtained.

6.2.1 Roll Angle Estimation

In a first step, the estimation quality of the hybrid method is determined concerning the roll behavior. The validation focuses on the estimation quality with respect to the roll angle. The evaluation of the estimation quality is first carried out qualitatively. For this purpose, the roll angle curves are plotted in the bottom part of Figure 6.3. In addition to the ground-truth roll angle and the roll angle estimated by the hybrid method, the representation is enhanced by the estimations purely based on the artificial neural network respectively the physical model.

The coloring is consistent with the open-loop validation in Chapter 4.3. The ground-truth roll angle φ_{Meas} is represented by a dotted red line, the roll angle resulting from the physical model φ_{P} by a solid green line, the roll angle resulting from the artificial neural network φ_{Ann} by a fine dashed blue line and the roll angle based on the hybrid method φ_{Est} by a dashed black line.

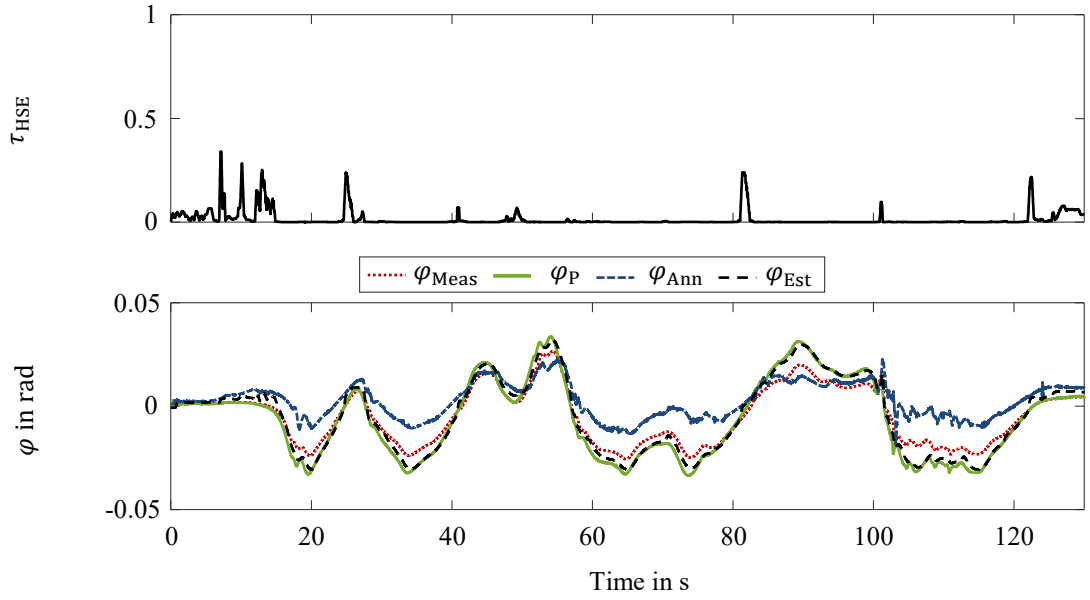

Figure 6.3 Hybrid State Estimation Validation – Roll Behavior: Top: Confidence Level; Bottom: Roll Angle Curves

Here, only in certain areas the artificial neural network results in a higher estimation quality than the physical model. The physical model provides a higher estimation quality considering one run over the Hockenheimring racetrack. Due to the lack of excitations present at the Hockenheimring during the training of the artificial neural network, it is not capable to achieve a higher estimation quality for this unknown track compared to the physical model. Exactly this aspect is considered in the hybrid method of state estimation. The hybrid method relies almost exclusively on the physical model during the validation maneuver, except for individual situations. Only in phases of known excitation the artificial neural network is trusted.

The confidence level τ_{HSE}, which reflects the confidence in the artificial neural network, is illustrated in the top part of Figure 6.3. By using the hybrid method the estimation quality can be enhanced compared to the two individual estimators. For a more detailed examination the deviations $\Delta\varphi_i$ of the estimations to the ground truth roll angle according to (4.79) are shown in Figure 6.4.

The hybrid method provides the best estimation quality over the whole maneuver. Furthermore, the artificial neural network as well as the physical model result in parts in noisy estimations. By using the unscented Kalman filter within the hybrid method, this noise is filtered so that an undistorted estimation is present.

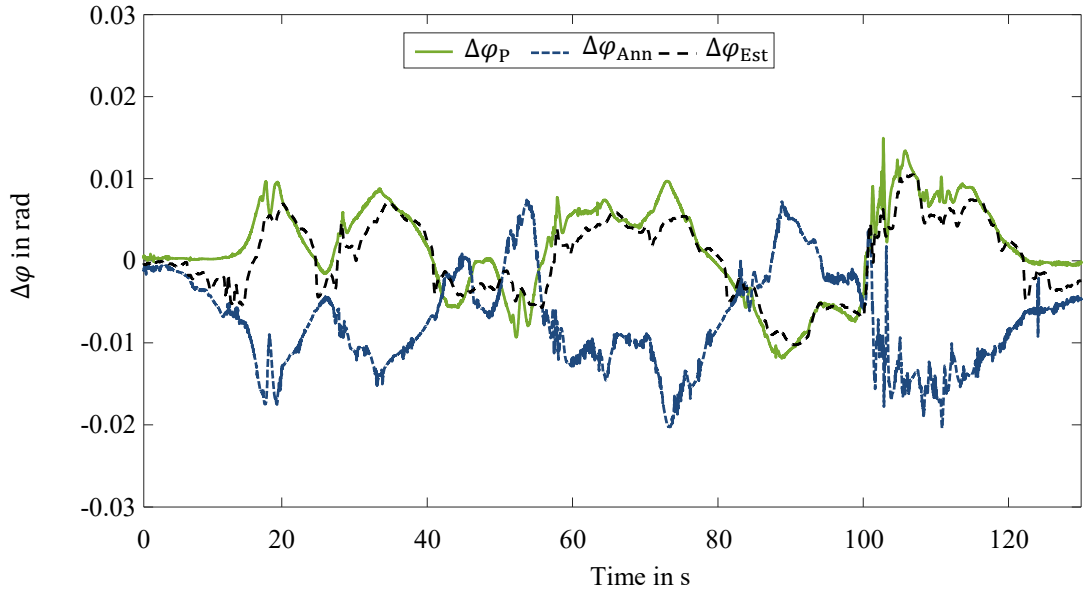

Figure 6.4 Hybrid State Estimation Validation – Roll Behavior: Roll Angle Deviations

For the quantitative evaluation of the estimation quality the root mean squared error is determined for the individual estimators by

$$RMSE(\varphi_{\text{Meas}}, \varphi_i) = \sqrt{\frac{\sum_{k=1}^{n}\left(\varphi_{\text{Meas}}(k) - \varphi_i(k)\right)^2}{n}}, \qquad i \in \{\text{Ann}, \text{Est}, \text{P}\}. \tag{6.1}$$

The assumption that the artificial neural network possesses the worst estimation quality is confirmed by the root mean squared errors. It results in a root mean squared error of 0.00929 rad, which is equivalent to 0.53228°. The physical model yields a root mean squared error of 0.00563 rad, which corresponds to 0.32258°. By using the hybrid method the highest estimation quality is achieved with a root mean squared error of 0.00466 rad, which is equivalent to 0.26700°. Table 6.3 lists these root mean squared errors.

Table 6.3 Hybrid State Estimation Validation – Roll Angle Estimation Quality

Estimation	RMSE	Unit
Artificial Neural Network	0.00929	rad
Hybrid State Estimation	0.00466	rad
Physical Model	0.00563	rad

Compared to the physical model, the hybrid method of state estimation increases the estimation quality by 17.23 %. In comparison with the artificial neural network there is even an improvement of 49.84 %.

6.2.2 Pitch Angle Estimation

In the following Section, the estimation quality of the hybrid method concerning the pitch angle is evaluated for one lap on the Hockenheimring racetrack. The evaluation of the estimation quality is first done in a qualitative way. For this purpose, the pitch angle curves for one lap on the Hockenheimring are displayed in the bottom part of Figure 6.5.

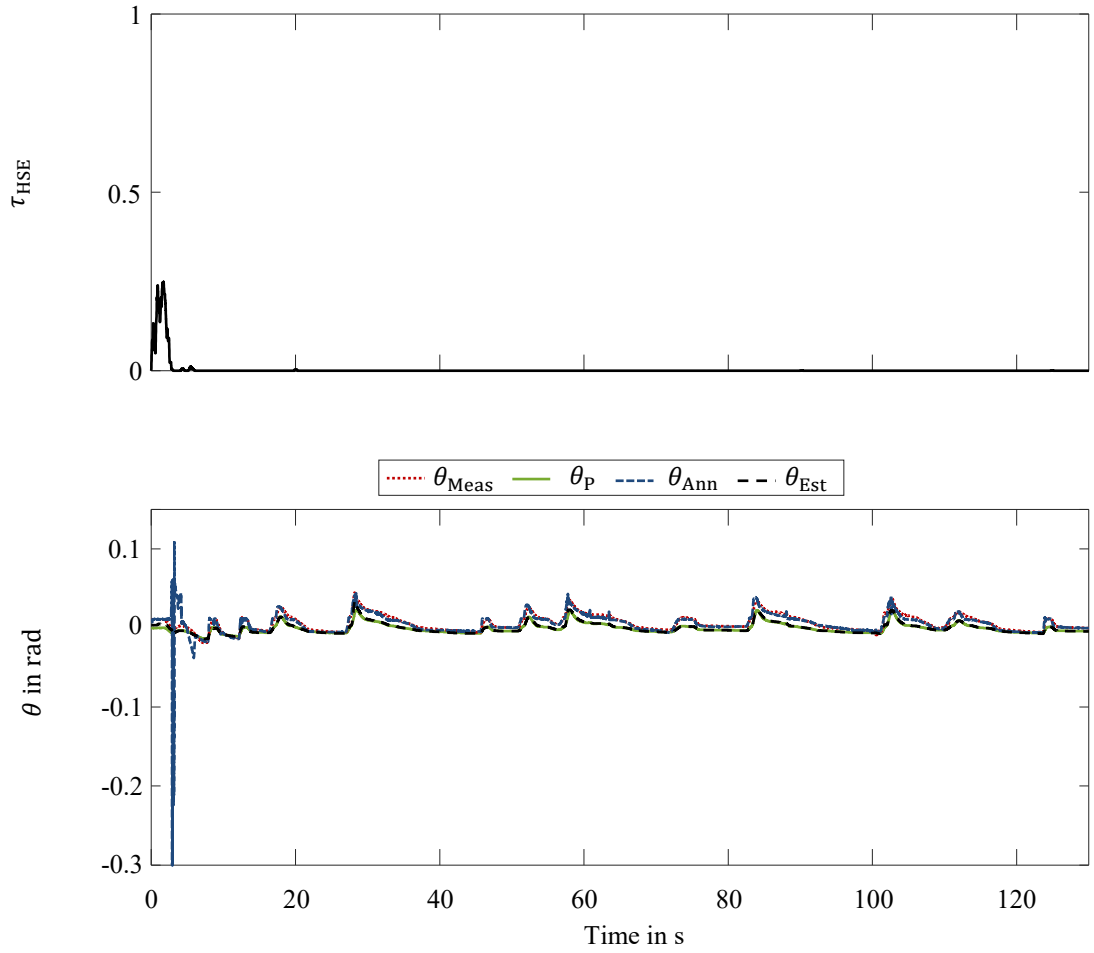

Figure 6.5 Hybrid State Estimation Validation – Pitch Behavior: Top: Confidence Level; Bottom: Pitch Angle Curves

Whereas the physical model can estimate the entire course of the pitch angle well, the artificial neural network provides an insufficient estimation shortly after the start of the lap. The unrecognized input data by the artificial neural network causes this incorrect estimation. Excluding this outlier at the beginning, the artificial neural network provides a valid state estimation. The hybrid method detects this outlier. Since the artificial neural network is supplied with completely unrecognized input data after the third second, the hybrid method relies almost exclusively on the physical model. This is also indicated by the confidence level τ_{HSE}, which is illustrated in the top part of Figure 6.5 for the lap at the Hockenheimring. Only at the beginning there is an increase in the confidence level, followed by nearly no confidence in the artificial neural network introduced by the outlier.

A detailed consideration of the estimation quality is based on the deviations $\Delta\theta_i$ of the estimations from the ground truth according to (4.78). For this purpose these deviations are plotted in Figure 6.6 for the validation maneuver.

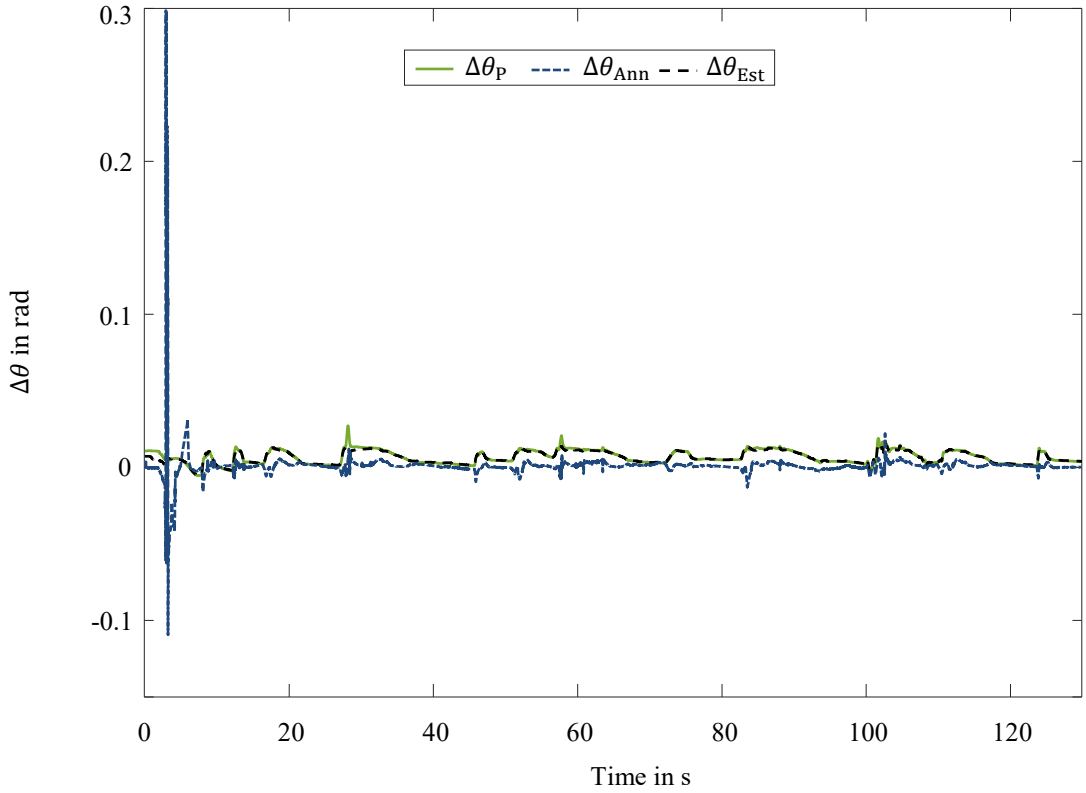

Figure 6.6 Hybrid State Estimation Validation – Pitch Behavior: Pitch Angle Deviations

The physical model results in a higher estimation quality than the artificial neural network in terms of the entire validation maneuver. Besides the outlier, the artificial neural network estimation exhibits an accurate estimation which outperforms the physical model partly. The estimation obtained from the hybrid method is also almost completely based on the estimation of the physical model. Only at the beginning of the driving maneuver the artificial neural network is slightly more trusted. By using the unscented Kalman filter within the hybrid method, additionally noise within the estimations of the individual estimators is filtered.

In order to evaluate the estimation quality also in a quantitative way, the root mean squared errors are determined for the individual estimators by

$$RMSE(\theta_{\mathrm{Meas}}, \theta_i) = \sqrt{\frac{\sum_{k=1}^{n}\left(\theta_{\mathrm{Meas}}(k) - \theta_i(k)\right)^2}{n}}, \qquad i \in \{\mathrm{Ann}, \mathrm{Est}, \mathrm{P}\}. \tag{6.2}$$

The artificial neural network results in a root mean squared error of 0.00910 rad, which is equivalent to 0.52139°. The qualitative evaluation of the estimation quality is confirmed in this case in a quantitative way. The physical model exhibits a better estimation quality, which is shown by a root mean squared error of 0.00802 rad, which corresponds to 0.45951°. By using

the hybrid method, the estimation quality can be further increased. The hybrid method results in a root mean squared error of 0.00753 rad, which is equivalent to 0.43144°. Table 6.4 summarizes the root mean squared errors of the individual estimators.

Table 6.4 Hybrid State Estimation Validation – Pitch Angle Estimation Quality

Estimation	RMSE	Unit
Artificial Neural Network	0.00910	rad
Hybrid State Estimation	0.00753	rad
Physical Model	0.00802	rad

By using the hybrid method the weakness of the artificial neural network in the estimation of the pitch angle for the unknown excitations is recognized and intercepted. Thus the estimation quality is improved through the hybrid method by 17.25 % compared to the artificial neural network. Due to the partial confidence in the artificial neural network in familiar vehicle dynamics segments, such as at the beginning of the lap, the hybrid method also leads to an improvement of the estimation quality of 6.11 % compared to the physical model.

6.2.3 Side-Slip Angle Estimation

The following Section focuses on the evaluation of the estimation quality of the hybrid method in the use case of the side-slip angle estimation. The evaluation is done first in a qualitative way analogous to the evaluation of the roll angle and pitch angle estimations. For this purpose the side-slip angle curves for one lap on the Hockenheimring racetrack are examined, which are plotted in the bottom part of Figure 6.7.

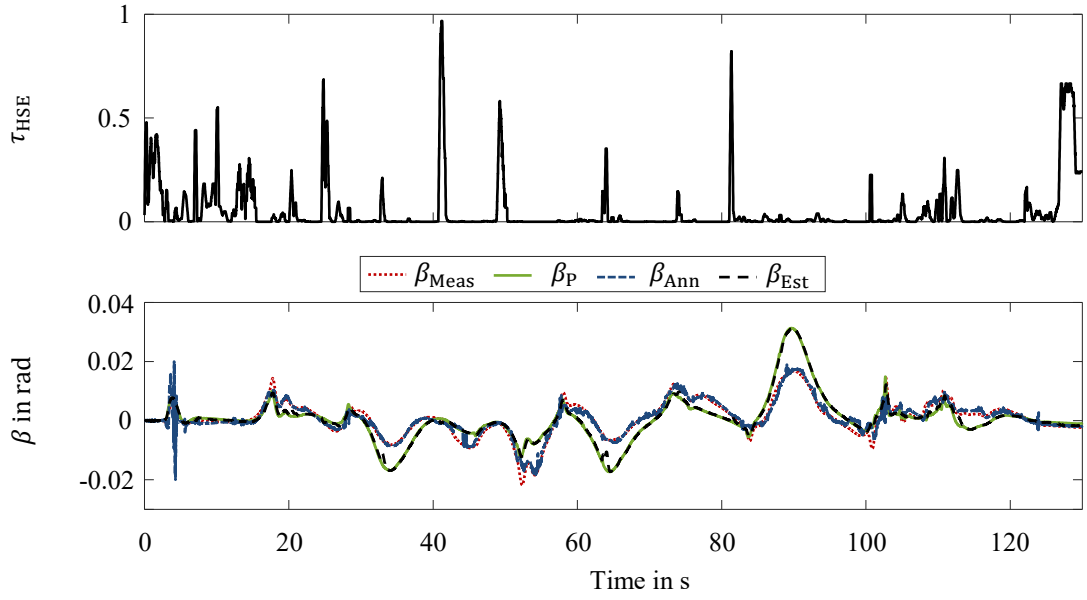

Figure 6.7 Hybrid State Estimation Validation – Side-Slip Behavior: Top: Time Confidence Level; Bottom: Side-Slip Angle Curves

The artificial neural network results in a higher estimation quality than the physical model for the entire validation maneuver. Only at the beginning of the lap, at about the fourth second, the artificial neural network results in an incomprehensible estimation. The physical model can basically reproduce the dynamics, however it fails to reproduce the corresponding amplitudes of the side-slip angle estimation due to the dynamic excitations present during the lap at the Hockenheimring racetrack. These excitations have already been recognized at least partially within the training of the artificial neural network. This is evident considering the confidence level τ_{HSE}, which is illustrated in the top part of Figure 6.7.

Compared to the roll angle and pitch angle estimation, there is a higher confidence level for the whole lap with respect to the side-slip angle estimation. The hybrid method therefore trusts the artificial neural network more than in the previous applications. In the critical situation at the beginning of the driving maneuver, however, the artificial neural network is not trusted, so that this invalid estimation of the artificial neural network is intercepted by the hybrid method. This is also shown in the detailed consideration of the side-slip angle deviations $\Delta\beta_i$ according to (4.79) in Figure 6.8.

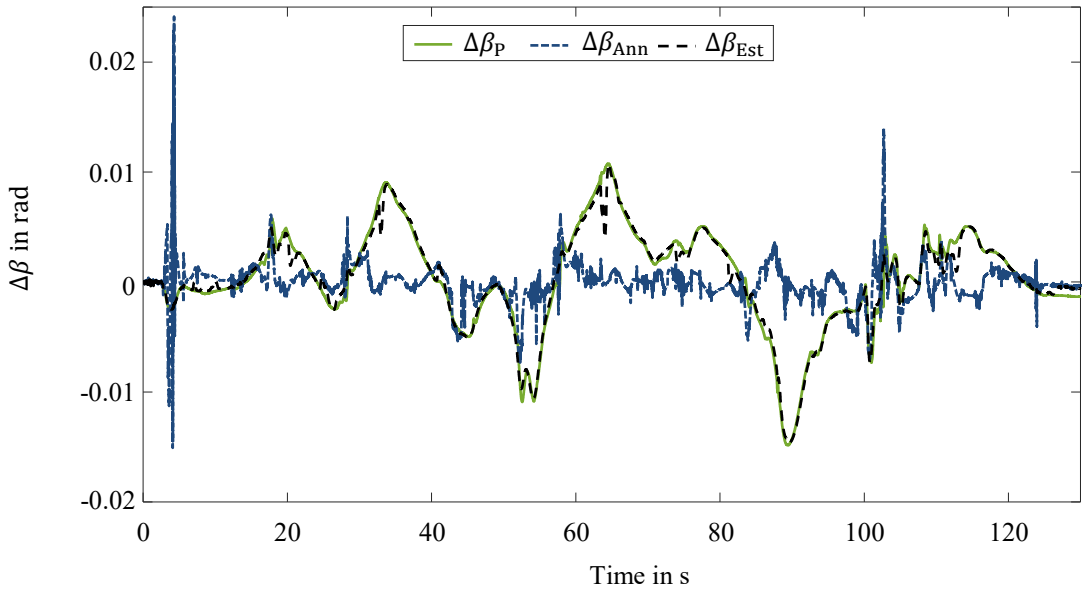

Figure 6.8 Hybrid State Estimation Validation – Side-Slip Behavior: Side-Slip Angle Deviations

The estimation by the artificial neural network is affected by noise again. The hybrid method, which still relies on the physical model in most instances, does not result in a noisy estimation similar to the previous applications within the roll angle and pitch angle estimation, which is due to the use of the unscented Kalman filter. Taking into account the depicted deviations, a higher confidence in the artificial neural network for this particular case would result in a higher estimation quality of the hybrid method. An outlook on the impact of the characteristic value $p_{\max}$ used within the determination of the confidence level τ_{HSE} on the estimation is critically examined in Chapter 7.3.

In addition to the qualitative evaluation, the estimation quality is evaluated analogous to the previous evaluations in a quantitative way by the root mean squared error:

$$RMSE(\beta_{\text{Meas}}, \beta_i) = \sqrt{\frac{\sum_{k=1}^{n}\left(\beta_{\text{Meas}}(k) - \beta_i(k)\right)^2}{n}}, \qquad i \in \{\text{Ann}, \text{Est}, \text{P}\}. \tag{6.3}$$

The physical model results in the worst estimation quality, which is also confirmed by the largest root mean squared error of 0.00447 rad, which corresponds to 0.25611°. The artificial neural network yields a root mean squared error of 0.00170 rad, which is equivalent to 0.09740°. The artificial neural network possesses the highest estimation quality. Due to the partial confidence in the artificial neural network, the hybrid method results in a root mean squared error of 0.00428 rad, which corresponds to 0.24523°. Table 6.5 summarizes the estimation quality of the individual estimators in relation to the side-slip angle estimation concerning the root mean squared errors.

Table 6.5 Hybrid State Estimation Validation – Side-Slip Angle Estimation Quality

Estimation	RMSE	Unit
Artificial Neural Network	0.00170	rad
Hybrid State Estimation	0.00428	rad
Physical Model	0.00447	rad

By using the hybrid method, the estimation quality can be improved by 4.25 % compared to an estimation based purely on the physical model. With a higher confidence in the artificial neural network, the existing potential of increasing the estimation quality by additional 60.28 % could be further exploited by the hybrid method.

6.2.4 Conclusion

In conclusion of this first part of the closed-loop validation with focus on the hybrid method of state estimation, the use of the hybrid method can further improve the estimation quality while preserving reliability. The validation of the hybrid method is deliberately done against the individual estimators to allow them to be contrasted. The integration of the physical model into an observer or a filter probably would increase its estimation quality, however, it is subordinated to the objective of a direct comparison. The results obtained highlight and confirm the working principle of the hybrid method. These results can be divided into two categories.

The first category comprises the application cases of roll and pitch angle estimation. The dynamic excitations of the roll and pitch behavior present during the validation maneuver, a lap on the Hockenheimring racetrack, were only included to a marginal extent in the training data

for the artificial neural network estimators. Therefore, this leads to rather small confidence levels within the hybrid state estimators. For this reason, the confidence of the hybrid methods is mainly based on the physical models with respect to the reliability. However, in the few cases of excitations that the artificial neural networks have encountered during training, the confidence levels in the artificial neural network estimators are raised. Since in these well-known segments, the artificial neural networks result in estimations of higher quality than the physical model. Therefore, an even higher estimation quality is achieved by the hybrid method compared to the individual state estimators.

The second category is represented by the application case of the side-slip angle estimation. In comparison to the application cases of rolling and pitching, the excitations regarding the side-slip angle were encountered more often during the training of the artificial neural network. This is indicated by the increased confidence level. However, the hybrid method basically trusts the physical state estimator more than the artificial neural network during the whole validation maneuver with regard to reliability. The state estimation based on the artificial neural network thus features unexploited potential, which is subordinated to the objective of reliability and thus neglected by a conservative interpretation of the hybrid method with respect to the determination of the confidence level. This reveals the influence of the characteristic value $p_{\max}$, which is used for the determination of the confidence level. If this characteristic value is reduced, the confidence in the artificial neural network is increased, thus the estimation quality of the hybrid method could be further enhanced. Similar to the first category, this would allow the hybrid method to achieve an even higher estimation quality than those of the individual estimators. The impact of the choice of this characteristic value is further discussed in Chapter 7.3.

6.3 Validation of the Central Predictive Vehicle Dynamics Control

In the following Section the hybrid method of predictive vehicle dynamics control in a closed-loop operation mode is evaluated individually. The evaluation is based again on one lap on the Hockenheimring racetrack. The central predictive vehicle dynamics control is in closed-loop operation within this Section along with the physical state estimators. The evaluation is done with regard to the control quality as well as the computational effort. Table 6.6 provides an overview of the current setup.

Table 6.6 Central Predictive Vehicle Dynamics Control Validation – Setup

Task	Method
Control	Co-Active Neuro-Fuzzy Inference System
State Estimation	Physical Model

The Section closes with a conclusion on the results achieved by the utilization of the hybrid method for the vehicle dynamics control.

6.3.1 Control Quality

In the first step the control quality of the central predictive vehicle dynamics control is determined. For this purpose the domains of roll, pitch and self-steering are considered. In addition to the comparison between the non-linear model-based predictive control and the control based on the co-active neuro-fuzzy inference system, the behavior of the test vehicle equipped with passive chassis elements and thus without vehicle dynamics control is considered.

Roll Behavior

The control of the roll behavior is the main control objective of the central predictive vehicle dynamics control. To achieve this objective the roll angle is controlled. To evaluate the control quality, the course of the roll angle for one lap on the Hockenheimring is analyzed. This is illustrated in Figure 6.9.

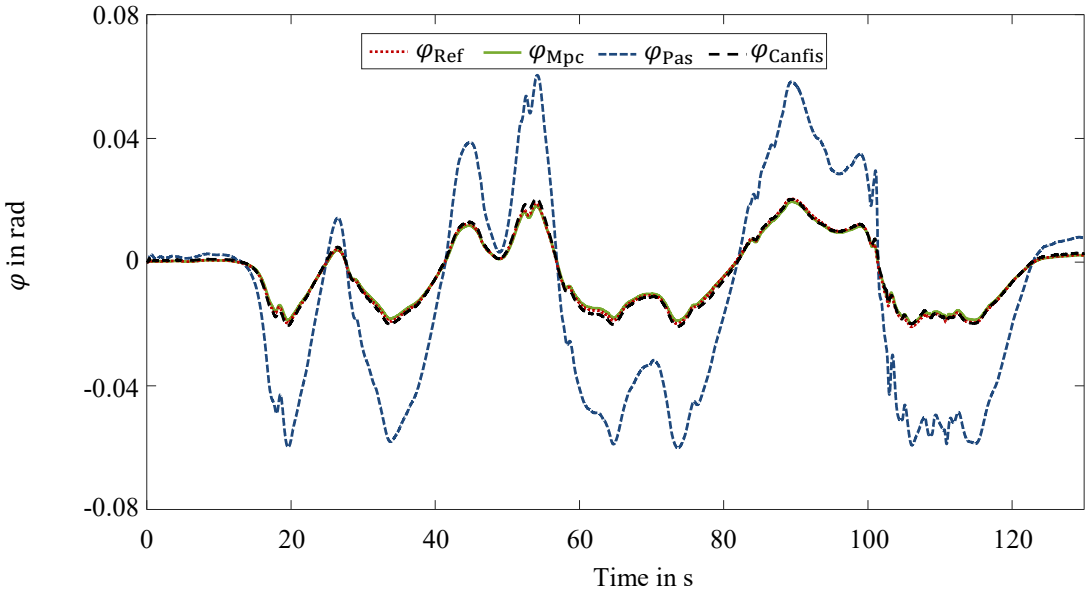

Figure 6.9 Central Predictive Vehicle Dynamics Control Validation – Roll Behavior: Roll Angle Curves

A dotted red line illustrates the reference trajectory of the roll angle φ_{Ref} for the validation maneuver. The roll angle φ_{Mpc} resulting from the non-linear model-based predictive control is represented by a solid green line. In addition, Figure 6.9 depicts the roll angle course φ_{Pas} of the test vehicle, which results from a passive chassis without a vehicle dynamics control. A blue fine dashed line represents this course φ_{Pas}. A dashed black line indicates the roll angle $\varphi_{\mathrm{Canfis}}$ resulting from the co-active neuro-fuzzy inference system.

The reference trajectory of the roll angle φ_{Ref} provides a reduction of about 75 % compared to the roll angle of the passive vehicle φ_{Pas} regarding the whole validation maneuver. Both the roll angle φ_{Mpc} resulting from the non-linear model-based predictive control and the roll angle $\varphi_{\mathrm{Canfis}}$ resulting from the co-active neuro-fuzzy inference system follow the reference trajectory φ_{Ref} without any noticeable deviation. In order to evaluate the control qualities in more detail, the control deviations $\Delta\varphi_i$ are determined by

$$\Delta\varphi_i = \varphi_{\mathrm{Ref}} - \varphi_i, \qquad i \in \{\mathrm{Canfis}, \mathrm{Mpc}\}. \tag{6.4}$$

The control deviations resulting from the control algorithms are shown in Figure 6.10. The color scheme remains consistent.

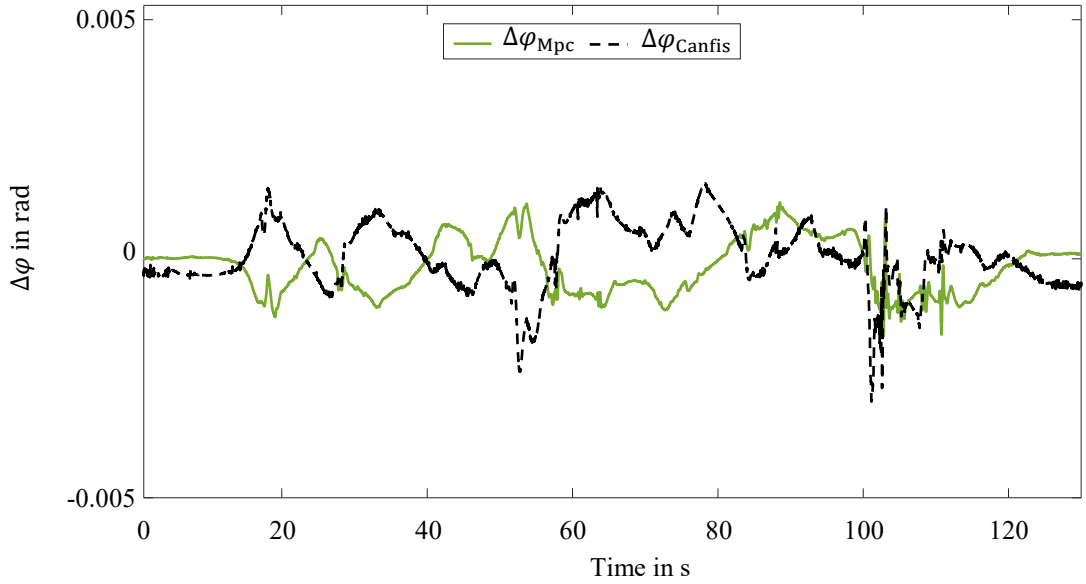

Figure 6.10 Central Predictive Vehicle Dynamics Control Validation – Roll Behavior: Roll Angle Deviations

Both control algorithms exhibit an excellent control quality. Based on the qualitative analysis, the non-linear model-based predictive control shows a slightly better control quality. This is confirmed by examining the maximum absolute control deviations. The non-linear model-based predictive control results in a maximum absolute control deviation of 0.00162 rad, which corresponds to 0.09282°. In contrast, the co-active neuro-fuzzy inference system results in a maximum absolute control deviation of 0.00299 rad, which is equivalent to 0.17131°.

In order to evaluate the control quality in a quantitative way for the entire validation maneuver, the root mean squared error is utilized:

$$RMSE(\varphi_{\mathrm{Ref}}, \varphi_i) = \sqrt{\frac{\sum_{k=1}^{n}\left(\varphi_{\mathrm{Ref}}(k) - \varphi_i(k)\right)^2}{n}}, \qquad i \in \{\mathrm{Canfis}, \mathrm{Mpc}\}. \tag{6.5}$$

The non-linear model-based predictive control results in a root mean squared error of 0.00058 rad corresponding to 0.03323°. The predictive vehicle dynamics control based on the

co-active neuro-fuzzy inference system yields a root mean squared error of 0.00068 rad, which is equivalent to 0.03896°. Table 6.7 highlights the root mean squared errors of both predictive vehicle dynamics control algorithms.

Table 6.7 Central Predictive Vehicle Dynamics Control Validation – Roll Behavior Control Quality

Estimation	RMSE	Unit
Co-Active Neuro-Fuzzy Inference System	0.00068	rad
Model-Based Predictive Control	0.00058	rad

Considering the whole validation maneuver, the non-linear model-based predictive control possesses a slightly better control quality. In principle, however, both control algorithms feature an outstanding control quality with regard to the roll behavior. The co-active neuro-fuzzy inference system is able to reproduce the non-linear model-based predictive control in a sufficient quality with regard to the roll behavior.

Pitch Behavior

In the following, the hybrid method of vehicle dynamics control is evaluated with respect to the pitch behavior. Here the control objective of the central predictive control is the reduction of pitching movements. Compared to the control of the roll behavior the reduction of pitching movements is a secondary objective. For the evaluation, first of all the arising pitch angle courses for one lap on the Hockenheimring are evaluated. The pitch angle curves are illustrated in Figure 6.11.

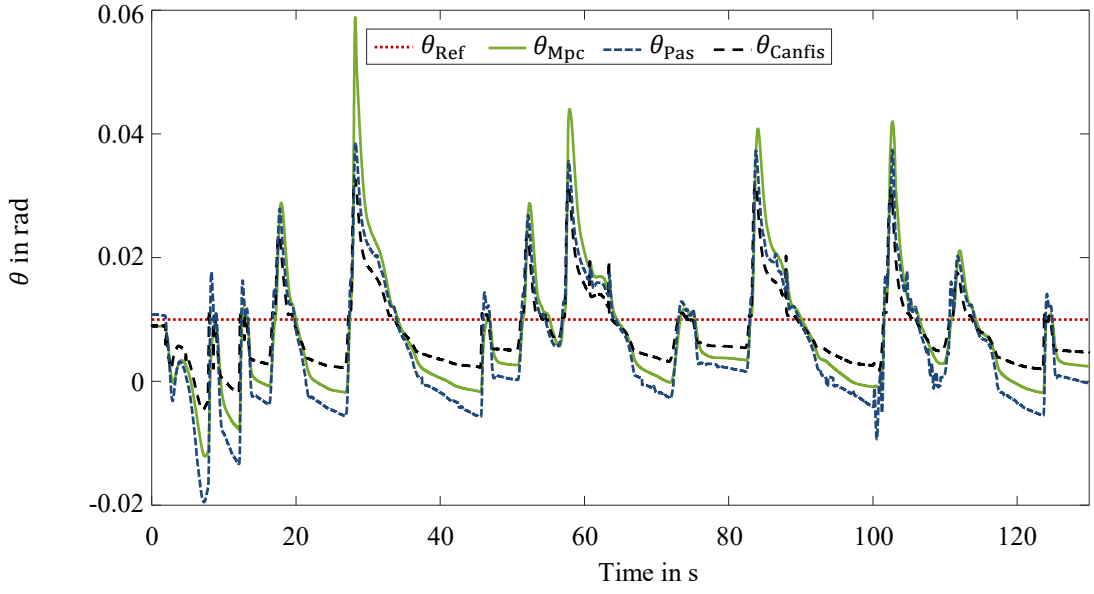

Figure 6.11 Central Predictive Vehicle Dynamics Control Validation – Pitch Behavior: Pitch Angle Curves

In principle, due to the current equipment of the vehicle with active stabilizers and semi-active dampers in combination with the prioritization of the objectives of the central predictive vehicle dynamics control, only a reduction of pitching movements is feasible. For this reason, a constant pitch angle is preset for the reference value θ_{Ref}.

The evaluation of the pitch reduction of the central predictive vehicle dynamics control algorithms is conducted in comparison to the pitch angle course of the vehicle equipped with a passive chassis. The non-linear model-based predictive control results in a pitch reduction for negative pitch angles. In the segment of positive pitch angles, however, there is no permanent reduction of the pitch angle. Sometimes even larger pitch angles are generated than in the passive pitch angle course. This is due to the prioritization of the control targets in the cost function of the non-linear model-based predictive control.

In contrast, the co-active neuro-fuzzy inference system performs a reduction of pitching movements for both positive and negative pitch angles. This results from the deviations in the damping factors which have already been investigated and highlighted in Section 5.3. Basically, the damping factors of the semi-active dampers serve as the main influencing factor on the pitch behavior.

In order to confirm this, the reduction of the pitch behavior is analyzed in detail by the control deviations:

$$\Delta\theta_i = \theta_{\mathrm{Ref}} - \theta_i, \qquad i \,\epsilon\, \{\mathrm{Canfis}, \mathrm{Mpc}\}. \tag{6.6}$$

The control deviations are plotted for this purpose additionally in Figure 6.12 for the validation maneuver.

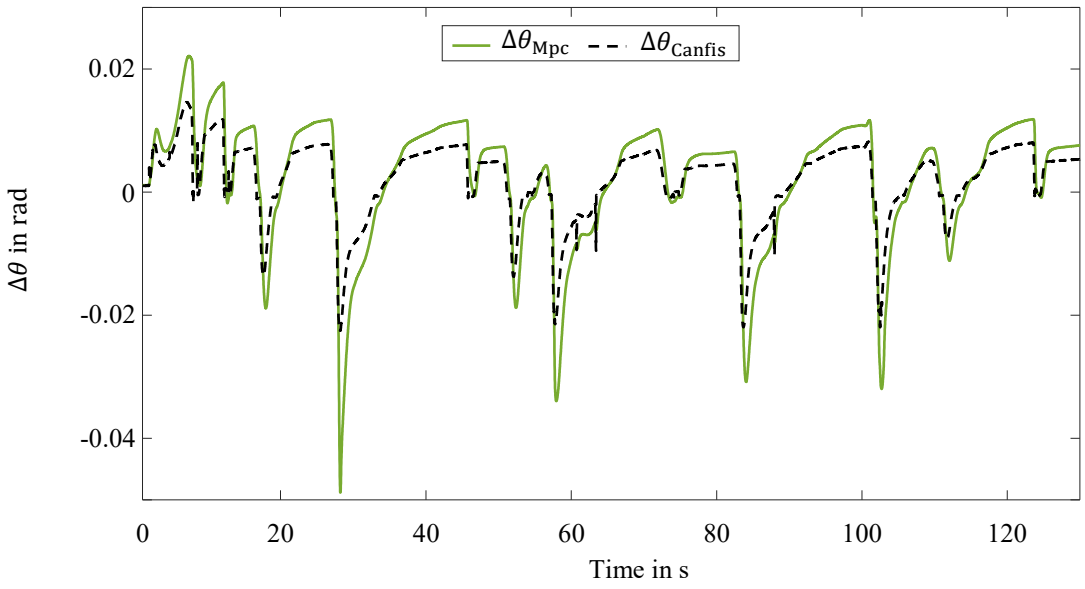

Figure 6.12 Central Predictive Vehicle Dynamics Control Validation – Pitch Behavior: Pitch Angle Deviations

This representation verifies that the co-active neuro-fuzzy inference system results in a higher reduction of the pitch behavior than the non-linear model-based predictive control. The maximum absolute deviation in the pitch angle for the co-active neuro-fuzzy inference system of 0.02267 rad is also significantly lower than that of the non-linear model-based predictive control of 0.04885 rad, which corresponds to 1.29890° for the co-active neuro-fuzzy inference system and 2.79890° for the non-linear model-based predictive control.

The root mean squared error is used for the further quantitative evaluation of the entire validation maneuver:

$$RMSE(\theta_{\mathrm{Ref}}, \theta_i) = \sqrt{\frac{\sum_{k=1}^{n}\left(\theta_{\mathrm{Ref}}(k) - \theta_i(k)\right)^2}{n}}, \qquad i \in \{\mathrm{Canfis}, \mathrm{Mpc}\}. \tag{6.7}$$

In principle, the root mean squared errors and the deviations in general are larger for this control objective than for the ones achieved for the roll behavior due to the already described influence factors.

The non-linear model-based predictive control results in a root mean squared error of 0.01023 rad, which is equivalent to 0.58614°. In contrast the co-active neuro-fuzzy inference system yields a root mean squared error of 0.00651 rad corresponding to 0.37300°. Table 6.8 provides a summary over the root mean squared errors of the two central predictive control algorithms.

Table 6.8 Central Predictive Vehicle Dynamics Control Validation – Pitch Behavior Control Quality

Estimation	RMSE	Unit
Co-Active Neuro-Fuzzy Inference System	0.00651	rad
Model-Based Predictive Control	0.01023	rad

Both central predictive control algorithms perform a reduction of the pitch behavior. The non-linear model-based predictive control reduces pitching movements by 5.01 % compared to a vehicle with passive chassis. The co-active neuro-fuzzy inference system even reduces pitching movements by 39.55 %. These differences are caused by the deviations in the manipulated variables of the damping factors shown in Chapter 5.3.2, which represent the main influencing factors in terms of the pitch behavior.

Self-Steering Behavior

The third objective of the central predictive vehicle dynamics control is the manipulation of the self-steering behavior. In comparison to the control of the roll behavior, this control objective is a secondary objective just like the objective of the pitch reduction. For the evaluation of the

self-steering behavior, a pseudo quantity $\tilde{\alpha}_i$ is used in the following for reasons of presentation. This pseudo quantity $\tilde{\alpha}_i$ describes the difference between the mean slip angles of the front and rear axle:

$$\tilde{\alpha}_i = \alpha_{\mathrm{f},i} - \alpha_{\mathrm{r},i} = a_y \, SSG_i, \qquad i \in \{\mathrm{Canfis}, \mathrm{Mpc}, \mathrm{Pas}, \mathrm{Ref}\}. \tag{6.8}$$

$\tilde{\alpha}_i$ thus represents the product of the self-steering gradient SSG_i and the lateral acceleration a_y. In a first step, the course of the pseudo quantity $\tilde{\alpha}_i$ is evaluated for one lap on the Hockenheimring racetrack. This representation suggests the impression of a dynamic reference quantity, which is due to the variability in the lateral acceleration a_y. Analogous to the control objective of the pitch reduction, a constant reference value SSG_{Ref} is also present here.

The courses of the pseudo quantities $\tilde{\alpha}_i$ are illustrated in Figure 6.13.

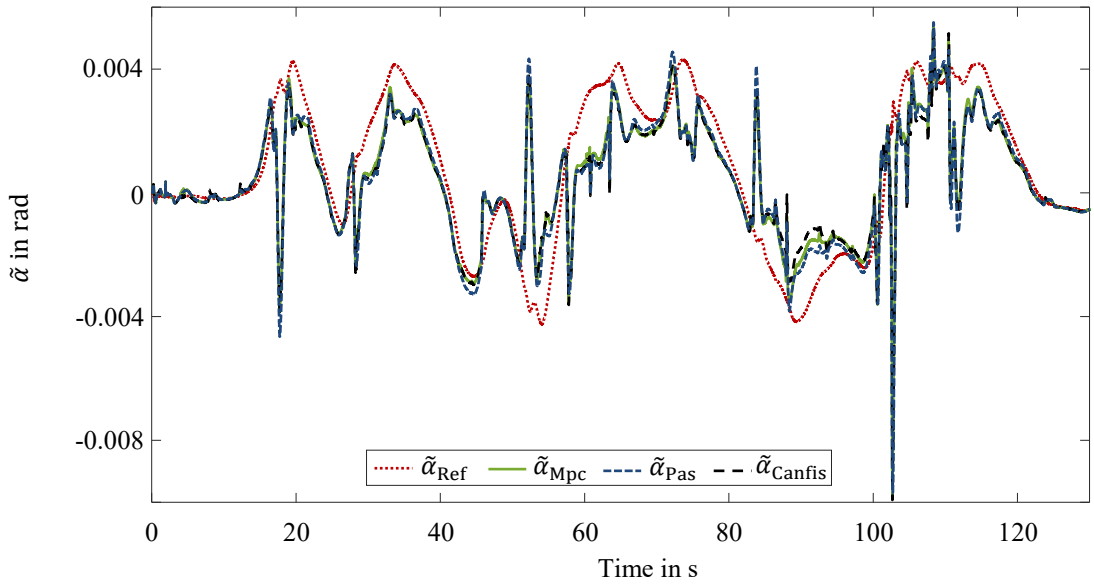

Figure 6.13 Central Predictive Vehicle Dynamics Control Validation – Self Steering Behavior: Slip Angle Difference Curves

In general, the courses of the pseudo quantity $\tilde{\alpha}_i$ resulting from the two central predictive controls do not differ significantly from the course resulting from the vehicle with passive chassis. The prioritization of the control targets is relevant here as well as the possibility of only indirect influence analogous to the area of pitch reduction.

For a detailed analysis the control deviations converted to the pseudo quantity $\Delta\tilde{\alpha}_i$ are determined by

$$\Delta\tilde{\alpha}_i = \tilde{\alpha}_{\mathrm{Ref}} - \tilde{\alpha}_i, \qquad i \in \{\mathrm{Canfis}, \mathrm{Mpc}\}. \tag{6.9}$$

These converted control deviations $\Delta\tilde{\alpha}_i$ are plotted in Figure 6.14.

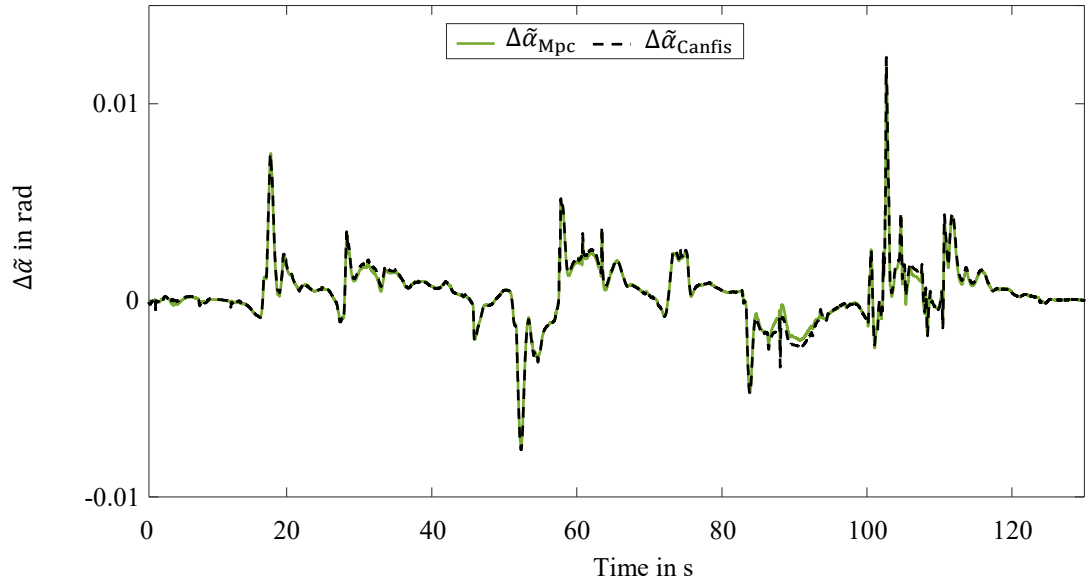

Figure 6.14 Central Predictive Vehicle Dynamics Control Validation – Self-Steering Behavior: Slip Angle Difference Deviations

In the detailed analysis there are almost no differences between the curves resulting from the non-linear model-based predictive control $\Delta\tilde{\alpha}_{\mathrm{Mpc}}$ and the co-active neuro-fuzzy inference system $\Delta\tilde{\alpha}_{\mathrm{Canfis}}$. With regard to the influencing variables of the self-steering behavior, which are mainly realized by the distribution of the counter roll torques between the front and the rear axle, the evaluation presented in Section 5.3 is confirmed. Already during the open-loop validation an excellent representation quality with respect to the manipulated variables of the counter roll torques are determined.

This is also confirmed by the observation of the maximum absolute control deviations, which are nearly equal. The non-linear model-based predictive control yields a maximum absolute control deviation of 0.01223 rad corresponding to 0.70073°. In contrast the co-active neuro-fuzzy inference system results in a maximum absolute control deviation of 0.01237 rad, which is equivalent to 0.70875°.

The quantitative evaluation of the control quality is done consistently by considering the root mean squared errors:

$$RMSE(\tilde{\alpha}_{\mathrm{Ref}}, \tilde{\alpha}_i) = \sqrt{\frac{\sum_{k=1}^{n}\left(\tilde{\alpha}_{\mathrm{Ref}}(k) - \tilde{\alpha}_i(k)\right)^2}{n}}, \qquad i \in \{\mathrm{Canfis}, \mathrm{Mpc}\}. \tag{6.10}$$

The impression is confirmed that both control systems achieve almost identical results with regard to the self-steering behavior, which has already been obtained by the qualitative evaluation. The non-linear model-based predictive control results in a root mean squared error of 0.00150 rad, which corresponds to 0.08594°. The root mean squared error obtained through the co-active neuro-fuzzy inference system amounts to 0.00158 rad, which is equivalent to

0.09053°. Table 6.9 highlights the root mean squared errors resulting from the two central predictive control algorithms.

The principal factor influencing the control quality in relation to the self-steering behavior is the weighting of the control objectives within the cost function of the non-linear model-based predictive control. In the context of this thesis the segment of self-steering behavior represents a minor control objective.

Table 6.9 Central Predictive Vehicle Dynamics Control Validation – Self-Steering Behavior Control Quality

Estimation	RMSE	Unit
Co-Active Neuro-Fuzzy Inference System	0.00158	rad
Model-Based Predictive Control	0.00150	rad

6.3.2 Computational Effort

Besides the consideration of the control quality, the evaluation of the computational effort is an important aspect of the validation. The reduction of the computational effort by the co-active neuro-fuzzy inference system is the main reason for the implementation of this hybrid method.

Analogous to the evaluation of the computational effort in the context of the open-loop validation in 5.3, the following Section determines and compares the quantities of the runtime, the utilization of the central processing unit as well as the usage of the random access memory for both central predictive control algorithms. The results within this Section represent values averaged over ten simulations of one lap of the Hockenheimring racetrack. The hardware used is identical to the one used for the open-loop validation, which is listed in Table 5.8.

In the first step the computational effort is determined regarding the non-linear model-based predictive control. The average runtime for one lap on the Hockenheimring racetrack involving the non-linear model-based predictive control is 947.58160 s. With an original duration of the validation maneuver of 130.8 s, the simulation including the non-linear model-based predictive control takes about 7.24 times longer. During the execution of the central predictive control an average central processing unit utilization of 9.94958 % is present. The maximum utilization of the central processing unit within all runs equals 13.54167 %. Moreover, an average random access memory usage of 2.44773 % occurs.

In contrast, the co-active neuro-fuzzy inference system results in an average runtime for one lap at the Hockenheimring racetrack of 102.10748 s. Thus, during the execution of the co-active neuro-fuzzy inference system a simulation is conducted, which is about 1.28 times faster than the original duration. The average utilization of the central processing unit is 8.33283 %. Within all ten runs a maximum central processing unit utilization of 9.11783 % is present. The average

usage of the random access memory during the execution of the co-active neuro-fuzzy inference system equals 2.45411 %.

An overview of the averaged quantities in relation to the runtime, the central processing unit utilization and the random access memory usage for the two central predictive vehicle dynamic controls is provided in Table 6.10.

Table 6.10 Central Predictive Vehicle Dynamics Control Validation – Computational Effort

Control Algorithm	Criterion	Averaged Value	Unit
Co-Active Neuro-Fuzzy Inference System	Central Processing Unit Utilization	8.33283	%
	Random Access Memory Usage	2.45411	%
	Runtime	102.10748	s
Model-Based Predictive Control	Central Processing Unit Utilization	9.94958	%
	Random Access Memory Usage	2.44773	%
	Runtime	947.58160	s

6.3.3 Conclusion

In conclusion, the hybrid method of vehicle dynamics control can be evaluated with respect to its general objective. By using the co-active neuro-fuzzy inference system, the computational effort of the central predictive vehicle dynamics control based on the non-linear model-based predictive control algorithm has to be reduced while preserving the control quality.

At first the focus is on the control quality regarding the hybrid method of vehicle dynamics control. For this purpose, the relative deviations with respect to the control quality in terms of the root mean squared errors between the non-linear model-based control and the control based on the co-active neuro-fuzzy inference system are determined. These relative deviations are related to the mean absolute value of the respective reference variables.

For the control of the roll behavior a reduction of the control quality by the co-active neuro-fuzzy inference system of 1.02 % results. Concerning the control of the self-steering behavior, the application of the hybrid method results in a reduction of the control quality by 3.81 %. The absolute control deviations for these two control objectives are minimal, so that the control quality is still preserved by the use of the co-active neuro-fuzzy inference system. With regard to the control objective of reducing pitching movements, an even larger reduction is achieved by using the hybrid method of vehicle dynamics control. Compared to the non-linear model-based predictive control, the co-active neuro-fuzzy inference system reduces pitching movements even more by 37.20 %. This improvement, however, is not a systematic advantage but results from the deviations in the representation of the damping factors, as presented in Chapter 5.3.2.

In general, the hybrid method for vehicle dynamics control allows the co-active neuro-fuzzy inference system to map the non-linear model-based predictive control while preserving the

control quality. The characteristic of the central predictive vehicle dynamics control is thus preserved.

The second decisive characteristic with regard to the implementation of the hybrid method of vehicle dynamics control is the reduction of the computational effort. As with the open-loop validation, this is also accomplished successfully in the case of the closed-loop validation. By using the co-active neuro-fuzzy inference system as the central predictive vehicle dynamics control algorithm, the runtime is reduced by a factor of 9.28 compared to the non-linear model-based predictive control. This is not accompanied by an increase of the computational effort in relation to the central processing unit utilization. In contrast to this the utilization of the central processing unit is even reduced by using the co-active neuro-fuzzy inference system. In comparison to the non-linear model-based predictive control the average central processing unit utilization is reduced by a factor of 1.19 and the maximum utilization of the central processing unit even by a factor of 1.49. In analogy to the results of the open-loop validation, only the memory requirement in the form of the random access memory usage increases by a factor of 1.00261 for the use of co-active neuro-fuzzy inference system. This slight increase results from the utilization of the premise and consequence parameters. However, the increase remains negligibly small.

In conclusion, the hybrid method of vehicle dynamics control, in other words the mapping of the non-linear model-based predictive control by the co-active neuro-fuzzy inference system, is able to reduce the computational effort significantly without deteriorating the control quality of the central predictive vehicle dynamics control.

6.4 Collaborative Validation of the Hybrid Methods

In the following final Section of the validation the two hybrid methods of state estimation and vehicle dynamics control are evaluated in simultaneous application. The hybrid state estimation thus works in collaboration with the co-active neuro fuzzy inference system. The validation is performed in closed-loop operation mode for one lap on the Hockenheimring racetrack. The focus of the validation of this collaborative setup is on an aggravated validation scenario. This includes failures of input variables into the state estimators based on artificial neural networks. The Section is closed with a conclusion on the obtained results regarding the aggravated circumstances in this special validation scenario.

Table 6.11 summarizes the setup within the collaborative validation scenario.

Table 6.11 Collaborative Validation – Setup

Task	Method
Control	Co-Active Neuro-Fuzzy Inference System
State Estimation	Hybrid Method

6.4.1 Aggravated Validation Scenario

For the evaluation of the collaborative setup of both hybrid methods, the validation scenario based on the lap at the Hockenheimring is made especially challenging. For this purpose two failures of input signals are simulated. The input signals are limited to signals into the artificial neural networks, which are used within the state estimation.

First, a failure into the artificial neural network for the estimation of the pitch behavior is simulated. The input variable used for this is the time derivative of the velocity $\frac{dv}{dt}$. The failure occurs at the third second, afterwards this input signal is not available. The second input variable for which a failure is simulated is the mean wheel speed $\bar{n}_{\mathrm{V}}$. This variable is used as an input quantity into the artificial neural network for the estimation of the side-slip angle. The failure occurs at second 21. After each failure, the corresponding signals are characterized by "Not a Number".

Table 6.12 provides an overview of the aggravated validation scenario with regard to the input signal failures.

Table 6.12 Collaborative Validation – Aggravated Scenario

Estimation Target	Signal	Malfunction	Time
Pitch Behavior	Time Derivative of the Velocity $\frac{dv}{dt}$	Failure	Second 3
Side-Slip Angle	Average Wheel Speed $\bar{n}_{\mathrm{V}}$	Failure	Second 21

In the following, the impact of the signal failures on the three target quantities of the central predictive vehicle dynamics control is evaluated.

Roll Behavior

The evaluation of the control quality with respect to the roll behavior for this aggravated scenario is first performed qualitatively. For this purpose the roll angle curves for the lap on the Hockenheimring are evaluated. These curves are shown in the bottom part of Figure 6.15.

The reference trajectory for the roll angle control φ_{Ref} is represented by a dotted red line. The roll angle curve $\varphi_{\mathrm{P,Mpc}}$ resulting from the state estimation based on the physical model in combination with the non-linear model-based predictive control is displayed by a solid green line. This curve $\varphi_{\mathrm{P,Mpc}}$ is generated without sensor failures. Additionally, the roll angle φ_{Pas} resulting from the vehicle with passive chassis is illustrated by a fine dashed blue line. The roll angle curve $\varphi_{\mathrm{Est,Canfis}}$ resulting from the hybrid method of state estimation in combination with the control by the co-active neuro-fuzzy inference system is represented by a dashed black line.

In principle both setups based on state estimation and control $\varphi_{\mathrm{P,Mpc}}$ and $\varphi_{\mathrm{Est,Canfis}}$ follow the reference trajectory φ_{Ref}. Whereas at the points of time of the signal failures at second 3 respectively 21 there are no direct effects recognizable due to the control by the co-active neuro-fuzzy inference system, partly larger deviations from the reference trajectory result in the further course of the validation maneuver.

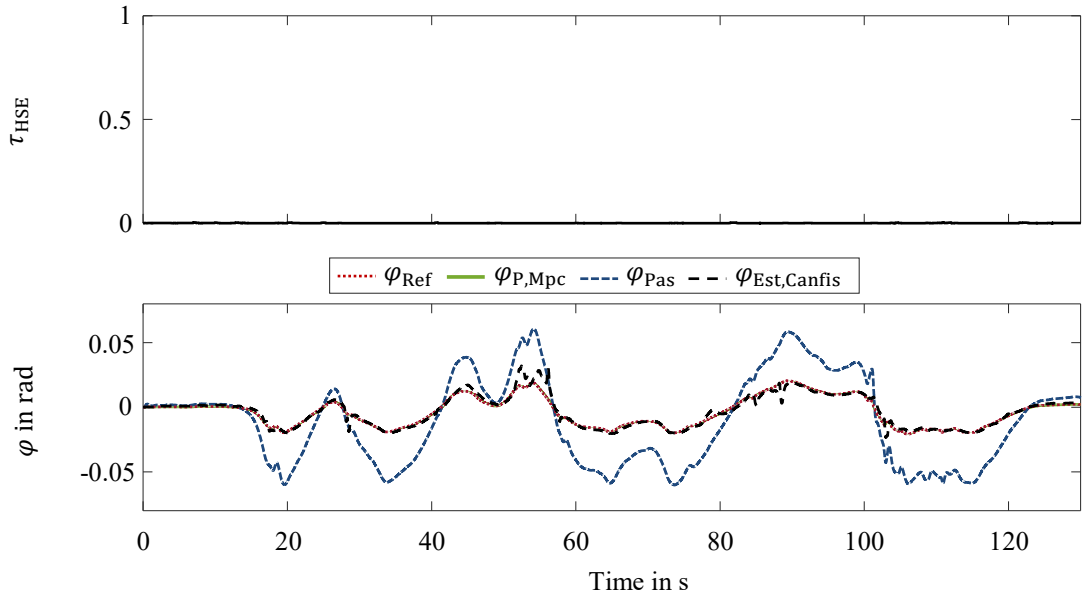

Figure 6.15 Collaborative Validation – Roll Behavior: Top: Confidence Level; Bottom: Roll Angle Curves

The functionality of the hybrid state estimation remains unaffected by the signal failures, so that a valid state estimation is available for the entire lap on the Hockenheimring. However, the changed situation is recognized by the hybrid method. This is illustrated by the very poor confidence level τ_{HSE}, which is shown in the top part of Figure 6.15.

For a detailed evaluation of the hybrid methods, the deviations from the reference value $\Delta\varphi_i$ for both setups according to (6.4) are determined. These deviations are shown in Figure 6.16. The coloring remains consistent so that the setup based on the non-linear model-based predictive control in combination with the physical state estimation is represented by a solid green line and the setup based on the co-active neuro-fuzzy inference system and the hybrid method of state estimation is represented by a dashed black line.

By this detailed examination minimal impacts of the signal failures on the control by the co-active neuro-fuzzy inference system are evident. Both at second 3 and at second 21 small changes in the course of the deviation $\Delta\varphi_{\mathrm{Est,Canfis}}$ occur. Subsequently, partly larger deviations occur in the course of the validation maneuver. This results in a maximum absolute deviation of 0.02480 rad for the setup based on both hybrid methods, which corresponds to 1.42094°. In comparison, the maximum absolute deviation for the setup based on the purely physical models is 0.00162 rad, which is equivalent to 0.09282°.

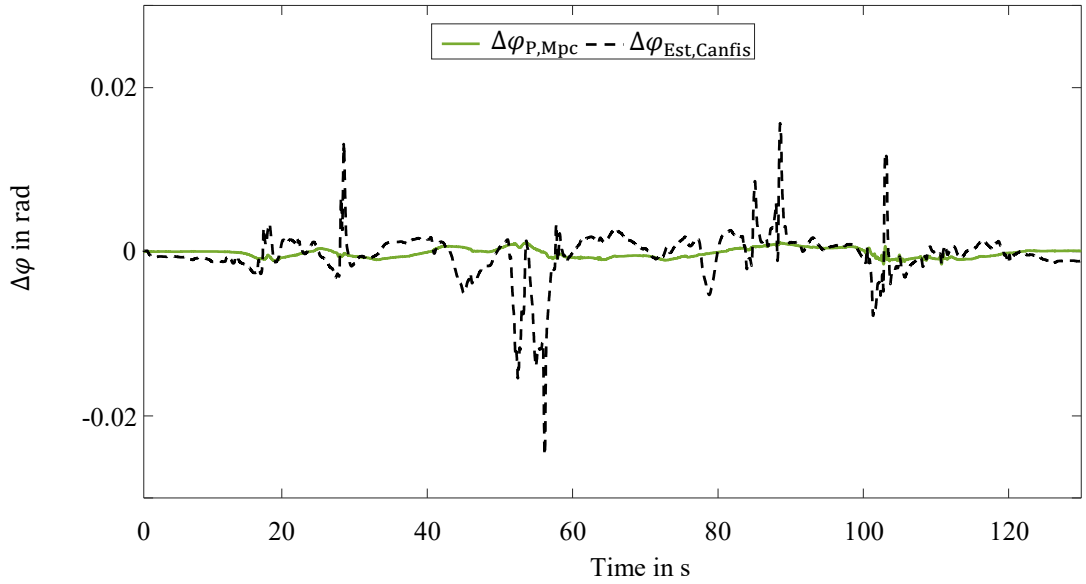

Figure 6.16 Collaborative Validation – Roll Behavior: Roll Angle Deviations

In order to evaluate both setups also in a quantitative way, the root mean squared errors according to (6.5) are determined. The setup based on the non-linear model-based predictive control and the state estimation using the physical model results in a root mean squared error of 0.00058 rad, corresponding to 0.03323°. The setup based on the co-active neuro-fuzzy inference system and the hybrid state estimation results in a root mean squared error of 0.00293 rad, which is equivalent to 0.16788°. Table 6.13 summarizes the root mean squared errors for both setups.

Table 6.13 Collaborative Validation – Roll Behavior Control Quality

Control	Estimation	RMSE	Unit
Hybrid State Estimation	Co-Active Neuro-Fuzzy Inference System	0.00293	rad
Physical Model	Model-Based Predictive Control	0.00058	rad

Basically the collaborative approach of the two hybrid methods results in a slightly worse control quality than the initial setup based on the pure physical models. In contrast, this collaborative approach guarantees a reliable function of the vehicle dynamics control and state estimation despite the failure of sensor signals, which have a direct influence on the central predictive control and thus also on the roll behavior. In general an adequate control quality is still available for this aggravated validation scenario.

Pitch Behavior

The second area of validation of the collaborative setup for the aggravated scenario is the consideration of the pitch behavior. The reduction of pitching movements is a secondary objective

of the central predictive control. In the area of state estimation, a direct influence of the signal failure in terms of the time derivative of the velocity acts as an additional hazard.

The impact of the signal failure on the mode of operation of the collaborative setup consisting of co-active neuro-fuzzy inference system and the hybrid state estimation is first qualitatively evaluated. For this purpose, the resulting pitch angle $\theta_{\mathrm{Est,Canfis}}$ is plotted in the bottom part of Figure 6.17. The further pitch angle curves $\theta_{\mathrm{P,Mpc}}$, θ_{Ref} and θ_{Pas} are not affected by the sensor failures.

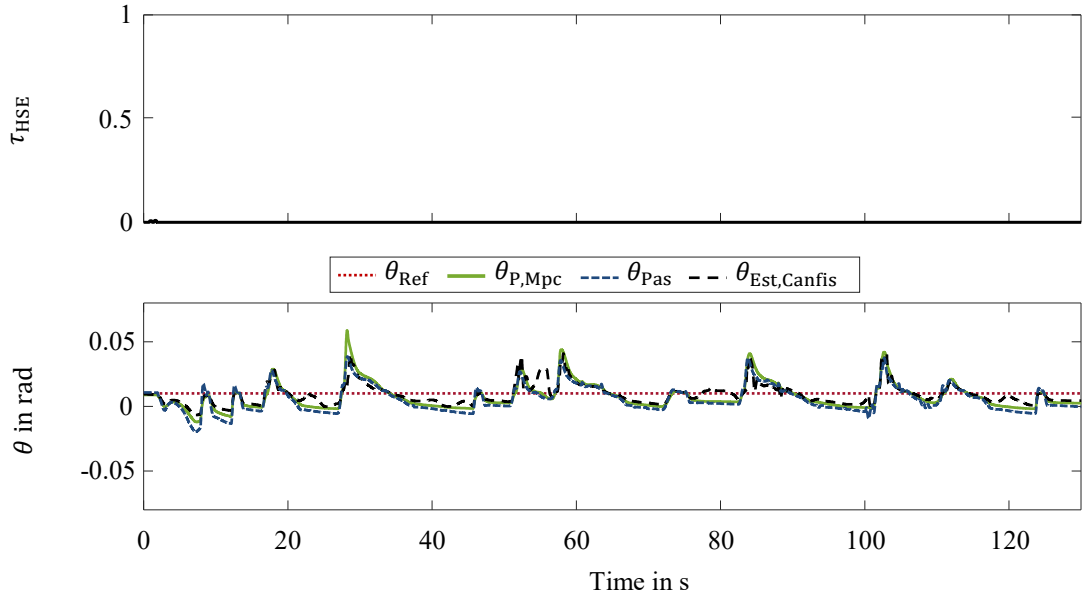

Figure 6.17 Collaborative Validation – Pitch Behavior: Top: Confidence Level; Bottom: Pitch Angle Curves

The signal failure occurs at the third second. The hybrid method of state estimation detects the signal failure and handles it. This results in a valid state estimation for the whole validation maneuver. The functionality of the hybrid state estimation is also shown by the confidence level τ_{HSE}, which is permanently $\tau_{\mathrm{HSE}} = 0$ after the third second. The course of the confidence level τ_{HSE} is illustrated in the top part of Figure 6.17.

In the course of the validation maneuver, however, the signal failures slightly affect the central predictive control based on the co-active neuro-fuzzy inference system with respect to the reduction of the pitch angle. This becomes especially obvious by the deviation at second 55.

To evaluate the impact of the aggravated scenario on the collaborative setup in more detail, the deviations from the reference value θ_{Ref} are determined according to (6.6). These deviations are illustrated for the setup based on the purely physical models and the setup of the two hybrid methods for the validation maneuver in Figure 6.18.

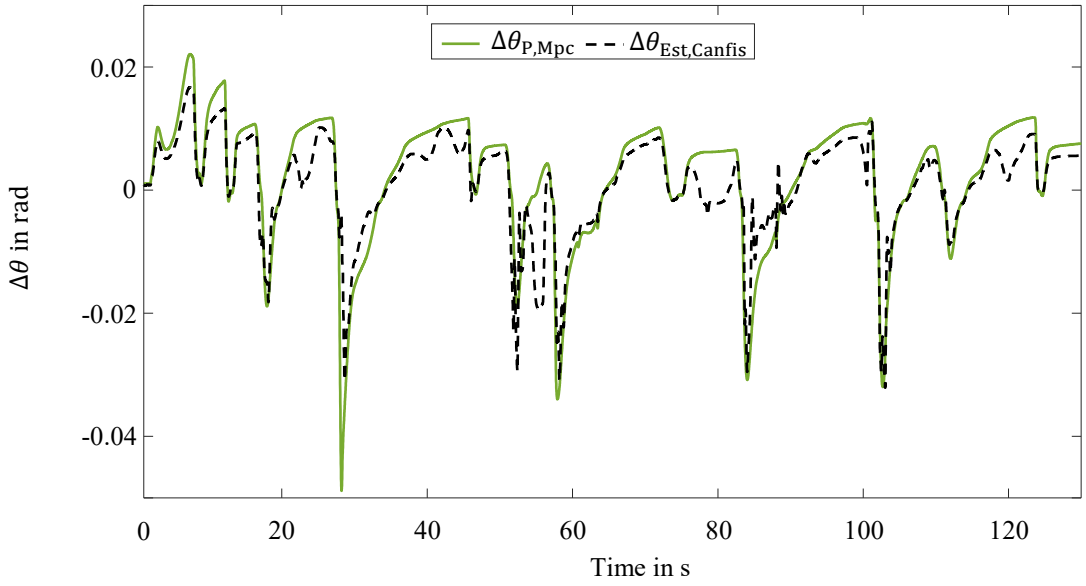

Figure 6.18 Collaborative Validation – Pitch Behavior: Pitch Angle Deviations

In principle, both central predictive control setups reduce the pitch behavior. However, analogous to the results obtained in Section 6.3.1, the co-active neuro-inference system again yields a stronger reduction of the pitch behavior. An exception is the period around second 55.

The maximum absolute deviation resulting from the non-linear model-based predictive control in combination with the state estimation based on the physical model equals 0.04885 rad, corresponding to 2.79890°. The collaborative setup of the co-active neuro-fuzzy inference system in combination with the hybrid state estimation results in a maximum absolute error of 0.03212 rad, which is equivalent to 1.84034°.

The further quantitative evaluation is based on the root mean squared errors according to (6.7). The purely physical setup results in a root mean squared error of 0.01023 rad, which corresponds to 0.58614°. The root mean squared error resulting from the collaborative setup of the two hybrid methods equals 0.00790 rad, which is equivalent to 0.45264°. The quantitative evaluation thus confirms that the co-active neuro-fuzzy inference system also achieves a greater pitch reduction within the collaborative setup compared to the purely physical setup with the non-linear model-based predictive control. A summary regarding the root mean squared errors for both setups is provided in Table 6.14.

Table 6.14 Collaborative Validation – Pitch Behavior Control Quality

Control	Estimation	RMSE	Unit
Hybrid State Estimation	Co-Active Neuro-Fuzzy Inference System	0.00790	rad
Physical Model	Model-Based Predictive Control	0.01023	rad

In general, despite the failure of input signals, a continuously valid state estimation is achieved in the collaborative setup of the hybrid method. This provides the foundation for a successful reduction of pitching movements in relation to the central predictive control by the co-active neuro-fuzzy inference system. The influence of the signal failures is only visible in the period around second 55. Nevertheless, the collaborative setup reduces the pitching movements over the whole validation maneuver significantly more than the setup based on non-linear model-based predictive control and the state estimation by the physical model.

Self-Steering Behavior

In the following, the collaborative setup composed of the two hybrid methods is evaluated for the control objective of manipulating the self-steering behavior within the aggravated scenario. The signal failure of the mean wheel speed $\bar{n}_V$ for the estimation of the side-slip angle in particular affects the self-steering behavior. The signal failure occurs at second 21, the artificial neural network for state estimation is thus no longer able to estimate the side-slip angle. By using the hybrid method this critical situation is detected and handled. This is demonstrated by the side-slip angle course resulting from the hybrid method of state estimation. The side-slip angle course is shown in the top part of Figure 6.19.

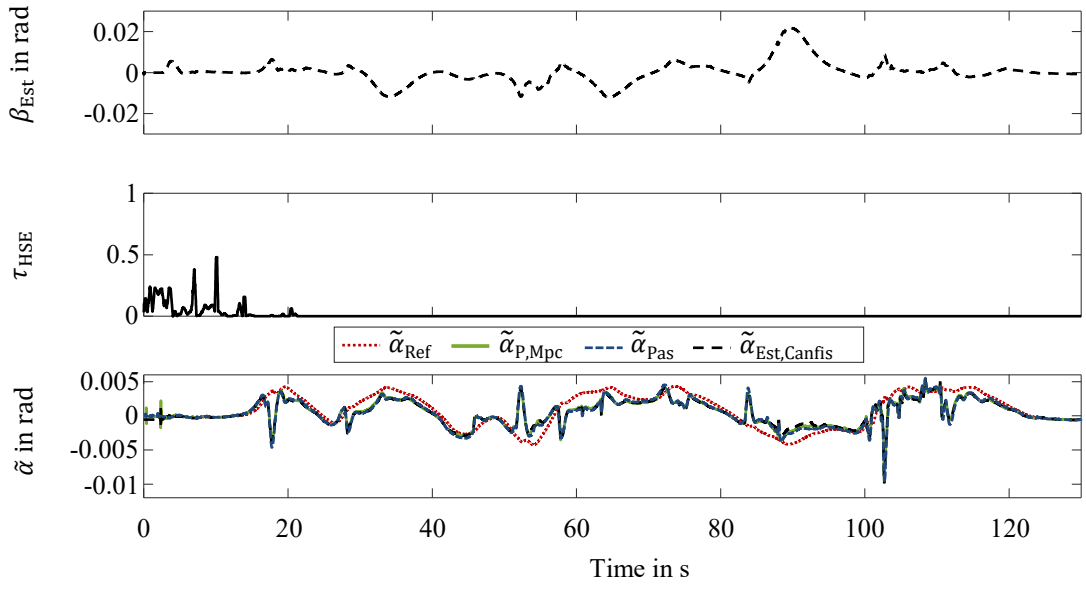

Figure 6.19 Collaborative Validation – Self-Steering Behavior: Top: Estimated Side-Slip Angle; Middle: Confidence Level; Bottom: Slip Angle Difference Curves

Despite the failure of the input signal, the hybrid method provides a continuously valid estimation of the side-slip angle. Moreover, no overshooting is present in the estimated side-slip angle at the time of the failure even with the closed-loop characteristic comprising the co-active neuro-fuzzy inference system.

The functionality of the hybrid method is confirmed by the course of the confidence level τ_{HSE} in the middle part of Figure 6.19. Whereas before the sensor failure the artificial neural network is partially trusted, the signal failure is correctly detected at the time of second 21 and the confidence level is then set to $\tau_{\mathrm{HSE}} = 0$. Consequently, the artificial neural network is no longer trusted from this point on as it completely fails to estimate the side-slip angle. As a result, the foundation for a successful manipulation of the self-steering behavior is created by using the hybrid method of state estimation.

In the following the focus is on the central predictive vehicle dynamics control by the co-active neuro-fuzzy inference system concerning the self-steering behavior. To determine the control quality, the courses of the pseudo quantity $\tilde{\alpha}_i$ for the validation maneuver are illustrated according to (6.8). The courses resulting from the two setups $\tilde{\alpha}_{\mathrm{P,Mpc}}$ and $\tilde{\alpha}_{\mathrm{Est,Canfis}}$ are supplemented by the course $\tilde{\alpha}_{\mathrm{Ref}}$ arising from the reference quantity and the course $\tilde{\alpha}_{\mathrm{Pas}}$ resulting from a vehicle with a passive chassis. These courses are visualized in the bottom part of Figure 6.19. Both setups exhibit a similar behavior and do not differ much in terms of the pseudo quantities $\tilde{\alpha}_{\mathrm{P,Mpc}}$ and $\tilde{\alpha}_{\mathrm{Est,Canfis}}$.

In order to achieve a detailed analysis of the discrepancy between the purely physical setup and the setup based on the hybrid methods, the respective deviations of the pseudo quantities from the reference quantity $\tilde{\alpha}_{\mathrm{Ref}}$ are determined according to (6.9).

These deviations are illustrated in Figure 6.20.

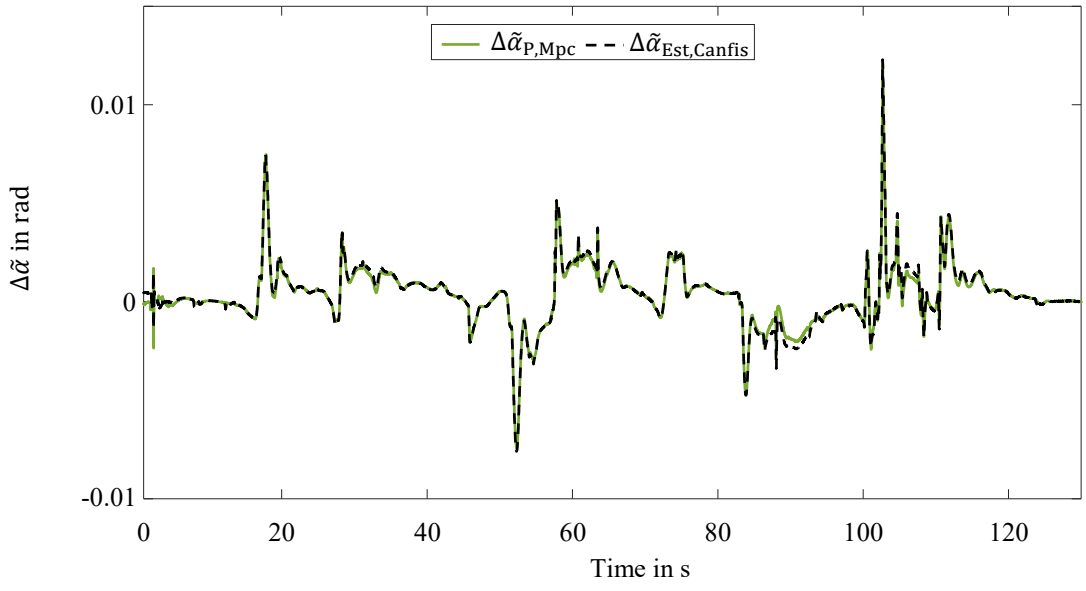

Figure 6.20 Collaborative Validation – Self-Steering Behavior: Slip Angle Difference Deviations

The deviations confirm the nearly identical control quality with respect to the self-steering behavior. Thus, similar results as in Section 6.3.1 are achieved. The main influencing factors are still the manipulated variables of the counter roll torques. Also within the collaborative setup

using the hybrid method of state estimation, nearly the same results are achieved by the co-active neuro-fuzzy inference system. No significant effects of the signal failures on the manipulation of the self-steering behavior can be determined.

Furthermore, the almost identical control quality between the two setups is confirmed by the evaluation of the maximum absolute deviations. The setup based on the non-linear model-based predictive control and the state estimation based on physical models yields a maximum absolute deviation of 0.01223 rad, which is equivalent to 0.70073°. The collaborative setup comprising the co-active neuro-fuzzy inference system and the hybrid method of state estimation results in a maximum absolute deviation of 0.01229 rad, which corresponds to 0.70417°.

In order to evaluate both setups also quantitatively for the entire validation maneuver, the root mean squared errors are determined according to (6.10). The setup based on the purely physical models results in a root mean squared error of 0.00150 rad corresponding to 0.08594°. The collaborative setup based on the hybrid methods achieves a root mean squared error of 0.00159 rad, which is equivalent to 0.09110°. By the additional use of the hybrid method of state estimation, the control quality of co-active neuro-fuzzy inference system is not significantly affected.

Table 6.15 summarizes the root mean squared errors for the different setups.

Table 6.15 Collaborative Validation – Self-Steering Behavior Control Quality

Control	Estimation	RMSE	Unit
Hybrid State Estimation	Co-Active Neuro-Fuzzy Inference System	0.00159	rad
Physical Model	Model-Based Predictive Control	0.00150	rad

By using the hybrid method of state estimation, the failure of the input signal into the artificial neural network for the state estimation is successfully detected and handled. Thus a valid state estimation is available for the entire validation maneuver. This is a mandatory condition for the successful implementation of the central predictive control. With regard to the control quality in terms of the self-steering behavior, no significant difference between the two setups is recognizable. Moreover, no significant differences with regard to the central predictive control based on the co-active neuro-fuzzy inference system collaborating with the hybrid method of state estimation respectively the state estimation on the physical model arise.

6.4.2 Conclusion

In conclusion, the collaborative setup consisting of the central predictive vehicle dynamics control based on the co-active neuro-fuzzy inference system as well as the hybrid method of state estimation is successfully realized for the validation maneuver, one lap on the Hockenheimring racetrack. Particularly remarkable is the fact that the validation maneuver is made significantly

more difficult through the simulation of two signal failures within the state estimation. Any further sensor signal failures into the artificial neural networks could also be detected and handled by the hybrid method of state estimation. Thus, the conducted validation is generalizable.

The hybrid method of state estimation allows a continuously valid state estimation for the whole duration of the validation maneuver. As a result, the segment of the roll behavior which is indirectly affected by the failures as well as the directly affected segments of the pitch behavior and the side-slip angle are successfully handled by the hybrid method of state estimation. By determining the confidence level, the failures are detected and handled. The oscillations determined in the open-loop validation of the hybrid method in the case of failures of an input signal in Section 4.3 have no significant effect on the control by the co-active neuro-fuzzy inference system within the collaborative setup.

The continuously available valid state estimation provides the mandatory foundation for the central predictive vehicle dynamics control. This is realized in the collaborative setup by the co-active neuro-fuzzy inference system. In principle, the central predictive control is successfully implemented even for the more aggravated validation scenario. Small deviations arise in the control quality with respect to the collaborative setup compared to the physical setup in the area of roll angle control. The control quality is preserved respectively even enhanced in the segments of manipulating the self-steering behavior respectively the reduction of pitching movements. The improvement in the segment of pitching, however, results from the deviation in the representation of the damping factors and is therefore not a systematic advantage. In general, the deviations in the overall control quality of the central predictive vehicle dynamics control are within an acceptable range.

The reason for the partially present deviations in the control quality, especially in the segment of the roll control, is the existing closed-loop issue between the hybrid state estimation and the central predictive vehicle dynamics control by the co-active neuro-fuzzy inference system. Both hybrid methods are trained with the same database. This database is derived from the purely physical setup obtained from the non-linear model-based predictive control and the state estimation based on the physical models. To minimize the deviations in the control quality, the data resulting from the hybrid method of state estimation for the driving scenarios can be included in the training database for the co-active neuro-fuzzy inference system. Thus, the unknown closed-loop issues presented in this Section are resolved and mitigated. This will further minimize the deviations in the control quality.

7 Conclusion

This Chapter concludes the thesis. To this end, it summarizes the results and highlights the scientific contribution. It critically reviews the results obtained in a discussion part. At the end, an outlook on future research tasks is presented. Within this thesis, two hybrid methods were developed and presented that exploit the potentials of artificial intelligence while still securing the reliability. The two hybrid methods are used for the implementation of a central predictive vehicle dynamics control system to perform the tasks of state estimation and control. By using the hybrid methods, the foundation for an increase in vehicle safety and ride comfort is built.

7.1 Summary

The thesis focuses on the objective of enhancing safety and ride comfort of future vehicles. This enhancement is achieved by a vehicle dynamics control system which influences both the vehicle safety and the ride comfort. In general, the domain of vehicle dynamics control represents a well-researched area. Nevertheless, this domain still features great unused potential which is exploited in this thesis by the integration of artificial intelligence. The domain of vehicle dynamics control is divided into the segments of the state estimation and the control algorithm itself. Accordingly, two novel hybrid methods are derived and presented within this thesis. For the implementation and validation of the hybrid methods, a development framework is built and used, which is based on a co-simulation of IPG CarMaker and MATLAB & Simulink.

The hybrid method of state estimation addresses the issue that the use of artificial intelligence can lead to an increase in estimation accuracy but at the same time does not provide a completely reliable system due to its black-box characteristics. However, the state estimation must be reliable, especially with respect to the use in a vehicle dynamics control system, so that the safety is not compromised. The domains of roll, pitch and side-slip behavior are considered separately as estimation targets. A separate estimator is thus created for each domain. Within the novel hybrid method of state estimation, artificial intelligence based models are merged and safeguarded by reliable simple physical models. The combination of both model types is real-

ized by unscented Kalman filters. The reliability is ensured by a novel method, which determines a confidence level τ_{HSE} for the respective artificial neural network. In this context the artificial neural networks represent the models based on artificial intelligence. The confidence level τ_{HSE} is based on the data used in the training of these models. The more often the respective artificial neural network has encountered the input data, the stronger the confidence and the higher the confidence level τ_{HSE}. Depending on this confidence level the covariances of transition and measurement of the unscented Kalman filter are adjusted. This results in a hybrid estimation, which in extreme cases relies completely on the physical model or completely on the artificial neural network. The artificial neural network is therefore only trusted in well-known areas. A preliminary open-loop validation is used to evaluate the functionality of the hybrid method of state estimation. In this context extreme situations like sensor malfunctions as well as a complete failure of an input signal into an artificial neural network are considered. Without the hybrid method, the artificial neural networks result in invalid and unreliable estimations, which would have fatal consequences for the control system. The hybrid method detects these critical situations and handles them accordingly. In these cases the hybrid method relies completely on the reliable simple physical models.

The second hybrid method of this thesis addresses the control task itself. A central predictive vehicle dynamics control system is desired. This control type offers enormous potential in terms of increasing safety and ride comfort. Common approaches regarding the central predictive control are based on model-based predictive control algorithms. Through complex non-linear models within this class of control algorithms, the control task is achieved with excellent control quality but at the expense of a greatly increased computational effort. The hybrid method of vehicle dynamics control addresses this issue and solves it by using a co-active neuro-fuzzy inference system to reproduce the non-linear model-based predictive control. The co-active neuro-fuzzy inference system represents a fuzzy inference system for a multiple input multiple output system in the structure of an artificial neural network. Thus the fuzzy inference system becomes trainable in terms of a desired behavior, but subsequent to this training it remains a fuzzy inference system. In the course of the hybrid method the non-linear model-based predictive control is implemented in the best possible way, thus without additional restrictions. A first open-loop validation highlights the functionality of the hybrid method. By using the co-active neuro-fuzzy inference system the computational effort is drastically reduced.

Both hybrid methods are validated further with closed-loop validations. For this purpose, a validation scenario based on a completely unknown maneuver is used which features dynamic excitations that exceed those in the training data. Thus it represents a special challenge for the validation. The hybrid methods are validated for three different setups.

In a first setup, the closed-loop validation of the hybrid method of state estimation is focused. For this purpose the hybrid method of state estimation is integrated into the development framework. The central predictive control within this setup is based on the non-linear model-based

predictive control in order to focus purely on the hybrid method of state estimation. Within the validation the focus is on the estimation accuracy and thus the quality of the estimation. In comparison to the purely physical models, the hybrid method improves the quality of the estimation in all three domains of the state estimation. With regard to the domains of rolling and pitching, additionally an improvement in terms of the estimation accuracy is achieved compared to the state estimation by the artificial neural networks. The hybrid method of state estimation thus outperforms the individual estimators. In the domain of the side-slip angle estimation the artificial neural network exhibits further potential to increase the estimation quality. The hybrid method partially disregards this potential in favor of reliability. In general, the closed-loop validation thus confirms the functionality of the hybrid method with respect to the objectives of increasing the estimation accuracy while ensuring reliability.

The second setup focuses on the closed-loop validation of the hybrid method of the vehicle dynamics control. In order to consider this hybrid method individually, the development framework contains the central predictive vehicle dynamics control based on the co-active neuro-fuzzy inference system while utilizing the state estimation based on the physical models. The closed-loop validation focuses on the main objectives of the control quality and the computational effort. Regarding the evaluation of the control quality the co-active neuro-fuzzy inference system results in an almost unchanged control performance for the roll and self-steering behavior. Concerning the control objective of reducing pitching movements, the performance of the non-linear model-based predictive control is even surpassed, which results mainly from the deviations in the representation of the damping factors and is therefore not a general systematic benefit. In general, however, the implementation of the hybrid method yields a preservation of the control quality. With focus on the computational effort, the results of the open-loop validation are confirmed. By using the co-active neuro-fuzzy inference system, the runtime is reduced by a factor of 9.28 and the average central processing unit utilization by a factor of 1.19. In general, the hybrid method regarding the central predictive control meets the required specifications of reducing the computational effort without a deterioration of the control quality.

Within the third setup, both hybrid methods are integrated into the framework in a collaborative setting and thus are validated together in a closed-loop manner. The focus is on the interrelated behavior of the hybrid methods. As an additional challenge, the validation scenario is further aggravated. During the validation maneuver, two input signals into the state estimation by the artificial neural network are set to fail. The estimations in the sections of the pitching as well as the side-slip angle are directly affected by these failures. By using the hybrid method the failures are correctly detected and handled. A valid state estimation is thus available for the entire validation maneuver. This provides the basis for a successful control. The impact of the signal failures on the control objectives of the pitch reduction as well as the on the influence of the self-steering behavior are not recognizable. Only in the section of the roll behavior there are minimal deviations compared to control quality achieved within the second validation setup. In

general, however, the use of both hybrid methods successfully masters this extremely aggravated validation scenario. Both hybrid methods thus meet the required specifications.

The thesis closes with a critically review of the achieved results. Moreover, the proposed hybrid methods are set into a wider scientific context and their impact on the development of future vehicles are outlined.

7.2 Scientific Contribution

The hybrid methods developed in this thesis constitute an important fundament for the development of vehicles of the future. Both methods contribute to safer vehicles and to the enhancement of ride comfort. The foundation for the success of the hybrid methods is the integration of artificial intelligence. In the following, the respective hybrid methods are presented individually with regard to their scientific contribution.

The hybrid method of state estimation addresses the issue that although models based on artificial intelligence possess an enhanced potential in terms of improving the estimation accuracy as well as a reduced modeling effort, they are only partially verifiable and thus not completely reliable. Basically, the lack of reliability applies to all black-box models, which result from experimental modeling. With regard to a collaboration with a control system, as it is considered in this thesis for a vehicle dynamics control system, it is indispensable to provide a consistently valid and reliable estimation. Otherwise, the safety of the vehicle occupants is directly compromised. In order to secure the state estimation by artificial intelligence, a novel hybrid method of state estimation is presented within this thesis. In general, this hybrid method yields a valid and reliable state estimation throughout. Thus it allows the potential of artificial intelligence to be exploited with respect to increasing the accuracy of estimation, but also provides the necessary validity and reliability. Even extreme scenarios of faulty sensor signals or complete failures of input signals in to the artificial intelligence based model can be detected and safely handled by this hybrid method. Consequently, the hybrid method provides an outstanding opportunity to use artificial intelligence based models in the vehicle as well as in combination with control systems without compromising reliability and thus safety. In general, this allows systems based on artificial intelligence to become legally approvable. Thus, the hybrid method represents a promising alternative in contrast to the integration of a human fallback level as it is proposed in (O'Sullivan et al., 2019).

The hybrid method of vehicle dynamics control addresses the issue that a central predictive vehicle dynamics control based on a non-linear model-based predictive control algorithm provides an outstanding control quality, however, it also involves an enormous computational effort. Moreover, the non-linear model-based predictive control used in this thesis performs a numerical optimization, which is not real-time capable without a limitation of iterations. The proposed hybrid method represents a novel approach to reduce the computational effort of the

control while preserving the control quality. Furthermore, the control implemented by the co-active neuro-fuzzy inference system is characterized by a direct mode of operation, so that a real-time application is possible. At the end of the training a fuzzy inference system is retained, which is much easier to comprehend and secure than an artificial neural network. The hybrid method thus represents a possibility to drastically reduce the computational effort of the central predictive vehicle dynamics control without deteriorating the control quality. This enables the implementation of central predictive vehicle dynamics control systems comprising the utilization of the existing synergies within the vehicle.

Whereas both hybrid methods have been presented in this thesis for the application in vehicle dynamics control systems, these hybrid methods can be easily extended into numerous and various fields of application.

The hybrid method of state estimation can be used for all kinds of black-box models resulting from experimental modeling, for which a reliable and fully validated model exists. In this way, the hybrid method addresses exactly the necessity of a possibility to reliably combine data-driven machine learning models with physical models in the field of seismology, as it is formulated by (Kong et al., 2018). Moreover, (Ryan, 2020) highlights the need for a reliable method to deploy artificial intelligence. In terms of human acceptance of systems based on artificial intelligence, reliability is a core characteristic. The hybrid method of state estimation represents an opportunity to use artificial intelligence while preserving a reliable system.

The hybrid method with respect to the control can be used for all control systems for which an excessive computational effort is a major issue or a direct method of operation is required for a real-time capable implementation. As an example, the hybrid method of control can likewise be used in the field of cooperative intelligent transportation systems. The method can contribute to the improvement of the control of inter-vehicle distances of multi-vehicle platoons. It provides an alternative to the approach presented by (Shalaby et al., 2019) in which a linearization is performed due to an increased computational effort. Another application example is represented by a trajectory tracking problem. To realize a predictive control, (Yue et al., 2018) have also applied a linearization. In both cases the hybrid method presents a promising approach to contribute to low computational efforts while further improving the control performance.

7.3 Discussion

The hybrid methods presented in this thesis are of course based on assumptions and therefore have limitations. The greatest influence on the implementation of the hybrid method is by far the data used. In this thesis, the data is generated by the presented development framework, which is based on a co-simulation.

Within this co-simulation standardized driving maneuvers are simulated for a defined vehicle setup. These driving maneuvers have been varied with respect to their main characteristics,

however, they still cover only discrete sections of the overall vehicle dynamics. With regard to a comprehensive implementation of the hybrid methods, further data should be added to the data set. Naturalistic driving data could close these remaining gaps. The data used was generated by simulation. Within the development framework, IPG CarMaker performs a very detailed multi-body simulation, however, it still remains a simulation. Therefore, the supplementation of the data set with experimental data is a reasonable approach. Besides using experimental data, the simulated data can also be deteriorated by noise. In conclusion, the supplementation of the simulation data with naturalistic driving data is recommended. It is expected that the mentioned extension of the data will further improve the performance of the hybrid methods. In an ideal case, an equally distributed database is available after this extension.

An important characteristic of the hybrid method of state estimation is the determination of the confidence level τ_{HSE}. Within this determination, the input data into the models based on artificial intelligence are classified into their training data, which have to be valid. Within the hybrid method the training data are divided into a grid structure. On the one hand, the number of individual grids for each input variable affects the resulting confidence level τ_{HSE}. A finer classification leads to a higher level of detail, but also to an increased memory requirement. On the other hand, the characteristic value $p_{\max}$ has a great influence on the determination of the confidence level τ_{HSE}. This value is used to scale the results obtained by the classification into the grid structure. In this thesis, the characteristic value is equated with the maximum value within the grid structure, thus following the principle that more data correlates with an improved estimation quality, (Halevy et al., 2009). This automatically results in a scaling between zero and one. Regarding the further application of the hybrid method in vehicles different characteristic values $p_{\max}$ can also be used depending on the driving conditions. As a result, the artificial intelligence based model can be trusted with less data under normal driving conditions than for situations near the vehicle dynamics limits, which require significantly more data. This can avoid different deviations in the estimation accuracy for the same confidence level value, as it is present for varying complex situations. Considering the legal approval of the hybrid method, the characteristic value can be implemented according to defined specifications. As an example, this specification can be based on a metric as it is considered for the approval of an automated driving function, (Winner et al., 2016). This metric is based on a minimum distance travelled without any accidents.

Within the thesis the hybrid method of state estimation is validated with respect to some extreme situations like sensor malfunction and signal failures. Here only the input signals into the models based on artificial intelligence are manipulated, as the safeguarding of these models is the focus of this thesis. The hybrid method of state estimation is furthermore able to detect and handle a failure of an input signal into the physical model. With regard to reliability and safeguarding, the resulting complete confidence in the model based on artificial intelligence is recommended initially to be only used to transfer the vehicle into a safe state.

The implementation of the confidence levels in the course of the combination of the individual models is done in the presented hybrid method by modifying the covariances of the transition and the measurement of the unscented Kalman filter. A further possibility of implementation would be the direct manipulation of the Kalman gain. With respect to noise reduction, however, the presented method of modifying the covariances is strongly recommended.

Within the hybrid method of control, the co-active neuro-fuzzy inference system is used to represent the non-linear model-based predictive control. The objective is to reduce the enormous computational effort of the non-linear model-based predictive control, while preserving the excellent control quality thereof. The non-linear model-based predictive control was designed in the context of this thesis with the objective of achieving the best possible control quality disregarding the associated computational effort. In principle, linearized models, a reduced prediction horizon or even a disregard of constraints could have reduced the computational effort. Considering the control quality, however, these adaptations of the non-linear model-based predictive control were deliberately neglected.

Another aspect to be discussed is that the same database is used for training both hybrid methods. This database is generated by the co-simulation within the development framework based on the non-linear model-based predictive control and the state estimation by the purely physical models. The individual validations of the hybrid methods show impressive results. With regard to the validation of the collaborative setup based on both hybrid methods, the control by the co-active neuro-fuzzy inference system and the state estimation by the hybrid method, slight deviations are obtained in the control of the roll behavior. By extending the training data set for the hybrid method of vehicle dynamics control with the behavior of the hybrid method of state estimation these smaller deviations could be counteracted. Extreme situations such as sensor malfunctions or even failures should also be included in the generation of the training data. By this measure, the collaborative setup of both hybrid methods can be further optimized with respect to all aspects.

In addition to the impact of the database on the performance of the co-active neuro-fuzzy inference system, its hyperparameters have to be discussed as well. Regarding the representation of the damping factors, the co-active neuro-fuzzy inference system is only partially able to follow the high dynamics of the non-linear model-based predictive control. The main influencing factor here is the number of membership functions. To limit the computational effort within the hyperparameter optimization, only two respectively three membership functions per input variable were provided in the search space. Moreover, it was determined that the number of membership functions is consistent for each input variable. By extending the search space of the hyperparameter optimization to include more membership functions as well as a variability with respect to the number of membership functions per input variable, a further improvement regarding the representation quality of the manipulated variables is expected.

A further influencing factor is the choice of the test vehicle used in the co-simulation. The test vehicle belongs to the class of sport utility vehicles. Basically, sport utility vehicles feature a higher center of gravity than, for example, compact class vehicles. Due to this higher center of gravity, a sport utility vehicle tends to show increased rolling and pitching movements. As a result, this vehicle class presents greater challenges in the area of roll and pitch control. Despite choosing the vehicle class with the highest rolling and pitching movements and thus presenting the greatest challenge in controlling these movements the hybrid state estimation and control of the vehicle dynamics feature an excellent performance. Consequently, no difficulties are expected regarding the applicability of the hybrid methods for the use with other vehicle classes.

7.4 Outlook

The application of the hybrid methods opens up new possibilities in the course of vehicle development, but also far beyond. The functionality of both hybrid methods has been impressively proven by simulative investigations within the scope of this thesis. Consequently, the next reasonable step for the future is to transfer the hybrid methods to a real vehicle in order to highlight the functionality of both methods under real world conditions as well. In this context, it can be examined how the transferability of models based purely on simulation data can be extended to an application in a real environment.

Another aspect that relates primarily to the overall vehicle dynamics control is the subjective investigation of how the ride comfort is improved by the use of the central predictive vehicle dynamics controller. In a user study, a test vehicle equipped with the central predictive vehicle dynamics control can be compared with one equipped with a standard control system, for example based on the control concept of peaceful coexistence. The objective results obtained in this thesis can thus be enriched by subjective assessments.

Whereas the hybrid methods have been implemented and presented within this thesis for the use case of a vehicle dynamics control system, both hybrid methods can be used in various application cases. With respect to the hybrid method of state estimation, an extension of estimation quantities will be pursued, whereby further costs can be saved. Furthermore, this hybrid method will be examined with respect to the choice of the artificial intelligence based models. Whereas in the thesis artificial neural networks represent artificial intelligence, in future work these will be replaced by different types of data-driven black-box model. Thus the generalizability of the hybrid method can be emphasized.

Another aspect that will be investigated and implemented in future research regarding the hybrid method of state estimation is a temporal dependency respectively a temporal lookback within the determination of the confidence level. In this thesis, the determination of the confidence level is based on the latest input data into the artificial intelligence based model. The

artificial neural networks used feature a recurrent structure with a temporal lookback, thus possessing information about past time steps. By taking into account the past confidence levels, which correspond temporally to the lookback of the artificial neural network, an additional improvement of the hybrid method is expected. This could simplify and support the identification of sensor malfunctions like a drift, which are currently recognized on the basis of a valid database. Moreover, this could also lead to an even smoother course of the confidence level.

At present, the use of artificial intelligence in vehicles but also in safety-critical applications in general is limited by legal regulations. This prevents the implementation of many promising artificial intelligence based algorithms and models despite their excellent performance. In (EuropeanCommission, 2020), the robustness and accuracy of artificial intelligence based systems are emphasized as key issues for a legal admissibility. This includes ensuring that systems based on respectively incorporating artificial intelligence operate reliably throughout. The hybrid method of state estimation satisfies exactly this requirement of the European Union. In principle, this thesis thus provides a possibility for the legal approval of artificial intelligence based systems. Of course, further aspects have to be considered regarding the legal approval, such as the documentation and storage of the training process and the training data. Ultimately, these aspects can be fulfilled on the basis of the hybrid method, so that a legal precedent for artificial intelligence based systems can be set.

Appendix

Utility-Analysis

Table A-1 Utility Analyses – Pair-by-Pair Comparison

	Additional Costs	Additional Functions	Integration Effort	Manipulation of the Pitch Behavior	Manipulation of the Roll Behavior	Manipulation of the Self-Steering Behavior
Additional Costs	1	2	2	1	0	1
Additional Functions	0	1	1	0	0	0
Integration Effort	0	1	1	1	0	1
Manipulation of the Pitch Behavior	1	2	1	1	0	2
Manipulation of the Roll Behavior	2	2	2	2	1	2
Manipulation of the Self-Steering Behavior	1	2	1	0	0	1

Bibliography

Abadi M., Barham P., Chen J., Chen Z., Davis A., Dean J. et al. (2016) *TensorFlow: A System for Large-Scale Machine Learning*. In 12th USENIX Conference on Operating Systems Design and Implementation, pp. 265 - 283, USENIX Association, Savannah, GA, USA. - ISBN 978-1-931971-33-1

Ahmadian M., Song X. and Southward S.C. (2004) *No-Jerk Skyhook Control Methods for Semiactive Suspensions*. In Journal of Vibration and Acoustics 126, - ISSN 1048-9002. pp. 580-584

Ahmed H. and Tahir M. (2017) *Accurate Attitude Estimation of a Moving Land Vehicle Using Low-Cost MEMS IMU Sensors*. In IEEE Transactions on Intelligent Transportation Systems 18, - ISSN 1558-0016. pp. 1723-1739

Aljazzar H., Fischer M., Grunske L., Kuntz M., Leitner-Fischer F. and Leue S. (2009) *Safety Analysis of an Airbag System Using Probabilistic FMEA and Probabilistic Counterexamples*. In 2009 Sixth International Conference on the Quantitative Evaluation of Systems, pp. 299-308

Antonov S., Fehn A. and Kugi A. (2011) *Unscented Kalman filter for vehicle state estimation*. In Vehicle System Dynamics 49, - ISSN 0042-3114. pp. 1497-1520

Beal C.E. and Gerdes J.C. (2010) *Predictive control of vehicle roll dynamics with rear wheel steering*. In Proceedings of the 2010 American Control Conference, pp. 1489-1494 - ISBN 2378-5861

Beal C.E. and Gerdes J.C. (2013) *Model Predictive Control for Vehicle Stabilization at the Limits of Handling*. In IEEE Transactions on Control Systems Technology 21, - ISSN 1558-0865. pp. 1258-1269

Bergstra J., Bardenet R., Bengio Y. and Kégl B. (2011) *Algorithms for Hyper-Parameter Optimization*. In 25th Annual Conference on Neural Information Processing Systems (NIPS 2011), Vol. 24, Neural Information Processing Systems Foundation, Granada, Spain.

Bergstra J., Komer B., Eliasmith C., Yamins D. and Cox D.D. (2015) *Hyperopt: a Python library for model selection and hyperparameter optimization*. In Computational Science & Discovery 8, - ISSN 1749-4699. pp. 014008

Bishop C.M. (2006) *Pattern Recognition and Machine Learning (Information Science and Statistics)*. Springer-Verlag - ISBN 0387310738

Blume S., Sieberg P.M., Maas N. and Schramm D. (2019) *Neural Roll Angle Estimation in a Model Predictive Control System*. In Proceedings of the IEEE Intelligent Transportation Systems Conference (ITSC) / ITSC 2019, pp. 1625 - 1630, IEEE, Auckland.

Boada B.L., Boada M.J.L. and Diaz V. (2016) *Vehicle sideslip angle measurement based on sensor data fusion using an integrated ANFIS and an Unscented Kalman Filter algorithm*. In Mechanical Systems and Signal Processing 72-73, - ISSN 0888-3270. pp. 832-845

Boada B.L., Boada M.J.L., Vargas-Melendez L. and Diaz V. (2018) *A robust observer based on H ∞ filtering with parameter uncertainties combined with Neural Networks for estimation of vehicle roll angle*. In Mechanical Systems and Signal Processing 99, - ISSN 0888-3270. pp. 611-623

Bosch (2020). *Electronic Stability Program*. Retrieved from https://www.bosch-mobility-solutions.com/en/products-and-services/passenger-cars-and-light-commercial-vehicles/driving-safety-systems/electronic-stability-program/. Access on 12.05.2020

Boyraz E., Kandler C., Gantikow M. and Schramm D. (2017a) *Investigation of methods for the objective assessment of the dynamic system behaviour of air springs*. In 17. Internationales Stuttgarter Symposium, Stuttgart. - ISBN Print ISBN: 978-3-658-16987-9; Electronic ISBN: 978-3-658-16988-6

Boyraz E., Kandler C., Gantikow M. and Schramm D. (2017b) *Objective assessment of the dynamic system behavior of multi-chamber air springs*. In 8. Münchner Fahrwerk-Symposium chassis.tech plus 2017, pp. 255-270, München. - ISBN Print ISBN: 978-3-658-18458-2 ; Electronic ISBN: 978-3-658-18459-9

Brown R. and Hwang P. (1997) *Introduction to random signals and applied kalman filtering*. 3rd (ed.), John Wiley & Sons, Inc.

Buma S., Ookuma Y., Taneda A., Suzuki K., Cho J.-S. and Kobayashi M. (2010) *Design and Development of Electric Active Stabilizer Suspension System*. In Journal of System Design and Dynamics 4. pp. 61-76

Butcher J.C. (2016) *Numerical Methods for Ordinary Differential Equations*. 3rd (ed.), John Wiley & Sons, Ltd - ISBN 978-1-119-12152-7

Camacho E.F. and Bordons C.A. (1998) *Model Predictive Control*. Springer-Verlag, Berlin.

Canale M., Fagiano L., Milanese M. and Borodani P. (2007) *Robust vehicle yaw control using an active differential and IMC techniques*. In Control Engineering Practice 15, - ISSN 0967-0661. pp. 923-941

Canale M., Fagiano L. and Signorile M.C. (2011) *A model predictive control approach to vehicle yaw control using identified models*. In Proceedings of the Institution of Mechanical Engineers, Part D: Journal of Automobile Engineering 226, - ISSN 0954-4070. pp. 577-590

Canale M., Milanese M. and Novara C. (2006) *Semi-Active Suspension Control Using "Fast" Model-Predictive Techniques*. In IEEE Transactions on Control Systems Technology 14, - ISSN 1558-0865. pp. 1034-1046

Chen B.C. and Hsieh F.C. (2008) *Sideslip angle estimation using extended Kalman filter*. In Vehicle System Dynamics 46, - ISSN 0042-3114. pp. 353-364

Chen S., Moshchuk N., Nardi F. and Ryu J. (2010) *Vehicle Rollover Avoidance*. In IEEE Control Systems Magazine 30, - ISSN 1941-000X. pp. 70-85

Chen W., Xiao H., Wang Q., Zhao L. and Zhu M. (2016) *Integrated Vehicle Dynamics and Control*. John Wiley & Sons

Chindamo D., Gadola M., Benini C. and Romano M. (2018) *Estimation of Vehicle Side-Slip Angle Using an Artificial Neural Network*. In Proceedings of the ICMAA 2018, Singapore.

Chiu S.L. (1994) *Fuzzy Model Identification Based on Cluster Estimation*. In J. Intell. Fuzzy Syst. 2, - ISSN 1064-1246. pp. 267–278

Choi M. and Choi S.B. (2014) *Model Predictive Control for Vehicle Yaw Stability With Practical Concerns*. In IEEE Transactions on Vehicular Technology 63, - ISSN 1939-9359. pp. 3539-3548

Cortes C. and Vapnik V. (1995) *Support-vector networks*. In Machine Learning 20, - ISSN 1573-0565. pp. 273-297

Cromer A. (1981) *Stable solutions using the Euler approximation*. In American Journal of Physics 49, - ISSN 0002-9505. pp. 455-459

De Pauw E., Daniels S., Thierie M. and Brijs T. (2014) *Safety effects of reducing the speed limit from 90km/h to 70km/h*. In Accident Analysis & Prevention 62, - ISSN 0001-4575. pp. 426-431

Dewancker I., McCourt M., Clark S., Hayes P., Johnson A. and Ke G. (2016) *A Strategy for Ranking Optimization Methods using Multiple Criteria*, pp. 11-20, PMLR

Doumiati M., Victorino A., Charara A. and Lechner D. (2009a) *Estimation of vehicle lateral tire-road forces: A comparison between extended and unscented Kalman filtering*. In 2009 European Control Conference (ECC), pp. 4804-4809

Doumiati M., Victorino A., Charara A. and Lechner D. (2009b) *Unscented Kalman filter for real-time vehicle lateral tire forces and sideslip angle estimation*. In 2009 IEEE Intelligent Vehicles Symposium, pp. 901-906 - ISBN 1931-0587

Eckstein L. and Zlocki A. (2013) *Safety Potential of ADAS – Combined Methods for an Effective Evaluation*. in *23rd International Technical Conference on the Enhanced Safety of Vehicles (ESV)*(ed.), Seoul, South Korea.

Elbanhawi M., Simic M. and Jazar R. (2015) *In the Passenger Seat: Investigating Ride Comfort Measures in Autonomous Cars*. In IEEE Intelligent Transportation Systems Magazine 7, - ISSN 1941-1197. pp. 4-17

EuropeanCommission (2020) *White paper on artificial intelligence : a European approach to excellence and trust.* pp. European Union, Nation.

EuropeanUnion (2009) *Regulation (EC) No. 661/2009 of the European Parliament and of the Council of July 13, 2009 concerning Type-approval Requirements for the General Safety of Motor Vehicles, their Trailers and Systems, Components and Separate Technical Units Intended therefor.* pp. European Union, Nation.

Fan X., Fan B. and Wang H. (2011) *Fuzzy control for vehicle stability*. In 2011 2nd International Conference on Artificial Intelligence, Management Science and Electronic Commerce (AIMSEC), pp. 2115-2118

Fan Y., Dao-Fei L. and Crolla D.A. (2008) *Integrated Vehicle Dynamics Control —state-of-the art review*. In 2008 IEEE Vehicle Power and Propulsion Conference, pp. 1-6 - ISBN 1938-8756

Farmer C.M. (2004) *Effect of Electronic Stability Control on Automobile Crash Risk*. In Traffic Injury Prevention 5, - ISSN 1538-9588. pp. 317-325

FGSV (2011) *RAA - Guidelines for the Design of Motorways*. Road and Transportation Research Association

FGSV (2012) *RASt 06 - Directives for the Design of Urban Roads*. Road and Transportation Research Association

Finnoff W., Hergert F. and Zimmermann H.G. (1993) *Improving model selection by nonconvergent methods*. In Neural Networks 6, - ISSN 0893-6080. pp. 771-783

Foody G.M. and Arora M.K. (1997) *An evaluation of some factors affecting the accuracy of classification by an artificial neural network*. In International Journal of Remote Sensing 18, - ISSN 0143-1161. pp. 799-810

Gadola M., Chindamo D., Romano M. and Padula F. (2014) *Development and validation of a Kalman filter-based model for vehicle slip angle estimation*. In Vehicle System Dynamics 52, - ISSN 0042-3114. pp. 68-84

Gers F.A., Schmidhuber J.A. and Cummins F.A. (2000) *Learning to Forget: Continual Prediction with LSTM*. In Neural Comput. 12, - ISSN 0899-7667. pp. 2451–2471

Gilbert E.G. (1963) *Controllability and oberservability in multivariable control systems*. In SIAM Journal on Control 1,

Giua A., Seatzu C. and Usai G. (1999) *Semiactive Suspension Design with an Optimal Gain Switching Target*. In Vehicle System Dynamics 31, - ISSN 0042-3114. pp. 213-232

Glorot X. and Bengio Y. (2010) *Understanding the difficulty of training deep feedforward neural networks*. (ed.), pp. 249-256, PMLR

Goebel K. and Yan W. (2008) *Correcting Sensor Drift and Intermittency Faults With Data Fusion and Automated Learning*. In IEEE Systems Journal 2, - ISSN 1937-9234. pp. 189-197

Gonzalez L.P., Sanchez S.S., Guzman J.G., Boada M.J.L. and Boada B.L. (2020) *Simultaneous Estimation of Vehicle Roll and Sideslip Angles through a Deep Learning Approach*. In Sensors 20, - ISSN 1424-8220

Goodfellow I., Bengio Y. and Courville A. (2016) *Deep Learning*. The MIT Press - ISBN 0262035618

Gräber T., Lupberger S., Unterreiner M. and Schramm D. (2019) *A Hybrid Approach to Side-Slip Angle Estimation With Recurrent Neural Networks and Kinematic Vehicle Models*. In IEEE Transactions on Intelligent Vehicles 4, - ISSN 2379-8904. pp. 39-47

Griffin R., McGwin G. and Kerby J. (2018) *Decomposition analysis of the effects of vehicle safety technologies on the motor vehicle collision–related mortality rate from 1994 to 2015*. In Traffic Injury Prevention 19, - ISSN 1538-9588. pp. S169-S172

Grüne L. and Pannek J. (2017) *Nonlinear Model Predictive Control*. In *Nonlinear Model Predictive Control: Theory and Algorithms*. Grüne L. and Pannek J. (ed.), pp. 45-69. Springer International Publishing, Cham. - ISBN 978-3-319-46024-6

Gulli A. and Pal S. (2017) *Deep Learning with Keras - Implementing Deep Learning Models and Neural Networks with the Power of Python*. Packt Publishing Ltd., Birmingham, UK. - ISBN 978-1-78712-842-2

Guo H., Cao D., Chen H., Lv C., Wang H. and Yang S. (2018) *Vehicle dynamic state estimation: state of the art schemes and perspectives*. In IEEE/CAA Journal of Automatica Sinica 5, - ISSN 2329-9274. pp. 418-431

Guzman J.G., Gonzalez L.P., Redondo J.P., Martinez M.M.M. and Boada M.J.L. (2018a) *Real-Time Vehicle Roll Angle Estimation Based on Neural Networks in IoT Low-Cost Devices*. In Sensors 18, - ISSN 1424-8220

Guzman J.G., Gonzalez L.P., Redondo J.P., Sanchez S.S. and Boada B.L. (2018b) *Design of Low-Cost Vehicle Roll Angle Estimator Based on Kalman Filters and an IoT Architecture*. In Sensors 18,

György K., Kelemen A. and Dávid L. (2014) *Unscented Kalman Filters and Particle Filter Methods for Nonlinear State Estimation*. In Procedia Technology 12, - ISSN 2212-0173. pp. 65-74

Halevy A., Norvig P. and Pereira F. (2009) *The Unreasonable Effectiveness of Data*. In IEEE Intelligent Systems 24, - ISSN 1941-1294. pp. 8-12

Harrer M. and Pfeffer P. (2017) *Steering handbook*. Springer International Publishing - ISBN 978-3-319-05448-3

Hecht N. (1989) *Theory of the backpropagation neural network*. In International 1989 Joint Conference on Neural Networks, pp. 593-605 vol.591

Heißing B. and Ersoy M. (2011) *Chassis Handbook*. 1st (ed.), Vieweg+Teubner Verlag, Wiesbaden. - ISBN 978-3-8348-0994-0

Hochreiter S. and Schmidhuber J. (1997) *Long Short-Term Memory*. In Neural Computation 9, - ISSN 0899-7667. pp. 1735-1780

Hou Y., Zhang J., Zhang Y. and Chen L. (2008) *Integrated chassis control using ANFIS*. In 2008 IEEE International Conference on Automation and Logistics, pp. 1625-1630 - ISBN 2161-816X

Hrovat D. (1997) *Survey of Advanced Suspension Developments and Related Optimal Control Applications*. In Automatica 33, - ISSN 0005-1098. pp. 1781-1817

Hutter F., Lücke J. and Schmidt-Thieme L. (2015) *Beyond Manual Tuning of Hyperparameters*. In KI - Künstliche Intelligenz 29, - ISSN 1610-1987. pp. 329-337

Ikenaga S., Lewis F.L., Campos J. and Davis L. (2000) *Active suspension control of ground vehicle based on a full-vehicle model*. In Proceedings of the 2000 American Control Conference. ACC (IEEE Cat. No.00CH36334), Vol. 6, pp. 4019-4024 vol.4016 - ISBN 0743-1619

Ioffe S. and Szegedy C. (2015) *Batch Normalization: Accelerating Deep Network Training by Reducing Internal Covariate Shift*. (ed.), pp. 448-456, PMLR

Isermann R. (2011) *Fault-Diagnosis Applications: Model-Based Condition Monitoring Actuators, Drives, Machinery, Plants, Sensors, and Fault-tolerant Systems*. Springer Publishing Company, Incorporated - ISBN 3642127665

Isermann R. and Münchhof M. (2011) *Identification of Dynamical Systems*. Springer-Verlag - ISBN 978-3-540-78878-2

ISO (2011a) *ISO 7401:2011 Road vehicles — Lateral transient response test methods — Open-loop test methods*. International Organisation for Standardization (ISO)

ISO (2011b) *ISO 8855:2011 Road vehicles — Vehicle dynamics and road-holding ability — Vocabulary*. International Organisation for Standardization (ISO)

ISO (2012) *ISO 4138:2012 Passenger cars - Steady-state circular driving behavior - Open-loop test methods*. International Organisation for Standardization (ISO)

ISO (2018) *ISO 3888-1:2018 Passenger cars — Test track for a severe lane-change manoeuvre — Part 1: Double lane-change*. International Organisation for Standardization (ISO)

ISO (2019) *ISO 7975:2019 Passenger cars — Braking in a turn — Open-loop test method*. International Organisation for Standardization (ISO)

Jang J.-S.R. and Sun C.-T. (1996) *Neuro-fuzzy and soft computing: a computational approach to learning and machine intelligence*. Prentice-Hall, Inc. - ISBN 0132610663

Jang J.R. (1993) *ANFIS: adaptive-network-based fuzzy inference system*. In IEEE Transactions on Systems, Man, and Cybernetics 23, - ISSN 2168-2909. pp. 665-685

Jang J.R. and Chuen-Tsai S. (1995) *Neuro-fuzzy modeling and control*. In Proceedings of the IEEE 83, - ISSN 1558-2256. pp. 378-406

Jantzen J. (2007) *Foundations of Fuzzy Control*. John Wiley & Sons, Inc. - ISBN 0470029633

Jarašūniene A. and Jakubauskas G. (2007) *Improvement of road safety using passive and active intelligent vehicle safety systems*. In Transport 22, - ISSN 1648-4142. pp. 284-289

Jazwinski A.H. (1970) *Stochastic Processes and Filtering Theory*. Academic, San Diego, CA, USA.

Jensen F.V. and Nielsen T.D. (2007) *Bayesian Networks and Decision Graphs*. Springer, New York, NY

Jianyong W., Houjun T., Li S. and Wan F. (2007) *Improvement of Vehicle Handling and Stability by Integrated Control of Four Wheel Steering and Direct Yaw Moment*. In 2007 Chinese Control Conference, pp. 730-735 - ISBN 1934-1768

Johansson R. (2009) *Vision Zero – Implementing a policy for traffic safety*. In Safety Science 47, - ISSN 0925-7535. pp. 826-831

Julier S.J. (2002) *The scaled unscented transformation*. In Proceedings of the 2002 American Control Conference (IEEE Cat. No.CH37301), Vol. 6, pp. 4555-4559 vol.4556 - ISBN 0743-1619

Julier S.J. and Uhlmann J.K. (1997) *New extension of the Kalman filter to nonlinear systems*. In Proc.SPIE, Vol. 3068

Julier S.J. and Uhlmann J.K. (2004) *Unscented filtering and nonlinear estimation*. In Proceedings of the IEEE 92, - ISSN 1558-2256. pp. 401-422

Kalman R.E. (1959a) *Contributions to the Theory of Optimal Control*. In Proceedings of the Conference on Ordinary Differential Equations, Bol. Soc. Mat. Mex., Mexico City, Mexico.

Kalman R.E. (1959b) *On the general theory of control systems*. In IRE Transactions on Automatic Control 4, - ISSN 1558-3651

Kalman R.E. (1960) *A New Approach to Linear Filtering and Prediction Problems*. In Journal of Basic Engineering 82, - ISSN 0021-9223. pp. 35-45

Kalman R.E. (1963) *Mathematical description of linear dynamical systems*. In SIAM Journal on Applied Mathematics 1. pp. 152 -192

Karaboga D. and Kaya E. (2019) *Adaptive network based fuzzy inference system (ANFIS) training approaches: a comprehensive survey*. In Artificial Intelligence Review 52, - ISSN 1573-7462. pp. 2263-2293

Kim S., Park K., Song H.J., Hwang Y.K., Moon S.J., Ahn H.S. et al. (2011) *Development of control logic for hydraulic active roll control system*. In International Journal of Automotive Technology 13, - ISSN 1976-3832. pp. 87

Kingma D.P. and Ba J. (2015) *Adam: A Method for Stochastic Optimization*. In CoRR abs/1412.6980,

Klir G.J. and Yuan B. (1994) *Fuzzy sets and fuzzy logic: theory and applications*. Prentice-Hall, Inc. - ISBN 0131011715

Kong Q., Trugman D.T., Ross Z.E., Bianco M.J., Meade B.J. and Gerstoft P. (2018) *Machine Learning in Seismology: Turning Data into Insights*. In Seismological Research Letters 90, - ISSN 0895-0695. pp. 3-14

Kraus M. (2014) *Schaeffler's electromechanical anti-roll system*. In 5th International Munich Chassis Symposium 2014. Pfeffer P.E. (ed.), pp. 361-365, Springer Fachmedien Wiesbaden, Wiesbaden. - ISBN 978-3-658-05978-1

Krogh A. and Hertz J.A. (1991) *A simple weight decay can improve generalization*. in *Proceedings of the 4th International Conference on Neural Information Processing Systems*(ed.), pp. 950–957, Morgan Kaufmann Publishers Inc., Denver, Colorado.

Kudarauskas N. (2007) *Analysis of emergency braking of a vehicle*. In Transport 22, - ISSN 1648-4142. pp. 154-159

Larochelle H., Erhan D., Courville A., Bergstra J. and Bengio Y. (2007) *An empirical evaluation of deep architectures on problems with many factors of variation*. in *Proceedings of the 24th international conference on Machine learning*(ed.), pp. 473–480, Association for Computing Machinery, Corvalis, Oregon, USA.

LeCun Y.A., Bottou L., Orr G.B. and Müller K.-R. (2012) *Efficient BackProp*. In *Neural Networks: Tricks of the Trade: Second Edition*. Montavon G., Orr G.B. and Müller K.-R. (ed.), pp. 9-48. Springer Berlin Heidelberg, Berlin, Heidelberg. - ISBN 978-3-642-35289-8

Leekwijck W.V. and Kerre E.E. (1999) *Defuzzification: criteria and classification*. In Fuzzy Sets and Systems 108, - ISSN 0165-0114. pp. 159-178

Lei H. and Shiguo L. (2006) *Design considerations of time constant mismatch problem for inductor DCR current sensing method*. In Twenty-First Annual IEEE Applied Power Electronics Conference and Exposition, 2006. APEC '06., pp. 7 pp. - ISBN 1048-2334

Liebemann E.K., Meder K., Schuh J. and Nenninger G. (2005) *Safety and Performance Enhancement: The Bosch Electronic Stability Control (ESP)*. In 19th International Technical Conference on the Enhanced Safety of Vehicles (ESV), pp. 8 pp., Washington DC, United States.

Liu Y., Waters T.P. and Brennan M.J. (2005) *A comparison of semi-active damping control strategies for vibration isolation of harmonic disturbances*. In Journal of Sound and Vibration 280, - ISSN 0022-460X. pp. 21-39

Luenberger D. (1971) *An introduction to observers*. In IEEE Transactions on Automatic Control 16, - ISSN 1558-2523. pp. 596-602

Luenberger D.G. (1964) *Observing the State of a Linear System*. In IEEE Transactions on Military Electronics 8, - ISSN 2374-9520. pp. 74-80

Mamdani E.H. and Assilian S. (1975) *An experiment in linguistic synthesis with a fuzzy logic controller*. In International Journal of Man-Machine Studies 7, - ISSN 0020-7373. pp. 1-13

Mann R.E., Macdonald S., Stoduto G., Bondy S., Jonah B. and Shaikh A. (2001) *The effects of introducing or lowering legal per se blood alcohol limits for driving: an international review*. In Accident Analysis & Prevention 33, - ISSN 0001-4575. pp. 569-583

McCulloch W.S. and Pitts W. (1943) *A logical calculus of the ideas immanent in nervous activity*. In The bulletin of mathematical biophysics 5, - ISSN 1522-9602. pp. 115-133

Mehra R.K., Amin J.N., Hedrick K.J., Osorio C. and Gopalasamy S. (1997) *Active suspension using preview information and model predictive control*. In Proceedings of the 1997 IEEE International Conference on Control Applications, pp. 860-865

Melzi S. and Sabbioni E. (2011) *On the vehicle sideslip angle estimation through neural networks: Numerical and experimental results*. In Mechanical Systems and Signal Processing 25, - ISSN 0888-3270. pp. 2005-2019

Miao Y., Choi S.B., Dong X.M. and Liao C.R. (2008) *Fuzzy Neural Network Control for Vehicle Stability Utilizing Magnetorheological Suspension System*. In Journal of Intelligent Material Systems and Structures 20, - ISSN 1045-389X. pp. 457-466

Michalska H. and Mayne D.Q. (1993) *Robust receding horizon control of constrained nonlinear systems*. In IEEE Transactions on Automatic Control 38, - ISSN 1558-2523. pp. 1623-1633

Misawa E.A. and Hedrick J.K. (1989) *Nonlinear Observers—A State-of-the-Art Survey*. In Journal of Dynamic Systems, Measurement, and Control 111, - ISSN 0022-0434. pp. 344-352

Mitchell T.M. (1999) *Machine learning and data mining*. In Commun. ACM 42, - ISSN 0001-0782. pp. 30–36

Mizuta Y., Suzumura M. and Matsumoto S. (2010) *Ride comfort enhancement and energy efficiency using electric active stabiliser system*. In Vehicle System Dynamics 48, - ISSN 0042-3114. pp. 1305-1323

Mizutani E. and Jang J.R. (1995) *Coactive neural fuzzy modeling*. In Proceedings of ICNN'95 - International Conference on Neural Networks, Vol. 2, pp. 760-765 vol.762

Münster M., Mair U., Gilsdorf H.-J. and Thomä A. (2009) *Electromechanical active body control*. In ATZ worldwide 111, - ISSN 2192-9076. pp. 44-48

Nam K., Oh S., Fujimoto H. and Hori Y. (2013) *Estimation of Sideslip and Roll Angles of Electric Vehicles Using Lateral Tire Force Sensors Through RLS and Kalman Filter Approaches*. In IEEE Transactions on Industrial Electronics 60, - ISSN 1557-9948. pp. 988-1000

Niemz T. (2007) *Reducing Braking Distance by Control of Semi-Active Suspension*. Dissertation, TU Darmstadt, Hamburg.

Novi T., Capitani R. and Annicchiarico C. (2018) *An integrated artificial neural network–unscented Kalman filter vehicle sideslip angle estimation based on inertial measurement unit measurements*. In Proceedings of the Institution of Mechanical Engineers, Part D: Journal of Automobile Engineering 233, - ISSN 0954-4070. pp. 1864-1878

O'Sullivan S., Nevejans N., Allen C., Blyth A., Leonard S., Pagallo U. et al. (2019) *Legal, regulatory, and ethical frameworks for development of standards in artificial intelligence (AI) and autonomous robotic surgery*. In The International Journal of Medical Robotics and Computer Assisted Surgery 15, - ISSN 1478-5951. pp. e1968

Pacejka H.B. (2006) *Tyre and vehicle dynamics*. 2nd (ed.), Butterworth-Heinemann, Oxford. - ISBN 978-0-7506-6918-4

Pahl H.J. (2016) *Air Springs In Commercial Vehicles: Design, Calculation and in Practice*. 2nd (ed.), CreateSpace Independent Publishing Platform - ISBN 978-1517084998

Passino K.M. and Yurkovich S. (1997) *Fuzzy Control*. Addison-Wesley Longman Publishing Co., Inc. - ISBN 020118074X

Patterson D.W. (1998) *Artificial Neural Networks: Theory and Applications*. Prentice Hall PTR - ISBN 0132953536

PorscheAG (2020). *Porsche Cayenne*. Retrieved from https://www.porsche.com/germany/models/cayenne/. Access on 03.05.20

Rahimi Fetrati S., Kandler C., Kärcher C. and Schramm D. (2016a) *Inversion Based Feedforward Design To Improve the Lateral Dynamics of High Performance Sports Cars*. In 13th International Symposium on Advanced Vehicle Control, München.

Rahimi Fetrati S., Teufel S. and Schramm D. (2016b) *Electrification of Torque-Vectoring system to improve the vehicle driving dynamics*. In 7th International Munich Chassis Symposium 2016, pp. 307-321, München. - ISBN 978-3-658-14218-6

Reif K. (2014) *Fundamentals of Automotive and Engine Technology - Standard Drives, Hybrid Drives, Brakes, Safety Systems*. Springer Vieweg - ISBN 978-3-658-03971-4

Rieger G., Scheef J., Becker H., Stanzel M. and Zobel R. (2005) *Active Safety Systems Change Accident Environment of Vehicles Significantly - A Challenge for Vehicle Design*. In Proceedings: International Technical Conference on the Enhanced Safety of Vehicles 2005. pp. 11p-11p

Robertson L.S. (1996) *Reducing death on the road: the effects of minimum safety standards, publicized crash tests, seat belts, and alcohol*. In American Journal of Public Health 86, - ISSN 0090-0036. pp. 31-34

Rokach L. and Maimon O. (2008) *Data Mining with Decision Trees: Theory and Applications*. World Scientific Publishing

Rossiter J.A. (2004) *Model-Based Predictive Control - A Practical Approach*. CRC Press, Boca Raton. - ISBN 9781315272610

Rumelhart D.E., Hinton G.E. and Williams R.J. (1986) *Learning representations by back-propagating errors*. In Nature 323, - ISSN 1476-4687. pp. 533-536

Rumelhart D.E. and McClelland J.L. (1987) *Learning Internal Representations by Error Propagation*. In *Parallel Distributed Processing: Explorations in the Microstructure of Cognition: Foundations*, pp. 318-362. MITP - ISBN 9780262291408

Ryan M. (2020) *In AI We Trust: Ethics, Artificial Intelligence, and Reliability*. In Science and Engineering Ethics 26. pp. 2749-2767

Sagewka S., Fiebig T., Schmid C. and Wostal D. (2017) *Mechatronic Roll Control for the 48-V Electrical System*. In ATZ worldwide 119, - ISSN 2192-9076. pp. 58-63

Sanchez E.N., Ricalde L.J., Langari R. and Shahmirzadi D. (2004) *Rollover prediction and control in heavy vehicles via recurrent neural networks*. In 2004 43rd IEEE Conference on Decision and Control (CDC) (IEEE Cat. No.04CH37601), Vol. 5, pp. 5210-5215 Vol.5215 - ISBN 0191-2216

Sasaki H. and Nishimaki T. (2000) *A Side-Slip Angle Estimation Using Neural Network for a Wheeled Vehicle*. In SAE Transactions 109, - ISSN 0096736X, 25771531. pp. 1026-1031

Schmidhuber J. (2015) *Deep learning in neural networks: An overview*. In Neural Networks 61, - ISSN 0893-6080. pp. 85-117

Schonlau M., Welch W.J. and Donald R.J. (1998) *Global versus Local Search in Constrained Optimization of Computer Models*. In Lecture Notes-Monograph Series 34, - ISSN 07492170. pp. 11-25

Schramm D., Hesse B., Maas N. and Unterreiner M. (2020) *Vehicle Technology - Technical foundations of current and future motor vehicles*. De Gruyter Oldenbourg, Berlin, Boston. - ISBN 978-3-11-059570-3

Schramm D., Hiller M. and Bardini R. (2018) *Vehicle Dynamics: Modeling and Simulation*. 2nd (ed.), pp. 440, Springer, Berlin, Heidelberg. - ISBN 978-3-662-54482-2

Shalaby M.K., Farag A., AbdelAziz O.M., Mahfouz D.M., Shehata O.M. and Morgan E.I. (2019) *Design of Various Dynamical-Based Trajectory Tracking Control Strategies for Multi-Vehicle Platooning Problem*. In 2019 IEEE Intelligent Transportation Systems Conference (ITSC), pp. 1631-1637

Sharp R.S. and Crolla D.A. (1987) *Road Vehicle Suspension System Design - a review*. In Vehicle System Dynamics 16, - ISSN 0042-3114. pp. 167-192

Sieberg P.M., Blume S., Harnack N., Mass N. and Schramm D. (2019a) *Hybrid State Estimation Combining Artificial Neural Network and Physical Model* In Proceedings of the IEEE Intelligent Transportation Systems Conference (ITSC) / ITSC 2019, pp. 894 - 899, IEEE, Auckland, New Zealand.

Sieberg P.M., Blume S., Reicherts S., Maas N. and Schramm D. (2021a) *Hybrid State Estimation – A Contribution Towards Reliability Enhancement of Artificial Neural Network Estimators*. In IEEE Transactions on Intelligent Transportation Systems - ISSN 1558-0016

Sieberg P.M., Blume S., Reicherts S. and Schramm D. (2019b) *Nichtlineare modellbasierte prädiktive Regelung der Fahrzeugdynamik in Bezug auf eine aktive Wankstabilisierung und eine Nickreduzierung*. In *Forschung im Ingenieurwesen*,Vol. 83, pp. 119–127. Springer Berlin Heidelberg, Berlin.

Sieberg P.M., Blume S. and Schramm D. (2021b) *Side-Slip Angle Estimation by Artificial Neural Networks for Vehicle Dynamics Control Applications*. In AmE 2021 - Automotive meets Electronics; 12th GMM-Symposium

Sieberg P.M., Hürten C. and Schramm D. (2020) *Representation of an Integrated Non-Linear Model-Based Predictive Vehicle Dynamics Control System by a Co-Active Neuro-Fuzzy Inference System*. In 2020 IEEE Intelligent Vehicles Symposium (IV), pp. 572-577 - ISBN 978-1-7281-6673-5

Sieberg P.M., Reicherts S. and Schramm D. (2018) *Nichtlineare modellbasierte prädiktive Regelung zur aktiven Wankstabilisierung von Personenkraftwagen*. in *Vierte IFToMM D-A-CH Konferenz 2018*(ed.), pp. 1 - 8, Lausanne.

Sieberg P.M., Schmid M., Reicherts S. and Schramm D. (2019c) *Computation time optimization of a model-based predictive roll stabilization by neuro-fuzzy systems*. In *19. Internationales Stuttgarter Symposium*, Stuttgart.

Singh P.S.A. and Darus I.Z.M. (2011) *Enhancement of SUV Roll Dynamics Using Fuzzy Logic Control*. In 2011 First International Conference on Informatics and Computational Intelligence, pp. 106-111

Sjöberg J., Zhang Q., Ljung L., Benveniste A., Delyon B., Glorennec P.-Y. et al. (1995) *Nonlinear black-box modeling in system identification: a unified overview*. In Automatica 31, - ISSN 0005-1098. pp. 1691-1724

Söffker D., Yu T.-J. and Müller P.C. (1995) *State estimation of dynamical systems with nonlinearities by using proportional-integral observer*. In International Journal of Systems Science 26, - ISSN 0020-7721. pp. 1571-1582

Sorenson H.W. (1970) *Least-squares estimation: from Gauss to Kalman*. In IEEE Spectrum 7, - ISSN 1939-9340. pp. 63-68

Sorenson H.W. (1985) *Kalman Filtering: Theory and Application*. IEEE Press

Spurgeon S.K. (2008) *Sliding mode observers: a survey*. In International Journal of Systems Science 39, - ISSN 0020-7721. pp. 751-764

Srivastava N., Hinton G., Krizhevsky A., Sutskever I. and Salakhutdinov R. (2014) *Dropout: a simple way to prevent neural networks from overfitting*. In J. Mach. Learn. Res. 15, - ISSN 1532-4435. pp. 1929–1958

Sugeno M. (1985) *An introductory survey of fuzzy control*. In Information Sciences 36, - ISSN 0020-0255. pp. 59-83

Sun C., Shrivastava A., Singh S. and Gupta A. (2017) *Revisiting Unreasonable Effectiveness of Data in Deep Learning Era*. In 2017 IEEE International Conference on Computer Vision (ICCV), pp. 843-852 - ISBN 2380-7504

Tahami F., Farhangi S. and Kazemi R. (2004) *A Fuzzy Logic Direct Yaw-Moment Control System for All-Wheel-Drive Electric Vehicles*. In Vehicle System Dynamics 41, - ISSN 0042-3114. pp. 203-221

Takagi T. and Sugeno M. (1985) *Fuzzy identification of systems and its applications to modeling and control*. In IEEE Transactions on Systems, Man, and Cybernetics SMC-15, - ISSN 2168-2909. pp. 116-132

Vargas-Melendez L., Boada B.L., Boada M.J.L., Gauchía A. and Díaz V. (2016) *A Sensor Fusion Method Based on an Integrated Neural Network and Kalman Filter for Vehicle Roll Angle Estimation*. In Sensors 16, - ISSN 1424-8220

Waltz R.A., Morales J.L., Nocedal J. and Orban D. (2006) *An interior algorithm for nonlinear optimization that combines line search and trust region steps*. In Mathematical Programming 107, - ISSN 1436-4646. pp. 391-408

Wan E.A. and Merwe R.V.D. (2000) *The unscented Kalman filter for nonlinear estimation*. In Proceedings of the IEEE 2000 Adaptive Systems for Signal Processing, Communications, and Control Symposium (Cat. No.00EX373), pp. 153-158

Wan E.A. and Van Der Merwe R. (2000) *The unscented Kalman filter for nonlinear estimation*. In Proceedings of the IEEE 2000 Adaptive Systems for Signal Processing, Communications, and Control Symposium (Cat. No.00EX373), pp. 153-158

Wang Z., Qin Y., Gu L. and Dong M. (2017) *Vehicle System State Estimation Based on Adaptive Unscented Kalman Filtering Combing With Road Classification*. In IEEE Access 5, - ISSN 2169-3536. pp. 27786-27799

Wei W., Shaoyi B., Lanchun Z., Kai Z., Yongzhi W. and Weixing H. (2016) *Vehicle Sideslip Angle Estimation Based on General Regression Neural Network*. In Mathematical Problems in Engineering 2016, - ISSN 1024-123X. pp. 3107910

Welch G. and Bishop G. (1995) *An introduction to the Kalman filter*. Organisation, Chapel Hill.

Werbos P.J. (1990) *Backpropagation through time: what it does and how to do it*. In Proceedings of the IEEE 78, - ISSN 1558-2256. pp. 1550-1560

Wielitzka M., Dagen M. and Ortmaier T. (2014) *State estimation of vehicle's lateral dynamics using unscented Kalman filter*. In 53rd IEEE Conference on Decision and Control, pp. 5015-5020 - ISBN 0191-2216

Wilson D.R. and Martinez T.R. (2001) *The need for small learning rates on large problems*. In IJCNN'01. International Joint Conference on Neural Networks. Proceedings (Cat. No.01CH37222), Vol. 1, pp. 115-119 vol.111 - ISBN 1098-7576

Winner H., Hakuli S., Lotz F. and Singer C. (2016) *Handbook of Driver Assistance Systems: Basic Information, Components and Systems for Active Safety and Comfort*, Springer

Won D., Ahn J., Sung S., Heo M., Im S.-H. and Lee Y.J. (2015) *Performance Improvement of Inertial Navigation System by Using Magnetometer with Vehicle Dynamic Constraints*. In Journal of Sensors 2015, - ISSN 1687-725X. pp. 435062

Wu Y., Biaobiao Zhang, Lu J. and Du K.-L. (2011) *Fuzzy Logic and Neuro-fuzzy Systems: A Systematic Introduction*. In International Journal of Artificial Intelligence and Expert Systems 2. pp. 47 - 80

Yildirim E.A. and Wright S.J. (2002) *Warm-Start Strategies in Interior-Point Methods for Linear Programming*. In SIAM J. on Optimization 12, - ISSN 1052-6234. pp. 782–810

Ypma T.J. (1995) *Historical Development of the Newton-Raphson Method*. In SIAM Review 37, - ISSN 00361445. pp. 531-551

Yue M., An C. and Sun J.-Z. (2018) *An Efficient Model Predictive Control for Trajectory Tracking of Wheeled Inverted Pendulum Vehicles with Various Physical Constraints*. In International Journal of Control, Automation and Systems 16, - ISSN 2005-4092. pp. 265-274

Zadeh L.A. (1988) *Fuzzy logic*. In Computer 21, - ISSN 1558-0814. pp. 83-93

Author's Publications Related to the Dissertation

2021

Bahr M., Reicherts S., Sieberg P., Morss L. and Schramm D. (2021) *Application of Artificial Neural Networks for Active Roll Control Based on Actor-Critic Reinforcement Learning*. In Simulation and Modeling Methodologies, Technologies and Applications. Obaidat M.S., Ören T. and Szczerbicka H. (ed.), pp. 61-82, Springer International Publishing, Cham. - ISBN 978-3-030-55867-3

Sieberg P.M., Blume S. and Schramm D. (2021) *Side-Slip Angle Estimation by Artificial Neural Networks for Vehicle Dynamics Control Applications*. In AmE 2021 - Automotive meets Electronics; 12th GMM-Symposium

Sieberg P.M., Blume S., Reicherts S., Maas N. and Schramm D. (2021) *Hybrid State Estimation – A Contribution Towards Reliability Enhancement of Artificial Neural Network Estimators*. In IEEE Transactions on Intelligent Transportation Systems

Sieberg P.M. and Schramm D. (2021) *Central Non-Linear Model-Based Predictive Vehicle Dynamics Control*. In Appl. Sci. 2021, 11, 4687. https://doi.org/10.3390/app1110468

2020

Harnack N., Blume S., Reicherts S., Sieberg P.M. and Schramm D. (2020) *Simulation der Gesamtfahrzeugdynamik durch KNN mittels LSTM-Zellen*. In *Neue Dimensionen Der Mobilität: Technische Und Betriebswirtschaftliche Aspekte*. Proff H. (ed.), pp. 689-706. Springer Fachmedien Wiesbaden, Wiesbaden. - ISBN 978-3-658-29746-6

Sieberg P.M., Hürten C. and Schramm D. (2020) *Representation of an Integrated Non-Linear Model-Based Predictive Vehicle Dynamics Control System by a Co-Active Neuro-Fuzzy Inference System*. In 2020 IEEE Intelligent Vehicles Symposium (IV), pp. 572-577 - ISBN 978-1-7281-6673-5

2019

Bahr M., Reicherts S., Sieberg P.M., Morss L.N. and Schramm D. (2019) *Development and Validation of Active Roll Control Based on Actor-Critic Neural Network Reinforcement Learning*. In Proceedings of the 9th International Conference on Simulation and Modeling Methodologies, Technologies and Applications / SIMULTECH 2019, pp. 36-46, Prag. - ISBN 9789897583810

Blume S., Sieberg P.M., Maas N. and Schramm D. (2019) *Neural Roll Angle Estimation in a Model Predictive Control System*. In Proccedings of the IEEE Intelligent Transportation Systems Conference (ITSC) / ITSC 2019, pp. 1625 - 1630, IEEE, Auckland.

Rahim L., Blume S., Reicherts S., Sieberg P.M. and Schramm D. (2019) *Zustandsschätzung des Wankverhaltens von Personenkraftwagen mittels künstlicher neuronaler Netze.* In Mobilität in Zeiten Der Veränderung : Technische Und Betriebswirtschaftliche Aspekte. Proff H. (ed.), pp. 229-239. Springer Fachmedien Wiesbaden, Wiesbaden. - ISBN 978-3-658-26107-8

Sieberg P.M., Blume S., Harnack N., Mass N. and Schramm D. (2019) *Hybrid State Estimation Combining Artificial Neural Network and Physical Model* In Proccedings of the IEEE Intelligent Transportation Systems Conference (ITSC) / ITSC 2019, pp. 894 - 899, IEEE, Auckland, New Zealand.

Sieberg P.M., Blume S., Reicherts S. and Schramm D. (2019) *Nichtlineare modellbasierte prädiktive Regelung der Fahrzeugdynamik in Bezug auf eine aktive Wankstabilisierung und eine Nickreduzierung*. In *Forschung Im Ingenieurwesen*,Vol. 83, pp. 119–127. Springer Berlin Heidelberg, Berlin.

Sieberg P.M., Schmid M., Reicherts S. and Schramm D. (2019) *Computation Time Optimization of a Model-Based Predictive Roll Stabilization by Neuro-Fuzzy Systems*. In *19. Internationales Stuttgarter Symposium*, Stuttgart.

2018

Sieberg P.M., Reicherts S. and Schramm D. (2018) *Nichtlineare modellbasierte prädiktive Regelung zur aktiven Wankstabilisierung von Personenkraftwagen*. in *Vierte IFToMM D-A-CH Konferenz 2018*(ed.), pp. 1 - 8, Lausanne

DuEPublico

Duisburg-Essen Publications online

UNIVERSITÄT DUISBURG ESSEN

Offen im Denken

ub | universitäts bibliothek

Diese Dissertation wird via DuEPublico, dem Dokumenten- und Publikationsserver der Universität Duisburg-Essen, zur Verfügung gestellt und liegt auch als Print-Version vor.

DOI: 10.17185/duepublico/74460
URN: urn:nbn:de:hbz:464-20210609-104002-0

Alle Rechte vorbehalten.